



Provided by the author(s) and University of Galway in accordance with publisher policies. Please cite the published version when available.

Title	A multiscale biomechanical investigation of bone fragility in Type-2 Diabetes using a Zucker Diabetic Fatty (ZDF) rat
Author(s)	Monahan, Genna
Publication Date	2024-04-18
Publisher	NUI Galway
Item record	http://hdl.handle.net/10379/18164

Downloaded 2024-05-20T00:15:04Z

Some rights reserved. For more information, please see the item record link above.



A Multiscale Biomechanical Investigation of Bone Fragility in Type-2 Diabetes using a Zucker Diabetic Fatty (ZDF) Rat

Genna Monahan B.E.



OLLSCOIL NA GAILLIMHÉ
UNIVERSITY OF GALWAY

A thesis submitted to the University of Galway as fulfilment of the requirements for the
Degree of Doctor of Philosophy

2023

Discipline of Biomedical Engineering,
College of Science and Engineering,
University of Galway

Supervisor of Research:

Dr. Ted Vaughan

ABSTRACT

Patients with type-2 diabetes (T2D) face an elevated risk of bone fracture, despite often exhibiting normal or increased bone mineral density (BMD). The prevailing theory suggests that the hyperglycaemic environment in T2D leads to an accumulation of non-enzymatic Advanced Glycation End-Products (AGEs) in the collagen matrix, resulting in a more brittle behaviour. Yet, no causal relationship has been established suggesting that other mechanisms may be responsible for bone fragility in T2D.

The objective of this thesis is to elucidate the underlying biological, biophysical and biomechanical mechanisms that contribute to bone fragility in T2D using a multiscale approach in a 46-week longitudinal study with a Zucker Diabetic Fatty (ZDF) (*fa/fa*) rat model, by investigating geometrical, compositional and mechanical alterations of the ulnar bone in ZDF rats. It was found that longitudinal alterations in bone growth and reduced bone strength was better correlated with altered mineral properties rather than AGEs. This led to the conclusion that bone fragility in ZDF (*fa/fa*) rats occurs through a multifactorial process, prompting further investigation into various biological, biophysical, and biomechanical factors that contribute to bone fragility.

A detailed investigation of the sequence of events from cellular- to tissue- to the whole-bone biomechanical-level in femoral bones of ZDF (*fa/fa*) rats was conducted on femoral tissue. It was found that the diabetic state disrupted bone metabolism and cell activity, which showed downstream effects on the mineral and organic components of the bone matrix. Together, these sub-tissue alterations coincided with deterioration of the fracture resistance, with biomechanical testing showing significantly reduced cracking toughness and work-to-fracture in 46-week diabetic (*fa/fa*) rats, compared to lean, healthy controls.

Finally, impaired longitudinal bone growth was investigated by assessing regional alterations in bone composition and tissue-level mechanical properties using site-matched Raman spectroscopy, nanoindentation and micro-pillar compression testing. Regional differences were mainly found in the periosteal region of the control and ZDF (*fa/fa*) rats. In particular, the mineral composition was found to be altered in the ZDF (*fa/fa*) rats indicating a regional interplay in bone formation and resorption during growth. Despite compositional changes, tissue-level mechanical properties, did not significantly differ between strains in both regions, contributing valuable insights into the complex dynamics of tissue composition, mechanics, and disease progression in the growth and maintenance of cortical bone in ZDF (*fa/fa*) rats with T2D.

Overall, the findings in this thesis reveal that bone fragility in the ZDF rats occurs through a complex process that was not solely attributed to AGE accumulation in the collagen matrix, but instead arose due to altered bone cellular metabolism and its subsequent effects on bone growth, microstructure and the spatial and temporal alterations to the mineral phase of the bone matrix.

LIST OF PUBLICATIONS

Journal Articles

The following publications have arisen from the work presented in this thesis:

- **Monahan, G.**, Schiavi-Tritz, J, Britton, M, Vaughan, T.J. “Longitudinal alterations in bone morphometry, mechanical integrity and composition in Type-2 diabetes in a Zucker diabetic fatty (ZDF) rat.” (2023) *Bone*, 170, 116672
<https://doi.org/10.1016/j.bone.2023.116672>

The following manuscripts are currently under review:

- **Monahan, G.E.**, Schiavi-Tritz, J, Britton, M, Jaisson, S, Okwika, A, Kerdjoudj, H, Vaughan, T.J. “Experimental and Computational Mechanics of Bone Fragility in Type-2 Diabetes: A Longitudinal Investigation using Zucker Diabetic Fatty (ZDF) Rats.”
Under review

The following manuscripts are currently in preparation:

- **Monahan, G.E.**, Schiavi-Tritz, J, Britton, M, Kochetkova, T, Minniert, C, Schwiedrzik, J, Vaughan, T.J. “An Investigation of Regional Alterations in the Compositional and Mechanical Properties of Cortical Bone from Zucker Diabetic Fatty (ZDF) Rats.” *In preparation*

The following publications have been generated separate to this thesis:

- Britton M., **Monahan, G.E.**, Schiavi-Tritz, J., Beljebbar, A., Van Gulick, L., Owieka, A., Jaisson, S., Kerdjoudj, H., Vaughan, T.J. “Investigating the Mechanical Properties and Microdamage Accumulation of Human Type-2 Diabetic Bone”. *In preparation*
- Britton M., **Monahan, G.E.**, Vaughan, T.J. “An Investigation of Regional Heterogeneity within the *ex vivo* Femoral Head of Type-2 Diabetic Patients” *In preparation*

Peer-Reviewed International Conference Proceedings

- Poster presentation at the annual meeting of American Society of Bone and Mineral Research, Vancouver, Canada. October 2023.
- Poster presentation at the annual meeting of Orthopaedic Research Society, Dallas, Texas, USA. February 2023.
- Poster presentation at the annual meeting of ICORS World Orthopaedic Congress, Edinburgh, Scotland, September 2022.
- Podium presentation at the annual meeting of European Solid Mechanics Conference, Galway, Ireland. July 2022.
- Podium presentation at the annual meeting of the European Society of Biomechanics, Porto, Portugal, June 2022.
- Podium presentation at the annual meeting of Orthopaedic Research Society, Tampa, Florida, USA. February 2022.
- Podium presentation at the annual meeting of the European Orthopaedic Research Society, Rome, Italy, September 2021.

Peer-Reviewed National Conference Proceedings

- Podium presentations at 26th , 27th and 28th Annual conference of the Section of Bioengineering of the Royal Academy of Medicine in Ireland (BINI), January 2020, May 2022 and January 2023.
- Podium presentation representing the University of Galway at 24th Annual Sir Bernard Crossland Symposium, September 2021.

ACKNOWLEDGEMENTS

Firstly, I would like to express my deepest gratitude to my supervisor Dr. Ted Vaughan, for his mentorship, support, patience and guidance. Whilst working with him I have gained invaluable scientific knowledge and confidence in my abilities as an academic writer, which I know I will carry with me after this PhD. He sets an exemplary standard in research and wordcraft, which will always serve as a lasting inspiration for me.

I must also convey my utmost appreciation for Dr. Jessica Schiavi-Tritz. I am truly grateful to have had the opportunity to learn from and work alongside her. She is someone I am happy to call both a friend and mentor. I will forever think back fondly of our trip to EORS in Rome (and the multiple daily ice-cream stops).

A special thank you to Masooma, Ruth, Ciara, Swati, Vatsal, Vinnie, Ryan, Dave, Tecla, Hannah, Martina, Mahtab, Sam, Darshan, Conall, Thomas, and all the members of Pints for PhDs. I honestly don't know how I got so lucky to be surrounded by such a wonderful, kind, energetic and dedicated group of people. You all have been so supportive throughout these past four years and I am so grateful to have met each and every one of you! I would like to extend my sincere thanks to Marissa. Her hardwork and dedication throughout her PhD has been inspiring to me. I'm so thankful for her support throughout the years. I could not have had a better friend to work, travel and taste German champagne in France with (lets also not forget the porto breakfast)! A big thank you to Flavia, for your kind-heartedness, feeding me snacks from her drawer, being my biggest motivator and always making me smile. I am so thankful for our scientific chats and friendship. A special thank you also to Anneke, who always took the time to help me when I was a bit lost, provide constructive advice and feedback (which I am forever grateful for) as well as being a wonderful friend and making me laugh. My sincerest appreciation goes to the technical staff, especially Dave Connolly, for his assistance and expertise in the lab and to Pat Kelly for machining all the necessary rigs and parts!

To my friends Katie, Gemma, Rachel and Laura. Thank you for all the "coffees", dinner dates, walks, laughter, support and care throughout the years. I also appreciate your patience with me even when I sometimes wasn't the best with replying to my WhatsApps, I still loved all your messages and am forever grateful to have you all as my friends.

To my Dad and Brother, Ryan – you have both given me so much love, support and patients. I appreciate every single call, text and moment we spend together. To my Mom, words cannot describe how much your support has meant to me over the last few years. This is truly your PhD as much as it is mine. I appreciate you being there for me through all the dinners cooked, walks done, coffee and lunch breaks taken, hot-water bottles made and hours of listening, your enduring love, unwavering support, and constant encouragement over the years. Last but certainly not least, Connor, I know you didn't want a sappy acknowledgement but here it is... I wouldn't have been able to get through these last four years without you. Thank you so much for your patience, your unconditional love and support and for always wanting the best for me. From your long train rides back and fourth to Galway when I couldn't come to Dublin, to your supportive little notes and snacks hidden at my desk to your funny cat memes, I appreciate all of it. Well folks we finally made it!

DECLARATION OF ORIGINALITY

I declare that the work presented in this thesis is my own.

Genna Monahan

ACRONYMS & NOMENCLATURE

Acronyms & nomenclature are defined below for content from Chapters 3 to 5.

Acronyms

AGE	Advanced Glycation End-Product
AP	Anterior-Posterior
APEDS	Activated Papain Enzyme Digestion Solution
ATR	Attenuated Total Reflectance
BMD	Bone Mineral Density
BMDD	Bone Mineral Density Distribution
BV	Bone Volume
BV/TV	Bone volume fraction
Ca ²⁺	Calcium ion
CML	Carboxymethyl-lysine
CO ₃ ²⁻	Carbonate ions
Conn.D	Connectivity Density
CTX-I	C-telopeptide of collagen alpha-I
Ct.Ar	Cortical bone tissue cross-sectional area
Ct.Po	Cortical porosity
Ct. Th	Cortical bone tissue thickness
DA	Degree of anisotropy
DICOM	Digital Imaging and Communications in Medicine (scan)
fAGE	Fluorescent Advanced Glycation End-Product
FEA	Finite Element Analysis
FTIR	Fourier Transform Infrared Spectroscopy
FWHM	Full Width at Half Maximum
HA	Hydroxyapatite
HbA1	Haemoglobin subunit alpha-1/2
HbA1c	Glycated haemoglobin
HFD	High Fat Diet
HPLC	High Performance Liquid Chromatography
HU	Hounsfield Units

IGF-I	Insulin-like growth factor hormone-I
IL-6	Interleukin-6
IPL	Image Processing Language (Scanco Medical)
KVp	Peak kilovoltage
L	Length
Micro-CT	Micro-Computed Tomography
ML	Medial-Lateral
M_{mean}	Mean mineral density
M_{mode}	Mode mineral density
P1NP	Procollagen type 1 amino terminal propeptide
PBS	Phosphate Buffer Saline
PEN	Pentosidine
PO_4^{3-}	Phosphate ions
PYD	Post-yield displacement
qPRS	Quantitative Polarised Raman Spectroscopy
ROI	Region of interest
Sost	Sclerostin
SMI	Structural model index
T2D	Type-2 Diabetes
TMD	Tissue Mineral Density
TV	Total Volume
TV_{25}	Tissue volume at low mineral density (25 th percentile)
TV_{50}	Tissue volume at medium mineral density (50 th percentile)
TV_{75}	Tissue volume at high mineral density (75 th percentile)
VOI	Volume of interest
ZDF	Zucker Diabetic Fatty
ZDSD	Zucker Diabetic Sprague Dawley
ZL	Zucker Lean

Nomenclature

A_c	Area of contact of indenter
C_{ml}	Cross-sectional distance from the centroid to outermost point
d	Displacement
d'	Normalised displacement
E	Young's (elastic) modulus
E_i	Indenter modulus
E_r	Reduced modulus
F_b	A geometry factor
H	Material hardness
I_{ap}	Anterior-Posterior moment of inertia
I_{ml}	Medial-Lateral moment of inertia
k	Bending rigidity
μA	Microampere
$\mu\varepsilon$	Microstrain
M	Moment
θ_c	Notch angle
ν	Poisson's ratio
ν_i	Indenter Poisson's ratio
P_{max}	Maximum force
$pMOI$	Polar moment of inertia
ρ_{Ash}	Ash density
ρ_{CT}	Computed Tomography measured density
R_i	Endosteal radius
R_m	Mean radius
R_o	Periosteal radius
S	Span length or Material stiffness
ε	Strain
σ	Stress
W_f	Area under the force-displacement curve or work-to-fracture

TABLE OF CONTENTS

1. Introduction	1
1.1 T2D and Bone Fragility	1
1.2 Mechanisms of Bone Fragility in T2D.....	3
1.2.1 Advanced Glycation End-Products	3
1.2.2 Pathophysiological Mechanisms of Bone Fragility in T2D	3
1.3 Animal Models of T2D	5
1.4 Objectives.....	7
1.5 Thesis Structure.....	9
1.6 References	10
2. Literature Review	17
2.1 Bone Structure, Function and Matrix.....	17
2.1.1 The Hierarchical Structure of Bone.....	18
2.1.2 Bone Matrix Composition	20
2.2 Bone Biology and Turnover.....	26
2.2.1 Bone Cells	27
2.2.2 Bone Modelling and Remodelling.....	31
2.2.3 Cellular and General Health Markers.....	33
2.3 Bone Quality	36
2.3.1 Multiscale Analysis of Bone Quality	37
2.3.2 Bone Mineralisation and Density Distribution.....	48
2.4 Bone Disease and T2D.....	49
2.4.1 Epidemiology and Pathophysiology of T2D	49
2.4.2 Bone Fragility in T2D	51
2.5 Rodent Bone.....	52
2.5.1 Growth, Structure and Function	52
2.5.2 Pre-Clinical Models of T2D	54
2.6 Multiscale Bone Biomechanics.....	56
2.6.1 Mechanical Testing of Small Animal Bone	57
2.6.2 Computational Modelling.....	71
2.6.3 Mechanisms of Fracture Resistance in Bone.....	72

2.7 Mechanisms of Bone Fragility in T2D.....	75
2.7.1 T2D and Impaired Cellular Metabolism.....	75
2.7.2 T2D and Altered Bone Matrix.....	83
2.7.3 T2D and Tissue Mechanical Integrity	100
2.8 Summary	109
2.9 References	110
3. Longitudinal Alterations in Bone Morphometry, Mechanical Integrity and Composition in Type-2 Diabetes in a Zucker Diabetic Fatty (ZDF) Rat	150
3.1 Introduction	150
3.2 Materials and Methods	153
3.2.1 Animal model and tissues.....	153
3.2.2 Geometric and Morphometric Properties	156
3.2.3 Structural and Material Properties	156
3.2.4 Biochemical Analysis.....	158
3.2.5 Fluorescence Advanced Glycated End-Products (fAGE) Analysis	159
3.3 Statistical Analysis	160
3.4 Results	161
3.4.1 Geometric and Morphometric Properties	161
3.4.2 Structural and Material Properties	164
3.4.3 Biochemical Analysis.....	167
3.4.4 Fluorescence Advanced Glycated End-Products (fAGE) Analysis	169
3.4.5 Correlation results among serum levels, skin and bone composition	170
3.4.6 Correlation results for biomechanical properties	170
3.5 Discussion	171
3.6 Concluding Remarks	178
Appendix 3.1	179
Details of animal study	179
Body mass loss of 46-week cohort with long-term diabetes.....	179
Appendix 3.2	181
Linear regression analysis of ultimate moment vs. section modulus (I_{ml}/C_{ml}) between type-2 diabetic (<i>fa/fa</i>) and Control (<i>fa/+</i>) rats.....	181
3.7 References	184

4. Experimental and Computational Mechanics of Bone Fragility in Type-2 Diabetes: A Longitudinal Investigation Using Zucker Diabetic Fatty (ZDF) Rats	197
4.1 Introduction	197
4.2 Material and Methods	200
4.2.1 Animal Model and Tissues	200
4.2.2 Cellular Metabolism	201
4.2.3 Organic Matrix Composition.....	202
4.2.4 Microarchitecture and Mineralisation	204
4.2.5 Biomechanical Analysis	205
4.3 Statistical Analysis	208
4.4 Results	209
4.4.1 Cellular Metabolism – Serum Analysis.....	209
4.4.2 Organic Matrix Composition – Bulk fAGEs and HPLC.....	210
4.4.3 Bone Microarchitecture – Micro-CT Analysis.....	211
4.4.4 Bone Mineralisation – BMDD Analysis	216
4.4.5 Biomechanical Analysis	220
4.4.6 Micro-FE Analysis	223
4.5 Discussion	224
4.6 Concluding Remarks	233
4.7 Appendix 4.1	234
4.7.1 Bone mineral density distribution data obtained for the femoral neck and midshaft	235
4.8 Appendix 4.2	237
4.8.1 Correlation analysis	237
4.9 References	242
5. An Investigation of Regional Alterations in the Compositional and Mechanical Properties of Cortical Bone from Zucker Diabetic Fatty (ZDF) Rats	252
5.1 Introduction	252
5.2 Materials and Methods	254
5.2.1 Sample preparation	255
5.2.2 Tissue composition.....	256
5.2.3 Tissue-level mechanical properties	258
5.2.4 Statistical Analysis	260

5.3 Results	260
5.3.1 Tissue composition	260
5.3.2 Tissue-level mechanical properties	267
5.4 Discussion	273
5.5 Concluding Remarks	279
5.6 References	280
6. Concluding Remarks and Future Perspectives	285
6.1 Summary of Key Contributions	285
6.2 Future Recommendations.....	288
6.3 References	290

CHAPTER 1

Introduction

1.1 T2D and Bone Fragility

Type-2 Diabetes (T2D) mellitus is a metabolic disorder that is characterised by insulin resistance, where the body's cells do not respond effectively to insulin, a hormone that regulates blood sugar. It is estimated that T2D accounts for 90-95% of diabetic cases (Valderrábano and Linares, 2018). and currently affects over 500 million adults globally. By 2045, this number is projected to grow to over 700 million (Robertson, 2023; Saeedi et al., 2019). Unlike Type-1 diabetes, T2D results from reduced insulin sensitivity and impaired insulin secretion, leading to hyperglycaemia. Patients with T2D can experience a wide range of micro- and macro-vascular complications, including retinopathy, nephropathy, neuropathy and atherosclerosis, as they age, which has a significant impact on their quality of life and increases their risk of mortality (Duckworth, 2001; Faselis et al., 2019; Laakso, 2014).

Patients with T2D also experience an increased risk of bone fragility fractures, with up to a 3-fold increase in hip fracture risk being reported, even after body mass and falling risk has been accounted for (Bonds et al., 2006; Janghorbani et al., 2007; Strotmeyer et al., 2005). While there are a variety of different factors that can influence the incidence of fragility fractures such as increased falling risk, secondary complications such as peripheral neuropathy and insulin use, research has shown that disease duration also plays a role, where individuals with long-term T2D have a higher incidence of fracture than short-term sufferers, even after adjusting for age and body mass index (BMI) (Janghorbani et al., 2006). Paradoxically, this increased risk of fracture in T2D is not associated with any reduction in bone mineral density (BMD) (Strotmeyer et al., 2005; Vestergaard, 2007), as would be the case in osteoporosis, a disease characterised by bone loss. Instead, patients with T2D usually present with a normal or high bone mineral density BMD, compared to non-diabetics (Vestergaard, 2007). This presents distinct clinical challenges when applying diagnostic criteria for fracture risk in patients with

T2D, as traditional screening methods that are based on bone density, such as Dual X-Ray Absorptiometry (DEXA) and the fracture risk prediction tool FRAX, are unable to provide quantitative measures of fracture probability (Vandenput et al., 2022). This implies that T2D is associated with a deterioration of bone quality, whereby the bone geometry, microarchitecture and intrinsic properties of the bone tissue matrix itself may be impaired leading to an impaired fracture resistance. Previous research has widely hypothesised that elevated levels of glucose, due to hyperglycaemia, results in an increased accumulation of non-enzymatic cross-links or adducts in the form of advanced glycated end-products (AGEs), which are thought to influence the organic matrix either by stiffening the collagen network leading to a more brittle tissue behaviour (Delmas et al., 1984; Vashishth, 2007) or altering the protein structure (Nagai et al., 2014). However, the difficulty in obtaining direct measurements from bone tissue *in vivo* means that quantitative data describing precisely how bone tissue properties are impaired in T2 diabetic patients are limited. In a previous large population based Health Aging, Body and Composition (Health ABC) study, circulating AGEs such as urinary pentosidine correlated with increased prevalence of vertebral fractures in the patient cohort with T2D even after adjustment for BMD (Schwartz et al., 2009). Additionally, serum carboxymethyl-lysine have been found to be significantly correlated with the clinical fracture risk in the T2 diabetic cohort (Dhaliwal et al., 2022). However, there has still been no clear causal relationship established in epidemiological studies between AGEs and bone fragility in T2D and highlights that other mechanisms may be responsible for this increased fragility, which have yet to be elucidated (Britton and Vaughan, 2023). **The work of this thesis uses a multiscale approach to examine bone quality and how this may play a role in impairing the mechanical integrity of bone from Zucker Diabetic Fatty (ZDF) rats as the disease progresses.**

This research is timely as the worldwide prevalence of diabetes has seen a significant rise, resulting in a substantial economic impact, with the global expenditure estimated to be €900 billion (Sun et al., 2022). In 2019, it was estimated that approximately €1 billion was spent on diabetes related complications in Ireland alone, accounting for 10-12% of the national health budget of €16 billion (Diabetes Ireland, 2021). Protecting against fracture in this patient population is vital as patients with T2D have impaired fracture healing as a result of increased inflammation, reduced bone turnover, vascularization and osteoblast differentiation (Marin et al., 2018; Murray and Coleman, 2019), resulting in increased recovery time, non-union and risk of fracture recurrence. A better understanding of the factors that contribute to this increased

fragility could help to establish a quantitative relationship between bone biomechanics and bone quality, ultimately improving the development of an effective fracture risk assessment technique for patients with T2D.

1.2 Mechanisms of Bone Fragility in T2D

1.2.1 Advanced Glycation End-Products

During T2D, elevated levels of glucose in the blood leads to a hyperglycaemic environment, which has been hypothesised to increase the formation of non-enzymatic cross-links or adducts throughout the proteins network in the organic phase of bone, known as advanced glycated end-products (AGEs) (Furst et al., 2016; Goldin et al., 2006). AGEs are present as both cross-linked and non-cross-linking adducts that are formed through reactions between amino components of proteins or lipids and glucose or its degradation products (Thorpe and Baynes, 2003; Willett et al., 2022). It has been widely hypothesised that AGE accumulation alters protein mechanics throughout the organic components of the bone matrix, thereby compromising the mechanical integrity of the bone tissue leading to increased fragility in T2D. However, much of the evidence supporting this has been derived through use of *in-vitro* glycation models, whereby animal or human tissue is immersed in a ribose solution to facilitate non-enzymatic glycation of the protein network (Catanese et al., 1999; Poundarik et al., 2015; Vashishth et al., 2001; Viguet-Carrin et al., 2008; Zimmermann et al., 2011). Importantly, these *in-vitro* glycation models are severely limited by the fact that they generate AGEs levels that can be an order of magnitude higher than those observed occurs physiologically, either through the natural aging process or during T2D (McCarthy et al., 2001a; Zimmermann et al., 2015, 2011). In fact, the majority of human studies have reported no significant differences in AGE levels in the bone tissue of T2D patients (Karim et al., 2018; Wölfel et al., 2022b, 2022a) compared to age-matched controls, with only a limited number of studies actually observing significant increases (Piccoli et al., 2020; Wölfel et al., 2020). **Together, this implies that there is limited experimental evidence that establishes any mechanistic link between AGE accumulation and bone fragility in T2D patients. This implies that other mechanisms must be responsible for impaired tissue behaviour.**

1.2.2 Pathophysiological Mechanisms of Bone Fragility in T2D

Normal maintenance of the bone tissue matrix is achieved through careful coordination between the bone cells, whereby osteoclasts are responsible for removal of damaged bone tissue and osteoblasts are responsible for the production of the bone matrix. During this process, osteoblasts secrete Type-I collagen, which becomes mineralised over time through the

availability of suitable nucleation sites to form the tissue matrix. This process is carefully orchestrated through local and systemic biochemical factors, in addition to targeted remodelling in response to mechanical loading. However, with the onset of T2D, various metabolic and cellular functions are disrupted throughout the body leading to complex pathophysiological changes that may disrupt normal bone metabolism. In particular, there is evidence of a direct link between hyperglycaemia and increased AGE accumulation with an increase in adiposity, suggesting a feed-forward cycle, switching Mesenchymal Stem Cell (MSC) fate from osteoblastogenesis to adipogenesis (Napoli et al., 2017). In fact, a study by Cassidy *et al.* (2020) reported a reduced number of bone-marrow derived MSCs in patients with T2D when compared to age-matched controls. This cycle may play a key role in the progression of metabolic dysfunction into an irreversible diabetic state resulting in pathophysiological changes such as an increased inflammatory state, disrupted cellular functions, increased in bone marrow adiposity and higher oxidative stress (Picke et al., 2019). There is evidence that patients with T2D present with low bone turnover, with reduced levels of bone formation and resorption serum markers, P1NP and CTX, respectively (Lekkala et al., 2023) and impaired expression of the bone formation controlling genes, sclerostin (Sost) and RUNX2 (Piccoli et al., 2020). This altered bone remodelling process could negatively impact the normal maintenance of both the organic and mineral components of the bone tissue, which could have devastating effects on the tissue's mechanical integrity. In particular, a recent *in-vitro* study has demonstrated that hyperglycaemia disrupts the mineralisation phase of osteoblasts exhibited by severely decreased mineral formation and matrix mineralisation (mineral: matrix ratio assessed via Raman spectroscopy) (Entz et al., 2022), while investigations on human tissue have demonstrated that mineral is more heterogeneously distributed in T2D (Parle et al., 2020; Wölfel et al., 2020), which are consistent with other observations of altered mineralisation patterns (Roschger et al., 2008). Furthermore, studies have demonstrated that changes in tissue composition can take place regionally, with altered carbonate: amide I ratios (Wölfel et al., 2022a) and crystallinity (Wölfel et al., 2020) in endocortical regions of the tibia and femoral of patients with T2D with high porosity that is likely a result of an altered bone remodelling process. **While this provides clear evidence that alterations to both mineral and organic phases of the bone matrix are likely responsible for diabetic bone fragility, a mechanistic understanding of how these changes are driven at a cellular level and how such sub-tissue alterations affect overall bone mechanics remains poorly understood.**

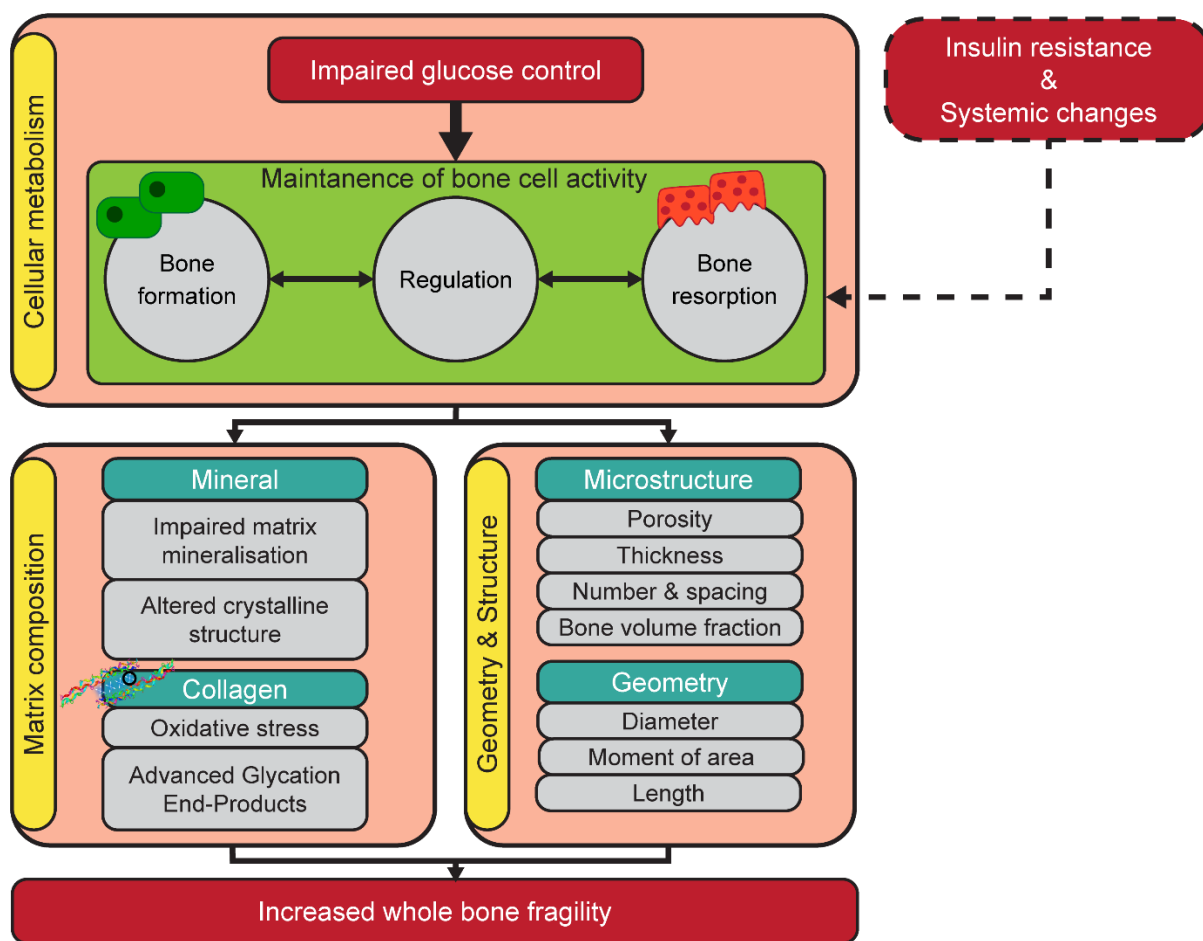


Figure 1.1. A summary of the pathophysiological mechanisms that may play a role in leading to increased whole-bone fragility in type-2 diabetes whereby impaired glucose control combined with increased insulin resistance and other systemic factors such as obesity and inflammation playing a role in altering bone cell metabolism which can affect bone maintenance. This may have a downstream effect on the matrix composition and the microstructure of the tissue both of which play a role in bone fracture resistance.

1.3 Animal Models of T2D

A major challenge in understanding the pathophysiological mechanisms of bone fragility in T2D is the difficulty of acquiring direct *in-vivo* tissue measurements, which restricts the availability of quantitative data that accurately describes the impairment of bone tissue properties in patients with T2D. This, coupled with bones complex hierarchical structural organisation and associated fracture mechanics, means there is a severe lack of understanding of the sub-tissue physiochemical alterations that take place in T2 diabetic bone disease and how these changes compromise overall structural integrity of the tissue. Even when human tissue has been examined, there are numerous associated challenges. For instance, pinpointing the precise diabetic onset in patients and determining the disease duration is generally difficult.

The use of medication can affect bone density, while the absence of key patient information (age, gender, body mass index, blood glucose, HbA1c levels) can limit the true understanding of bone fragility in T2D. Using a rodent model of Type 2 Diabetes (T2D) can mitigate confounding factors like age, gender, and disease duration, offering a cost-effective approach to unravel the factors contributing to bone fragility in T2D. However, the complex and diverse nature of this disease means there is currently no single animal model that can fully replicate all human characteristics. Furthermore, rodent bones lack Haversian systems and do not undergo human-like remodelling (Wittig and Birkedal, 2022), but can still provide important insight into appositional growth, bone loss and T2 diabetic bone fragility.

There are a variety of animal studies that have provided insight into bone quality and fragility in T2D. Hamann *et al.* (2011) examined the impact of T2D on bone physiology and regeneration in 21-week old ZDF rats (disease duration for ~9-weeks) and found that while osteoblast differentiation was impaired in these rats, osteoclast biology was not and thus the ZDF (*fa/fa*) rats exhibited delayed bone regeneration with only 21% of defect filling in comparison to 57% by non-diabetic controls. Hunt *et al.* (2018b) investigated bone tissue composition of a 20-week old KK-Ay murine model of T2D using Fourier transform infrared (FTIR) imaging and high-performance liquid chromatography (HPLC) and reported that KK-Ay mice had increased collagen maturity, mineral content, and less heterogeneous mineral properties than controls but did not report differences in pentosidine or other non-enzymatic crosslinks, concluding that the characteristics of KK-Ay mice align with those of aged bone and correspond to observations indicating decreased remodelling in T2D. Creecy *et al.* (2016) has carried out one of the longest investigations of T2 diabetic bone fragility at 16-, 22- and 29-weeks using ZDSD rats (disease duration ~1-, 7- and 14-weeks). While they did not report any difference in tissue-mechanical properties compared to controls, they did report alterations with disease progression such as reduced bone toughness and fracture toughness in the ZDSD rats with age. While these animal studies have provided important insight into bone fragility in T2D, it is notable that several existing studies have been limited by disease duration and have only investigated properties in animals that were overtly diabetic for a few weeks (Devlin *et al.*, 2014; Hamann *et al.*, 2011; Mehta *et al.*, 2023; Micheletti *et al.*, 2023; Prisby *et al.*, 2008; Woolley *et al.*, 2023). **Furthermore, whilst existing studies have examined cellular, compositional, and biomechanical aspects of T2 diabetic bone fragility, these investigations have tended to examine these factors independently of one another (Creecy *et al.*, 2016; Hamann *et al.*, 2011; Hunt *et al.*, 2018; Zeitoun *et al.*, 2019), resulting in a**

fragmented understanding of the underlying mechanisms involved. More comprehensive longitudinal animal studies are required to fully elucidate the connection between diabetes pathophysiology and compromised skeletal strength.

1.4 Objectives

The global objective of this thesis is to elucidate the underlying biological, biophysical and biomechanical mechanisms that contribute to bone fragility in T2D. As a model for long-term T2D, this work conducts a 46-week longitudinal study using a Zucker Diabetic Fatty (ZDF) (*fa/fa*) rat model and investigates longitudinal alterations in cellular behaviour, tissue composition, bone morphometry and multiscale mechanical properties across different tissue types from these animals. Furthermore, insight into the onset of progressing of bone fragility in more animal models of T2D will provide invaluable information towards establishing an animal model that can mimic the characteristics of the human disease.

The specific objectives of this thesis are:

1. To investigate the geometrical, compositional and mechanical alterations of ulnar bone in ZDF (*fa/fa*) rats to determine whether AGEs from radius cortical bone are the main contributing factor to the increased risk of fracture observed in subjects with T2D.
2. To examine the biological, biophysical and biomechanical factors that contribute to bone fragility in a ZDF (*fa/fa*) rat using serum and femoral bone to establish the sequence of events that occur from the cellular-level to the tissue-level that impact the whole-bone fracture mechanics during T2D.
3. To explore regional differences in tissue composition and mechanics during growth and maintenance of cortical bone as disease progressed in ZDF (*fa/fa*) rats to identify differences in bone tissue quality in T2D.

Three hypotheses have been formed to address these three objectives, with each hypothesis addressed in the respective studies presented in Chapters 3, 4 and 5.

- **Hypothesis 1:** Mechanical properties and composition of cortical bone becomes altered as a result of increased AGE concentration in the Zucker Diabetic Fatty (ZDF) (*fa/fa*) rats.
- **Hypothesis 2:** Bone fragility in ZDF (*fa/fa*) rats occurs through of a variety of biological, biophysical and biomechanical contributing factors.

- **Hypothesis 3:** Regional alterations in bone composition leads to impaired bone growth, maintenance and tissue-level mechanical properties in ZDF (*fa/fa*) rats.

1.5 Thesis Structure

This thesis is structured as follows:

Chapter 2 outlines the existing relevant literature on the topic of bone and T2D. This Chapter provides information on bone structure, function, composition and mechanics. The techniques used to assess bone quality and mechanical in small animal bones are described in detail, as well as the effects of T2D on bone cell metabolism, matrix and mechanics. *Chapter 3* outlines the first technical Chapter of this thesis, which is an investigation of bone morphometry via micro-computed tomography, mechanical integrity via three-point bend testing and composition using FTIR and measuring fluorescent AGE (fAGEs) accumulation as the disease progresses in a Zucker Diabetic Fatty (ZDF) Rat model of T2D. *Chapter 4* presents the second technical Chapter which considers the downstream effects of an altered cellular metabolism on bone fragility and determines whether AGEs are a significant contributor to bone fragility for these ZDF rats. Cellular metabolism is evaluated by measuring a variety of serum markers. AGE accumulation is again investigated by measuring fAGEs and using high-performance liquid chromatography to assess furosine and carboxymethyl-lysine. Bone microarchitecture and mineralisation is explored using micro-CT and finally biomechanics is evaluated through fracture toughness testing, sideways fall testing and computational modelling. *Chapter 5* is a regional analysis of bone composition and tissue-level mechanics to further inform patterns of bone growth and loss in the ZDF rats. The endocortical and periosteal region of cortical bone from the femora is assessed using polarised Raman spectroscopy to investigate the tissue composition, nanoindentation to measure tissue-level mechanical properties and micropillar compression testing to provide some information on the elastic and plastic deformation behaviour. Finally, *Chapter 6* will discuss the main findings of this thesis and provide future recommendations for the field.

1.6 References

- Bonds, D.E., Larson, J.C., Schwartz, A. V., Strotmeyer, E.S., Robbins, J., Rodriguez, B.L., Johnson, K.C., Margolis, K.L., 2006. Risk of fracture in women with type 2 diabetes: The women's health initiative observational study. *J. Clin. Endocrinol. Metab.* 91, 3404–3410. <https://doi.org/10.1210/jc.2006-0614>
- Britton, M., Vaughan, T., 2023. An experimental investigation on the biomechanics of bone fragility in type-2 diabetes. University of Galway.
- Cassidy, F.C., Shortiss, C., Murphy, C.G., Kearns, S.R., Curtin, W., De Buitléir, C., O'brien, T., Coleman, C.M., 2020. Impact of type 2 diabetes mellitus on human bone marrow stromal cell number and phenotypic characteristics. *Int. J. Mol. Sci.* 21, 1–20. <https://doi.org/10.3390/ijms21072476>
- Catanese, J., Bank, R., TeKoepple, J., Keaveny, T., 1999. Increased cross-linking by non-enzymatic glycation reduces the ductility of bone and bone collagen. *ASME-PUBLICATIONS-BED* 42, 267--268.
- Creecy, A., Uppuganti, S., Merkel, A.R., O'Neal, D., Makowski, A.J., Granke, M., Voziyan, P., Nyman, J.S., 2016. Changes in the Fracture Resistance of Bone with the Progression of Type 2 Diabetes in the ZDSD Rat. *Calcif. Tissue Int.* 99, 289–301. <https://doi.org/10.1007/s00223-016-0149-z>
- Delmas, P.D., Tracy, R.P., Riggs, B.L., Mann, K.G., 1984. Identification of the noncollagenous proteins of bovine bone by two-dimensional gel electrophoresis. *Calcif. Tissue Int.* 36, 308–316. <https://doi.org/10.1007/BF02405335>
- Devlin, Van Vliet, M., Motyl, K., Karim, L., Brooks, D.J., Louis, L., Conlon, C., Rosen, C.J., Bouxsein, M.L., 2014. Early-onset type 2 diabetes impairs skeletal acquisition in the male TALLYHO/JngJ mouse. *Endocrinol. (United States)* 155, 3806–3816. <https://doi.org/10.1210/en.2014-1041>
- Dhaliwal, R., Ewing, S.K., Vashishth, D., Semba, R.D., Schwartz, A. V., 2022. Greater Carboxy-Methyl-Lysine Is Associated With Increased Fracture Risk in Type 2 Diabetes. *J. Bone Miner. Res.* 37, 265–272. <https://doi.org/10.1002/jbmr.4466>
- Diabetes Ireland, 2021. Diabetes Prevalence in Ireland Report. Dublin.
- Duckworth, W.C., 2001. Hyperglycemia and Cardiovascular Disease. *Curr. Atheroscler. Rep.*

3, 383–391.

- Entz, L., Falgayrac, G., Chauveau, C., Pasquier, G., Lucas, S., 2022. The extracellular matrix of human bone marrow adipocytes and glucose concentration differentially alter mineralization quality without impairing osteoblastogenesis. *Bone Reports* 17, 101622. <https://doi.org/10.1016/j.bonr.2022.101622>
- Faselis, C., Katsimardou, A., Imprialos, K., Deligkaris, P., Kallistratos, M., Dimitriadis, K., 2019. Microvascular Complications of Type 2 Diabetes Mellitus. *Curr. Vasc. Pharmacol.* 18, 117–124. <https://doi.org/10.2174/1570161117666190502103733>
- Furst, J.R., Bandeira, L.C., Fan, W., Agarwal, S., Nishiyama, K.K., McMahon, D.J., Dworakowski, E., Jiang, H., Silverberg, S.J., Rubin, M.R., 2016. Advanced Glycation Endproducts and Bone Material Strength in Type 2 Diabetes. *J. Clin. Endocrinol. Metab.* 101, 2502–2510. <https://doi.org/10.1210/jc.2016-1437>
- Goldin, A., Beckman, J.A., Schmidt, A.M., Creager, M.A., 2006. Advanced Glycation End Products. *Circulation* 114, 597–605. <https://doi.org/10.1161/CIRCULATIONAHA.106.621854>
- Hamann, C., Goettsch, C., Mettelsiefen, J., Henkenjohann, V., Rauner, M., Hempel, U., Bernhardt, R., Fratzl-Zelman, N., Roschger, P., Rammelt, S., Günther, K.-P., Hofbauer, L.C., 2011. Delayed bone regeneration and low bone mass in a rat model of insulin-resistant type 2 diabetes mellitus is due to impaired osteoblast function. *Am. J. Physiol. Metab.* 301, 1220–1228. <https://doi.org/10.1152/ajpendo.00378.2011>
- Hunt, H.B., Pearl, J.C., Diaz, D.R., King, K.B., Donnelly, E., 2018. Bone Tissue Collagen Maturity and Mineral Content Increase With Sustained Hyperglycemia in the KK-Ay Murine Model of Type 2 Diabetes. *J. Bone Miner. Res.* 33, 921–929. <https://doi.org/10.1002/jbmr.3365>
- Janghorbani, M., Feskanich, D., Willett, W.C., Hu, F., 2006. Prospective Study of Diabetes and Risk of Hip Fracture. *Diabetes Care* 29, 1573–1578. <https://doi.org/10.2337/dc06-0440>
- Janghorbani, M., Van Dam, R.M., Willett, W.C., Hu, F.B., 2007. Systematic review of type 1 and type 2 diabetes mellitus and risk of fracture. *Am. J. Epidemiol.* 166, 495–505. <https://doi.org/10.1093/aje/kwm106>

- Karim, L., Moulton, J., Van Vliet, M., Velie, K., Robbins, A., Malekipour, F., Abdeen, A., Ayres, D., Bouxsein, M.L., 2018. Bone microarchitecture, biomechanical properties, and advanced glycation end-products in the proximal femur of adults with type 2 diabetes. *Bone* 114, 32–39. <https://doi.org/10.1016/j.bone.2018.05.030>
- Laakso, M., 1999. Hyperglycemia and cardiovascular disease in type 2 diabetes. *Diabetes* 48, 937–942. <https://doi.org/10.2337/diabetes.48.5.937>
- Lekkala, S., Sacher, S.E., Taylor, E.A., Williams, R.M., Moseley, K.F., Donnelly, E., 2023. Increased Advanced Glycation Endproducts, Stiffness, and Hardness in Iliac Crest Bone From Postmenopausal Women With Type 2 Diabetes Mellitus on Insulin. *J. Bone Miner. Res.* 38, 261–277. <https://doi.org/10.1002/jbmr.4757>
- Marin, C., Luyten, F.P., Van der Schueren, B., Kerckhofs, G., Vandamme, K., 2018. The Impact of Type 2 Diabetes on Bone Fracture Healing. *Front. Endocrinol. (Lausanne)*. 9, 1–15. <https://doi.org/10.3389/fendo.2018.00006>
- McCarthy, Etcheverry, S.B., Bruzzone, L., Lettieri, G., Barrio, D.A., Cortizo, A.M., 2001. Non-enzymatic glycosylation of a type 1 collagen matrix: Effects on osteoblastic development and oxidative stress. *BMC Cell Biol.* 2. <https://doi.org/10.1186/1471-2121-2-16>
- Mehta, D., Sihota, P., Tikoo, K., Kumar, S., Kumar, N., 2023. Type 2 diabetes alters the viscoelastic behavior and macromolecular composition of vertebra. *Bone Reports* 18, 101680. <https://doi.org/10.1016/j.bonr.2023.101680>
- Micheletti, C., Jolic, M., Grandfield, K., Shah, F.A., Palmquist, A., 2023. Bone structure and composition in a hyperglycemic, obese, and leptin receptor-deficient rat: Microscale characterization of femur and calvarium. *Bone* 172, 116747. <https://doi.org/10.1016/j.bone.2023.116747>
- Murray, Coleman, 2019. Impact of Diabetes Mellitus on Bone Health. *Int. J. Mol. Sci.* 20, 4873. <https://doi.org/10.3390/ijms20194873>
- Nagai, R., Shirakawa, J., Fujiwara, Y., Ohno, R., Moroishi, N., Sakata, N., 2014. Detection of AGEs as markers for carbohydrate metabolism and protein denaturation 55, 1–6. <https://doi.org/10.3164/jcbn.13>
- Napoli, N., Chandran, M., Pierroz, D.D., Abrahamsen, B., Schwartz, A. V, Ferrari, S.L., 2017.

- Mechanisms of diabetes mellitus-induced bone fragility. *Nat. Rev. Endocrinol.* 13, 208–219. <https://doi.org/10.1038/nrendo.2016.153>
- Parle, E., Tio, S., Behre, A., Carey, J.J., Murphy, C.G., O'Brien, T.F., Curtin, W.A., Kearns, S.R., McCabe, J.P., Coleman, C.M., Vaughan, T.J., McNamara, L.M., 2020. Bone Mineral Is More Heterogeneously Distributed in the Femoral Heads of Osteoporotic and Diabetic Patients: A Pilot Study. *JBMR Plus* 4, 1–10. <https://doi.org/10.1002/jbm4.10253>
- Piccoli, A., Cannata, F., Strollo, R., Pedone, C., Leanza, G., Russo, F., Greto, V., Isgrò, C., Quattrocchi, C.C., Massaroni, C., Silvestri, S., Vadalà, G., Bisogno, T., Denaro, V., Pozzilli, P., Tang, S.Y., Silva, M.J., Conte, C., Papalia, R., Maccarrone, M., Napoli, N., 2020. Sclerostin Regulation, Microarchitecture, and Advanced Glycation End-Products in the Bone of Elderly Women With Type 2 Diabetes. *J. Bone Miner. Res.* 35, 2415–2422. <https://doi.org/10.1002/jbmr.4153>
- Picke, A., Campbell, G., Napoli, N., Hofbauer, L.C., Rauner, M., 2019. Update on the impact of type 2 diabetes mellitus on bone metabolism and material properties. *Endocr. Connect.* 8, R55–R70. <https://doi.org/10.1530/EC-18-0456>
- Poundarik, A.A., Wu, P.-C., Evis, Z., Sroga, G.E., Ural, A., Rubin, M., Vashishth, D., 2015. A direct role of collagen glycation in bone fracture. *J. Mech. Behav. Biomed. Mater.* 52, 120–130. <https://doi.org/10.1016/j.jmbbm.2015.08.012>
- Prisby, R.D., Swift, J.M., Bloomfield, S.A., Hogan, H.A., Delp, M.D., 2008. Altered bone mass, geometry and mechanical properties during the development and progression of type 2 diabetes in the Zucker diabetic fatty rat. *J. Endocrinol.* 199, 379–388. <https://doi.org/10.1677/JOE-08-0046>
- Robertson, R.P., 2023. Type 2 diabetes mellitus: Prevalence and risk factors [WWW Document]. UpToDate.
- Roschger, P., Paschalis, E.P., Fratzl, P., Klaushofer, K., 2008. Bone mineralization density distribution in health and disease 42, 456–466. <https://doi.org/10.1016/j.bone.2007.10.021>
- Saeedi, P., Petersohn, I., Salpea, P., Malanda, B., Karuranga, S., Unwin, N., Colagiuri, S., Guariguata, L., Motala, A.A., Ogurtsova, K., Shaw, J.E., Bright, D., Williams, R., 2019. Global and regional diabetes prevalence estimates for 2019 and projections for 2030 and

- 2045: Results from the International Diabetes Federation Diabetes Atlas, 9th edition. *Diabetes Res. Clin. Pract.* 157, 107843. <https://doi.org/10.1016/j.diabres.2019.107843>
- Schwartz, A. V, Garnero, P., Hillier, T.A., Sellmeyer, D.E., Strotmeyer, E.S., Feingold, K.R., Resnick, H.E., Tylavsky, F.A., Black, D.M., Cummings, S.R., Harris, T.B., Bauer, D.C., 2009. Pentosidine and Increased Fracture Risk in Older Adults with Type 2 Diabetes 94, 2380–2386. <https://doi.org/10.1210/jc.2008-2498>
- Strotmeyer, E.S., Cauley, J.A., Schwartz, A. V., Nevitt, M.C., Resnick, H.E., Bauer, D.C., Tylavsky, F.A., De Rekeneire, N., Harris, T.B., Newman, A.B., 2005. Nontraumatic fracture risk with diabetes mellitus and impaired fasting glucose in older white and black adults: The health, aging, and body composition study. *Arch. Intern. Med.* 165, 1612–1617. <https://doi.org/10.1001/archinte.165.14.1612>
- Sun, H., Saeedi, P., Karuranga, S., Pinkepank, M., Ogurtsova, K., Duncan, B.B., Stein, C., Basit, A., Chan, J.C.N., Mbanya, J.C., Pavkov, M.E., Ramachandaran, A., Wild, S.H., James, S., Herman, W.H., Zhang, P., Bommer, C., Kuo, S., Boyko, E.J., Magliano, D.J., 2022. IDF Diabetes Atlas: Global, regional and country-level diabetes prevalence estimates for 2021 and projections for 2045. *Diabetes Res. Clin. Pract.* 183, 109119. <https://doi.org/10.1016/j.diabres.2021.109119>
- Thorpe, S.R., Baynes, J.W., 2003. Maillard reaction products in tissue proteins : New products and new perspectives Review Article 275–281. <https://doi.org/10.1007/s00726-003-0017-9>
- Valderrábano, R.J., Linares, M.I., 2018. Diabetes mellitus and bone health: epidemiology, etiology and implications for fracture risk stratification. *Clin. Diabetes Endocrinol.* 4, 9. <https://doi.org/10.1186/s40842-018-0060-9>
- Vandenput, L., Johansson, H., McCloskey, E. V., Liu, E., Åkesson, K.E., Anderson, F.A., Azagra, R., Bager, C.L., Beudart, C., Bischoff-Ferrari, H.A., Biver, E., Bruyère, O., Cauley, J.A., Center, J.R., Chapurlat, R., Christiansen, C., Cooper, C., Crandall, C.J., Cummings, S.R., da Silva, J.A.P., Dawson-Hughes, B., Diez-Perez, A., Dufour, A.B., Eisman, J.A., Elders, P.J.M., Ferrari, S., Fujita, Y., Fujiwara, S., Glüer, C.C., Goldshtein, I., Goltzman, D., Gudnason, V., Hall, J., Hans, D., Hoff, M., Hollick, R.J., Huisman, M., Iki, M., Ish-Shalom, S., Jones, G., Karlsson, M.K., Khosla, S., Kiel, D.P., Koh, W.P., Koromani, F., Kotowicz, M.A., Kröger, H., Kwok, T., Lamy, O., Langhammer, A.,

- Larijani, B., Lippuner, K., Mellström, D., Merlijn, T., Nordström, A., Nordström, P., O'Neill, T.W., Obermayer-Pietsch, B., Ohlsson, C., Orwoll, E.S., Pasco, J.A., Rivadeneira, F., Schei, B., Schott, A.M., Shiroma, E.J., Siggeirsdottir, K., Simonsick, E.M., Sornay-Rendu, E., Sund, R., Swart, K.M.A., Szulc, P., Tamaki, J., Torgerson, D.J., van Schoor, N.M., van Staa, T.P., Vila, J., Wareham, N.J., Wright, N.C., Yoshimura, N., Zillikens, M.C., Zwart, M., Harvey, N.C., Lorentzon, M., Leslie, W.D., Kanis, J.A., 2022. Update of the fracture risk prediction tool FRAX: a systematic review of potential cohorts and analysis plan, *Osteoporosis International*. Springer London. <https://doi.org/10.1007/s00198-022-06435-6>
- Vashishth, D., 2007. The Role of the Collagen Matrix in Skeletal Fragility. *Curr. Osteoporos. Rep.* 5, 62–66.
- Vashishth, D., Gibson, G., Khoury, J., Schaffler, M., Kimura, J., Fyhrie, D., 2001. Influence of nonenzymatic glycation on biomechanical properties of cortical bone. *Bone* 28, 195–201. [https://doi.org/10.1016/S8756-3282\(00\)00434-8](https://doi.org/10.1016/S8756-3282(00)00434-8)
- Vestergaard, P., 2007. Discrepancies in bone mineral density and fracture risk in patients with type 1 and type 2 diabetes—a meta-analysis. *Osteoporos. Int.* 18, 427–444. <https://doi.org/10.1007/s00198-006-0253-4>
- Viguet-Carrin, S., Farlay, D., Bala, Y., Munoz, F., Bouxsein, M.L., Delmas, P.D., 2008. An in vitro model to test the contribution of advanced glycation end products to bone biomechanical properties. *Bone* 42, 139–149. <https://doi.org/10.1016/j.bone.2007.08.046>
- Willett, T.L., Voziyan, P., Nyman, J.S., 2022. Causative or associative: A critical review of the role of advanced glycation end-products in bone fragility. *Bone* 163, 116485. <https://doi.org/10.1016/j.bone.2022.116485>
- Wittig, N.K., Birkedal, H., 2022. Bone hierarchical structure: spatial variation across length scales. *Acta Crystallogr. Sect. B Struct. Sci. Cryst. Eng. Mater.* 78, 305–311. <https://doi.org/10.1107/S2052520622001524>
- Wölfel, E.M., Fiedler, I.A.K., Dragoun Kolibova, S., Krug, J., Lin, M.-C., Yazigi, B., Siebels, A.K., Mushumba, H., Wulff, B., Ondruschka, B., Püschel, K., Glüer, C.C., Jähn-Rickert, K., Busse, B., 2022a. Human tibial cortical bone with high porosity in type 2 diabetes mellitus is accompanied by distinctive bone material properties. *Bone* 165, 116546. <https://doi.org/10.1016/j.bone.2022.116546>

- Wölfel, E.M., Jähn-Rickert, K., Schmidt, F.N., Wulff, B., Mushumba, H., Sroga, G.E., Püschel, K., Milovanovic, P., Amling, M., Campbell, G.M., Vashishth, D., Busse, B., 2020. Individuals with type 2 diabetes mellitus show dimorphic and heterogeneous patterns of loss in femoral bone quality. *Bone* 140, 115556. <https://doi.org/10.1016/j.bone.2020.115556>
- Wölfel, E.M., Schmidt, F.N., vom Scheidt, A., Siebels, A.K., Wulff, B., Mushumba, H., Ondruschka, B., Püschel, K., Scheijen, J., Schalkwijk, C.G., Vettorazzi, E., Jähn-Rickert, K., Gludovatz, B., Schaible, E., Amling, M., Rauner, M., Hofbauer, L.C., Zimmermann, E.A., Busse, B., 2022b. Dimorphic Mechanisms of Fragility in Diabetes Mellitus: the Role of Reduced Collagen Fibril Deformation. *J. Bone Miner. Res.* 37, 2259–2276. <https://doi.org/10.1002/jbmr.4706>
- Woolley, W., Obata, Y., Martin, K., Acevedo, C., 2023. Whole-Bone Toughness Is Linked to Canal and Osteocyte Lacunae Deficits in the ZDSD Type 2 Diabetic Rat Model. *Jom* 20–24. <https://doi.org/10.1007/s11837-023-05882-8>
- Zeitoun, D., Caliaperoumal, G., Bensidhoum, M., Constans, J.M., Anagnostou, F., Bousson, V., 2019. Microcomputed tomography of the femur of diabetic rats: alterations of trabecular and cortical bone microarchitecture and vasculature—a feasibility study. *Eur. Radiol. Exp.* 3, 17. <https://doi.org/10.1186/s41747-019-0094-5>
- Zimmermann, E.A., Busse, B., Ritchie, R.O., 2015. The fracture mechanics of human bone: influence of disease and treatment. *Bonekey Rep.* 4, 1–13. <https://doi.org/10.1038/bonekey.2015.112>
- Zimmermann, E.A., Schaible, E., Bale, H., Barth, H.D., Tang, S.Y., Reichert, P., Busse, B., Alliston, T., Ager III, J.W., Ritchie, R.O., 2011. Age-related changes in the plasticity and toughness of human cortical bone at multiple length scales. *Proc Natl Acad Sci* 35, 14416–14421. <https://doi.org/10.1073/pnas.1107966108>

CHAPTER 2

Literature Review

This Chapter provides an overview of the literature relevant to the technical Chapters of this thesis. Section 2.1 outlines the structure and function of bone and its matrix, while Section 2.2 includes an overview of the bone cells and their role in bone turnover as well as providing details on some relevant markers of bone and general health. Bone quality and biomechanics are detailed in Section 2.3 and 2.4, respectively. Rodent bone growth, structure and function is outlined in Section 2.5, where various rodent models of T2D are also discussed. Finally, Section 2.6 reviews various human and animal studies of type-2 diabetes and the factors that may impair mechanical integrity of bone in these subjects.

2.1 Bone Structure, Function and Matrix

Bone is a living, anisotropic, dynamic tissue that is constantly renewing and repairing itself throughout its lifespan. Its primary function within the skeleton is to provide support and protection for internal organs, while enabling movement and locomotion. Whole bones can withstand substantial loads in a variety of deformation modes including compression, tension, bending and torsion loading with the response to these loads being dependent of the bone type and structure (Currey, 2012).

Bone has a complex assembly and is often described by the various hierarchical levels of organisation (Rho et al., 1998). This hierarchical organisation provides a highly optimised structure that exhibits high stiffness and strength and excellent resistance to fracture (Weiner and Wagner, 1998). While the primary role of bone is often considered to be a mechanical one, it also performs several other critical functions, with many bones acting as major reservoirs of calcium and phosphate that are responsible for a wide variety of metabolic functions throughout the body (Boskey, 2006). Bone also provides a structure for the niche of hematopoietic stem

cells, which are the progenitors of all blood cells and mesenchymal stem cells that are the precursors of bone cells. However, with aging and the onset of metabolic diseases such as type-2 diabetes (T2D), the dynamic capability of bone can become altered (Briot et al., 2017; Schultz, 2001; Unnanuntana et al., 2011; Zimmermann et al., 2015).

2.1.1 The Hierarchical Structure of Bone

Bone is intricately comprised of an organic protein matrix that is combined with a stiff mineral phase to form a hierarchical composite structure, which is assembled using a universal basic building block – the mineralised collagen fibril (Ascenzi and Bonucci, 1976; Currey, 1984; Hofmann et al., 2006). Bone has multiple structural length scales (Rho et al., 1998), ranging from the microstructural organ level (> 1 mm) down to the nano- and even sub-nanoscale (< 100 nm) as seen in Figure 2.1.

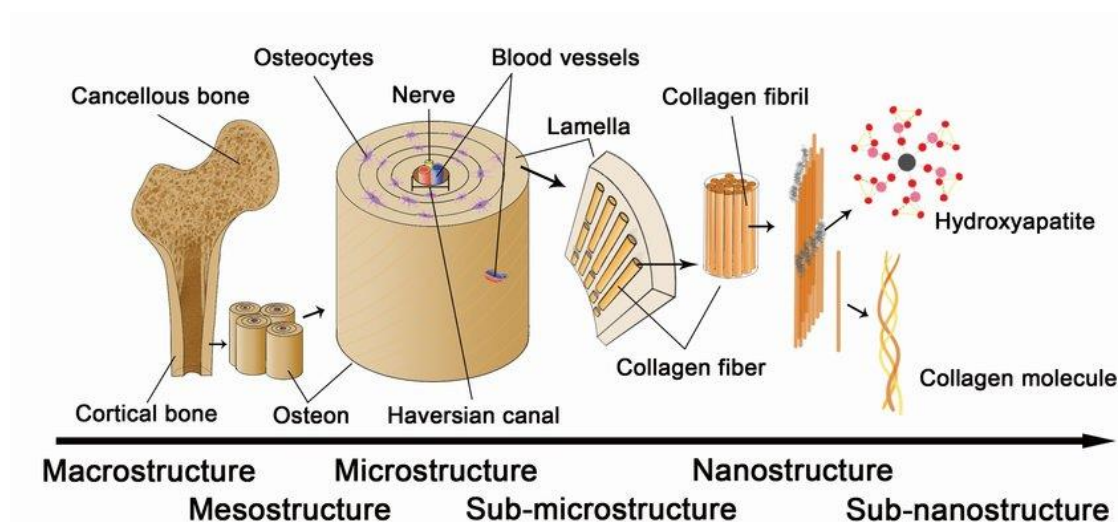


Figure 2.2: The hierarchical structure of bone. At the macrolevel, bone consists of cortical and trabecular tissue, which is then reduced to a single osteon at the microlevel and further reduced to a mineralised collagen fibril consisting of a collagen molecule and hydroxyapatite mineral crystals at the nano- and sub-nano level, respectively (J. Fan et al., 2022).

At the macroscale (> 1 mm), there are two types of bone, cortical (compact) and trabecular (cancellous). All bones have an outer shell of dense cortical tissue; with a thickness that can vary from bone to bone. Trabecular bone may be present in the whole inner region of bones, such as in the vertebrae, ribs and calvaria bones, or may only be partially present in long bones at specific regions, such as the epiphyses and metaphysis (Reznikov et al., 2014a). The outer surface of bone is covered in a sheet of fibrous connective tissue known as the periosteum, from which bone can form and grow (Cowin, 2001). The marrow cavity is lined with the endosteum, which is a thin cellular membrane of bone surface cells such as osteoclasts,

osteoblasts and bone lining cells (Cowin, 2001). The porosity of cortical bone varies from 5% to 30% with an apparent density of about 1.8 g cm^{-3} , while the porosity of trabecular bone varies from 30% to $> 90\%$ with an apparent density of $0.1 - 0.9 \text{ g cm}^{-3}$ (Bonucci, 1999). Although it is more widely accepted that cortical and trabecular bone are comprised of similar constituents, there are distinct structural and biological differences between these tissue types, with trabecular bone being more metabolically active than cortical bone on average, exhibiting a 26% yearly turnover rate in comparison to cortical bones with 3% per year (Jee, 1983; Oftadeh et al., 2015; Rho et al., 1998).

During development, the formation of cortical and trabecular bone begins as “woven” tissue, which is formed by endochondral and intramembranous ossification. Woven bone is made up of randomly distributed osteocytes and disorganised mineralised collagen fibres. Over time, the woven bone is replaced by lamellar tissue, which is comprised of a series of lamellae that are oriented in bundles of unidirectional and fanning arrays of mineralised collagen fibrils (Reznikov et al., 2014a). At the microscale, adult cortical tissue in long bones is found in three different patterns: (1) the circumferential lamellae, which are layers of lamellae found all along the circumference of the bone, often found in the outer layer (Cowin, 2001); (2) concentric rings of lamellae, known as osteons, that surround vascular channels, nerves, cells and Volkmann’s canals, which are canals connecting to other osteons (Lacroix, 2019); and (3) interstitial lamellae, which is lamellar tissue that fills the gaps between osteons and angular fragments of what was previously concentric or circumferential lamellae (Cowin, 2001). Trabecular bone consists of a network of interconnected struts of trabeculae that can be plate- or rod-like in structure (Currey, 2012). These are usually $100\text{-}200 \mu\text{m}$ thick in human or large animal bone and $20\text{-}60 \mu\text{m}$ thick in small mouse or rat bone (Bouxsein et al., 2010), which the trabecular direction typically oriented according to the external principal loading direction as proposed by Wolff’s law (Frost, 1994; Wolff, 1986). The human trabecular microstructure differs to cortical bone, where trabeculae are mainly composed of lamellar and woven tissue. Osteons are absent from trabecular bone, which means that the mineralised tissue itself is not vascularised and the surrounding bone marrow must provide the trabecular tissue with nutrients and oxygen via fluid exchange (Cowin, 2001; Oftadeh et al., 2015).

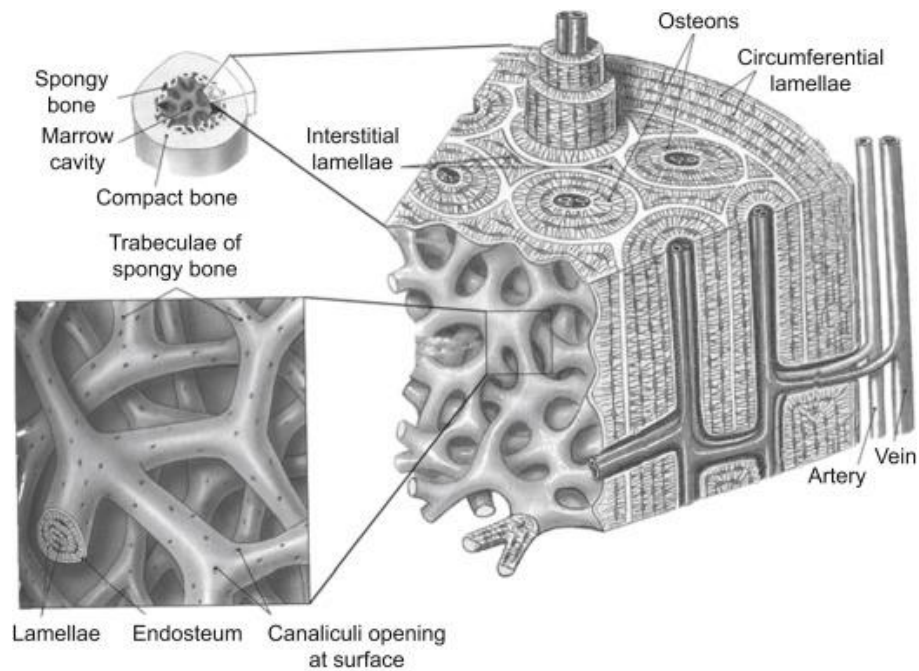


Figure 2.3: A detailed schematic of the structure of osseous tissue (Lacroix, 2019).

2.1.2 Bone Matrix Composition

Bone is a heterogeneous composite material and makes up the largest portion of the body's connective tissue mass. It comprises of a mineral phase, hydroxyapatite ($\text{Ca}_{10}(\text{PO}_4)_6(\text{OH})_2$), an organic phase (~90% type-I collagen, ~5% non-collagenous glycoproteins and ~2% lipids by water) and water (Boskey, 2013). However, the composition and local structural arrangements of these constituents can vary greatly. Despite being assembled from the relatively limited number of building blocks, the range of mechanical properties that bone can exhibit is remarkable, which a set of highly optimised properties being achieved through intricate organisation of the organic and inorganic components.

Mineral

The mineral phase, also known as the inorganic phase of bone, is mainly made up of hydroxyapatite crystals. In human adult bone, there are different stages of the bone forming processes, (1) primary bone formation or “modelling”, which is a rapid process of forming new “osteoid” bone in an area where no bone was present prior to the formation, (2) secondary mineralisation, which follows the primary mineralisation phase and is a slow process where mineral content is gradually deposited and increases over a time frame of many years and (3) replacement bone formation or “remodelling”, where old lamellar or mature bone is removed by osteoclasts and replaced with new bone (Roschger et al., 2008). During primary mineralisation, the main function is to ensure osteoblast cells deposit the hydroxyapatite

microcrystals between the collagen fibrils in the organic matrix (Reznikov et al., 2014b) in a process that is known as mineral nucleation (Gorski, 2011). The first step in mineralisation is the nucleation of mineral to form crystals ~15-20 nm in c-axis length. Then, during secondary mineralisation, the number of mineral crystals are increased and become more mature. Over time, the crystals grow and interlock with the collagen fibres of the organic matrix to create a composite structure that provides bone with its stiffness and resistance to fracture (Blair et al., 2017; Gorski, 2011; Vallet-Regi; and Navarrete, 2015). Specific proteins in the organic matrix, known as non-collagenous proteins, help to regulate the nucleation and growth of hydroxyapatite crystals. As the matrix begins to mature, the hydroxyapatite crystals become highly organised and aligned within the collagen layers along the long axis of the fibril (Blair et al., 2017) as seen in Figure 2.3. This is known as intrafibrillar mineralisation, which generally occurs during the secondary bone formation phase (Olszta et al., 2007). Hydroxyapatite crystals are small in size (~20-50 nm long, 15 nm wide and 2-5 nm thick) and have a unique lattice structure (Morgan and Gerstenfeld, 2020). However, the mineral phase of bone is not purely made up of hydroxyapatite, with bone mineral also consisting of anionic and cationic impurities such as carbonate (CO_3^{2-}), monohydrogen-phosphate (HPO_4^{2-}), sodium (Na^+) and magnesium (Mg^{2+}) ions, along with ion vacancies within the lattice structure (Morgan and Gerstenfeld, 2020; Von Euw et al., 2019). These impurities can freely move in and out of the crystal lattice. For example, CO_3^{2-} ions can easily substitute into phosphate (PO_4^{3-}) (known as a type-B substitution) within the lattice structure, and in some cases can make up to ~5-9% of the weight proportion of bone mineral (Morgan and Gerstenfeld, 2020; Von Euw et al., 2019). The substitution of impurities of different shapes and sizes can reduce apatite crystallinity and distort the lattice structure. This solubility of the apatite may become impaired, in turn negatively impacting mineral homeostasis (McConnell, 1962; Ou-Yang et al., 2001). Previous research has found that disruptions to the normal lattice structure can lead to reduced mechanical integrity. For example, one study compared the composition of bones with and without fragility fractures using Fourier transform infrared microspectroscopy and found that increased fracture risk was positively correlated with cancellous mineral crystallinity and a negative correlation between carbonate: phosphate ratio (or type-B substitution) and fracture risk (Gourion-Arsiquaud et al., 2009). Another study found decreased carbonate: phosphate ratio in both cancellous and cortical bone to be an explanatory variable for fracture risk (Boskey et al., 2016). Other studies have found bone diseases to affect crystal size and crystallinity, with crystal size being decreased in Paget's disease (Whyte, 2006) and diabetes (Boskey and Marks, 1985) but increased in patients with osteopetrosis (Einhorn et al., 1988).

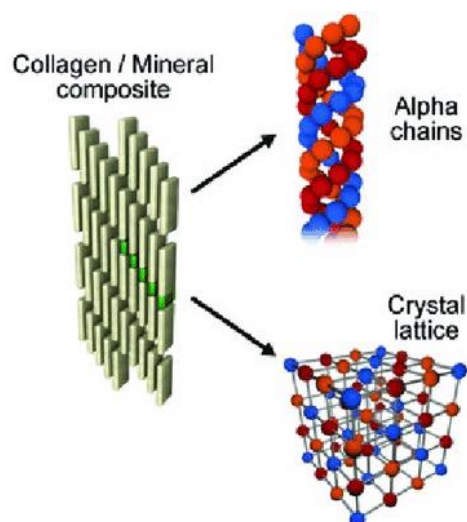


Figure 2.4: A schematic of the collagen-mineral composite at the nano- and ultrastructural level of bone, where mineral is deposited along and between collagen fibres. At the molecular level this structure consists of a triple helix of alpha chains and a mineral crystal lattice (Gasser and Kneissel, 2017).

Collagen

The organic phase of bone is primarily composed of type-I collagen (~90%), forming the main basis of the extracellular matrix (Cowin, 2001; Rosa et al., 2022). The collagenous matrix plays an important role in preserving the bone structure and shape, providing the tissue with high tensile strength, ductility and toughness (Currey, 2003; Olszta et al., 2007; Tzaphlidou, 2005). Collagen has a unique and complex structure known as tropocollagen that is formed by a polypeptide chain of repetitive amino acid sequences known as glycine-X-Y, where X and Y are usually proline and hydroxyproline residues, respectively. This configuration leads to the triple helical structure, where three-polypeptide strands are right-hand twisted and tightly stabilised by interchain hydrogen bonds (Figure 2.4) (Olszta et al., 2007; Rosa et al., 2022). Dense bundles of tropocollagen form collagen fibrils, and mineral crystals are embedded within the spaces between the collagen fibrils, resulting in the formation of a rigid and durable structure known as the mineralised collagen fibril. Multiple collagen fibrils are stabilised by the formation of covalent cross-links that join non-helical and helical regions of proximate collagen molecules together to form a collagen fibre (Saito and Marumo, 2010). Collagen fibres are aligned parallel to one-another to form what are termed lamellae and this composite structure gives bone its elasticity, durability and provides bone with an excellent tensile strength (Viguet-Carrin et al., 2006).

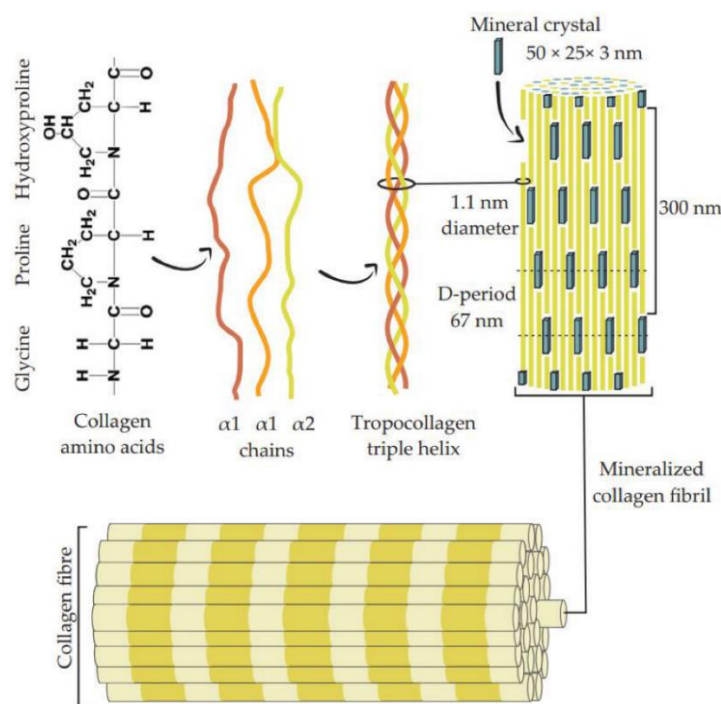


Figure 2.5: At the smallest level collagen amino acids, glycine, proline and hydroxyproline make-up the alpha chains, which is woven to form the triple-helix tropocollagen structure. Mineral crystals embed within and between the tropocollagen structure to form the mineralised collagen fibril. Multiple fibrils bundle together to form collagen fibres (Rosa et al., 2022).

Enzymatic and Non-Enzymatic Crosslinks

There are two types of collagen cross-links: (1) enzymatic, where the formation is regulated by lysine hydroxylase and lysyl oxidase and (2) non-enzymatic crosslinks, formed by the exposure of glycation, oxidation or glycooxidation between lysine or hydroxylysine residues and sugar (Saito and Marumo, 2010). Initially, during enzymatic cross-link formation, immature and unstable divalent crosslinks such as dehydro-dihydroxylysinonorleucine (deH-DHLNL), dehydro-hydroxylysinonorleucine (deH-HLNL) and deH-lysinonorleucine (deH-LNL) are formed due to a post-translational modification (Saito et al., 2014, 1997; Saito and Marumo, 2010) and eventually undergo Amadori rearrangement to form pyridinium (the family to which pyridinoline (PYD) and deoxypyridinoline (DPD) belong) and pyrrole (the family to which pyrrolodine (PYL) and deoxy-pyrrolodine (DPL) belong) which are mature, trivalent cross-links (Saito et al., 2014) (Figure 2.5). Immature cross-links are the most abundant form of cross-link in bone, since the transformation of immature cross-links to mature cross-links in bone is quite a slow process (Eyre et al., 1988; Saito et al., 2014). It is thought that enzymatic cross-links may have a positive role to play in bone strength (Vashishth, 2007; Viguet-Carrin et al., 2006). There is evidence to suggest that enzymatic crosslinks may

be a determinant of bone strength (Saito et al., 2006). Bones toughness is greatly dependant on the collagen matrix, which is stabilised (providing the tissue with elasticity and tensile strength) by enzymatic cross-links during the early stages of collagen fibril formation and mineralisation (Yamauchi et al., 1988). Previous studies have used Fourier transform infrared spectroscopy (FTIR) to quantify collagen cross-links (Farlay et al., 2011; Garcia et al., 2016; Hunt et al., 2018; Paschalis et al., 2001). However, there is still ambiguity as to whether this is a measurement of collagen maturity, or the modification of enzymatic cross-links and further research is needed to allow for correct interpretation.

Conversely, non-enzymatic cross-links, known as Advanced Glycation End-products (AGEs) are thought to negatively impact bone. There are a wide variety of AGEs that fall under two main categories, determined by whether they form as (i) cross-links or (ii) non-cross-linking adducts (Saito and Marumo, 2010; Willett et al., 2022) (Figure 2.5). AGEs are created via multiple pathways with various intermediates, but in general terms, AGEs form due to a reaction between the amino component of protein or lipids and either (1) glucose and/ or (2) products that remain after glucose degradation and metabolism (Thorpe and Baynes, 2003; Willett et al., 2022). When proteins and lipids bind to one-another, this forms cross-links, which have been hypothesised to stiffen the collagen network, leading to a more brittle tissue behaviour, reducing the tissue toughness (Vashishth, 2007; Viguet-Carrin et al., 2006). Adducts are formed when the protein structure itself is altered, which can ultimately impair protein function (Nagai et al., 2014). Similar to the post-translational modifications of enzymatic cross-links that enhance the protein stability, non-enzymatic cross-links also undergo post-translational modifications that are often influenced by factors including pH, oxidative stress and glucose levels (Willett et al., 2022). There are a wide range of non-enzymatic cross-links and adducts caused by various post-translational modifications, with the most common and widely studied of these being pentosidine (cross-linking) and carboxymethyl-lysine (adduct). Intrinsic toughening (or plasticity) is what provides a material with the ability to resist fracture (Ritchie, 2011) via a fibrillar sliding mechanism, where mineralised collagen fibrils slide past one another to allow bone to deform and absorb energy without fracturing through sacrificial bonds, which break and reform as they slide (see *Non-Collagenous Proteins*). However, fibrillar sliding is dependent on the alignment and orientation of the collagen fibres (Kamml et al., 2023; Ritchie, 2011; Zimmermann and Ritchie, 2015). With aging and certain diseases, this toughening mechanism can be affected by an increase in AGE cross-linking that is thought to over-stabilize the collagen structure leading to reduced

fibrillar sliding and a more brittle tissue behaviour (Saito et al., 1997; Tang et al., 2007; Wang et al., 2002; Zimmermann et al., 2011).

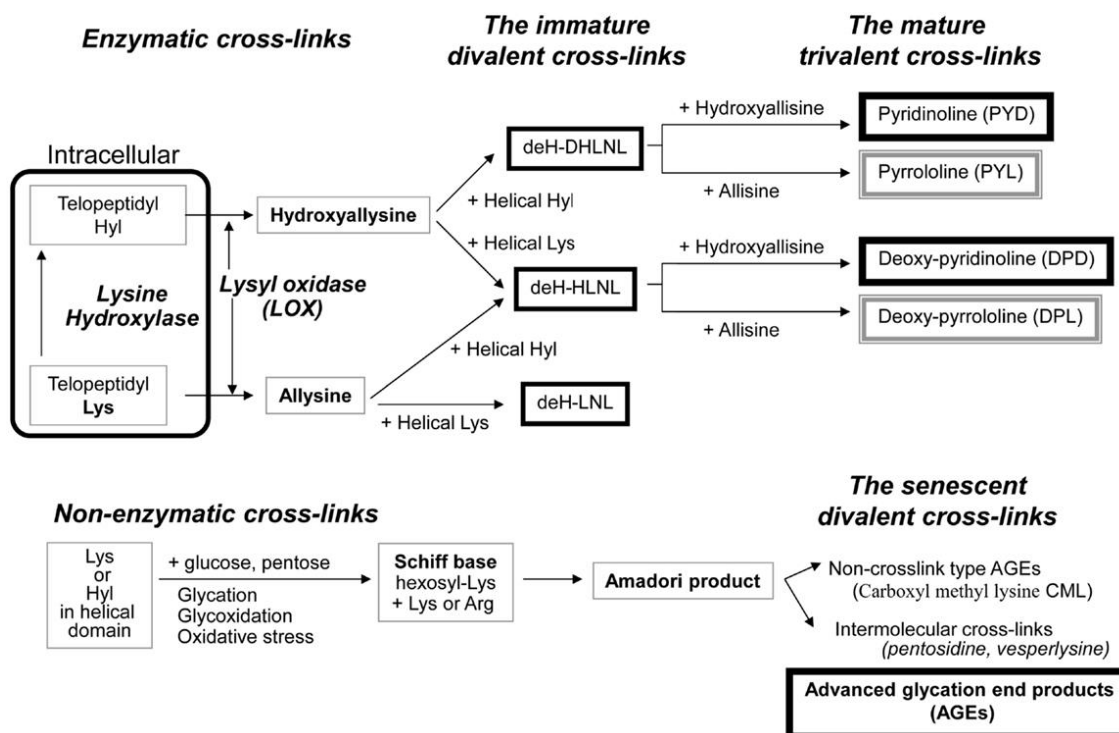


Figure 2.6: The formation pathway of enzymatic and non-enzymatic crosslinks and adducts in bone collagen, where the first step of enzymatic formation require Lysine hydroxylase and Lysyl oxide, whereas the first step of non-enzymatic formation requires glycation, glycooxidation or oxidative stress (Saito and Marumo, 2013).

Non-collagenous proteins

Non-collagenous proteins (NCPs) make up approximately 10% of the organic matrix of bone. While over 200 different NCPs have been reported, the most commonly known are osteocalcin, osteonectin and osteopontin (Delmas et al., 1984). It is understood that NCPs play a critical role in bone mineralisation and may act as nucleators, aiding the growth of the mineral crystals within the collagen fibrils (Glimcher, 1989; Gorski, 2011; Roach, 1994). NCPs have also described as a protein-based “glue” that fuses mineralised collagen fibrils to one another, reducing separation and influencing bones’ ability to resist fracture due to what are termed sacrificial bonds and hidden lengths (Fantner et al., 2005) (see Figure 2.6). Although data is limited, NCPs are thought to influence bone quality, particularly in patients with bone disease such as osteoporosis, where studies have found disruptions in the organisation and a reduced amount of NCPs present in osteoporotic patients when compared to healthy controls, consequentially, impairing fracture resistance (Ferris et al., 1987; Grynepas et al., 1994; Morgan

et al., 2015). Extracellular NCPs have a wider role outside of the initial understanding of their part to play in calcium binding and cell adhesion and it is possible that a better understanding of the effect NCPs have on bone quality could allow for a more accurate estimation of fracture risk.

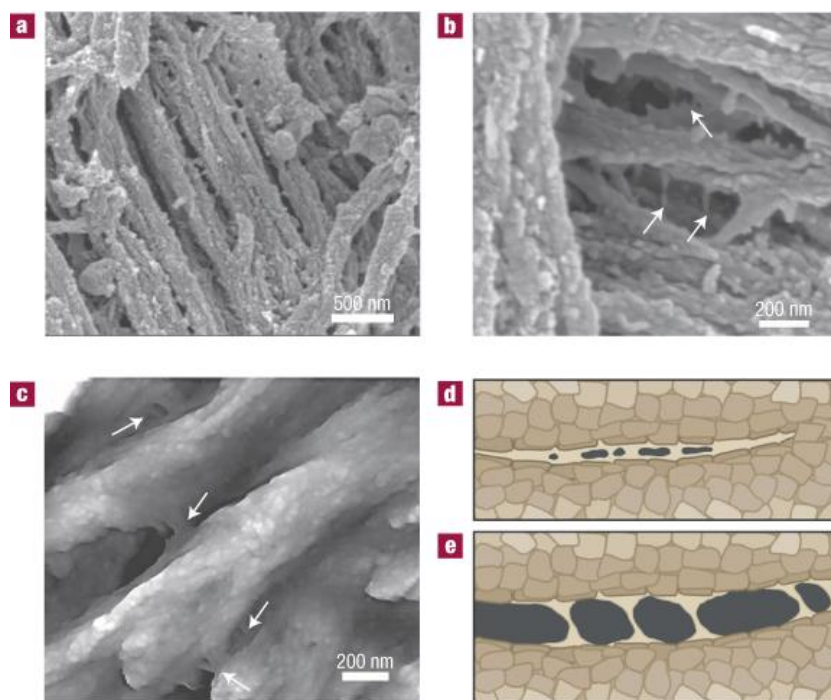


Figure 2.7: Mineralised collagen fibrils are interconnected glue-like non-collagenous proteins, where (a) shows mineralised collagen fibrils on a fractured human bone surface, (b) Scanning Electron Micrographs show fibrils are held together by a glue-like substance known as, non-collagenous proteins, (c) Atomic Force Microscope image of a fractured bone surface also showing connected fibrils and (d & e) shows a schematic depicting how the non-collagenous proteins help to resist separation of fibrils (Fantner et al., 2005).

2.2 Bone Biology and Turnover

Bone cells play a vital role in creating bone tissue and maintaining bone function and strength. There are four main types of bone cells: osteoblasts, osteocytes, osteoclasts and bone lining cells. Bone has a unique mineralised matrix that is continuously renewing throughout life by a process called ‘bone turnover’. In healthy individuals, this process removes old or damaged tissue, replaces it with new tissue and ensures that the individual constituents of the bone matrix (e.g., hydroxyapatite mineral crystals and collagen proteins) are optimally arranged to maximise the load-bearing capacity of the structure.

2.2.1 Bone Cells

Osteoblasts derived from mesenchymal stem cells (MSCs). MSCs are found in bone marrow, muscle and fat tissue and are known as multipotent cells, meaning they have the potential to differentiate into various types of tissue such as bone, cartilage, muscle and fat. Osteoblasts make up ~ 4 – 6% of bone cells in the adult skeleton and are essential for formation of new tissue during bone turnover as they synthesize collagen and mineralise the organic matrix – including many proteoglycans, non-collagenous proteins, cell attachment proteins and type-I collagen, which makes up 90% of the organic matrix (Mohamed, 2008). During initial stages of bone formation, new osteoid (which is the unmineralised organic tissue) is deposited to replenish and maintain the bone matrix volume (Trammell and Kroman, 2012). After the bone formation phase, osteoblasts have multiple possible fates, whereby they can (1) become embedded in the matrix and differentiate into an osteocyte, (2) become an inactive flattened and elongated osteoblast called, bone lining cells or (3) undergo apoptosis (Einhorn, 1998; Franz-Odenaal et al., 2006). There are various markers that are secreted from osteoblasts into the blood that can be used to give an indication of bone formation including: alkaline phosphatase (ALP), type I collagen, type I amino-terminal propeptide (P1NP), osteopontin (OPN), osteocalcin (OCN) and bone-specific alkaline phosphatase (BAP) (Bilezikian et al., 2018; Hygum et al., 2017). Particularly, serum P1NP is regarded as a reliable marker to monitor bone formation in humans and rats (Hale et al., 2007). The type-I collagen triple helix are bordered by various components including P1NP, which then spontaneously develop into collagen fibrils, where in bone mineralisation can occur and circulating P1NP has been shown to be linearly proportional to newly mineralised tissue (Hale et al., 2007). Bone is unique, in the fact that a network of mechanosensing cells known as osteocytes traverse through the tissue. The spaces found in the lamellar and woven tissue are known as lacunae that house osteocytes. Channelling away from the lacunae are canaliculi that join to the Haversian canal, allowing the cells to communicate through the mineralised matrix as well as the flow of nutrients and oxygen, known as the lacuno-canalicular network.

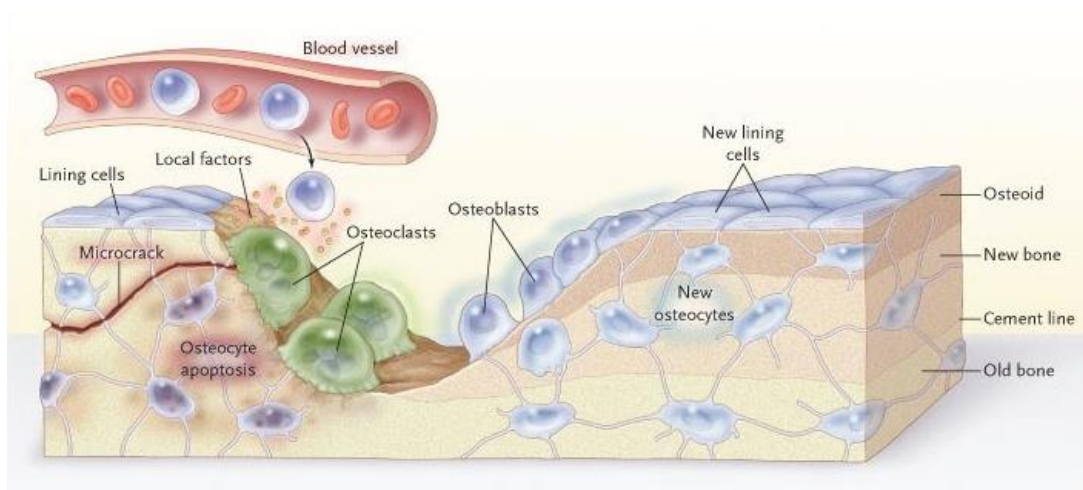


Figure 2.8: Schematic of the bone remodelling cycle whereby microcracks occur and can sever the canaliculi, cutting off communication between osteocytes and increasing osteocyte apoptosis, causing damage to the tissue. Lining cells and osteocytes release signals to blood and marrow cells to stimulate osteoclastogenesis. Osteoclasts break down the damaged tissue and osteoblasts deposit new bone to rebuild the tissue. Osteoblasts either embed themselves into the matrix to become osteocytes, flatten to become bone lining cells or go through apoptosis (Seeman, 2008).

Osteocytes are the most mature stage of the osteoblast lineage and are the most abundant bone cell type, making up ~95% of the cells in the tissue (Frost, 1960). Moreover, osteocytes have a longer lifespan than osteoblasts, with an estimated average half-life of ~25 years for a human osteocyte in comparison to approximately three months and 10-20 days for a human osteoblast (Frost, 1964; Manolagas, 2000). Similar to a network of neurons, osteocytes are connected to each other to allow communication between cells. This network is known as the osteocyte lacunar-canalicular network and provides microporosity in the mineralised bone matrix (Burger and Klein-Nulend, 1999; Knothe Tate et al., 2004). Osteocytes occupy the lacunar spaces from which canals called canaliculi distribute off in multiple directions and allow for the exchange of oxygen, nutrients, factors and waste (Crockett et al., 2011). The wide distribution and interconnections of osteocytes allow these cells to detect stresses and strains on the bone and hence, osteocytes are considered the main mechanosensory of bone. Although other bone cell's respond to mechanical loading, osteocytes are the most responsive and sensitive cell for detecting stimuli, such as deformation of the bone matrix, fluid flow shear stress due to changes in canalicular fluid flow and associated streaming potentials (Burger and Klein-Nulend, 1999). Commonly measured markers of osteocyte activity include osteocalcin

(OCN), which is expressed by mature osteoblasts and young osteocytes, and sclerostin (Sost) that is solely expressed by mature osteocytes.

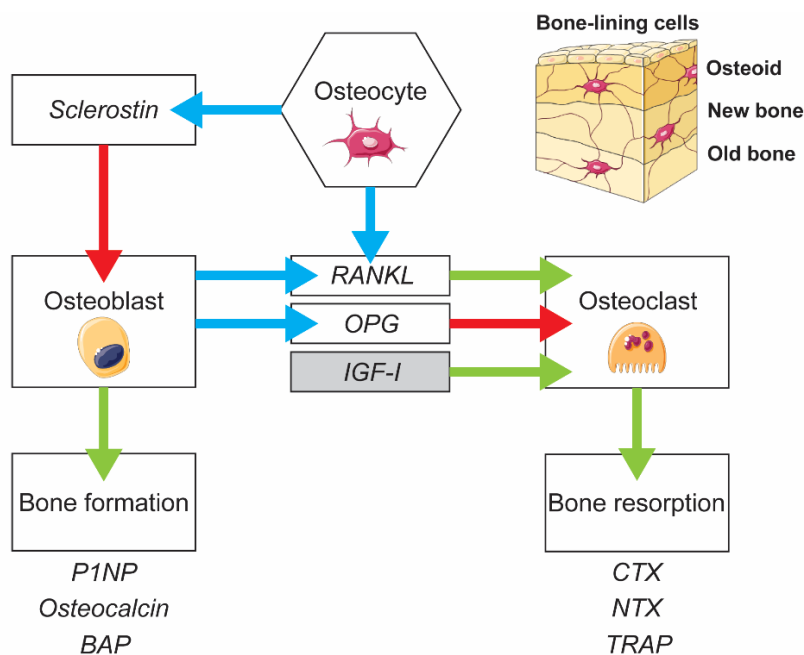


Figure 2.9: Schematic adapted from (Hygum et al., 2017), where blue arrows represent the products that are secreted, red arrows represent the inhibitory actions of those products onto cells, green arrows represent the stimulatory actions of the secreted products onto cells and grey represents products released by the liver. RANKL, receptor activator of nuclear factor- κ B ligand; OPG, osteoprotegerin; IGF-I, Insulin growth-factor hormone-I; P1NP, type I amino-terminal propeptide; BAP, Bone alkaline phosphate; CTX, C-terminal cross-linking telopeptide of collagen; NTX, N-terminal telopeptide of type 1 collagen; TRAP, enzyme tartrate resistant acid phosphatase.

Osteocytes secrete Sost and receptor activator of nuclear factor- κ B ligand (RANKL) (a cytokine essential to osteoclast differentiation and activation) to coordinate osteoblast and osteoclast function by inhibiting the wingless (Wnt) signalling and promoting osteoclastogenesis, respectively (Spencer et al., 2006). Wingless or Wnt signalling is thought to be important in skeletal function such as maintaining bone mass and regulating bone cell functions, particularly bone formation and resorption (Zákány and Duboule, 1993). Wnts are glycoproteins that are secreted to activate three or more receptor-mediated signalling pathways in order to maintain cellular homeostasis (Milat and Ng, 2009). Previous studies have demonstrated the importance of the Wnt/ β -catenin pathways in determining the fate of mesenchymal precursor cells into either osteoblasts, chondrocytes and even adipocytes (Day

et al., 2005; Grey et al., 2012; Hill et al., 2005; Kim and Schafer, 2016). Sclerostin is a protein, secreted by mature osteocytes and has an antagonistic effect on Wnt signalling (Delgado-Calle et al., 2017) Sclerostin is thought to play a role in bone mass homeostasis, reducing bone formation by inhibiting osteoblasts and stimulating bone resorption via osteoclast formation, dependant of RANKL (Baron and Kneissel, 2013; Glass et al., 2005; Li et al., 2008). All indicative that osteocytes play a central role in bone remodelling during bone turnover and can regulate bone mass using a combination of hormonal and mechanical signals. Elevated sclerostin has been reported in studies of obese, type-2 diabetic patients and in patients with reduced kidney function (Amrein et al., 2014; Daniele et al., 2015; Pelletier et al., 2013; Sheng et al., 2012), suggesting sclerostin may be an important factor for insulin resistance.

In healthy bone tissue, the formation process carried out by osteoblasts needs to be balanced by a resorption process, which are carried out by osteoclasts. Unlike osteoblasts and osteocytes, osteoclasts are generally not as prevalent in bone, which usually consists of two to three per μm^3 (Roodman, 1996). Osteoclasts are large, multinucleated cells that are derived from hematopoietic stem cells (an immature cell that can develop into all types of blood cells) and differentiate along the monocyte/ macrophage lineage (Kartsogiannis and Ng, 2004; Martini et al., 2012). Osteoclasts possess several characteristics to aid bone resorption, with the two main characteristics being; (1) the ruffled border, which secretes various organic acids and preserves a low pH at the surface of bone, critical to dissolving mineral components (2) the sealing zone, which is a tight ring-like zone of osteocyte adhesion that prevents important cell-to-bone exchanges from affecting the extracellular environment (Suda et al., 1992). The driving force in osteoclastogenesis is its ligand, RANKL, which is expressed in osteoblasts, osteocytes and stromal cells and is stimulated by parathyroid hormone (PTH), PGE₂, endocrine hormone - 1.25(OH)₂D₃, interleukin 1 β (IL- 1 β) and IL-11 (Hofbauer et al., 1999; Horwood et al., 1998; Yasuda et al., 1998). However, RANKL is also the inhibitor of osteoprotegerin (OPG) (Figure 2.8) (Bucay et al., 1998; Mizuno et al., 1998). Osteoclasts are key to the long-term maintenance of blood calcium homeostasis and secrete the enzyme tartrate resistant acid phosphatase (TRAP) during bone resorption that is necessary for balancing cartilage mineralisation and maintaining its integrity during growth and development (Sawyer et al., 2003). Hence, TRAP is a suitable biochemical marker for osteoclastic bone resorption (Figure 2.8). Additionally, C-terminal cross-linking telopeptide of collagen type-I (CTX-I) is another common marker of bone resorption. Individual molecules of collagen are joined together via crosslinks within the triple helix. There are two main sites for crosslinking that are found at both ends of the collagen

molecule, the amino- (N) and carboxyl- (C) terminal (Herrmann and Seibel, 2008). During the degradation of type-I collagen, CTX fragments are released into circulation and can be measured from both urine and serum (Herrmann and Seibel, 2008). Following bone resorption, osteoclasts leave behind a concave surface of eroded bone as seen in Figure 2.7, where osteoblasts are called upon to deposit new bone to replace the old/ resorbed bone, starting the cycle of bone remodelling again.

2.2.2 Bone Modelling and Remodelling

The early stages of bone formation occur through intramembranous and endochondral ossification. During intramembranous ossification, the number of bone cells and fibres increase, individual trabeculae begin to form into primary cancellous and cortical bone begins to form by filling the spaces of the primary cancellous bone with primary osteons or Haversian systems, which are eventually replaced by osteons (Secondary Haversian systems) (Cowin, 2001). On the other hand, endochondral ossification occurs when chondrocytes grow and develop a cartilaginous pattern that will turn into a calcified matrix. Where MSCs will colonise and differentiate into osteoblasts to form bone tissue. Primary cancellous bone forms from woven bone with calcified islands embedded throughout that are later replaced by bone marrow or lamellar trabecular bone (Ortega et al., 2004). Once a bone surface has formed, modelling can begin. During the early stages of life, bone is growing rapidly from the growth plate and bone modelling is most prominent to increase bone volume and support the growth of the skeleton. Both bone formation and resorption occurs during bone modelling to control bone shape, size and mass (Allen and Burr, 2013).

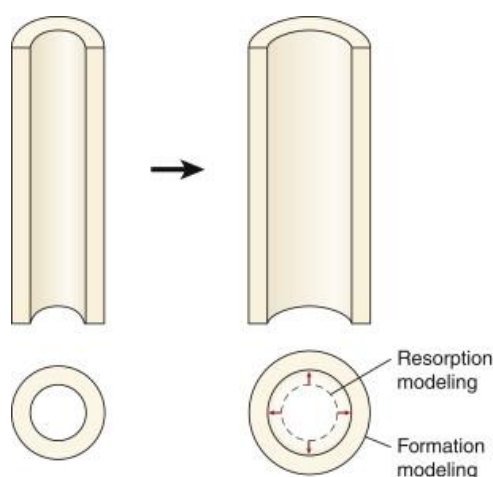


Figure 2.10: Bone grows radially on the periosteal surface via formation modelling and is removed on the endocortical surface via resorption modelling, which preserved bone thickness (Allen and Burr, 2013).

In the diaphysis, *formation modelling* is when osteoblasts add bone to a periosteal surface faster than bone is resorbed endocortically, while *resorption modelling* occurs on the endocortical surface (Figure 2.9). This process is distinctly different from the bone remodelling process, since in bone remodelling formation and resorption occur on different surfaces. Formation modelling results in a consistent cortical thickness and ensures radial growth of the bone (Allen and Burr, 2013). In addition, bone architecture and mass are regulated through mechanical stimulus (Cowin, 2001). If bone strains exceed a certain range, known as the modelling threshold, the minimum effective strain (MES) of $1,000 \mu\epsilon$, formation modelling or drift becomes activated and bone mass and strength increases, otherwise when strains remain below this threshold formation modelling stays inactive (Frost, 1997).

Bone remodelling is the process in which bone has been modelled and is now being maintained. Bone remodelling occurs in a cycle controlled by a group, known as the bone multicellular unit (BMU), whereby old and damaged tissue is removed and replaced with new tissue and can take approximately 4-6 months to complete (Allen and Burr, 2013). Bone remodelling via the BMU occurs in 5 stages: (1) Activation, (2) Resorption, (3) Reversal, (4) Formation and (5) Termination (Kenkre and Bassett, 2018) (See Figure 2.10). The resting bone period represents the stage in human bone when over 80% of the surface is dormant and not actively remodelled (Kenkre and Bassett, 2018). The activation period, which usually lasts 10 days, is when circulating osteoclast precursor cells differentiate, this process itself is controlled by osteocytes. A canopy is then formed from detached bone lining cells, this canopy encapsulates the BMU and limits the remodelling process to this region. Resorption is the next stage where osteoclasts begin to remove the old and damaged tissue via a macrophage-like process lasting approximately 2- to 3-weeks. Reversal occurs between resorption and formation to remove the remaining debris from the osteoclasts in the resorbed area by macrophage cells, lasting approximately four months. Following removal, bone formation begins, where differentiated osteoblasts infiltrate the concave surface of eroded bone and begin to deposit osteoid, which soon becomes mineralised to build new bone. The formation stage can take up to 90 days whilst the mineralization phase can take approximately a year to complete (Allen and Burr, 2013). The final stage is termination, at this stage osteocytes signal for osteoblastogenesis to decline. It is at this stage that osteoblasts either undergo apoptosis or become buried deep within the mineralised matrix to become osteocytes (Allen and Burr, 2013; Kenkre and Bassett, 2018).

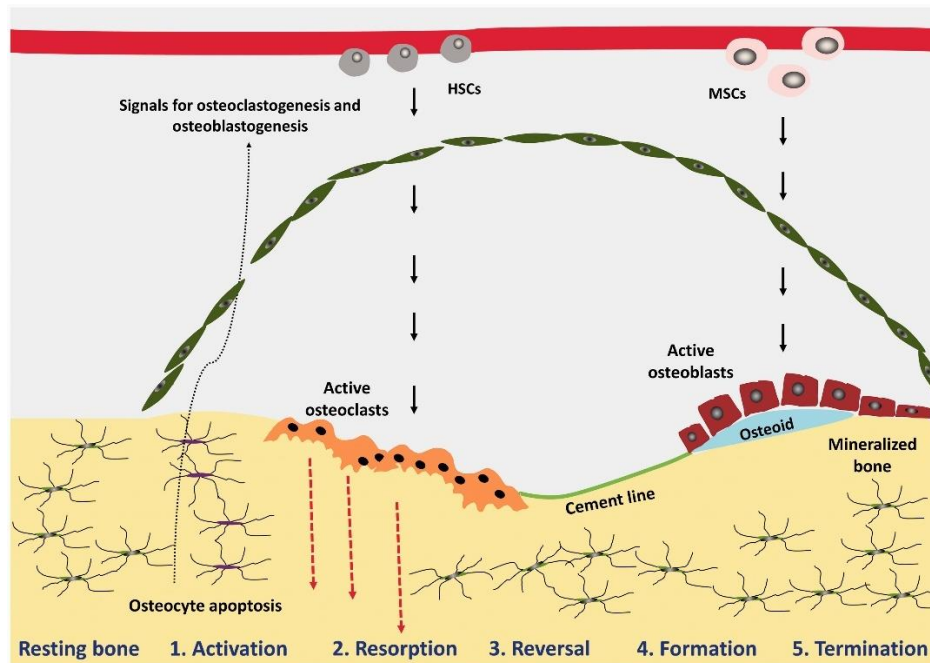


Figure 2.11: Bone remodelling occurs at five stages via the bone multicellular unit that consists of a resting phase followed by (1) activation, (2) resorption, (3) reversal, (4) formation and (5) termination (Kenkre and Bassett, 2018).

2.2.3 Cellular and General Health Markers

Calcium

Bone is a major reservoir for calcium. There is approximately 1 - 1.3 kg of calcium in a healthy adult and roughly 99% of that calcium is found in bone, with the remaining 1% found in soft tissues and extracellular fluid (Houillier et al., 2006). Calcium is essential in ensuring normal cell signalling as well as controlling muscle contraction and nerve impulse transmission (Peacock, 2010). Calcium levels may reflect the capability of maintaining glucose and bone cell metabolism homeostasis in the body and hence it is important that serum calcium levels are within the normal range for healthy subjects (total calcium levels: 2.2 – 2.6 mmol/ L) to ensure proper physiological function (Song, 2017). Calcium homeostasis is tightly regulated by two hormonal systems and receptors including the parathyroid hormone (PTH) and its receptor (PTHr) and 1,25-dihydroxyvitamin D [$1, 25(\text{OH})_2\text{D}$], an active form of vitamin D and its receptor (VDR). The calcium sensing receptor (CaR) is also important in calcium homeostasis (Peacock, 2010). When serum calcium levels fall, the CaR is deactivated within the parathyroid gland, and this signals the release of PTH into the bloodstream. This increased PTH secretion stimulates the PTHr in the kidney to increase tubular calcium and in bone to signal osteoclasts to release calcium from the bone surfaces into the bloodstream (Jeon, 2008;

Song, 2017). The secretion of $1, 25(\text{OH})_2\text{D}$ is also increased by the kidney during high levels of the PTH, which causes the gut to absorb more calcium and bone to increase resorption and reduces PTH secretion from the parathyroid gland (Song, 2017). This cycle is shown in Figure 2.11.

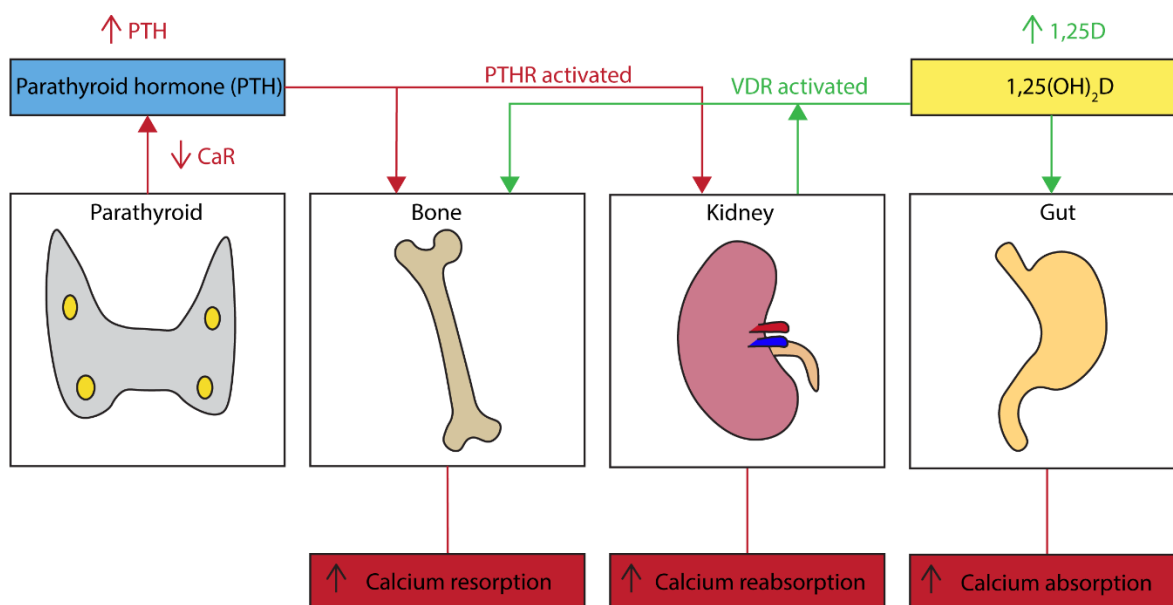


Figure 2.12: Schematic of calcium homeostasis adapted from (Peacock, 2010). Red arrows represent the secretion of parathyroid hormone (PTH) when serum calcium levels reduce and the calcium receptor (CaR) is inactivated, this activates the parathyroid receptor (PTHR) signal bone to release calcium into the bloodstream and the kidney to increase calcium reabsorption to increase calcium levels. Green arrows represent how the kidney increased its secretion of vitamin D ($1,25\text{D}$) when PTH secretion is increased that signals the vitamin D receptor (VDR) to stimulate calcium absorption and resorption in the gut and bone, respectively.

When diagnosing diseases and pathological conditions, calcium levels are commonly measured from serum and extracellular fluid since calcium equilibrium is often affected. Typically, calcium equilibrium is affected in disorders where PTH secretion is altered, such as primary hyperparathyroidism (Houillier et al., 2006). Hyperparathyroidism occurs when one or more of the parathyroid glands are overactive resulting in the secretion of too much PTH, which increases serum calcium levels and can have a detrimental effect on bone mineral density and kidney function (Marcocci and Cetani, 2018). In the case of post-menopausal women presenting with osteoporosis, calcium is often not being absorbed effectively and it is commonly found that these patients present with increased serum calcium levels, although PTH

and 1,25(OH)₂D is reduced. However, in the case of osteoporosis that has occurred as a result of old age, serum calcium levels are found to be reduced along with a reduction in PTH and 1,25(OH)₂D. Hence, measuring serum calcium concentration can be a good indicator for homeostasis in the body and for disease diagnosis (Gallagher, 1990).

Insulin Growth Factor Hormone-I (IGF-I)

Growth factors are essential for normal bone growth and development, with one of the most common markers being IGF-I or insulin growth-factor hormone-I. IGF-I is a polypeptide that acts both as an endocrine hormone and a tissue growth factor and interestingly, circulating IGF-I is mainly released in bone and the liver and its secretion is often controlled by growth hormone (Rosen and Pollak, 1999). IGF-I is synthesised by osteoblasts and is an important regulator in bone cell function, collagen synthesis and can stimulate anabolic activity within the bone tissue (Crockett et al., 2011; Johansson et al., 1992; McCarthy et al., 1989). Interestingly, a study by Lean *et al* (1996) found that when osteocytes detect mechanical stress, in response they secrete paracrine factors, such as, IGF-I. IGF-I is generally most abundant at puberty and naturally declines with age (Jones, 1995), with it being understood to play a vital role in longitudinal bone growth. Interestingly, there have been reports of increased insulin sensitivity when IGF-I levels are increased and previous research investigating childhood obesity and T2D, found that during puberty IGF-I levels rose and fell in a pattern similar to the rise and fall of insulin resistance, suggesting that the growth hormone IGF-I axis contributes to the insulin resistance of puberty (Hannon et al., 2005). Indicating the importance of circulating IGF-I in normal bone growth and development.

Interleukin-6 (IL-6)

Cytokines are a diverse group of small cell-secreted proteins or peptides that can be either pro- or anti-inflammatory (Zhang and An, 2007). There are many different types of cytokines, however one that has gained particular interest in the field of bone is interleukin-6 (IL-6). IL-6 has many different functions such as, regulating immune responses, haemopoiesis (the formation of blood cells and platelets), inflammation and is thought to influence some osteoclast and osteoblast activities (Mihara et al., 2012; Sims, 2021). IL-6 is produced via two pathways, classic- and trans-signalling. The classic signalling pathway is thought to be involved with inducing an anti-inflammatory and regenerative response while the trans-signalling pathway is thought to induce the pro-inflammatory response (Rose-John, 2012; Schaper and Rose-John, 2015). It is understood that IL-6 trans-signalling promotes bone

formation and osteoclast formation. IL-6 has been associated with osteoclastogenesis, whereby IL-6 has been found to stimulate the expression of RANKL that promotes osteoclast precursors to progress into mature osteoclasts and increases their resorptive activity (Rose-John, 2012). Conversely, literature has also demonstrated the opposite effect, where IL-6 has also been shown to play an inhibitory role on osteoclasts and osteoblasts resulting in a reduced expression of a variety of osteoclastic markers such as TRAP and hindering RANKL signalling pathways (Yoshitake et al., 2008). Additionally, IL-6 is also thought to influence bone formation. IL-6 has been shown to increase the expression of osteoblastic markers such as alkaline phosphatase (ALP), which aids in the formation and deposition of extracellular matrix mineralisation (Bellido et al., 1997; Itoh et al., 2006). IL-6 has also been associated with increasing the production of IGF-I, promoting bone growth, collagen synthesis and bone matrix mineralisation (Pass et al., 2009). A study on mice found that when IL-6 (or tumour necrosis factor α , TNF α) was overexpressed, IGF-I levels were reduced resulting in stunted growth, similar results were observed in studies on human patients (De Benedetti et al., 2001, 1997). However, IL-6 is understood to be associated with various pathological conditions, particularly in conditions associated with abnormal bone resorption such as rheumatoid arthritis and Paget's disease (Fonseca et al., 2009). IL-6 cytokines are known to play a direct and indirect role in the bone metastasis "vicious cycle" (Blanchard et al., 2009). Moreover, IL-6 is understood to play a role in the pathogenesis of T2D (Akbari and Hassan-Zadeh, 2018). Adipose tissue and adipocytes are major sources for circulating IL-6 (Makki et al., 2013), hence there have been many studies suggesting a link between obesity and circulating IL-6 levels as well as studies trying to provide an understanding as to how heightened circulating levels of IL-6 can lead to reduced insulin sensitivity, resistivity or maintenance of elevated glucose levels (Bastard et al., 2002; Rotter et al., 2003).

2.3 Bone Quality

With disease and aging, tissue quality can become altered and can increase a patient's likelihood of fracture. Since bone is arranged hierarchically, these alterations can be examined at multiple length scales from the nano- to the macroscale using a wide range of techniques (Donnelly, 2011; Hernandez and Keaveny, 2006). Tissue mechanical integrity can be explained by bone quality with the inclusion of bone quantity such as, bone mineral density (BMD), as shown in Figure 2.12.

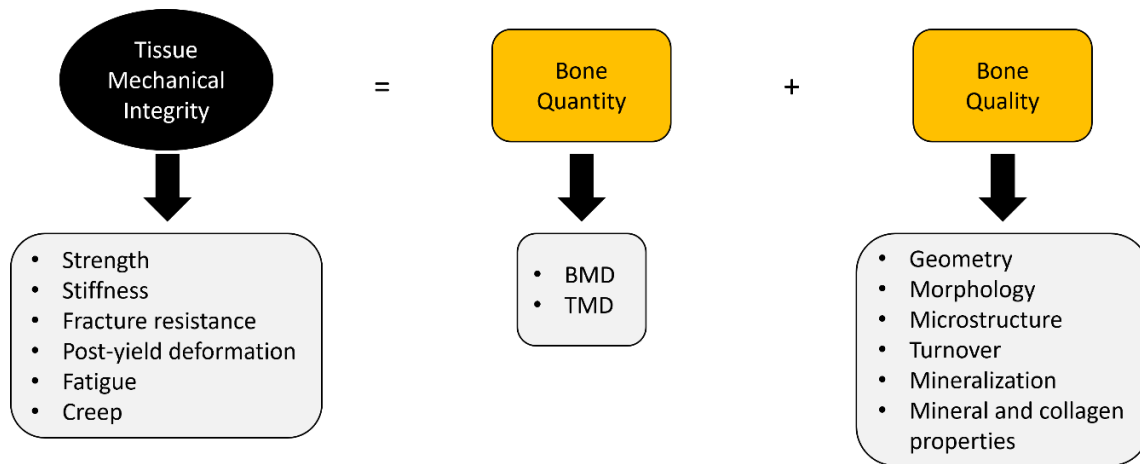


Figure 2.13: Schematic adapted from (Boskey and Imbert, 2017) outlining the different variables of bone quality that contribute to the mechanical integrity of the tissue.

2.3.1 Multiscale Analysis of Bone Quality

To understand the full picture of bones resistance to fracture, the bone features that can alter tissue quality at different length scales must be considered. There are a variety of techniques that can be applied to explore the different physico-chemical components at the nano- to the macroscale, which will be discussed in this Section.

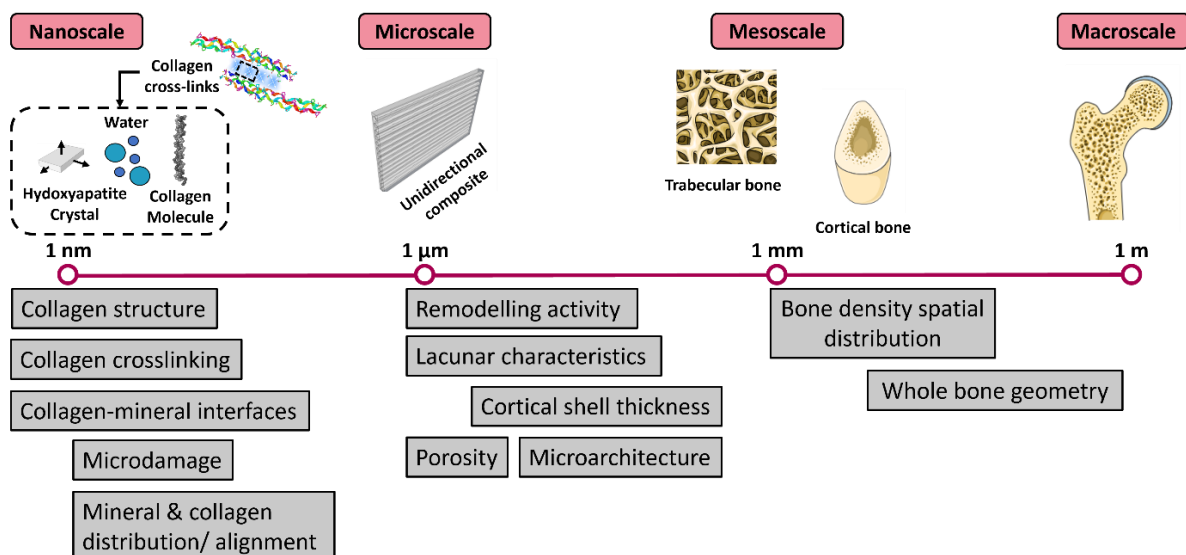


Figure 2.14: Image adapted from (Donnelly, 2011; Hernandez and Keaveny, 2006) showing the different techniques used to assess bone quality at the different length scales of bone.

Nanoscale

Fluorometric assays and High Performance Liquid Chromatography (HPLC)

At the nanoscale, collagen crosslinks are often measured to explore the crosslink type (enzymatic or non-enzymatic) and quantities present. Fluorometric assays are often used to quantify a bulk measurement of AGEs, including pentosidine, crossline and versperlysines A, B and C to name a few. This techniques measures hydroxyproline content form a hydrolysate, which provides a measure of the total amount of collagen (by assuming 14% hydroxyproline by weight) and normalises it against quinine to quantify the amount of bulk fluorescent non-enzymatic AGEs (Sell and Monnier, 1989; Tang et al., 2007). To gain a more detailed insight to the types and quantities of collagen crosslinks, high-pressure liquid chromatography (HPLC) techniques can be applied, where a liquid sample (which in this case can be in the hydrolysate of bone samples) is injected into a filled column material such as a liquid or gel (stationary phase) that is connected to a pump. At high pressure, the pump system pushes a solvent carrying the sample through the column to a detector. The components of the different samples become separated depending on the speed of the liquid or gas through the stationary phase and how long it takes to reach the detector (retention time). A raw spectra is obtained for the elution of the different crosslinks (Czaplicki, 2013) (Figure 2.14), such as immature and mature enzymatic crosslinks, non-enzymatic crosslinks (pentosidine) and even non-enzymatic non-crosslinking adducts (CML) (Creecy et al., 2016; Romanowicz et al., 2022). Furosine is an early marker of glycation that can also be quantified via HPLC (Sell, 1997).

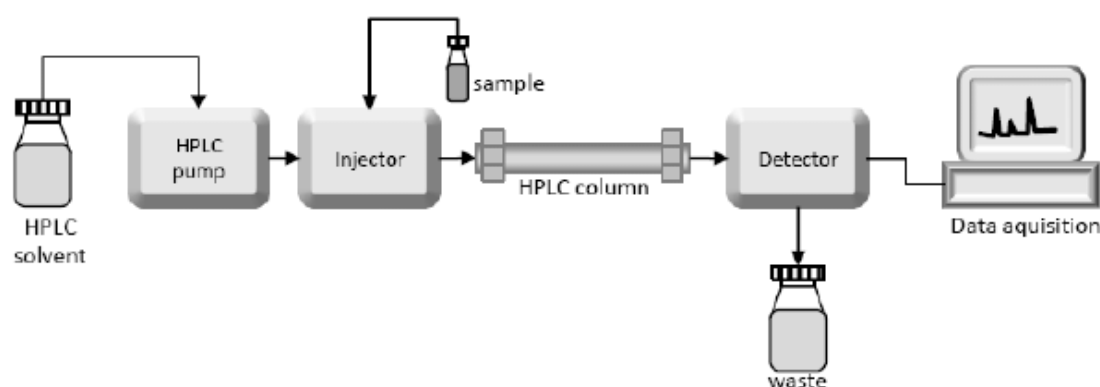


Figure 2.15: Schematic diagram the High Performance Liquid Chromatography, where solvent and sample are pushed through the column via a pump and injector which move into a detector and a raw spectra is gotten (Czaplicki, 2013).

Microscale

Fourier Transform Infrared Microspectroscopy (FTIR)

At the microscale, there are a wide range of techniques that can be implemented to assess bone quality such as Energy-dispersive x-ray (EDX), quantitative Backscattering Electron Imaging (qBEI), small/ wide angle X-Ray scattering (SAXS/ WAXS), vibrational spectroscopy such as Fourier transform infrared (FTIR) and Raman and Micro-Computed Tomography (Micro-CT). The main focus will be on FTIR, Raman Spectroscopy and Micro-CT techniques since these have been used to assess bone quality of the Type-2 Diabetic rat bone in this thesis.

FTIR and Raman are both vibrational spectroscopy techniques that have both been used to quantify chemical features in the tissue and assess bone matrix composition. In both techniques, an incident light is focused onto the sample, where the chemical bonds of the mineral and collagen components become excited and vibrate (Donnelly, 2011). These vibrations that occur are molecule specific and correspond to different absorption peaks that produces an infrared FTIR or Raman spectra that can provide information about the biochemical composition of the measured sample. There are a variety of different ways to assess bone with FTIR such as using a transmission, reflection and attenuated total reflectance (ATR-FTIR) probe. Additionally, others have adopted the use of an optical microscope and a focal plane array detector to allow the sample surface to be imaged whilst also collecting spatial information about the tissue composition, known as FTIR imaging (FTIR-I). A drawback of using spectroscopy on unfixed, untreated bone samples is that they can quickly become dehydrated during measurements due to the intensity of the IR beam. In cases where transmission is used, samples must be homogenized with KBr and formed into tiny pellets for measuring, which can become a very time-consuming sample preparation process (Kourkoumelis et al., 2019) (Figure 2.15). ATR-FTIR is considered advantageous due to its low cost, rapid sample preparation and measuring. ATR-FTIR commonly measures a spectra from solid or powdered bone and employs the use of a crystal to reflect the IR beam creating an evanescent wave, which is absorbed by the sample and the reflected radiation is returned to the detector (Taylor and Donnelly, 2020) (Figure 2.15). It is understood that using powdered bone samples is more favourable than larger sample Sections as the powdered samples allow for deeper penetration depth of the IR radiation into the sample and removes the possibility of taking measurements from void spaces (i.e. in the presence of a pore) (Kontopoulos et al., 2018). However, a disadvantage of ATR-FTIR is that the particle size of the powdered bone tissue can affect some parameters such as crystallinity,

carbonate: phosphate and phosphate: amide (Kontopoulos et al., 2018). FTIR-I is considered quite an advantageous method of spectroscopy as each pixel in the FTIR image contains a spectrum, which can be mapped onto the image to create a biochemical fingerprint of that sample, making it easier to compare diseased tissue to non-diseased. However, since FTIR-I is measured through transmission, bone samples must be embedded, polished and sliced thinly, which can be a time consuming preparation process. Moreover, during the tissue embedding process the sample must be dehydrated that may potentially alter the bone structure at the nanoscale and therefore, it is important to remove the effects of the embedding material from the spectra via subtraction (Lievers et al., 2010; Taylor and Donnelly, 2020).

Raman Spectroscopy

Raman spectroscopy detects scattering light from biological molecules and ions that become excited by an incident laser light (Morris and Mandair, 2011). The molecules vibrate and this causes energy loss from a small fraction of light, which is then deflected at longer wavelengths. Each molecule has a unique vibrational characteristic, which is related to the difference in wavelength between the incident and scattered light (Morris and Mandair, 2011). The output is a Raman spectra with bands that reflect specific molecular vibrations of mineral and collagen components, known as frequency shifts, that are labelled in wavenumber units (cm^{-1}), similar to an FTIR spectra. Raman spectroscopy is quite a universal technique as it can be used with fresh or embedded tissue and allows for a higher spatial resolution to be used (Gamsjaeger et al., 2010). Unlike FTIR, Raman spectra do not have strong water contributions when used in conjunction with bone and hence, Raman may be used on hydrated samples (Donnelly, 2011; Taylor and Donnelly, 2020). However, tissue embedding is often preferred for Raman spectroscopy and Raman imaging measurements on bone samples, despite possible dehydration, since embedding samples surfaces are flat that minimizes the effect of surface scattering and maximised the signal-to-noise ratio (Taylor and Donnelly, 2020).

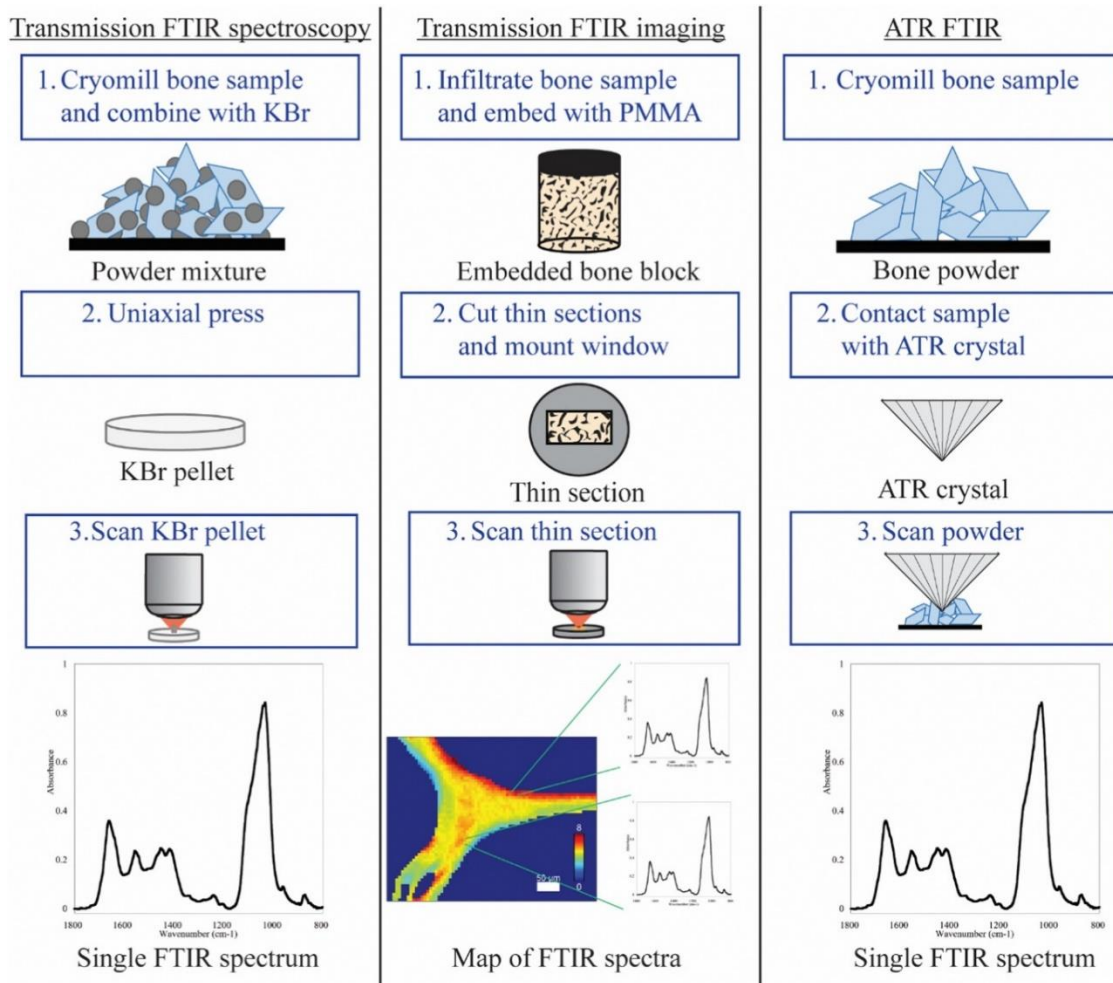


Figure 2.16: Different bone sample preparation methods where potassium bromide (KBr) pellets are formed for transmission FTIR spectroscopy (left), a polished bone sample embedded in PMMA is prepared for transmission FTIR imaging (centre) and bone is milled into a powder for ATR-FTIR (right) (Taylor and Donnelly, 2020).

Different spectral peaks represent the inorganic (PO_4 and CO_3) organic (Amide and CH_2) components of bone and are found at different peak positions or integration ranges. The most common outcomes measured via FTIR and Raman spectroscopy include the mineral: matrix ratio, carbonate: phosphate ratio, mineral maturity (or interchangeably termed “crystallinity”) and collagen maturity (or the enzymatic collagen crosslink ratio), among other less common measurements (Taylor and Donnelly, 2020). Table 2.1 and Figure 2.16 below shows the different parameters measured, the range in which they are found in and a description for each outcome.

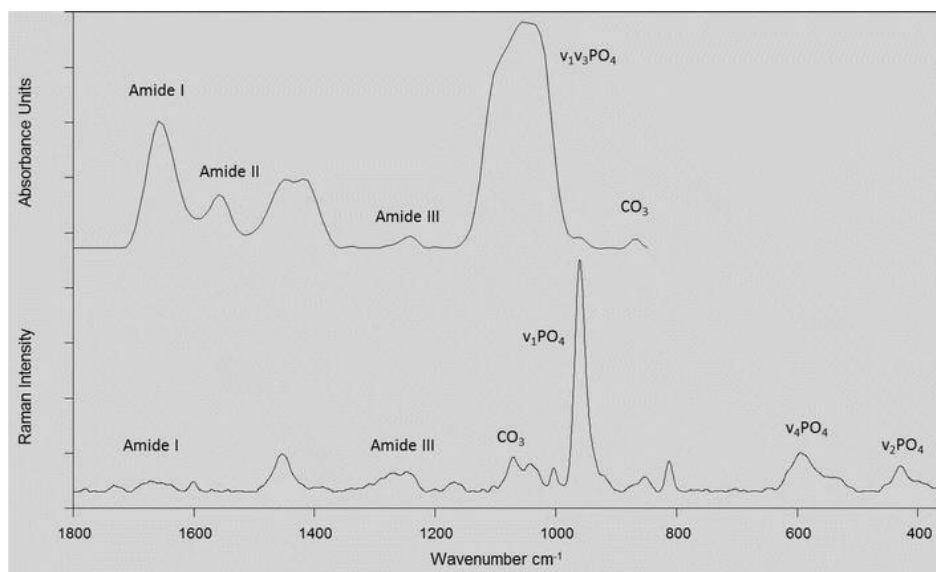


Figure 2.17: Example of a typical FTIR (top) and Raman (bottom) spectra with peaks labelled according to its composition (Paschalis *et al.*, 2017).

It is important to note that due to laser polarisation, some Raman bands are more orientation-dependant than others, which can affect some commonly used measurements and lead to polarisation bias if not accounted for (Makowski *et al.*, 2013). It is understood that the intensity of the mineral Raman bands are solely dependent on the c-axis orientation (Kazanci *et al.*, 2006; Tsuda and Arends, 1994). In addition, a study by Kazanci *et al.* (2006) explored which peaks were more sensitive to orientation and polarisation direction and found that the major $\nu_1\text{PO}_4$ and Amide I bands were found to be sensitive to polarisation-orientation. However, they did find other peaks such as the ν_2 , $\nu_4\text{PO}_4$ and Amide III bands were less susceptible to orientation effects and thus concluded that in order to avoid bias and to allow for more consistent comparison between literature, peaks that have a lesser effect of orientation should be used to measure parameters such as the mineral: matrix and carbonate: phosphate (Kazanci *et al.*, 2006; Makowski *et al.*, 2013). However, the use of polarisation with a Raman spectrometer provides orientation-related information specific to the tissue being examined. With polarisation, Raman spectra can be collected at different excitation polarisation angles. The intensity of the Raman spectra is dependent on the orientation of the molecular bonds relative to the laser polarisation vector and excitation vibration mode (Kochetkova *et al.*, 2021).

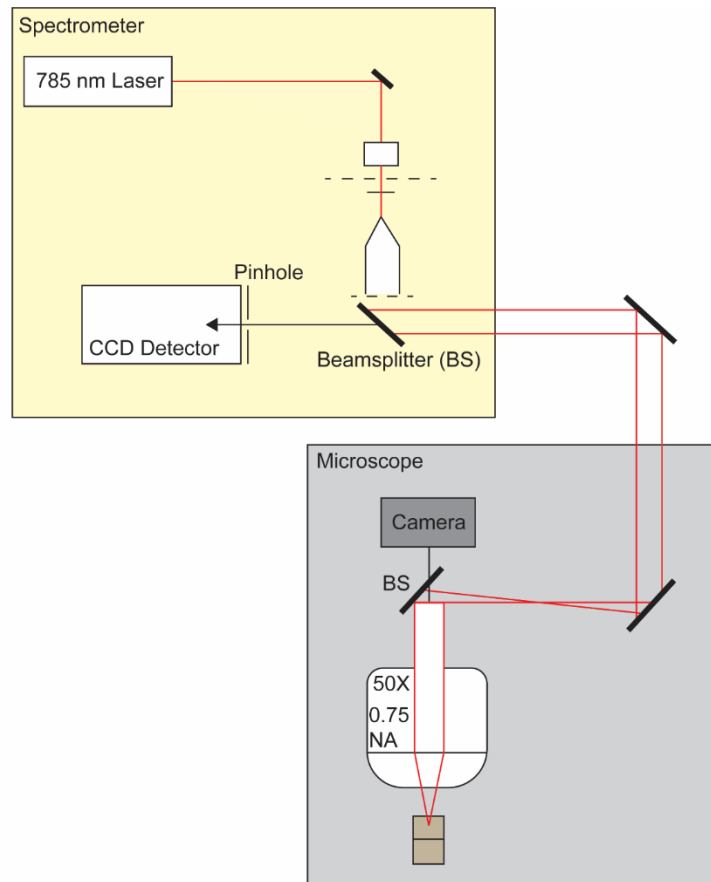


Figure 2.18: Schematic diagram of a typical Raman spectrometer set-up.

Table 2.1: FTIR and Raman ratio parameters to assess bone quality adapted from (Kourkoumelis et al., 2019; Taylor and Donnelly, 2020).

Outcome	Description	FTIR (integration range or peak)	Raman (integration range or peak)	Ref
Mineral: matrix ratio	Measure of mineral per the amount of collagen in the tissue (reflects BMD), Relates to ash density, Increases with age, A predictor of bone stiffness.	$\nu_1 - \nu_3$ PO ₄ : Amide I (900–1200 : 1600–1720 cm ⁻¹)	$\nu_1 - \nu_2$ PO ₄ : Amide I (930–980, 410-460 : 1620–1700 cm ⁻¹) $\nu_1 - \nu_2$ PO ₄ : Amide III (930–980, 410-460: 1215–1300 cm ⁻¹) ν_1 PO ₄ : CH ₂ (930–980: 1446 cm ⁻¹)	(Boskey et al., 1992; Donnelly et al., 2010b; Gamsjaeger et al., 2014; Taylor et al., 2017)
Carbonate: phosphate ratio	Measure of carbonate substitution into the mineral crystal lattice at the A-type, B-type and labile positions, Indirectly related to carbon content, Increases with age.	ν_2 CO ₃ : $\nu_1 - \nu_3$ PO ₄ (850–890 : 900–1200 cm ⁻¹) A-type, B-type and labile subband positions: (878, 871, 865 cm ⁻¹)	ν_1 CO ₃ : $\nu_1 - \nu_2$ PO ₄ (1050-1100 : 930–980, 410-460 cm ⁻¹)	(Awonusi et al., 2007; Donnelly et al., 2010b; Handschin and Stern, 1995; Ou-Yang et al., 2001)
Mineral maturity	Transformation of non-apatitic domains into apatitic crystals, Often interrelated to crystallinity	Stoichiometric apatite/ Nonstoichiometric apatite (1030/1020 or 1110 cm ⁻¹)	-	(Farlay et al., 2010; Gamsjaeger et al., 2017a; Paschalis et al., 2017)
Mineral crystallinity	Reflects crystal size and perfection	FWHM of ν_4 PO ₄ (604 cm ⁻¹)	1/FWHM ν_1 PO ₄	
Acid Phosphate substitution (HPO₄)	HPO ₄ Substitution into bone mineral crystal lattice is associated with newly deposited mineral, Inversely correlated to crystallinity, Decreases with age	$\nu_1 - \nu_3$ PO ₄ sub-bands 1127 : 1096 cm ⁻¹	-	(Rey et al., 1991; Spevak et al., 2013)
Enzymatic crosslink ratio (collagen maturity)	Ratio of mature trivalent crosslinks to immature divalent crosslinks, Measure of the secondary structure of collagen fibres	Amide I sub-bands 1660 : 1690 cm ⁻¹	Amide I sub-band 1660 : 1690 cm ⁻¹	(Gamsjaeger et al., 2017b; Paschalis et al., 2001)
Non-enzymatic crosslink ratio	Positively correlated to bulk fluorescent AGE levels, Relates to glucose-mediate crosslinks that irreversibly form between collagen proteins	Amide I sub-bands 1678 : 1692 cm ⁻¹	-	(Schmidt et al., 2017; Sihota et al., 2020a)
Pentosidine (PEN)	Commonly measured non-enzymatic crosslink	-	Area ratio PEN : CH ₂ 1495 : 1450 cm ⁻¹	(Rubin et al., 2016)
Carboxymethyl-lysine (CML)	Commonly measured non-enzymatic adduct	-	Area ratio CML : CH ₂ 1150 : 1450 cm ⁻¹	

Micro-Computed Tomography (Micro-CT)

Micro-CT is a non-destructive 3D imaging techniques and is considered as the “gold standard” for assessing bone morphology and microarchitecture in *ex vivo* small animal studies, since it allows for the use of higher resolutions (1 – 6 μm), which enable accurate analysis of the cortical and trabecular components (Bouxsein et al., 2010). *In vivo* micro-CT is also available for imaging in longitudinal small animal studies, however higher resolutions can be more difficult to achieve (up to $\sim 10 \mu\text{m}$). Before beginning a scan, the micro-CT scanner must be calibrated to phantom samples of different hydroxyapatite densities (0, 100, 200, 400, 800 mg HA/ cm^3) to allow for the conversion of the X-Ray attenuation to a given bone density for the sample (Burghardt et al., 2008). A micro-CT scanner contains a micro-focus X-Ray tube, rays are passed through a collimator and the emitted photons are focused into a beam, which then passes through an aluminium filter to eliminate beam-hardening artifacts as shown in Figure 2.18. The beam hits the sample and then the detector, which compares the X-Ray attenuation of the bone to the hydroxyapatite (HA) standard, to estimate the bone density. The sample is rotated approximately 0.5 degrees and the cycle begins again until full rotation is complete and a series of 2D projections known as slices are gotten (Figure 2.18). The 2D projections are then reconstructed into a 3D image of the scanned region of interest. Defining the voxel size is an important consideration when imaging small animal bones (Müller et al., 1996). A voxel size is a 3D volume related to pixel size and slice thickness and can be equated to nominal resolution (Scanco Medical, 2023). Ideally, when determining the image resolution all three dimensions should be equal and the smallest voxel size giving the highest resolution should be chosen. However, the higher the resolution the longer the acquisition times as more projections must be collected and it is important to find the right balance between the two (Bouxsein et al., 2010).

There are two main steps to take during image processing: (1) filtration and (2) segmentation. Filtration is used to remove image noise, this is done firstly by implementing the aluminium filter to reduce beam-hardening that are generated when low energy photons are attenuated as the X-Ray beam passes through the sample (Bouxsein et al., 2010). Additionally, a Gaussian filter may be applied that reduces ring artifacts that can be present in 2D slices around the rotation centre. Generally, a Gaussian filter of 0.8 and support of 1 or 2 voxels is selected for small animal bone studies of morphology (Stauber and Müller, 2008). Segmentation is used by applying a minimum and maximum threshold where those inside the range capture mineralised structures considered to be bone and outside the range eliminates the non-mineralised

structures such as adipose and cartilage tissue. It is preferred that a single global threshold for all scans is possible to ensure consistent comparison between groups, however, sometimes this may not be possible when trying to compare results to another study and thus sometimes applying a global threshold is not possible (Bouxsein et al., 2010). Whilst many previous studies fail to report their applied segmentation thresholds (Bagi et al., 1997; Christiansen, 2016; Mohsin et al., 2019; Yamako et al., 2006), it is important that current studies do report it, in mg HA/cm^3 , to allow for comparison between studies.

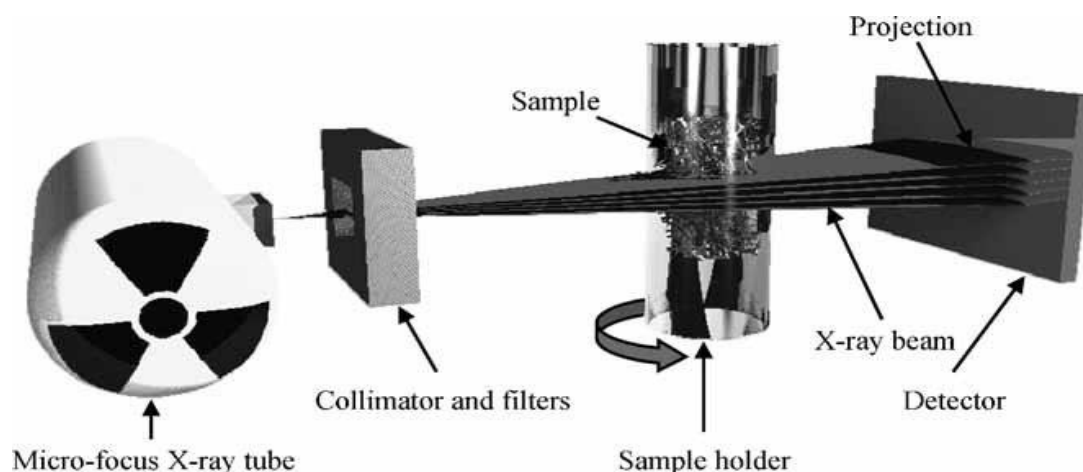


Figure 2.19: A standard micro-CT scanner components where X-rays are emitted from an X-ray tube and are passed through a collimator and filter to eliminate beam hardening and narrow the energy spectrum. C-rays then travel through the sample and the resulting image is projected onto the detector (Bouxsein et al., 2010).

Bone volume fraction of BV/TV , is the volume of bone within a total volume of interest and is determined by applying a threshold that separates the densities of bone from the background and other tissue densities, such as cartilage or marrow (Bouxsein et al., 2010). The area of the bone surface (BS) can also be measured using marching-cubes algorithms to triangulate the bone surface and can be normalised against the total volume (bone surface density, BS/TV) or bone volume (specific bone surface, BS/BV) (Lorensen and Cline, 1987). When estimating the trabecular micro-architecture such as trabecular thickness (Tb.Th), spacing (Tb.Sp) and number (Tb.N) a 3D sphere-fitting or distance-transformation method must be used whereby spheres are fitted into the trabecular structure (Tb.Th) or outside the structure (background or marrow space) (Tb.Sp), the largest diameter of the fitted sphere that can fit in each voxel is determined and each spherical diameter is then averaged (Figure 2.19) (Bouxsein et al., 2010; T. Hildebrand and Rüegsegger, 1997). To calculate Tb.N Euclidean distance mapping is

applied to find the average distance between the mid-axes of each trabeculae (Danielsson, 1980).

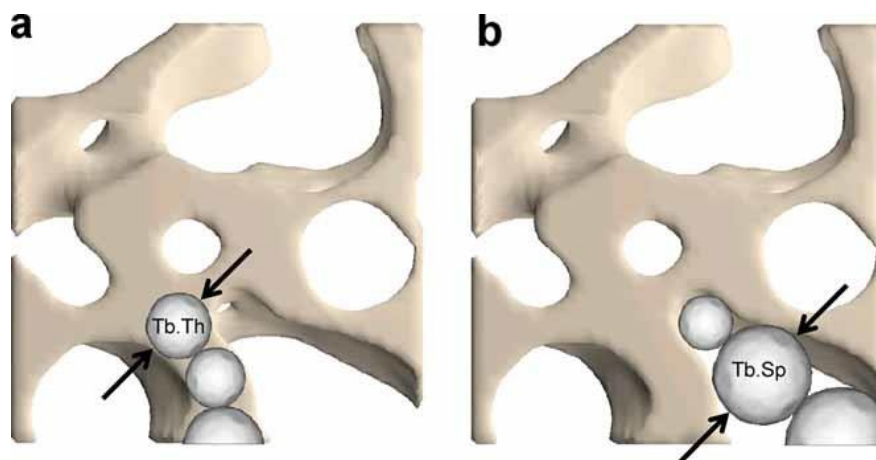


Figure 2.20: Schematic representation describing how (a) trabecular thickness (*Tb.Th*) and (b) separation (*Tb.Sp*) is calculate with micro-CT using a 3D sphere fitting algorithm (Bouxsein et al., 2010).

Connectivity density (Conn.D), gotten from the Euler number, can be used to examine how well trabeculae are connected within the structure. The Euler number is a topological measure that counts the number of trabecular objects, the cavities enclosed by bone minus the number of structures that would have to be broken to split the structure in half and then normalised by TV (Odgaard and Gundersen, 1993). The structural model index (SMI) provides a measure of whether the trabeculae present with a more rod-like or plate-like structure, where an SMI closer to 0 represents a more parallel plate-like structure and an SMI closer to 3 reflects a more cylindrical rod-like structure and in some cases an SMI of 4 represents a more spherical structure (Tor Hildebrand and Rüegsegger, 1997; Salmon et al., 2015). The SMI may also be negative or positive, where a negative SMI indicates a more concave surface and a positive SMI indicates a convex surface (Salmon et al., 2015). Additionally, the Ellipsoid factor (EF) is an alternative method to determine rod/ plate geometry as there is a concern for using SMI on samples with more concave surfaces (Doube, 2015; Salmon et al., 2015). SMI is calculated by using surface mesh dilation as described in (Salmon et al., 2015). The EF is measured using an ellipsoid optimization algorithm, which assumes that the maximal ellipsoids are centred on the medial axis and then dilates, rotates and slightly translates each ellipsoid until it reaches it maximum volume (Doube, 2015). Trabecular orientation can vary depending on mechanical loading and hence, where bone can become anisotropic (Whitehouse, 1974). The degree of anisotropy (DA) describes how highly oriented the trabeculae are within a specified volume of

interest and is commonly measured via the mean intercept length method (Harrigan and Mann, 1985; Whitehouse, 1974). Micro-CT can provide important information on cortical morphometry, as long as the region of interest scanned is at least as long as the cortical thickness (Bouxsein et al., 2010). These properties measured include cortical bone area (Ct.Ar), cortical thickness (Ct.Th) and cortical bone area fraction (Ct.Ar/ total area (Tt.Ar)), where Ct.Th is preferable measured via the distance-transform method (Bouxsein et al., 2010). Additionally, micro-CT can be used to provide information about the moment of inertia (I and J), which can describe the geometric contribution of the bone to resist bending and torsion loading (Jepsen et al., 2015). The I_{\max} or $I_{\text{anterior-posterior(AP)}}$ and I_{\min} or $I_{\text{medial-lateral(ML)}}$ can be measured, which is the moment of inertia along the axis that is hardest and easiest to bend, respectively (Jepsen et al., 2015). The polar moment of inertia (J or pMOI), which is often used when considering resistance to twisting a bone about its long axis, can also be measured using micro-CT where $J = I_{\min} + I_{\max}$ (Bouxsein et al., 2010). When measuring cortical porosity (Ct.Po), total pore volume (Po.V) and number (Po.N) the resolution of the scan must be sufficient since vascular pores can range from 10 μm in diameter down to canaliculi (0.1 μm to 1 μm in diameter). Ideally, the ratio of voxels to object size should be equal or greater than 2, where the higher the ratio the more accurate the morphological measurements.

2.3.2 Bone Mineralisation and Density Distribution

Micro-CT can be an efficient and non-destructive way to include a measure of mineralisation for both cortical and trabecular bone to a study. These properties include bone mineral density (BMD) and tissue mineral density (TMD), where BMD reflects a whole-bone measure of density bone and marrow (non-bone voxels) spaces whereas, TMD represents just the mineral density of the bone tissue itself and does not include the marrow, non-bone spaces (Bouxsein et al., 2010). More recently, bone density information has been used to mineral distribution through a bone mineral density distribution (BMDD) analysis. A BMDD is often created using techniques such as quantitative backscattering electron microscopy (qBEL) or micro-computed tomography (Micro-CT), where the grey levels of the pixels or voxels within the region/ volume of interest are converted into a histogram to describe bone mineral content in g HA/cm^3 (Roschger et al., 2008). From this histogram, the average mineral content (Ca_{mean} or M_{mean}), most frequent mineral content (Ca_{mode} or M_{mode}), mineral heterogeneity or the full width at half maximum of the histogram that describes the varied degree of mineralisation within a given region (Ca_{width} or FWHM), the amount of lowly mineralised bone areas according to the

25th (Ca_{low} or M_{low}) and the amount of highly mineralised bone areas according to the 75th percentile of density distribution (Ca_{high} or M_{high}) can be measured, and this information can be used to interpret bone turnover and the mineralisation process (Donneys et al., 2012; Fratzl et al., 2004; Mashiatulla et al., 2017; Sullivan et al., 2020) (Figure 2.20). Previous studies have used the BMDD to assess how patients with certain bone diseases respond to treatment by examining the histogram shifts towards lower or higher mineralisation (Pritchard et al., 2013; Roschger et al., 2003, 2001). For example, in diseases where the BMDD is shifted towards higher mineralisation, the Ca_{mean} and Ca_{peak} will be greater than normal, and this may be a result of hypermineralisation or low bone turnover (Roschger et al., 2008). In diseases where BMDD is shifted towards lower mineralisation, Ca_{mean} and Ca_{peak} will be lower than normal as an indication of hypomineralisation or a greater amount of lower mineralised tissue present as a result of increased bone turnover (Roschger et al., 2008).

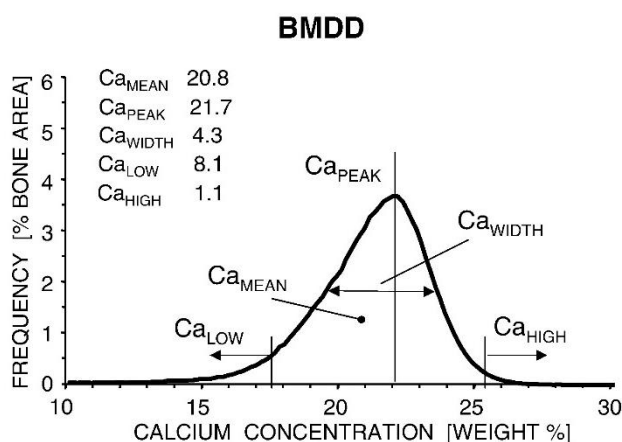


Figure 2.21: Example of a bone mineral density distribution (BMDD) graph resulting from *qBEI* showing the different parameters: Ca_{MEAN} , average calcium concentration from a defined bone area; Ca_{PEAK} , maximum height of the histogram indicating the most frequently measured calcium concentration; Ca_{WIDTH} , the full width at half maximum (FWHM) of the histogram representing mineral heterogeneity or distribution; Ca_{LOW} , percentage of bone area that is lowly mineralised at a given percentile cut-off range; Ca_{HIGH} , percentage of bone area that is highly mineralised at a given percentile cut-off range (Roschger et al., 2008).

2.4 Bone Disease and T2D

2.4.1 Epidemiology and Pathophysiology of T2D

T2D is a metabolic disorder and accounts for 90-95% of diabetic cases (Valderrábano and Linares, 2018), with development often occurring in people over the age of 45 (CDC, 2023)

Alarming with the increased rates of childhood obesity, the development of T2D during childhood or adolescence is a growing concern (Wu et al., 2022) that will result in a continued increase in the prevalence of T2D. Moreover, the prevalence of T2D can be higher among certain groups. A 2022 study compared various countries and explored the prevalence of T2D in 2021 and projections for 2045 and found that the Middle East and North Africa regions to have the highest prevalence of T2D in 2021 (16.2 (8.5–18.3)%) and predicted prevalence for 2045 (19.3 (10.1–21.9)%), followed by North America and the Caribbean (2021: 14.0 (12.3–15.8)%), 2045: 15.2 (13.4–17.3)%) (Sun et al., 2022). Diabetes is regarded as a heterogeneous disease often characterised by elevated blood glucose levels, insulin resistance and impaired insulin secretion. During type-1 diabetes (also known as juvenile diabetes due to diagnosis often occurring early in life), patients possess antibodies that create an autoimmune response against pancreatic islet β -cell antigens, impairing insulin secretion, resulting in a build-up of glucose in the bloodstream, known as hyperglycaemia and are often administered insulin to control the symptoms. Unlike type-1 diabetes, T2D patients often present with reduced insulin sensitivity at different severities, whereby the demand for insulin increases as a result of some insulin resistance within the body but the demand is not met due to impaired insulin secretion (Beck-Nielsen and Groop, 1994; Kahn, 1994) through a variety of mechanisms that contribute to insulin resistance, β -cell dysfunction and an increased inflammatory state (Donath and Shoelson, 2011). It is common with T2D that both microvascular (such as retinopathy, nephropathy and neuropathy) (Faselis et al., 2019) and macrovascular (such as cardiovascular comorbidities) (Duckworth, 2001; Laakso, 2014) complications arise as the patient gets older and the disease progresses, which can negatively impact the patients quality of life and increase their risk of falling or mortality. Interestingly, a study carried out in Ireland by Sanz-Nogués *et al* (Sanz-Nogués et al., 2020) explored the current knowledge, perceptions and concerns of the long-term health complications associated with patients living with type-1 and T2D and found that while retinopathy, amputation and nephropathy were among the most identified complications, diabetes-related osteopathy (represented as “bone fractured” on the questionnaire) was under recognised by both groups.

T2D is normally diagnosed via a diagnostic blood test to measure percentage of glycated haemoglobin (HbA1c), which reflects the mean plasma glucose levels over the past 8- to 12-weeks (Nathan et al., 2007). A diabetic state is confirmed by a HbA1c of $\geq 6.5\%$ (48 mmol/mol) (Bennett et al., 2007). Additionally, an oral glucose tolerance test (OGTT) may be carried out by administering 75 g of an oral glucose solution to the patients and the recording their

blood glucose levels at various time points within a 2-hour window following the consumption. A blood glucose level < 7.8 mmol/L (140 mg/dL) is considered normal, between 7.7 to 11 mmol/L (140 – 199 mg/dL) is considered pre-diabetic and > 11.1 mmol/L (200 mg/dL) confirms a diabetic-state (Bartoli et al., 2011).

2.4.2 Bone Fragility in T2D

Osteoporosis is by far the most-studied bone disease that causes skeletal fragility. It is a disease of bone loss, with the term osteoporosis literally meaning “porous” bone. During osteoporosis, a patient experiences an imbalance in their bone remodelling process, indicated by increased bone resorption with no compensation in bone formation, leading to a net loss of bone and reduced bone density (Christodoulou and Cooper, 2003). Dual X-Ray absorptiometry (DEXA) is the current gold-standard to predict fracture risk of osteoporotic patients, where the clinician gets a measure of the patient’s BMD that can be converted into a T-Score, which describes the number of standard deviations from the population mean (Normal: T-score ≥ -1 ; Osteoporotic: T-score < -2.5) to classify the severity of the disease and the probability of fracture (Lash et al., 2009). The fracture risk algorithm (FRAX®) score can also be used to predict fracture risk whilst also considering other factors such as age, gender and family history (Kanis et al., 2010). Today, more and more patients with T2D are experiencing fractures, with T2D having up to a 3-fold increase in incidence of fracture risk in comparison to non-diabetics (Janghorbani et al., 2006). However, unlike osteoporotic patients, T2 diabetic patients do not present with a reduction in BMD and using a DEXA scan as the current diagnostic technique to predict fracture risk is simply not adequate enough for patients with T2D who often present with normal or high BMD (Bonds et al., 2006; Janghorbani et al., 2007; Schwartz et al., 2013; Vestergaard, 2007). Hence, a re-evaluation of the current diagnostic criteria and the development of an effective fracture risk assessment technique for T2 diabetic bone disease is needed. A summary of several studies that have investigated and report the relative fracture risk in patients with T2D is shown in Table 2.2.

Table 2.2: Summary of fracture risk in patients with T2D from various studies.

Fracture location	Gender (sample number)	Relative risk (RR) [95% CI]	Ref
All	Male & Female (T2D: n = 2979)	RR = 1.64, [1.07 – 2.51]	(Strotmeyer et al., 2005)
All	Female (T2D: n = 5285)	RR = 1.2, [1.11 – 1.30]	(Bonds et al., 2006)
Hip	Male & Female (Systematic review)	M: RR = 2.8, [1.2 – 6.6] F: RR = 2.1, [1.6 – 2.7]	(Janghorbani et al., 2007)
Hip	Female (Systematic review)	RR = 1.38, [1.25 – 1.53]	(Vestergaard, 2007)
Hip (h) and non-spine (ns)	Male & Female (M: n = 5994, F: n = 7926)	M (h): RR = 5.71, [3.42 – 9.53], (ns): RR = 2.17, [1.75 – 2.69] F (h): RR = 1.88, [1.43 – 2.48], (ns): RR = 1.52, [1.31 – 2.69]	(Schwartz et al., 2011)

2.5 Rodent Bone

2.5.1 Growth, Structure and Function

While rodent models are often used to better understand skeletal fragility there are distinct differences between human and rodent bone structure, function and metabolism that are important to consider, to build effective animal studies and make correct conclusions. Human and rodent bone are thought share a similar initial process of cortical bone development, via intramembranous and endochondral ossification, whereby cartilage from the cartilaginous growth plate of long bones becomes gradually mineralised and eventually replaced by new bone tissue (Isojima and Sims, 2021; Wittig and Birkedal, 2022). However, unlike humans, rodent bones do not have Haversian systems and therefore do not undergo Haversian remodelling that is seen in human bone (see Section 2.1). Instead, in rodents, bone begins to mature in the outer and inner circumference of the cortex, depositing a surrounding layer of lamellar bone, while a band of unorganised woven bone remains intra-cortically from endochondral ossification, where residual calcified cartilage remains, as shown in Figure 2.21 (Vanleene et al., 2008). These remaining calcified cartilage islands tend to be highly mineralised and stiffer than the surrounding bone tissue and hence are thought to play a role in bone toughness (Bach-Gansmo et al., 2013). However, it has also been argued that due to the lack of Haversian remodelling it is likely that these cartilage islands accumulate microdamage, which could ultimately contribute to a loss of bone toughness with aging (Launey et al., 2010; Schaffler et al., 1995). Moreover, since the central region of bone was initially formed from endochondral ossification and due to the low remodelling in the central region, it is understood that this region is more mature than outer lamellar regions (Bach-Gansmo et al., 2015, 2013; Busa et al., 2005; Shipov et al., 2013). In addition, the central region is regarded as isotropic since lacunar orientation is randomly organised and less interconnected

within the intracortical region, while in the circumferential lamellar regions, lacunae are highly aligned with the long axis and better connected in some Sprague-Dawley rat strains (Bach-Gansmo et al., 2015; Kerschnitzki et al., 2011), leading to the assumption that the central bone region is quite woven. However, other studies of the Wistar rat strain have used small angle x-ray scattering and found the collagen matrix of the central region to be quite aligned and that the central bone osteocyte lacunae are only randomly oriented in the transverse plane but are quite aligned with the longitudinal plane (Bach-Gansmo et al., 2015). This indicates that there is still confusion over whether this region should be referred to as woven or mature, and arrangement and structural behaviour of rodent bone is yet to be fully elucidated (Bach-Gansmo et al., 2015; Ip et al., 2016; Shipov et al., 2013; Vanleene et al., 2008).

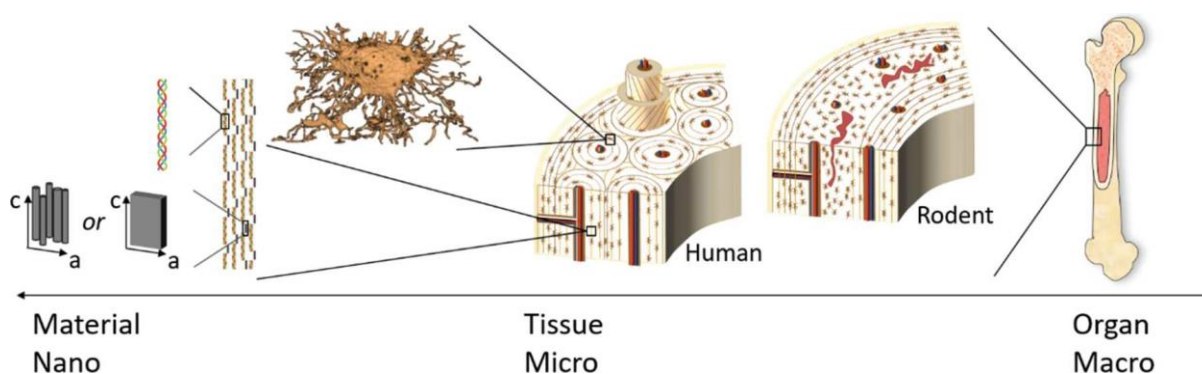


Figure 2.22: Comparison of the main features of human and rodent cortical bone. Both share the fact that at the nanolevel bone is made up of hydroxyapatite mineral crystals and collagen that forms the mineralised collagen fibril, and both have micropores, known as lacunae, that house the osteocyte cells. However, human bone possess Haversian systems and osteons that are important for bone remodelling, whereas rodents do not possess Haversian systems (Wittig and Birkedal, 2022).

The organised, circumferential lamellar regions are found in the periosteal and endocortical regions. It is thought that during bone growth and development, one region is more active in bone formation whilst another is in resorption, similar to that experienced in human bone during modelling. Busa *et al* (2005) explored the primary and secondary mineralisation process during growth in Sprague-Dawley rats and found that the circumferential lamellar bone regions established similar chemical and mechanical properties to that of the older intracortical region during the early stages of modelling, indicating that it may be possible to compare the circumferential lamellar properties to the properties of the intracortical region and determine the end-point of secondary mineralisation. Interestingly, Birkhold *et al* (2016) investigated bone formation and resorption on the periosteal and endocortical regions of bone and how this

was affected during ages and in response to mechanical stimulation. This study found that there was no difference in formation or resorption between endocortical and periosteal regions of control young mouse bone (10-weeks old), whereas, in the control adult (26-weeks) and elderly (78-weeks) mice it was found that bone resorption was increased endocortically, and no resorption activity was found periosteally. In the control elderly mice, there was an increase in bone formation in the endocortical region when compared to the periosteal (Birkhold et al., 2016). When comparing the net effects of bone resorption and formation between the ages it was found that young mice had increased formation and resorption on both surfaces leading to increased cortical thickening and bone volume fraction, whereas, the adult and elderly mice showed increased endocortical resorption and formation but periosteally bone formation and resorption was balanced - leading to cortical thinning and bone loss (Birkhold et al., 2016). It was also found that the periosteal surface was less mechano-responsive than the endocortical regions (Birkhold et al., 2016). This indicates that there are differences between the periosteal and endosteal circumferential lamellar regions of rodent bone.

2.5.2 Pre-Clinical Models of T2D

Table 2.3 and Table 2.4 below summarise the main rodent models that have been used to date to investigate bone fragility in T2D. There are four main classifications of mouse and rat models for T2D, which considers whether they are (1) spontaneous or diet-induced, (2) single gene or polygenic in aetiology, (3) obese or lean, and (4) become diabetic before or after skeletal maturity (Fajardo et al., 2014). Diet-induced models are seen as the more favourable choice to best imitate human T2D aetiology in most regions of the world (O’Hearn et al., 2023). However, the majority of animal studies investigating skeletal fragility have been on the spontaneous rodent breed since they can closely capture characteristic features of T2D such as obesity and insulin resistance and because of their ease of availability (Wang et al., 2013). However, in this spontaneous breed T2D is highly genetic, whereas in humans the development of T2D is more heterogenous. The spontaneous models are then split by single-gene or polygenic aetiologies, where although the polygenic models more closely match the genetic contributions of T2D in human, the single-gene mutation models provide a substantial platform to test specific mechanistic hypotheses (Fajardo et al., 2014). The next classification separates the animal models by a lean or obese characteristic. Obese models have been used quite extensively in research for T2D since 80-90% of human patients with T2D are overweight or obese (Nianogo and Arah, 2022). However, there is a growing cohort of patients in Asia and

other regions that experience T2D while presenting with a low body mass index (BMI) (Li et al., 2013).

Table 2.3: Murine models of bone fragility in type-2 diabetes.

	Tallyho/ JngJ (TH)	Yellow Kuo Kondo (KK/Ay)	Muscle IGF-1R- lysine-arginine (MKR)	C57BL/6J
Classification (age of onset)	Spontaneous, obese (prematurity)	Spontaneous, obese (prematurity)	Spontaneous, lean (prematurity)	Diet-induced, obese
Single or polygenic	Polygenic	Single gene	Single gene	Polygenic
Age of pre- diabetes	4-8 weeks	8 weeks	2 weeks	Never develops frank diabetes
Age of hyperglycaemia	10+ weeks	16 weeks	~8 weeks	\$\$
Gender	Male	Male	Male	Male

\$\$ Diet induced so severity depends on duration of HFD

Table 2.4: Rodent models of bone fragility in type-2 diabetes.

	Diabetic Wistar (WBN/Kob)	Zucker Diabetic Fatty (ZDF)	Zucker Diabetic Sprague Dawley (ZSD)	UCD-T2DM	HFD STZ Sprague Dawley	LepR -/ Lund MetS
Classification (age of onset)	Spontaneous, obese	Spontaneous, obese (prematurity)	Spontaneous, lean (prematurity)	Spontaneous, obese	Diet- induced, non-obese	Spontaneous, obese
Single or polygenic		Single gene	Polygenic			Single gene
Age of pre- diabetes	24-28 weeks	6-10 weeks			4 weeks	
Age of hyperglycaemia	48-52 weeks	~12 weeks	15-21 weeks	~14 weeks	~8 weeks\$\$	16 weeks
Gender	Male	Male	Male	Male	Female	Male

\$\$ Diet induced so severity depends on duration of HFD

Finally, age of onset of the disease is the final category to consider, where rodent models can either become hyperglycaemic or frank diabetic before (pre-maturity) or after (post-maturity) skeletal maturity (Fajardo et al., 2014). It is important to distinguish between the two as both cases may lead to different outcomes in terms of bone development and maintenance. A major downfall in using rodents to model T2D is the issue of male bias in most of the well-established models, whereby the female strains either cannot develop frank diabetes or the severity of the disease is very mild. This means that the majority of research on skeletal fragility in rodent models for T2D has been carried out on males, leaving a large gap in the literature and of the understanding of how skeletal fragility can present in females with T2D, particularly in the presence of oestrogen or oestrogen-deficiency (Díaz et al., 2019). It is important to note that normal and diabetic fasting glucose levels are different in rodents and humans. Rodents have

higher fasting glucose levels (~100 - 199 mg/dL) than humans (< 100 mg/dL) since no typical diabetic symptoms, such as polyuria and polydipsia, are experienced within this range (Clee and Attie, 2007; Svenson et al., 2007). Hence, rodents have higher fasting plasma glucose cut-off level for being considered as diabetic (>250 mg/dL) than humans (>125 mg/dL) (Fajardo et al., 2014).

The Zucker Diabetic Fatty (ZDF) (fa/fa) Rat

The model of interest in this thesis is the Zucker Diabetic Fatty (ZDF) (*fa/fa*) rat strain and compared to the normoglycemic, lean, heterozygous (*fa/+*) controls. The onset and progression of T2D has been well characterised in this model and permits examination of bone properties influenced by alterations to insulin resistance, impaired glucose tolerance and hyperglycaemia (Clark et al., 1983; Peterson et al., 1990). These animals are purposely bred with an abnormal leptin receptor/ leptin receptor signalling, leading to hyperphagia and eventually obesity. At approximately 7-weeks of age the (*fa/fa*) rats show the first signs of hyperglycaemia and at approximately 9-weeks these rats become overtly diabetic with fasting plasma glucose levels reaching 300 mg/ dL (Chen and Wang, 2005; Etgen and Oldham, 2000; Fajardo et al., 2014). Between 7- to 10-weeks serum insulin levels are high resulting in increased bone formation around and subsequently higher BMD than controls at this age (Chen and Wang, 2005; Prisby et al., 2008). However, with the progression of the disease, insulin levels fall as pancreatic β -cells stop responding to glucose stimulus, leading to insulin resistance (Peterson et al., 1990). The ZDF (*fa/fa*) rats are not considered skeletally mature before ~ 16-weeks of age and hence, these rats develop diabetes pre-skeletal maturity, which may have an impact on their bone growth and development (Fajardo et al., 2014; Hughes and Tanner, 1970), which is evident with their small bone phenotype (Prisby et al., 2008; Reinwald et al., 2009). Additionally, these ZDF (*fa/fa*) rats are leptin deficient, which may have an influence on bone size (Steppan et al., 2000).

2.6 Multiscale Bone Biomechanics

The physical function of the skeleton is to provide the body with support to enable movement and protect internal organs. Hence, bone must be able to withstand high, repetitive loads that are applied in a variety of ways including compression, tension, bending and torsion throughout our daily lives. Mechanical properties of bone can differ between tissue types (cortical or trabecular), anatomical location, loading direction (longitudinal or transverse) and, with external factors such as age, body mass index (BMI) and disease all found to influence overall

bone mechanics. The mechanical performance of the tissue depends on both the structural and material aspects of the tissue, whereby the structural mechanical properties are a function of the bone geometry (size and shape), while the material mechanical properties reflect the intrinsic, tissue-level properties regardless of bone geometry (elastic modulus, strength and toughness) (Augat and Schorlemmer, 2006). The tissue-level material properties can be influenced by a variety of things at various length scales, such as the microstructure (porosity and microcracks) and composition whereby alterations to the mineral and collagen arrangement or proportion will influence behaviour.

2.6.1 Mechanical Testing of Small Animal Bone

Macroscale Testing

Bending Tests

Animal studies provide the ability to examine the mechanical properties of bone at different length scales and can help to better understand how bone biomechanics are affected with disease and genetic modifications. At the organ-level, the most traditional types of mechanical testing include three- or four-point bending, compression of torsion loading tests, which in the case of small animal bones can often be carried out on whole-bone specimens. Table 2.5 summarised the structural properties, such as whole-bone stiffness, maximum force, post-yield displacement and work-to-fracture, which can be measured from a standard force-displacement curve from a uniaxial tests (Figure 2.22 (A)). Figure 2.22 (B) shows an example of a load-displacement curve of bone that has exhibited linear and non-linear deformation, also known as elastic and plastic deformation. Elastic deformation is recoverable deformation, whereby when the load is removed the specimen can recover most of its shape and structure, whereas plastic deformation is what occurs after a load is applied past the elastic region until failure where the sample becomes permanently deformed and unrecoverable. The point of transition from elastic to plastic deformation is known as the yield point that is often calculated using an offset method, where a line parallel to the linear region of the force-displacement curve is offset by 0.03% to 0.2% to define the yield point (Turner, 2006). Stiffness is calculated as the slope of the linear (elastic) region of the curve. Post-yield displacement (PYD) is calculated the difference between displacement at yield and at fracture.

Table 2.5: Table describing the different structural properties measured from mechanical testing bone adapted from (Jepsen et al., 2015).

Structural property (units)	Description
Stiffness (N/mm)	The amount of elastic deformation a structure undergoes when loaded.
Maximum force (N)	The greatest force applied before the structure reached a failure point.
Post-yield displacement (mm)	The displacement that occurs between yielding and fracture, indicates brittle or ductile behaviour.
Work-to-fracture (Nmm)	The amount of energy that can be absorbed before failure, measures a structures overall resistance to failure.

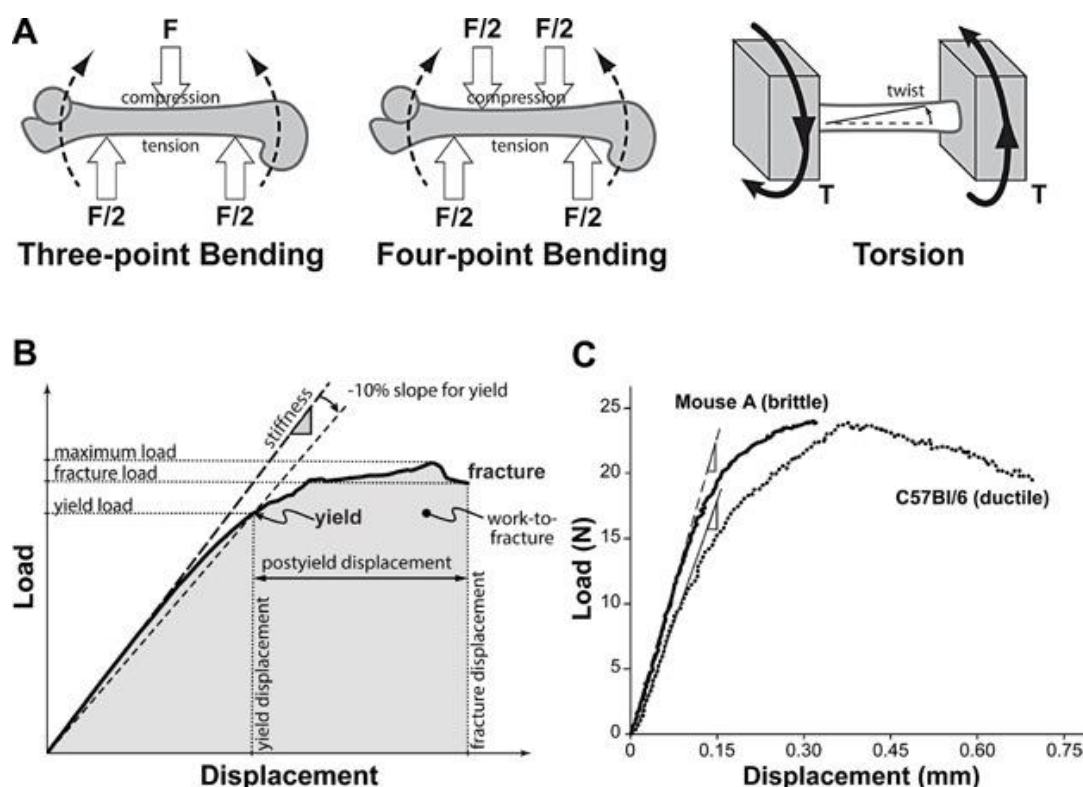


Figure 2.23: (A) Diagrammatic representation of the different loading regimes at the macroscale of small animal femurs such as three-point bending, four-point bending and torsion. (B) A typical load-displacement curve resulting from a standard bending test showing how the various structural-properties can be measured using the curve. (C) Comparing the load-displacement curves from a ductile and brittle bone sample, where post-yield performance of brittle bone is reduced in comparison to the ductile bone sample (Jepsen et al., 2015).

Likewise, tissue-level mechanical properties can be measured from force-displacement curves converted into stress (σ) -strain (ϵ) curves. Stress is fundamentally described as force (F)

normalised by area (A) over the region where the compressive or tensile force is applied. Uniaxial strain represents the deformation and is defined as the change in length (ΔL) of a sample normalised by the initial length (L_0). Tissue-level stiffness, known as elastic modulus, is measured as the slope of the linear part of the stress-strain curve reported in MPa (N/mm^2). Ultimate stress is the maximum stress reached before failure reported in MPa, while post-yield strain is the material-level equivalent of PYD reported as a unitless dimensions or percentage and toughness is essentially the material-level equivalent of work-to-fracture reported in MPa, however, measuring toughness in small animal bones is not recommended since beam theory are only valid within the linear region, and determining toughness entails significant consideration of nonlinear post-yield behaviour. Bending tests are often used to determine mechanical properties of long bones such as humeri, radii, ulnae, femora, and tibiae (Figure 2.22 (A)). In mechanical testing of small animal bones, the three-point bend test is preferred as it is easier to apply to smaller sized samples (Steiner et al., 2015). These bending tests use beam theory to relate the structural- and tissue-level response of long bone samples to account for test geometry and configuration. In this case, force must be converted to moment (M) and displacement into normalised displacement (d'). From the moment-normalised displacement curve, the above-described structural properties can be measured where stiffness is referred to as bending rigidity. Material-properties can then be calculated using beam theory Equations dependant of that sample shape, which often employs the use of moment of inertia that describes the geometric contribution of bone to resist bending (Jepsen et al., 2015). In many cases, elastic modulus is under-predicted when measured using beam theory from bending tests due to the aspect ratio (span length: bone width) of the samples, since beam theory assumes an aspect ratio $>16:1$ (van Lenthe et al., 2008). Nevertheless, bending tests are still deemed a useful way of estimating tissue-level properties of bone, since these tests are often quick to perform as they require little-to-no samples preparation.

Skeletal biomechanical properties of rodent bone can differ depending on the anatomical site tested and animal strain. Schriefer *et al.* (2005) compared the mechanical properties derived from multiple skeletal sites (femur, humerus, metatarsal, radius and tibia) from mice of different strains (C57BL/6J and C3H/HeJ) using a three-point bend test and using an FE model to examine measurement error. It was found that bones with the highest aspect ratio and greater thickness to radius ratio were better for bend testing and reduced measurement error. It was also concluded that the radius bone was preferred for mechanical testing due to its higher aspect ratio (Schriefer et al., 2005). Toughness can also be estimated by three-point bend testing;

however, it can also be misinterpreted via beam theory and essentially reflects tissue strength in the presence of defect distribution within the bone rather than the bone matrix structure and is written in units of energy (mJ) (Ritchie et al., 2008).

Fracture toughness test

Fracture toughness testing is a method to measure a material's resistance to fracture in the presence of a dominant flaw of a known size and is a more accurate measure of fracture resistance. Fracture toughness can be examined using linear elastic and non-linear elastic fracture mechanics. Linear-elastic fracture analysis is often used to determine stress required to induce a brittle fracture in the presence of a defect particularly when the size of the plastic zone is less than the cross-section of the specimen, which is known as “small-scale yielding” (Richard and Sander, 1973). Well-established methods for assessing fracture mechanics of metallic materials under mode I (K_I) (opening of a notch under tension) are described in the ASTM E-399 (ASTM E-399, 2014). This method has also been applied to cortical bone, whereby a sample is sectioned from the whole-bone, notched specimens tested using a single-edge notched three-point bend (SENB) or compact tension (CT) test (Ritchie et al., 2008). Fracture parameters are calculated using Equation 2.1 and 2.2, where P is the applied load, S is the loading span, $f(\frac{a}{W})$ and $f'(\frac{a}{W})$ are geometric functions of $(\frac{a}{W})$ taken from ASTM 1820 (ASTM E1820, 2012).

$$K_I = \frac{PS}{BW^{\frac{3}{2}}} f\left(\frac{a}{W}\right) \quad (2.1)$$

and,

$$K_I = \frac{P}{BW^{\frac{3}{2}}} f'\left(\frac{a}{W}\right) \quad (2.2)$$

Generating an atomically sharp notch is important as the stress intensity developed at a notch can be severely reduced if the stress concentrator is not sharp (Nishida and Hanak, 1994). Plane strain fracture toughness is denoted as K_{IC} , which measures the resistance of a material to crack extension under linear elastic conditions and can be taken at crack initiation or crack instability. For fracture toughness testing of small animal bones, due to their small and complicated geometry, it is difficult to section the tissue into a known dimension for testing as per a SENB or CT test and hence, the whole bone must be tested. In this case, long bones such as the femur are the preferred bones to use for fracture toughness testing (Vashishth, 2009), whereby femora

are notched on the posterior or anterior and loaded adjacent to the notch until failure in a three-point bend configuration where Equation 2.3 - 2.6 is used to calculate mode I stress intensity factor by assuming the long bone as a thick-walled hollow cylinder (Ritchie et al., 2008).

$$K_I = F_b \sigma_b \sqrt{\pi R_m \theta} \quad (2.3)$$

Where R_m is the mean radius, t is cortical thickness, θ is the half-crack angle and σ_b is the applied bending stress, defined as:

$$\sigma_b = \frac{MR_o}{\frac{\pi}{4}(R_o^4 - R_i^4)} \quad (2.4)$$

Where M is bending moment ($M = \frac{PS}{4}$), R_o and R_i is the outer and inner radius of the cortical shell, respectively, and F_b is a geometry factor given as:

$$F_b = \left(1 + \frac{t}{2R_m}\right) \left[A_b + B_b \left(\frac{\theta}{\pi}\right) + C_b \left(\frac{\theta}{\pi}\right)^2 + D_b \left(\frac{\theta}{\pi}\right)^3 + E_b \left(\frac{\theta}{\pi}\right)^4 \right] \quad (2.5)$$

$$A_b = 0.65133 - 0.5774\varepsilon - 0.3427\varepsilon^2 - 0.0681\varepsilon^3$$

$$B_b = 1.879 + 4.795\varepsilon + 2.343\varepsilon^2 - 0.6197\varepsilon^3$$

$$C_b = -9.779 - 38.14\varepsilon - 6.611\varepsilon^2 + 3.972\varepsilon^3$$

$$D_b = 34.56 + 129.9\varepsilon + 50.55\varepsilon^2 + 3.374\varepsilon^3 \quad (2.6)$$

$$E_b = -30.82 - 147.6\varepsilon - 78.38\varepsilon^2 - 15.54\varepsilon^3$$

$$\varepsilon = \log\left(\frac{t}{R_m}\right)$$

Crack initiation is regarded as the stress intensity required to form a crack whereas crack instability is the event that occurs well after crack initiation. There are several approaches that may be taken to measure both for small animal bones shown in Figure 2.23. The first approach that may be taken to calculate crack initiation using half-notch angle (θ_{init}) and the 5% secant method to find the load (P_Q) at the intercept of the load-displacement curve using a 5% secant line as per ASTM E-399 standard (ASTM E-399, 2014) as shown in Figure 2.23. However, this method requires that the ratio of P_{max} to P_Q is less than or equal to 1.1 and hence is deemed

to be an inaccurate method of calculating fracture toughness in small animal bones due to the presence of plasticity in smaller sized samples. This method also produces lower values for fracture toughness than the other two approaches (Ritchie et al., 2008). Therefore, the alternative approach is to use the maximum load method that calculates crack instability at maximum load (P_{max}) using θ_{init} . This is a more straightforward approach to calculate crack instability but can also be inaccurate since crack initiation rarely occurs exactly at the maximum load, although Ritchie *et al.* (2008) showed that the maximum load method produced the lowest coefficient of variation for all of the approaches. Hence, the last approach is the crack instability approach whereby the crack instability using the load at failure (P_f) and crack angle (θ_{inst}) is determined. Each of the three approaches can be applied to Equation 2.7 to calculate fracture toughness of small bones by interchanging θ_c and P_s depending on the method used.

$$K_c = F_b \frac{P_s S R_o}{\pi(R_o^4 - R_i^4)} \sqrt{\pi \theta_c} \quad (2.7)$$

Where S is the span length.

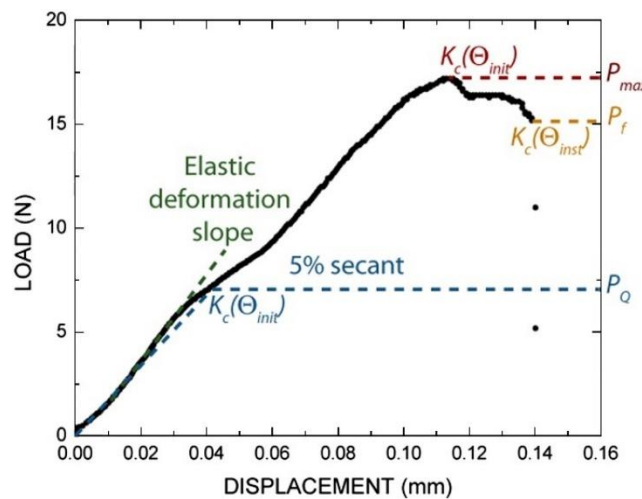


Figure 2.24: Different methods of measuring fracture toughness (K_c) using the resulting load-displacement curve such as crack initiation using load at the 5% secant (P_Q) and notch angle (θ_{init}), crack initiation at maximum load (P_{max}) using notch angle (θ_{init}) and crack instability using the load at failure (P_f) and crack angle (θ_{inst}) (Ritchie et al., 2008).

In addition to a linear elastic analysis, the non-linear elastic approach may be employed in the case where a material exhibits more extensive plastic deformation. In this case, the J-integral

can be measured as outlined in ASTM E1820 (ASTM E1820, 2012) . J-based measurements are important for bone due to the formation of diffuse damage and microcracks, which are generally thought to be mechanisms of inelastic behaviour (Yan et al., 2007). However, this method requires accurate observations over crack extension and load-line displacement that would require the use of an *in-situ* mechanical test set-up with an environmental SEM (Koester et al., 2008). This is not always feasible for testing carried out regularly and due to issues with validity of results Richie *et al.* (2008) concluded that using the J-integral to measure toughness of small-animal bones is not recommended.

Microscale testing

Nanoindentation

It can be difficult to accurately determine tissue-level properties of bone using macro-mechanical testing, due to its complex hierarchical structure. At the microscale, nanoindentation testing enables the local estimation of tissue properties such as hardness and elastic modulus. Nanoindentation is based on the principle of hardness testing and the standard method for estimating modulus and hardness by indentation was developed by Oliver and Pharr (Oliver and Pharr, 1992, 2004). An indentation test is performed using a depth-sensing diamond indenting tip that can be spherical, conical and most-commonly used with bone, Berkovich shaped.

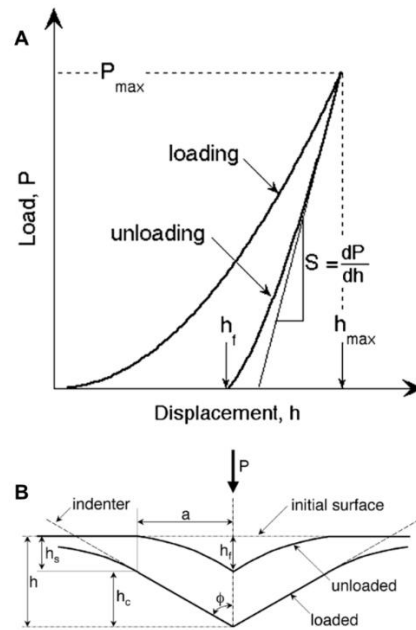


Figure 2.25: (A) Illustration of the indentation loading profile and (B) diagram of the unloading process of the indenter showing the parameters that characterize contact geometry (Oliver and Pharr, 2004).

During the test an electromagnetic actuation system drives the indenter tip into the polished sample surface under either load- (mN) or displacement-control (nm) at a constant rate and the load-displacement data is collected for each loading and unloading cycle by a high-resolution sensor. In this thesis the G200 Nano Indenter (Keysight Technologies, USA) was used that can test up to a maximum load of 500 mN and to a depth as low as 0.01 nm (Keysight Technologies Inc., 2017). Importantly, bone behaves in a viscoelastic manner due to the existence of collagen fibrils and water, which can result in buckling and creep of the material during indentation. Thermal drift, which should ideally stay below 0.001 mm/s, can also occur during nanoindentation (Keysight Technologies Inc., 2017). To control for the effects of viscoelasticity and thermal drift, a “hold” period is implemented such that the indenter is held at peak loading depth for a defined period of time (preferably 15 or more seconds) before measurements are recorded (Wu et al., 2011). Hardness is calculated using Equations 2.8 – 2.13, where P is the indentation load, α and m are power-law fitting constants, h is the indentation displacement and h_f is the final depth of indentation after complete loading.

$$P = \alpha(h - h_f)^m \quad (2.8)$$

From the power-law relation, initial loading stiffness (S) is determined by $= \frac{dP}{dh}$:

$$S = m\alpha(h_{max} - h_f)^{m-1} \Big|_{h=h_{max}} \quad (2.9)$$

Where h_{max} is the maximum depth. The contact depth (h_c) over which the indenter contacted the material, is calculated as the difference between the maximum and sink-in depth (h_s) by including a constant based on tip geometry (ε) ($\varepsilon = 0.75$ for a Berkovich indenter), such that:

$$h_c = h_{max} - h_s \quad (2.10)$$

$$h_c = h_{max} - \varepsilon \frac{P_{max}}{S} \quad (2.11)$$

To calculate hardness (H) the projected contact area (A_c) is required, which is calculated using an empirically determined area function at contact depth (h_c):

$$A_c = C_1 h_c^2 + C_2 h_c^1 + C_3 h_c^{\frac{1}{2}} + C_4 h_c^{\frac{1}{4}} + \dots + C_8 h_c^{\frac{1}{128}} \quad (2.12)$$

where C_1 to C_8 are constants calculated during instrument calibration. The initial term reflects the changing of the indenter tip shape from a pyramidal shape and the remaining describes the blunting of the tip from a conical shape. Finally, from this hardness (H) can be calculated:

$$H = \frac{P_{max}}{A_c} \quad (2.13)$$

According to Oliver and Pharr (1992), when using a Berkovich indenter tip, contact stiffness (S) is calculated from the slope of the maximum load (P) and the penetration depth (h) from the upper 25% of the unloading curve using Equations 2.14 – 2.15, since the unloading curve only measures elastic deformation recovery whereas the loading curve reflects both elastic and

plastic deformation (Oliver and Pharr, 1992) (Figure 2.24). The elastic modulus (E) is calculated by:

$$E_r = \frac{\sqrt{\pi}S}{2\beta\sqrt{A_c}} \quad (2.14)$$

where E_r is the reduced modulus, β is a constant ($\beta = 1.034$ for a Berkovich tip). Finally, elastic modulus (E) is calculated as:

$$\frac{1}{E_r} = \frac{(1 - \nu^2)}{E} + \frac{(1 - \nu_i^2)}{E_i} \quad (2.15)$$

where ν is Poisson's ratio ($\nu = 0.3$), E_i is the indenter elastic modulus ($E_i = 1141$ GPa), ν_i is the indenter Poisson's ratio ($\nu_i = 0.07$).

Micro-pillar compression testing

Whilst nanoindentation is useful to accurately measure elastic modulus and hardness, a limitation of this technique is that plastic deformation cannot be captured. Interestingly, research by Schwiedrzik *et al.* (2014) showed that the post-yield and failure behaviour of bone differs from the macrolevel to the microlevel, where bone behaved more ductile and exhibited an anisotropic elastoplastic behaviour at the microscale in comparison to displaying a quasi-brittle response at the macroscale. Hence, micropillar compression testing is an alternative micromechanical method to assess the yield and post-yield response of bone to loading, whereby micro-sized pillars are milled from a bulk sample using a focused ion beam and compressed under a controlled displacement to a defined maximum depth with an intermittent unloading segment in the elastic region, using an indenter tip of a known geometry (Kochetkova *et al.*, 2021; Wolfram and Schwiedrzik, 2016) (Figure 2.25). Milling a micro-sized bone sample removes the presence of a defect such as a microcrack or pore, which can result in increased failure stresses at the microscale when compared to stresses at the macroscale (Morgan *et al.*, 2018; Schwiedrzik *et al.*, 2014). This observation is in line with the scaling theory of quasi-brittle failure and highlights the presence of a size effect in bone (Bažant, 2004; Wolfram and Schwiedrzik, 2016). After compression testing is carried out on the micropillar samples, load-displacement curves are obtained and can be converted into

stress-strain curves following frame compliance and sink-in corrections, where then elastic modulus and yield stress can be calculated. These corrections must be made to allow for accurate measurement of the elastic modulus (Zhang et al., 2006). Methods for calculating the apparent elastic modulus and yield stress discussed in this Section were taken from (Kochetkova et al., 2021). The apparent elastic modulus (E_{app}) was modelled as a function of collagen fibre orientation, where a transverse isotropic compliance tensor shown in Equation 2.16, is rotated around one axis from the transverse plane and hence E_{app} can be expressed as a function of fibril angle after fitting. (Equation 2.17):

$$[[c]] = \begin{pmatrix} \frac{1}{E_t} & -\frac{\nu_t}{E_t} & -\frac{\nu_a}{E_a} & 0 & 0 & 0 \\ -\frac{\nu_t}{E_t} & \frac{1}{E_t} & -\frac{\nu_a}{E_a} & 0 & 0 & 0 \\ -\frac{\nu_a}{E_a} & -\frac{\nu_a}{E_a} & \frac{1}{E_a} & 0 & 0 & 0 \\ 0 & 0 & 0 & \frac{1}{2\mu_a} & 0 & 0 \\ 0 & 0 & 0 & 0 & \frac{1}{2\mu_a} & 0 \\ 0 & 0 & 0 & 0 & 0 & \frac{1+\nu_t}{E_t} \end{pmatrix}, \quad (2.16)$$

$$E_{app} = \left(\frac{\cos^4(\theta)}{E_a} + \frac{\sin^4(\theta)}{E_t} + \left(\frac{1}{\mu_a} - 2\frac{\nu_a}{E_a} \right) \cos^2(\theta) \sin^2(\theta) \right)^{-1} \quad (2.17)$$

Where E_a and E_t are elastic modulus in the axial and transverse direction, respectively, ν_a and ν_t are directional Poisson's ratios and μ_a is the shear modulus.

Yield stress was similarly modelled as a function of collagen fibril orientation using Tsai-Hill composite function criterion (Tsai and wu, 1971). For unidirectional fibre-reinforced composite materials experiencing in-plane stress, the failure criterion is written as:

$$\left(\frac{\sigma_a}{X} \right)^2 - \left(\frac{\sigma_a \sigma_t}{X^2} \right) + \left(\frac{\sigma_t}{Y} \right)^2 + \left(\frac{\tau}{S} \right)^2 = 1 \quad (2.18)$$

Where σ_a and σ_t are normal stresses in the axial and transverse directions, τ is the in-plane shear stress, X , Y and S represent strength of the material in the longitudinal, transverse and

shear direction. In the uniaxial loading direction, normal and shear stresses are written as a function of fibre angle (θ):

$$\sigma_a = \sigma_x \cos^2(\theta),$$

$$\sigma_t = \sigma_x \sin^2(\theta), \quad (2.19)$$

$$\tau = \sigma_x \sin(\theta) \cos(\theta)$$

By inserting Equation 2.19 to 2.18, the resulting stress applied along the uniaxial loading direction (σ_x) where fibres are oriented along $\theta = 0^\circ$:

$$\sigma_x = \left(\left(\frac{\cos^2(\theta)}{X} \right)^2 - \left(\frac{\sin(\theta) \cos(\theta)}{X} \right)^2 + \left(\frac{\sin^2(\theta)}{Y} \right)^2 + \left(\frac{\sin(\theta) \cos(\theta)}{S} \right)^2 \right)^{\frac{1}{2}}. \quad (2.20)$$

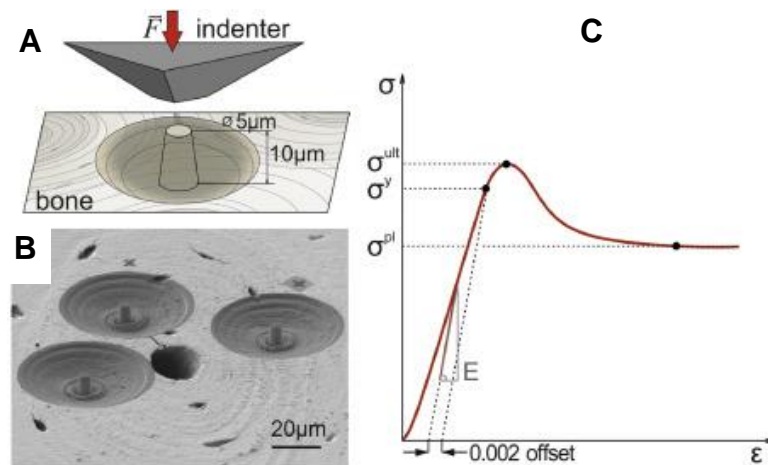


Figure 2.26: (A) An illustration of the compression configuration of a micropillar. (B) A HRSEM image of fabricated micropillars surrounding an osteon and (C) a stress-strain curve with output parameters marked on the curve, where elastic modulus (E) is calculated from the slope of the curve; yield stress (σ_y), defined as stress at 0.2% inelastic deformation; ultimate stress (σ_{ult}) is maximum stress and (σ_{pl}) is the plateau stress (Kochetkova et al., 2021).

Table 2.6 below compares the range of values of various tissue-level properties from the different types of mechanical testing. It can be seen that three-point bend testing greatly underpredicts elastic modulus in rodent tissue, when compared to results from the nanoindentation. Additionally, elastic modulus and hardness values are higher when tested in

the longitudinal direction versus the transverse, which shows the role collagen fibre direction plays in tissue mechanics. Fracture toughness values ranged from 2.6 – 9.6 MPa.m^{1/2} and it was also shown that carrying out mechanical testing on dry bone samples leads to markedly increased elastic modulus and Stress values in comparison to testing samples wet.

Table 2.6. Comparison of tissue-level properties over different bone types, specimen and mechanical tests.

Mechanical test	Ref	Specimen	Anatomical location	$\frac{E \text{ (GPa)}}{H \text{ (GPa)}}$	σ_u / σ_y (MPa)	Toughness
Three-point bend	(Stefan et al., 2010)	Human	Femur	17.9 ± 1.0	σ_u : 183.8 ± 15.1	Elastic: 86.7 ± 7.7 mJ/mm ³ Plastic: 148.7 ± 48.3 mJ/mm ³
	(Stefan et al., 2010)	Bovine	Femur	22.4 ± 1.4	σ_u : 231.4 ± 1.9	Elastic: 197.3 ± 55.5 mJ/mm ³ Plastic: 186.8 ± 79.9 mJ/mm ³
	(Zhang et al., 2018)	Bovine	Femur (L)	22.6 ± 2.8	σ_u : 218.6 ± 30.4	
			Femur (T)	13.8 ± 2.3	σ_u : 104.9 ± 21.9	
	(Rezaee et al., 2020)	Rat	Ulna	24.5 ± 4.1	σ_u : 6.62 ± 0.65	
	(Acevedo et al., 2018)	Rat	Ulna	18.3 ± 0.7	σ_u : 280 ± 5 σ_y : 251 ± 2	
	(Uppuganti et al., 2016)	Rat	Femur (6 months)	6.5 ± 0.7	σ_u : 215 ± 15	4.1 ± 1.2 mJ/m ³
			Femur (12 months)	5.9 ± 0.8	σ_u : 200 ± 25	3.2 ± 0.6 mJ/m ³
			Femur (24 months)	4.5 ± 0.7	σ_u : 180 ± 30	3.6 ± 0.7 mJ/m ³
	(Schriefer et al., 2005)	Mouse (C57B6/J)	Femur	10.9 ± 0.2	σ_u : 240 ± 10	9.8 ± 0.3 MPa
(Willett et al., 2019)	Human	Femur			$K_{c,init}$ (MPa.m ^{1/2}): 9.5 ± 2.4	
Fracture toughness (linear elastic)	(Yan et al., 2007)	Bovine	Femur (L)			2.6 ± 0.3 MPa.m ^{1/2}
			Femur (T)			5.1 ± 0.5 MPa.m ^{1/2}
	(Uppuganti et al., 2016)	Rat	Femur (6 months)			$K_{c,init}$ (MPa.m ^{1/2}): 8.3 ± 0.3 $K_{c,insta}$ (MPa.m ^{1/2}): 8.3 ± 0.6 T_{cr} (MJ/m ³): 0.35 ± 0.1
			Femur (12 months)			$K_{c,init}$ (MPa.m ^{1/2}): 9 ± 0.7 $K_{c,insta}$ (MPa.m ^{1/2}): 8.1 ± 0.8 T_{cr} (MJ/m ³): 0.22 ± 0.

Mechanical test	Ref	Specimen	Anatomical location	E (GPa)	σ_u / σ_y (MPa)	Toughness
				H (GPa)		
Nanoindentation			Femur (24 months)			$K_{c,init}$ (MPa.m ^{1/2}): 9.5 ± 0.9 $K_{c,insta}$ (MPa.m ^{1/2}): 9.6 ± 0.7 T_{cr} (MJ/m ³): 0.2 ± 0.09
	(Carriero et al., 2014)	Mouse (Balb)	Femur			$K_{c,init}$ (MPa.m ^{1/2}): 6.2 ± 0.3
	(Turner et al., 1999)	Human (dry)	Femur (Cortical)	20 ± 0.3	-	
			Femur (Trabecular)	18.1 ± 1.7	-	
			Femur (L) (Cortical O)	22.5 ± 1.3	0.61 ± 0.04	
	(Rho et al., 1997)	Human (dry)	Femur (L) (Cortical I)	25.8 ± 0.7	0.74 ± 0.03	
			Femur (T) (Trabecular)	13.4 ± 2.0	0.47 ± 0.08	
			Femur (L) (Cortical O)	15.8 ± 5.3	0.234 - 0.760	
	(Zysset et al., 1999)	Human (wet)	Femur (L) (Cortical I)	17.5 ± 5.3	0.234 - 0.760	
			Femur (T) (Trabecular)	11.4 ± 5.6	0.234 - 0.760	
	(Liu et al., 2021)	Rat (dry)	Femur	20.7 ± 4.6	0.7 ± 0.2	
	(Shipov et al., 2013)	Rat	Femur (Lamellar)	27.8 ± 3.2	1.13 ± 0.2	
			Femur (Woven)	30.1 ± 3.4	1.15 ± 0.2	
			Femur (L) (Proximal)	18 ± 3	0.7 ± 1	
	(Casanova et al., 2017)	Mouse (wet)	Femur (T) (Proximal)	12 ± 3	0.55 ± 1	
			Femur (L) (Central)	19 ± 2	0.65 ± 0.9	
			Femur (T) (Central)	13 ± 2	0.65 ± 1	
	Micro-pillar compression	(Indermaur et al., 2021)	Human (Dry)	Transiliac crest (Cortical)		σ_u :590 ± 128 σ_y :350 ± 97
			Dry (A)	27.5 ± 2.2 1.01 ± 0.1	σ_u :750 ± 60 σ_y :490 ± 10	
(Schwiedrzik et al., 2014)		Ovine (Tibia, Cortical)	Dry (T)	19 ± 1.8 0.67 ± 0.1	σ_u :590 ± 40 σ_y :300 ± 20	
			Wet (A)	22.8 ± 1.6 0.6 ± 0.11	σ_u :180 ± 21 σ_y :170 ± 22	
			Wet (T)	14.5 ± 1.6 0.51 ± 0.1	σ_u :170 ± 15 σ_y :130 ± 25	
(Kochetkova et al., 2022)		Minipig (Yucatan)	Jaw (Cortical)	12.9	σ_y : 295	
(Maghsoudi-Ganjeh et al., 2021)	Mouse (wild type)	Femur (Cortical)	13.9 ± 2.7	584 ± 157		

L, Longitudinal; T, Transverse; A, Axial; E, Elastic modulus; H, Hardness; σ_u , Ultimate stress; σ_y , Yield stress.

2.6.2 Computational Modelling

Finite element (FE) modelling provides a mathematical formulation of a structure that includes geometry and mechanical properties unique to that structure, where loading conditions can be applied to understand the mechanical environment. Finite element analysis (FEA) has been widely used in the mechanical analysis of bone as it provides a non-invasive and efficient way to assess the different stress-strain states and distributions in reaction to different applied forces. Image-based FE modelling has become increasingly popular particularly the use of patient-specific FE modelling, whereby Digital Imaging and Communications in Medicine (DICOM) files obtained from micro-CT have been used to generate a 3D reconstructed model containing voxel-specific density information for the tissue by converting grey values to Hounsfield units (HU). However, due to the heterogeneous nature of bone a correction is needed for this conversion since the phantoms used for density calibration in micro-CT are homogeneous, which is achieved by comparing a ratio relationship of CT density to ash density $\left(\frac{\rho_{qCT}}{\rho_{ash}}\right)$ (Dragomir-Daescu et al., 2011; Schileo et al., 2008). When establishing the relationship between bone mineral density and elastic modulus, a power-law is used, which can change depending on tissue type and subject (i.e. animal strain) (Cory et al., 2010; Verbruggen and McNamara, 2023). Imaging processing software, such as Materialise MIMICS (Belgium), allows for the ease of reconstructing 2D DICOM images to a 3D model with voxel-specific material properties mapped onto each element. Here, the 3D structure is separated into multiple smaller units known as elements that are attached to each other by nodal points (Figure 2.26). Each element is assigned a unique material property (i.e., density, elastic modulus and Poisson's ratio) and boundary conditions can be applied to the model to represent the forces or displacements that are physically encountered. The behaviour of the structure is predicted when the applied constitutive Equations are calculated for each element and matrix stiffness is then defined. Stress and strain can then be calculated from the entire model, incrementally, for each applied load or displacement at the nodes, via integration points within the elements. The stress distributions are then calculated through interpolation functions that may be either linear or quadratic to determine displacements at arbitrary points within the element, outputting what is known as a displacement field, which can then be differentiated to output the strain field (Dailey et al., 2023). Stress is then established via the defined material variables of each element such as density, elastic modulus and Poisson's ratio (Dailey et al., 2023).

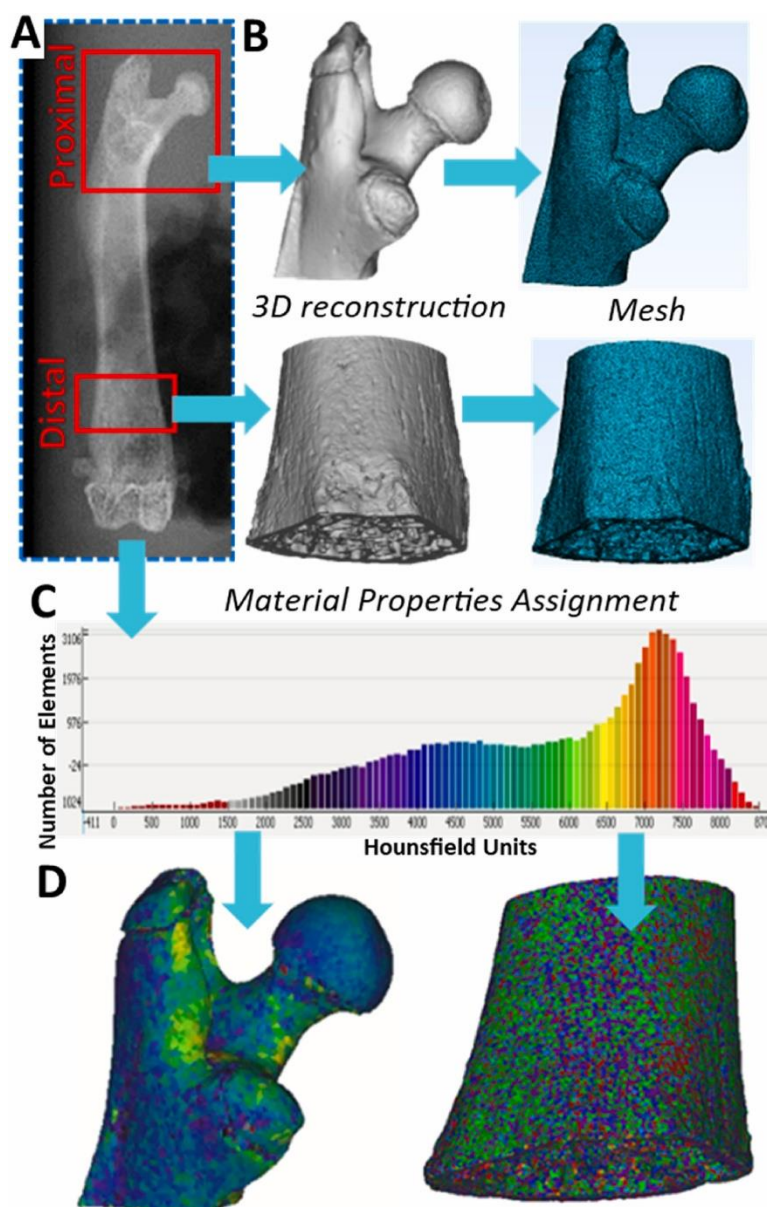


Figure 2.27: A schematic of the development of an FE model moving from (A and B) micro-CT 3D reconstructed images to (C) importing DICOM images into Mimics and 3-Matic software to (C and D) apply a mesh and voxel-specific material properties (Verbruggen and McNamara, 2023).

2.6.3 Mechanisms of Fracture Resistance in Bone

There are a variety of factors that contribute to fracture resistance such as bone density, mineral distribution and heterogeneity, tissue microarchitecture and quality of the collagen matrix components. These factors may become altered with aging and disease and lead to an increase in fracture risk. Bone's ability to resist fracture is mainly attributed to its toughness that can occur through, (1) intrinsic (ahead of crack tip) toughening mechanisms of deformation such as fibrillar sliding and, (2) extrinsic (behind crack tip) mechanisms that act to shield the crack

from the applied driving force, which results in crack bridging or crack deflection (Launey et al., 2010).

Intrinsic toughening mechanisms

At its most basic, plastic deformation starts to occur with individual collagen molecules undergoing an uncoiling phase during crack initiation. Hydrogen-bonds (H-bonds) are broken to allow molecular stretching and unwinding and intermolecular sliding of molecules are observed, which allows for larger plastic strains to be tolerated without the cause of catastrophic brittle failure (see Figure 2.27) (Launey et al., 2010; Ritchie, 2010). Once yielding begins, fibrillar sliding occurs, where mineral particles and tropocollagen molecules of the mineralised collagen fibrils are allowed to glide over one-another, thus, enabling efficient dissipative deformation (Gupta et al., 2006) (Figure 2.27). A study by Buehler *et al.* (2007), assessed the stress-strain response of an unmineralised and mineralised collagen fibril under a tensile load and found that mineral crystals allowed the fibril to reach large stresses and increases energy dissipation during deformation as the mineral crystals increased the fibrils resistance to slip. It is understood that at this scale enzymatic collagen crosslinks play an important role in controlling deformation and strength by stabilising the structure. Conversely, non-enzymatic crosslinks have been found to increase with age and with some diseases (i.e., T2D) (Nyman, 2013; Nyman et al., 2007; Wang et al., 2002), particularly the formation of AGEs. AGEs are proposed to impair the structural integrity of the fibrils by stiffening the collagen network and preventing fibrillar sliding (Buehler, 2007; Siegmund et al., 2008; Vashishth et al., 2001). Conversely, non-collagenous proteins contribute to the fracture resistance of bone, acting as a glue that holds mineralised collagen fibrils together to form the collagen fibre (Figure 2.27) (see Section on *non-collagenous proteins*). In an aqueous environment these bonds can re-form and in fact water can play a role in fracture resistance since water is bound to both the collagen and mineral component via H-H bonding (Nyman and Makowski, 2012). Microcracking is also an important feature of intrinsic toughening deformation at the microscale as it provides plastic deformation whilst also allowing the progression towards extrinsic toughening mechanisms.

Extrinsic toughening mechanisms

Extrinsic toughening mechanisms generally arise during crack growth. The main features of extrinsic toughening are constrained microcracking, crack deflection and bridging. In cortical bone, microcracking tends to occur in hyper-mineralised regions around cement lines that are

mainly aligned in the longitudinal direction. Whilst microcracking is deemed as an important mechanism of intrinsic toughening, microcracking provides a minimal contribution to extrinsic toughness. However, microcracking is important as it allows for crack bridging and deflection to occur, these are formidable toughening mechanisms of bone (Launey et al., 2010). Although cortical bone exhibits greater strength and stiffness in the longitudinal than the transverse direction, toughness is generally lower in the longitudinal direction since microcracks tend to run parallel to cement lines. Hence, the longitudinal direction (crack bridging) experiences a different toughening mechanism than the transverse direction (crack deflection).

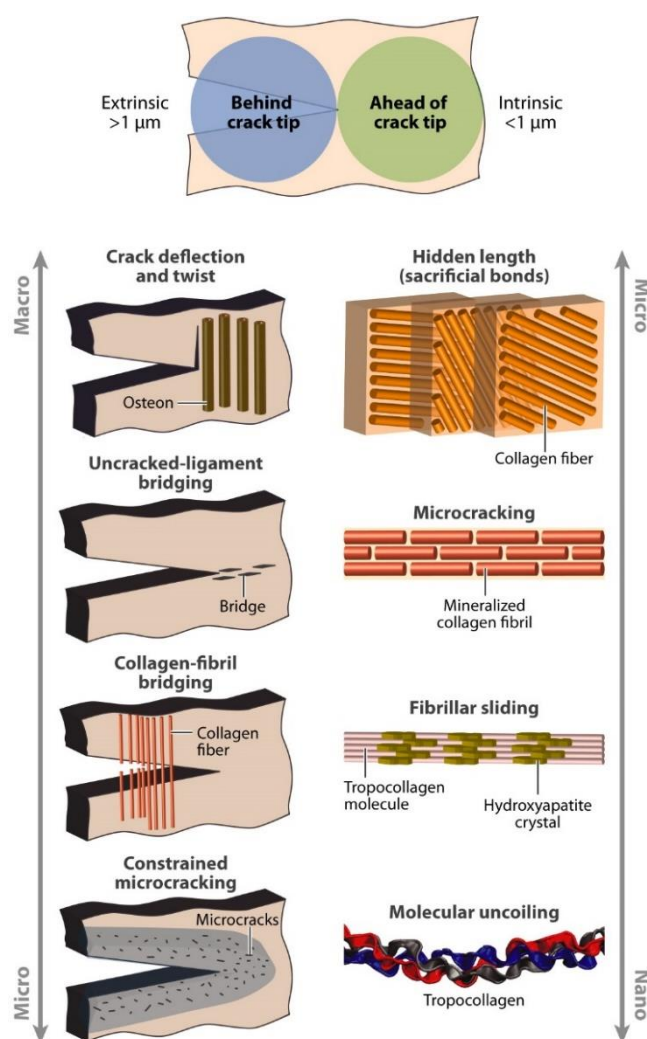


Figure 2.28: Schematic describing the toughening mechanisms of bone that occur on an intrinsic and extrinsic level at multiple length scales (Launey et al., 2010).

In the transverse direction, cement-line microcracks are perpendicular to the crack path, which restricts crack growth, acting as delamination barriers to cause cracks to twist and create very tortuous crack paths resulting in a high toughness. In the longitudinal direction cement-line

microcracks are aligned parallel to and ahead of the growing crack tip where the nearby intact regions can act as bridges across the crack, which can concentrate load in a different direction that would otherwise have increased unstable cracking (Launey et al., 2010).

2.7 Mechanisms of Bone Fragility in T2D

2.7.1 T2D and Impaired Cellular Metabolism

Patients presenting with uncontrolled T2D, particularly where blood glucose levels are not regulated due to increased insulin sensitivity, are at a higher risk of developing a variety of secondary complications such as macrovascular disease, retinopathy, nephropathy and neuropathy. More and more research suggest that glycaemic control and bone homeostasis becomes altered during T2D, which can either directly or indirectly (via bone marrow adiposity, inflammation and impaired bone vascularisation) effect bone cells, which likely explains the increased risk of fracture in these patients (Figure 2.28).

T2D has been shown to have a direct effect on bone cell behaviour, which can consequentially alter bone metabolism (Cassidy et al., 2020; Marin et al., 2018; Murray and Coleman, 2019; Picke et al., 2019; Sanches et al., 2017; Yamaguchi and Sugimoto, 2011). Table 2.7 and Table 2.8 summarise markers of cellular metabolism in human and animals with T2D, respectively. Under a controlled environment, insulin promotes osteoblast differentiation and glucose provides an energy source for these bone forming cells (Wei et al., 2015). However, in T2D, patients present with insulin resistant hyperglycaemia and high levels of glucose have been found to suppress osteoblast differentiation (Napoli et al., 2014). In fact, studies have found that serum biochemical bone formation markers such as P1NP and ALP to be reduced in patients with T2D (Hunt et al., 2021; Lekkala et al., 2023). Wnt signalling is a key pathway for deciding MSC fate, as osteoblast or adipocyte differentiation is coordinated by osteocytes. Due to the high glucose concentrations, the network of viable osteocytes have been found to be either reduced, leading to an increase in empty lacunar spaces (Tanaka et al., 2015; Woolley et al., 2023), or increased with decreased vascular canal volume (Ay et al., 2020). In patients with T2D, Sost levels are associated with glycated haemoglobin levels and are found to be elevated, leading to an increase in RANKL expression (Catalfamo et al., 2014; García-Martín et al., 2012; Hygum et al., 2017; Piccoli et al., 2020). This impairs Wnt signalling where MSC fate can switch to favour adipogenesis over osteoblastogenesis due to high glucose concentrations leading to increased bone marrow adiposity and reduced osteoblastogenesis in T2D (López-Herradón et al., 2013; Tanaka et al., 2015). There is further ambiguity when osteoclast activity during T2D is considered, since serum markers of bone resorption such as CTX-I have been

reported to be both increased or decreased in patients with T2D (Hygum et al., 2017; Starup-Linde and Vestergaard, 2016). In rodents, resorption serum markers such as CTX and TRAP have been found to be mostly elevated (Hamann et al., 2014, 2013, 2011; Picke et al., 2016a).

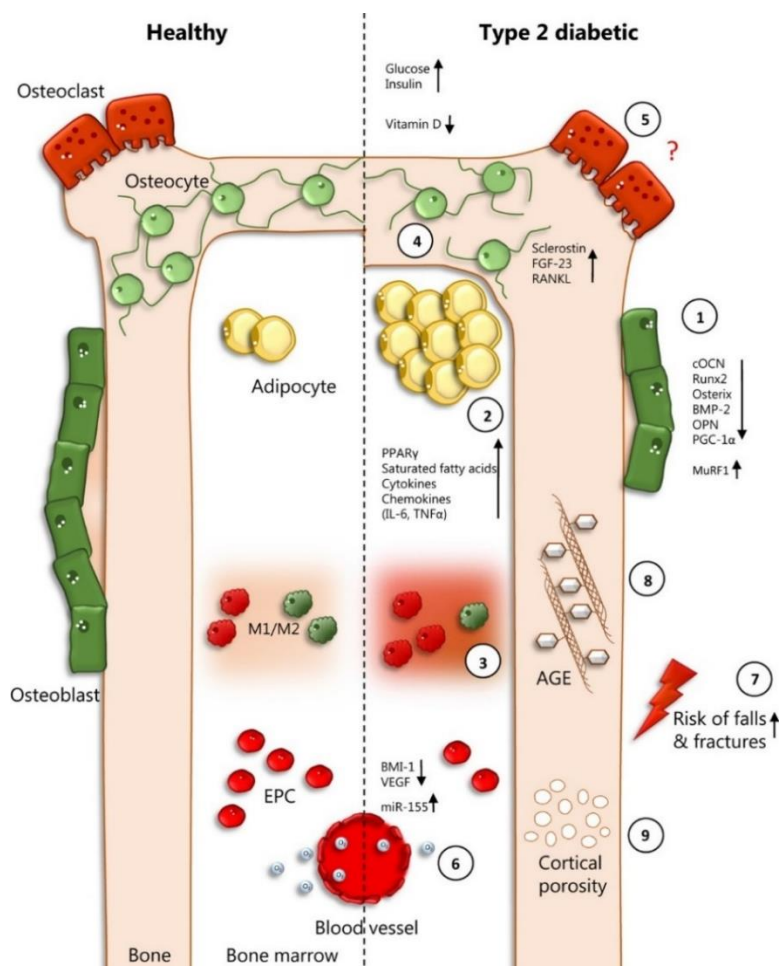


Figure 2.29: Factors that impact bone homeostasis in T2D. (1) Bone formation markers are reduced. (2) MSC fate is switched from osteoblastogenesis to adipogenesis, and bone marrow adiposity is increased. Cytokines and chemokine markers (such as IL-6) are elevated. (3) Supposedly, this leads to an increase in inflammation and an accumulation of pro-inflammatory M1 macrophages. (4) Markers such as Sost, fibroblast growth factor hormone (FGF-23) and RANKL are elevated as a result of impaired osteocyte activity and increased apoptosis. (5) It is generally accepted that due to reduced bone turnover, osteoclast activity is also reduced, however, there is still no clear understanding of how osteoclasts are affected in T2Ds. (6) Vessel permeability and micro-hypoxia is increased, (7) bone quality is reduced and patients are at a greater risk of falling and experiencing a fracture, (8) AGE formation is accelerated and (9) cortical porosity is increased (Picke et al., 2019).

In addition, it is thought that the hyperglycaemic state, increased inflammation, and oxidative stress leads to the increased formation of non-enzymatic crosslinks, known as AGEs, that form between collagen proteins in the organic component of the bone matrix, which is considered as a main variable in increasing bone stiffness and reducing the mechanical integrity of the tissue. AGEs have been shown to correlate with blood glucose levels and disease duration (Ali and Rao, 2020). AGEs are believed to have a negative impact on cellular activity in T2 diabetic bone, however there is no clear understanding of the exact mechanisms that are interrupted. It has been reported that AGEs can significantly inhibit osteoblast differentiation and proliferation through a variety of mechanisms. *In-vitro* studies have shown AGEs can increase osteoblast apoptosis (Alikhani et al., 2007; Kume et al., 2005) and disrupt osteoblast activity by reducing cell attachment to the collagen matrix, which can reduce differentiation and proliferation and inhibit mineralisation of the osteoblastic cells (McCarthy et al., 2004) as well as reducing the secretion of ALP, which in turn reduced osteoid mineralisation (Romero-Díaz et al., 2021).

It is understood that IGF-I plays an important role in regulating bone formation and growth. Interestingly, several *in-vitro* studies have shown that in a high glucose or AGE environment the stimulatory actions of IGF-I on osteoblasts becomes dulled (McCarthy et al., 2001b; Terada et al., 1998). Moreover, the receptor for AGEs (RAGE) mediates an inflammatory response via ligands such as AGEs through sustained activation of NF- κ B and it has been found that the AGE/RAGE signalling plays a heavy role in vascular calcification of diabetic patients as a result of increased oxidative stress and inflammation (Kay et al., 2016). Whilst the effects of AGE on osteoclast activity is not as clear, previous *in-vitro* work has found that AGE-modified proteins can enhance bone resorption (Miyata et al., 1997) and also stimulate IL-6 production (Takagi et al., 1997). However, the role IL-6 plays in the pathogenesis of T2D has been contradictory to date (Akbari and Hassan-Zadeh, 2018). It is important to consider how disruptions to bone cell metabolism may explain alterations to the trabecular and cortical bone microstructure in subjects with T2D, particularly in the instance when fracture risk is increased and independent of bone density.

From Table 2.7 and Table 2.8 it is clear that the majority of human and animal studies measure blood glucose but many fail to measure HbA1c. Additionally, a large number of human and animal studies have failed to report markers of bone cell metabolism. Only two human studies shown in Table 2.7 have reported markers of osteoblast, osteoclast and osteocyte activity (Hunt et al., 2021; Piccoli et al., 2020). However, there are many other human studies of bone fragility

in T2D that did not measure any cellular markers at all (Burghardt et al., 2010; Cirovic et al., 2022; Parle et al., 2020; Rodic et al., 2021; Wölfel et al., 2022a, 2020). As for the animal studies in Table 2.8 only two studies have reported markers of osteoblast, osteoclast and osteocyte activity (Hamann et al., 2013, 2011), while many other studies reported one but not the others.

Table 2.7: Markers Of cellular metabolism measured from blood serum in humans with T2D.

	Gender (Age)	Tissue type	Blood glucose	HbA1c	Insulin	Calcium	PTH	RUNX2	P1NP	OCN	Sost	TRAP	CTX
Karim et al. 2018	Male and female (63.8 ± 9.7)	Femoral neck (cort) ¹ and head (trab) ²	↑	↑									
Hunt et al. 2019	Male (64.8 ± 8.1)	Femoral neck (trab)	↑		↑								
Piccoli et al. 2020	Postmenopausal women (75.2 ± 8.5)	Femoral head (trab)	↑			=		↑ gene expression		= gene expression	↑ gene expression & serum		
Hunt et al. 2021^{&}	Postmenopausal women (94.3 ± 16.4)	Femoral neck (cort) ¹ and trab ²		↑		=	=			↓ uOCN	=		↓
Yadav et al. 2022	Male and female (67.1 ± 7.4)	Femoral head (trab)		↑									
Lekkala et al. 2023^{&}	Postmenopausal women (64 ± 6)	Iliac crest bone (cort) ¹ and trab)		↑			=			↓ uOCN	=		↓

[&]only focusing on T2D group; ↑, increase; ↓, decrease; =, no difference; Cort, Cortical; Trab, Trabecular; HbA1c, glycated haemoglobin; PTH, parathyroid hormone; RUNX2, Runt-related transcription factor 2; P1NP, procollagen type-1 N-propeptide; OCN, osteocalcin; Sost, Sclerostin; TRAP, tartrate-resistant acid phosphatase; CTX, cross-linked C-telopeptide of type I collagen; uOCN, uncarboxylated osteocalcin.

Table 2.8: Markers Of cellular metabolism measured from blood serum in animals with T2D.

	Animal (Strain) Gender	Age (Duration of T2D)	Tissue type	Blood glucose	HbA1c	Insulin	Calcium	PTH	RUNX2	P1NP	OCN	Sost	TRAP	CTX
Saito et al. 2006*	Rat (WBN/Kob) Male	1, 2, 4, 6, 8, 10, 12, 14, 16 & 18 months (24-28 weeks*)	Femur	↑							=			
Prisby et al. 2008*	Rat (ZDF (fa/fa)) Male	7, 13 & 20 weeks (8 weeks*)	Femur (midshaft) ^{1a} (neck) ^{1b} , vertebra ² , tibia ³	↑		=								
Reinwald et al. 2009	Rat (ZDF (fa/fa), ZDSD) Male	33 weeks (ZDF: 21 weeks, ZDSD: 12- 18 weeks)	Femur (midshaft) ¹ , vertebra ²	↑ ZDF, ↑ ZDSD	↑ ZDF, ↑ ZDSD	↑ ZDF, ↓ ZDSD								
Hamann et al. 2011	Rat (ZDF (fa/fa)) Male	21 weeks (9 weeks)	Femur (dm, midshaft) ¹ , vertebra ²	↑		=	↑	↑		↓	↓	=		↑
Hamann et al. 2013*	Rat (ZDF (fa/fa)) Male	23 weeks (11 weeks)	Femur (dm, midshaft) ^{1a} (neck) ^{1b} , vertebra ²	↑			↑				↓	=		↑
Gallant et al. 2013	Rat (ZDSD) Male	32 weeks (10 weeks)	Femur (midshaft) ¹ , vertebra ²	↑	↑									
Devlin et al. 2014*	Mouse (Tallyho/JngJ (TH)) Male	8 & 17 weeks (~7 weeks*)	Femur ¹ (dm) ^{1a} (midshaft) ^{1b} , vertebra ² , tibia ³	↑		↑				=				=
Hamann et al. 2014*	Rat (ZDF (fa/fa)) Male	23 weeks (11 weeks)	Femur (dm) ^{1a} (midshaft) ^{1b} , vertebra ²	↑			↑				↓ cOCN		↑	↑

	Animal (Strain) Gender	Age (Duration of T2D)	Tissue type	Blood glucose	HbA1c	Insulin	Calcium	PTH	RUNX2	PINP	OCN	Sost	TRAP	CTX
Hammond <i>et al.</i> 2014	Rat (ZDSB) Male	30 weeks (~12 weeks)	Tibia	↑	↑									
Stabley <i>et al.</i> 2015	Rat (ZDF (fa/fa)) Male	7, 13 & 20 weeks (8 weeks*)	Femur	↑		↑								
Picke <i>et al.</i> 2016⁺	Rat (ZDF (fa/fa)) Male	23 weeks (11 weeks)	Femur (dm) _{1a} (midshaft) ^{1b}	↑	↑		↑	=		↓			↑	↑
Creecy <i>et al.</i> 2016*	Rat (ZDSB) Male	16, 22 & 29 weeks (8-14 weeks*)	Femur (dm) _{1a} (midshaft) ^{1b} , vertebra ² , radius ³	↑										
Creecy <i>et al.</i> 2018*	Mouse (Tallyho/JngJ (TH)) Male	16 & 34 weeks (~24 weeks)	Femur (dm) _{1a} (midshaft) ^{1b} , vertebra ²	↑	↑	↑				↓			=	
Hunt <i>et al.</i> 2018	Mouse (KK-Ay) Male	20 weeks (12 weeks)	Femur (cortical (c), trabecular (t), whole bone (wb))	↑										
Zeitoun <i>et al.</i> 2019	Rat (ZDF (fa/fa)) Male	24 weeks (12 weeks)	Femur (head) ^a (neck) ^b (midshaft) ^c (dm) ^d	↑										
Acevedo <i>et al.</i> 2018⁺	Rat (UCD- T2DM) Male	6 months (9.9 ± 1 weeks)	Ulnae ¹ , vertebra ²	↑	↑	↑								
Ay <i>et al.</i> 2020	Rat (STZ Wistar Albino) Male	1 and 3 months (~12 weeks*)	Femur (dm)	↑										

	Animal (Strain) Gender	Age (Duration of T2D)	Tissue type	Blood glucose	HbA1c	Insulin	Calcium	PTH	RUNX2	P1NP	OCN	Sost	TRAP	CTX
Sihota <i>et al.</i> 2020	Rat (HFD STZ Sprague Dawley) Female	21-22 weeks (8 weeks)	Femur	↑	↑	↓								
Tice <i>et al.</i> 2022	Mouse (MKR) Male	15 weeks (14 weeks)	Femur	↑										
Llabre <i>et al.</i> 2022	Mouse (C57BL/6J) Male	32 weeks (~9 weeks)	Femur	↑										
Micheletti <i>et al.</i> 2023	Rat (LepR -/- Lund MetS) Male	20 weeks (~4 weeks)	Femur ¹ , Calvaria ²	↑										
Woolley <i>et al.</i> 2023	Rat (ZDSD) Male	19 weeks (~4 weeks)	Femur	↑										
Mehta <i>et al.</i> 2023	Rat (Sprague- Dawley) Female	21-22 weeks (8 weeks)	Vertebra		↑	↑								

*only focusing on oldest age group; †only comparing to vehicle group; #trending significance; ↑, increase; ↓, decrease; =, no difference; Cort, Cortical; Trab, Trabecular; dm, distal metaphysis; HbA1c, glycated haemoglobin; PTH, parathyroid hormone; RUNX2, Runt-related transcription factor 2; P1NP, procollagen type-1 N-propeptide; OCN, osteocalcin; Sost, Sclerostin; TRAP, tartrate-resistant acid phosphatase; CTX, cross-linked C-telopeptide of type I collagen; cOCN, carboxylated osteocalcin.

2.7.2 T2D and Altered Bone Matrix

Mineral

T2D alters bone cell function due to the hyperinsulinemic and hyperglycaemic environment, which can impair tissue mineralisation and mineral quality. In general, it has been shown that patients with T2D can present with increased mineralisation as presented by an increase in cortical and trabecular mineral: matrix ratio from the femoral neck region (Hunt et al., 2021, 2019; Wölfel et al., 2020) but as seen in Table 2.9 the literature is not fully conclusive with other research showing no change in mineral: matrix ratio from cortical bone from other regions such as the mandible or femoral midshaft region (Rodic et al., 2021; Wölfel et al., 2022b, 2022a) and even reductions in the trabecular bone from the femoral head region (Yadav et al., 2022), indicating a possible region influence on mineralisation in T2D. In general, human literature hasn't shown changes to mineral crystallinity, maturity, carbonate: phosphate ratio or acid phosphate content (Table 2.9). Mineral properties reported in animal studies of T2D is a bit more unclear likely due to the fact that properties may be influenced by the strain of animal used as well as the disease duration and tissue of interest. Nevertheless, the vast majority of animal studies have reported a greater cortical bone mineral: matrix ratio when measured from the femoral midshaft (Creedy et al., 2018a, 2016; Hunt et al., 2018) (Table 2.10). Conversely, other animal studies have shown no change (LLabre et al., 2022; Micheletti et al., 2023; Tice et al., 2022) and even a reduction in mineral: matrix ratio (Sihota et al., 2020b) (Table 2.10). Previous animal studies of bone fragility in T2D have reported alterations to the mineral structure of the cortical bone examined via XRD where crystal width and spacing was found to be greater (LLabre et al., 2022; Sihota et al., 2020b), with others finding greater crystal thickness and c-axis length (Tice et al., 2022). Llabre *et al.* (2022) concluded that these changes captured a poorer crystalline structure in the T2 diabetic mice. Whilst there is limited research on human tissue on mineralisation and crystal structure, Parle *et al.* (2020) examined bone mineral density distribution (BMDD) from trabecular bone from the femoral neck of T2D patients using micro-CT. Here, it was found that mineral heterogeneity was higher in the diabetic group when compared to the control. Similarly, Wölfel *et al.* (2020) reported increased mineral heterogeneity and an increase in lowly mineralised calcium content in the endocortical region. Although, a follow-up study by Wölfel *et al.* (2022a) found no differences in mineralisation parameters of cortical bone as measured via qBEI. Tissue composition in T2D has also been analysed using FTIR and Raman spectroscopy. It has been found that crystallinity, taken as the full width at half the maximum of the $\nu_1\text{PO}_4$ peak, was unchanged in

both cortical and trabecular human tissue in T2D (Hunt et al., 2021, 2019; Rodic et al., 2021; Wölfel et al., 2022a, 2020), with animal studies also generally finding no differences between strains in cortical and trabecular tissue (Creecy et al., 2018b; Hamann et al., 2014; Hunt et al., 2018; LLabre et al., 2022; Mehta et al., 2023; Tice et al., 2022). Regardless of crystallinity, studies have reported increased carbonate substitution into the crystal lattice structure, reported as carbonate: phosphate ratio. Tice *et al.* (2022) found an increase in the ratio of carbonate: phosphate of cortical mouse bone measured via Raman spectroscopy, where they stated that greater type-B carbonate substitutions parallel to the mineral c-axis can increase gaps in the lattice structure and deteriorate the symmetry of the structure. Similarly, Mehta *et al.* (2023b) reported an increase in the carbonate: phosphate ratio of vertebral bone powder from diabetic rats measured via ATR-FTIR, although, they reported no difference in crystal length or width measured from XRD. Likewise, a human study by Rodic *et al.* (2021) also reported a higher carbonate: phosphate ratio in the cortex of the femoral region from the T2 diabetic subjects compared to the controls.

Acid phosphate, which is a measure of HPO_4 substitutions into bone mineral crystal lattice and has been associated with newly deposited mineral, has not been widely reported in studies of T2D, perhaps since this is a relatively new parameter whose ratios have been debated (Spevak et al., 2013). Mineral: matrix ratio has generally found to be increased in animal models of T2D (Creecy et al., 2018b, 2016; Hamann et al., 2014; Hunt et al., 2018; Mehta et al., 2023), although others have reported no differences (LLabre et al., 2022; Micheletti et al., 2023; Tice et al., 2022), with a decreased mineral: matrix ratio also being observed (Sihota et al., 2020b). Similarly, human studies have reported no consistent outcome for the mineral: matrix ratio, again reporting it as increased (Hunt et al., 2021, 2019; Wölfel et al., 2020), decreased (Hunt et al., 2021; Wölfel et al., 2020; Yadav et al., 2022) or unchanged (Rodic et al., 2021; Wölfel et al., 2022a, 2022b). Interestingly, in research by Wölfel *et al.* (2020), subjects with T2D and T2D with high porosity (T2DwHP) were examined and they showed that the T2DwHP cohort had a lower mineral: matrix ratio in the periosteal region and lower crystallinity in the endocortical region than the normal T2 diabetic cohort. Additionally, they reported lower mineral maturity in both regions of the normal T2 diabetic and T2DwHP cohorts than the controls. Taken together it is clear there is evidence to suggest that the mineral component of the bone matrix can become altered in subjects with T2D. While the exact properties that are altered are a little unclear, human studies suggest that mineralisation may be increased leading to an increased mineral: matrix ratio, with some animal studies supporting

this, which may lead to increased stiffness. In addition, some animal studies have reported increases in crystallinity, which may impact fibrillar sliding and fracture resistance.

Collagen

Table 2.11 summarises alterations to the collagen matrix reported in animal studies of T2D. As with mineral, collagen is maintained via remodelling and this process can become altered within a hyperglycaemic environment and with that AGEs are thought to rapidly accumulate in patients with T2D altering the collagen matrix, consequentially impairing the mechanical integrity of the tissue. A previous population-based study showed that serum pentosidine levels increased with age (Takahashi et al., 2000). The large population-based Health ABC study further investigated whether circulatory pentosidine (a crosslinking, fluorescent AGE) measured from urine was associated with fractures in older patients with and without T2D and found that pentosidine was associated with increased clinical fracture incidence and increased vertebral fracture prevalence in those with diabetes but not in those without diabetes (Schwartz et al., 2009). Whilst they did not measure AGE levels directly from the bone collagen, previous research has shown evidence that circulatory levels of serum or urine AGEs may be used as a non-invasive biomarker for AGEs in the bone collagen (Odetti et al., 2005). A more recent population-based study has investigated the association of the non-crosslinking, non-fluorescing AGE, CML measured from serum, with incident clinical fractures and prevalent vertebral fractures in older adults with and without T2D from the Health ABC study and found that higher serum CML levels were associated with increased risk of incident clinical fractures in T2D, independent of BMD. Earlier epidemiological studies of T2D have quantified a bulk measurement of AGEs through fluorescence, known as fAGEs for bone tissue (as described in Section on *Bone Matrix Composition*). The majority of animal studies have measured bulk fAGEs from cortical tissue and have found increases (Acevedo et al., 2018; Creecy et al., 2016; LLabre et al., 2022; Sihota et al., 2020b; Tice et al., 2022; Woolley et al., 2023), although Devlin *et al.* (2014) found no differences in fAGE levels from cortical mouse bone. Human studies have also found increased fAGEs in cortical (Karim et al., 2018; Lekkala et al., 2023; Wölfel et al., 2020) and trabecular (Piccoli et al., 2020; Yadav et al., 2022) bone, while others have found no difference in both tissue types (Hunt et al., 2019; Karim et al., 2018; Wölfel et al., 2022a, 2022b). More recent studies of T2D have assessed individual AGEs rather than the bulk measurements as it is understood that certain AGEs correlate better to bone fragility than others. However, to date, the most commonly measured AGE is a crosslink measurement of pentosidine, due to its ease of quantifiability as it fluoresces naturally and survives acid

hydrolysis (Sell et al., 1991; Willett et al., 2022). Similar to fAGEs, animal and human studies have found greater (Hunt et al., 2019; Lekkala et al., 2023; LLabre et al., 2022; Saito and Marumo, 2010; Tice et al., 2022) or unchanged (Creecy et al., 2016; Hunt et al., 2021, 2018; Karim et al., 2018) levels of pentosidine in the bone tissue of T2 diabetic subjects. Karim *et al.* (2013) explored the relationship between pentosidine and fAGEs in cortical and cancellous bone that had undergone *in-vitro* glycation and found that their relationship was dependant on bones surface-to-volume ratio since the magnitude of accumulation differed in cancellous and cortical bone and they concluded that pentosidine only accounted for a small proportion of fAGEs. Furthermore, a recent mass spectrometry study by Arakawa *et al.* (2020) reported that the content of AGE crosslinks like pentosidine in bone are lower in comparison to other AGEs, particularly non-crosslinking AGE adducts, highlighting the importance of examining AGE adducts in subjects with T2D. Whilst studies measuring AGE adducts in T2 diabetic subjects are more limited, there are two animal studies and one human study of that have reported an increase in CML from cortical bone (LLabre et al., 2022; Tice et al., 2022; Wölfel et al., 2020) measured via confocal Raman spectroscopy and ultra-performance liquid chromatography tandem mass-spectrometry (UPLC MS/MS), respectively. Enzymatic crosslinks such as pyridinoline and deoxypyridinoline, have also been measured in subjects with T2D. Human and animal studies have mostly found no difference in these enzymatic crosslinks (Creecy et al., 2016; Hunt et al., 2019, 2018; Lekkala et al., 2023), although Saito *et al.* (2006) and Mehta *et al.* (2023) did find that the number of total enzymatic crosslinks measured via HPLC and the enzymatic crosslink ratio measured via ATR-FTIR from cortical bone were reduced in the diabetic rats. FTIR and Raman spectroscopy have also been used to assess the collagen quality by examining collagen maturity, sugar: matrix ratio and non-enzymatic crosslink ratio. Hunt *et al.* (2019) measured collagen maturity from trabecular bone of the femoral neck and found no difference but did find a higher sugar: matrix and non-enzymatic crosslink ratio. Similar results were found in animal studies by Sihota *et al.* (2022) and Mehta *et al.* (2023) who both found no difference in collagen maturity from cortical bone but an increase in the non-enzymatic crosslink ratio. Taken together these findings suggest that when measuring AGEs in subjects with T2D it is not enough to just measure fAGEs or AGE adducts but instead both should be quantified since various studies have reported no changes in one measurement but then did observe changes in the other. Especially since the relationship of fAGEs and pentosidine to bone was dependant on bones surface-to-volume ratio.

Table 2.9: Summary of the reported alterations to the mineral and collagen components of T2 diabetic human bone measured via FTIR or Raman.

	Gender (Age)	Tissue type	Mineral:Matrix ratio			Mineral properties				Collagen properties								
			(ν 1PO ₄ /AmI)	(ν 1PO ₄ /Pro)	(ν 1PO ₄ /AmIII)	Mineral maturity	Crystallinity	C:Pv1 ratio	AP content	Collagen maturity	NE-xLR	fAGEs	Pentosidine	CML	MGH1	PYD	DPD	
Karim et al. 2018	Male and female (63.8 ± 9.7)	Femoral neck (cort) ¹ and head (trab) ²											↑ ¹ , = ² , serum	= serum				
Hunt et al. 2019	Male (64.8 ± 8.1)	Femoral neck (trab)	↑			=	=	=	=	↑	=	↑				↓ [#]	=	
Wölfel et al. 2020	Male and female (T2DM ^a : 73 ± 7; T2DMw HP ^b : 76 ± 8)	Femoral midshaft (cort)	↑ ^a , ↓ ^b			= ^a , ↓ ^b					= ^a , ↑ ^{#b}	↑ ^{a, b}		↑ ^a , ↓ ^b				
Piccoli et al. 2020	Postmenopausal women (75.2 ± 8.5)	Femoral head (trab)										↑						
Hunt et al. 2021^{&}	Postmenopausal women (94.3 ± 16.4)	Femoral neck (cort) ¹ and trab ²)	↑ ^{1, 2#} (mean) ↓ ^{1, 2} (width)			= ^{1, 2} (mean) ↑ ^{1, 2} (width)	= ^{1, 2} (mean) = ^{1, 2} (width)	= ^{1, 2} (mean) ↓ ^{1, 2} (width)	= ^{1, 2} (mean) = ^{1, 2} (width)				=					
Rodic et al. 2021^{&}	Male (70.6 ± 4.5)	Mandible	=	=	=	=	↑											

	Gender (Age)	Tissue type	Mineral:Matrix ratio			Mineral properties				Collagen properties							
			(ν 1PO ₄ /AmI)	(ν 1PO ₄ /Pro)	(ν 1PO ₄ /AmIII)	Mineral maturity	Crystallinity	C:P ν 1 ratio	AP content	Collagen maturity	NE-xLR	fAGEs	Pentosidine	CML	MG-H1	PYD	DPD
Yadav et al. 2022	Male and female (67.1 \pm 7.4)	Femoral head (trab)	↓								↑						↓ enz xlinks
Wölfel et al. 2022	Male and female (T2DM ^a : 77.2 \pm 5.5; T2DMw HP ^b : 76 \pm 8.7)	Tibial midshaft (cort)	= ^{a, b}			= ^{a, b}		= ^{a, b}				= ^{a, b}					
Wölfel et al. 2022^{&}	Male (74.3 \pm 7.9)	Femoral midshaft (cort)	=			=		=			=			↑ [#]	↑		
Lekkala et al. 2023^{&}	Postmenopausal women (64 \pm 6)	Iliac crest bone (cort ¹ and trab ²)									↑ ^{1, 2} =2	↑ ^{1, 2}	↑ ^{1, 2}				= ^{1, 2}

[&]only focusing on T2D group; ↑, increase; ↓, decrease; =, no difference; Cort, Cortical; Trab, Trabecular; ν 1PO₄/AmI, ν 1 phosphate to Amide I; ν 1PO₄/Pro, ν 1 phosphate to proline; ν 1PO₄/AmIII, ν 1 phosphate to amide III; C:P ν 1 ratio, carbonate to phosphate ratio; AP content, Acid phosphate content; NE-xLR, non-enzymatic crosslink ratio; fAGEs, fluorescent AGEs; CML, carboxymethyl-lysine; MG-H1, 5-hydroxymethyl imidazolone; PYD, pyridinoline; DPD, deoxypyridinoline; enz xlinks, enzymatic crosslinks.

Table 2.10: Summary of the reported alterations to the mineral component of T2 diabetic animal bone measured via FTIR or Raman.

	Animal (Strain) Gender	Age (Duration of T2D)	Tissue type	Crystal structure					Mineral properties						
				Mean crystal length	Mean crystal width	HA crystal orientation	HA crystal size	D-spacing	(ν 1PO ₄ /AmI)	(ν 1PO ₄ /Pro)	(ν 1PO ₄ /AmIII)	ν 1PO ₄ /CH ₂ wag	Crystallinity	C:Px1 ratio	AP content
Hammond et al. 2014	Rat (ZDSD) Male	30 weeks (~12 weeks)	Tibia					↑		=	↑ [#]	↑	=	=	
Creecy et al. 2016*	Rat (ZDSD) Male	16, 22 & 29 weeks (8-14 weeks*)	Femur (dm) ^{1a} (midshaft) ^{1b} , vertebra ² , radius ³						↑ ^{1b}	↑ ^{1b}	= ^{1b}		↑ ^{1b}	= ^{1b}	
Creecy et al. 2018*	Mouse (Tallyho/JngJ (TH)) Male	16 & 34 weeks (~24 weeks)	Femur (dm) ^{1a} (midshaft) ^{1b} , vertebra ²						↑ ^{1b}	↑ ^{1b}	↑ ^{1b}		= ^{1b}	↓ ^{1b}	
Hunt et al. 2018	Mouse (KK-Ay) Male	20 weeks (12 weeks)	Femur (cortical (c), trabecular (t), whole bone (wb))						↑ ^{wb, c#}				= ^{wb, c, t (means)}	= ^{c, t (mean & width), =wb (mean)} , ↑ ^{wb (width)}	
Sihota et al. 2020	Rat (HFD STZ Sprague Dawley) Female	21-22 weeks (8 weeks)	Femur	=	↑				↓				↑ [#]	=	=

	Animal (Strain) Gender	Age (Duration of T2D)	Tissue type	Crystal structure					Mineral properties							
				Mean crystal length	Mean crystal width	HA crystal orientation	HA crystal size	D-spacing	(v1PO ₄ /AmI)	(v1PO ₄ /Pro)	(v1PO ₄ /AmIII)	v1PO ₄ /CH ₂ wag	Crystallinity	C:Pv1 ratio	AP content	
Tice et al. 2022	Mouse (MKR) Male	15 weeks (14 weeks)	Femur		↑	=				=		=			↑ [#]	
Llabre et al. 2022	Mouse (C57BL/6J) Male	32 weeks (~9 weeks)	Femur				↑	↑		=				=	=	
Micheletti et al. 2023	Rat (LepR -/- Lund MetS) Male	20 weeks (~4 weeks)	Femur ¹ , Calvaria ²									= _{1,2}		= _{1,2}	= _{1,2}	
Mehta et al. 2023	Rat (Sprague-Dawley) Female	21-22 weeks (8 weeks)	Vertebra	=	=					↑				=	↑	=

*only focusing on oldest age group; [#]only comparing to vehicle group; [#]trending significance; ↑, increase; ↓, decrease; =, no difference; Cort, Cortical; Trab, Trabecular; dm, distal metaphysis; HA, hydroxyapatite; v1PO₄/ AmI, v1 phosphate to Amide I; v1PO₄/ Pro, v1 phosphate to proline; v1PO₄/ AmIII, v1 phosphate to amide III; v1PO₄/ CH₂ wag, phosphate to CH₂ wag bend of the collagen matrix; C:Pv1 ratio, carbonate to phosphate ratio; AP content, Acid phosphate content.

Table 2.11: Summary of the reported alterations to the collagen component of T2 diabetic animal bone measured via FTIR or Raman.

	Animal (Strain) Gender	Age (Duration of T2D)	Tissue type	AGEs			Crosslink properties						Collagen properties			
				fAGEs	Pento sidine	C M L	P Y D	D P D	NE- xLR	E- xLR	Immature crosslinks	Mature crosslinks	Collagen maturity	Collagen denaturation (1670/1640)	Bound water	
Saito <i>et al.</i> 2006*	Rat (WBN/Kob) Male	1, 2, 4, 6, 8, 10, 12, 14, 16 & 18 months (24-28 weeks*)	Femur		↑						↓	↓	=			
Devlin <i>et al.</i> 2014*	Mouse (Tallyho/JngJ (TH)) Male	8 & 17 weeks (~7 weeks*)	Femur ¹ (dm) ^{1a} (midshaft) ^{1b} , vertebra ² , tibia ³	= ^{1b}												
Creecy <i>et al.</i> 2016*	Rat (ZDSD) Male	16, 22 & 29 weeks (8-14 weeks*)	Femur (dm) ^{1a} (midshaft) ^{1b} , vertebra ² , radius ³		= ^{1b}		= ^{1b}									
Creecy <i>et al.</i> 2018*	Mouse (Tallyho/JngJ (TH)) Male	16 & 34 weeks (~24 weeks)	Femur (dm) ^{1a} (midshaft) ^{1b} , vertebra ²	↑ ^{1b}	↑ ^{1b#}		↑ ^{1b}									↑ ^{1b}
Hunt <i>et al.</i> 2018	Mouse (KK-Ay) Male	20 weeks (12 weeks)	Femur (cortical (c), trabecular (t), whole bone (wb))		=		=									↑ ^{wb, c, t}
Acevedo <i>et al.</i> 2018	Rat (UCD- T2DM) Male	6 months (9.9 ± 1 weeks)	Ulnae ¹ , vertebra ²	↑												

	Animal (Strain) Gender	Age (Duration of T2D)	Tissue type	AGEs			Crosslink properties						Collagen properties			
				fAGEs	Pento sidine	C M L	P Y D	D P D	NE- xLR	E- xLR	Immature crosslinks	Mature crosslinks	Collagen maturity	Collagen denaturation (1670/1640)	Bound water	
Sihota <i>et al.</i> 2020	Rat (HFD STZ Sprague Dawley) Female	21-22 weeks (8 weeks)	Femur	↑						↑				=		
Tice <i>et al.</i> 2022	Mouse (MKR) Male	15 weeks (14 weeks)	Femur	↑	↑	↑										
Llabre <i>et al.</i> 2022	Mouse (C57BL/6J) Male	32 weeks (~9 weeks)	Femur	↑	↑	↑										↓
Woolley <i>et al.</i> 2023	Rat (ZDSD) Male	19 weeks (~4 weeks)	Femur	↑												
Mehta <i>et al.</i> 2023	Rat (Sprague- Dawley) Female	21-22 weeks (8 weeks)	Vertebra						↑	↓				=		

*only focusing on oldest age group; †only comparing to vehicle group; #trending significance; ↑, increase; ↓, decrease; =, no difference; Cort, Cortical; Trab, Trabecular; dm, distal metaphysis; fAGEs, fluorescent AGEs; CML, carboxymethyl-lysine; PYD, pyridinoline; DPD, deoxypyridinoline; NE-xLR, non-enzymatic crosslink ratio; E-xLR, enzymatic crosslink ratio.

Microarchitecture

Bone microarchitecture and structure can influence fracture resistance. While it is understood that patients with T2D don't often present with reduced BMD and in fact may have unchanged or increased BMD, it is important to consider how the cortical and trabecular microarchitecture may also be affected. In general, human studies have shown that the microarchitecture of the trabecular bone component seems to be preserved in subjects with T2D (Table 2.12). While it may be concluded that human studies have shown that the cortical microarchitecture is mostly preserved (Table 2.13), some studies have reported cases of increased porosity which would influence bones resistance to fracture (Burghardt et al., 2010; Patsch et al., 2013; Wölfel et al., 2022a, 2020). A recent review paper by Karim *et al.* (2019) concluded that there is no clear conclusion regarding how the cortical and trabecular microarchitecture are affected during T2D, particularly with pre-clinical studies. The ZDF (*fa/fa*) and ZDSD rat is the most common rat used to investigate bone biomechanics, with these rat strains often presenting with a reduced cortical and trabecular BMD and BV/TV (Creecy et al., 2016; Hamann et al., 2011; Prisby et al., 2008; Reinwald et al., 2009; Zeitoun et al., 2019) as shown in Table 2.13. This is a common characteristic of the current animal models of T2D that occur due to their genetic trait, especially in diet-induced models that develop diabetes before reaching skeletal maturity (Fajardo et al., 2014). Nevertheless, TMD is occasionally reported in animal studies of T2D, which is generally found unchanged and sometimes increased (Creecy et al., 2018b, 2016; Devlin et al., 2014; Micheletti et al., 2023; Sihota et al., 2020b; Woolley et al., 2023). Much of the *ex-vivo* human studies have found no differences in the BMD, TMD and BV/TV of the trabecular and cortical bone of patients with T2D, particularly taken from the femoral head or neck region (Cirovic et al., 2022; Karim et al., 2018; Parle et al., 2020; Wölfel et al., 2022a, 2022b, 2020). Cortical porosity is an important parameter to measure as increased porosity is thought to play a role in increasing fracture risk despite a normal or higher BMD. Burghardt *et al.* (2010) used HR-pQCT to investigate the cortical and trabecular microarchitecture of post-menopausal women with T2D and found that despite a slightly more advantageous trabecular microarchitecture, the cortical microarchitecture was compromised due to an increased porosity of the distal radius and similarly of the distal tibia, similar results were found in male and female patients with T2D in a study by Paccou and colleagues (2016) that assessed cortical porosity and pore volume. Patsch *et al.* (2013) also found increased cortical porosity in T2 diabetic patients with fragility fractures compared to diabetic patients without fracture, suggesting the preferential region of cortical bone may be compromised in patients that present

with a fracture in T2D. Cortical porosity has also been examined in animal studies of T2D. Creecy *et al.* (2016b) investigated cortical porosity in ZDSD rats at different stages of the disease – 16-, 22- and 29-week using micro-CT and interestingly they found that in the earlier stages of the disease (16- and 22-weeks) there was no difference in cortical porosity and pore number between diabetic and control rats, however at 29-weeks, the diabetic rats had significantly higher levels of porosity and pore number than the controls that coincided with a brittle bone effect with age. Zeitoun *et al.* (2019), also used micro-CT to measure cortical porosity in ZDF (*fa/fa*) rats along different regions of the femoral bone (neck and midshaft) and found cortical porosity to be higher in the diabetic rats. However, there are some animal studies of T2D that have found no difference in cortical porosity and even reductions, so more human and animal data is needed to fully understand the role porosity play in the cortical bone of patients with T2D. Other trabecular properties such as thickness, number, spacing, SMI and Conn.D can also be explored but most *ex vivo* human studies of T2D have reported no major changes in these parameters (Hunt *et al.*, 2019; Karim *et al.*, 2018; Parle *et al.*, 2020; Piccoli *et al.*, 2020) whilst one study by Sihota and colleagues (2021) reported reduced trabecular thickness, number, BV/TV and increased SMI for trabecular bone taken from the femoral head. While animal studies have frequently reported reductions in trabecular thickness and SMI (Acevedo *et al.*, 2018; Creecy *et al.*, 2018b; Devlin *et al.*, 2014; Reinwald *et al.*, 2009; Zeitoun *et al.*, 2019). Future studies need to explore cortical and trabecular bone without confounding factors such as age, disease duration, sex, BMI, ethnicity, whether or not a patient experience a fracture or not, height and region of interest. Furthermore, it is possible that there is a subgroup of patients with T2D and high cortical porosity, as indicated in work by Wölfel and colleagues, where the risk of fracture is greater in these patients in comparison to patients with T2D and normal porosity.

Table 2.12: Summary of cortical and trabecular microarchitecture from human studies of T2D.

	Gender (Age)	Tissue type	Cortical					Trabecular								
			BMD	TMD	Ct.Th	Ct.Po	Ct.Po.V	BMD	TMD	BV/TV	Tb.Th	Tb.N	Tb.Sp	SMI	Conn.D	
Burghardt et al. 2010	Postmenopausal women (62.9 ± 7.7)	Radius ¹ and tibia ² (cort ^a , trab ^b)	= ^{1a} , ↑ ^{2a}		= ^{1a} , ^{2a}	↑ ^{1a} , = ^{2a}		= ^{1b} , ^{2b}				= ^{1a} , ↑ ^{2b}	= ^{1b} , ^{2b}	= ^{1b} , ^{2b}		
Patsch et al. 2013	Postmenopausal women without ^a and with ^b fracture (61.3 ± 5.7)	Ultradistal radius ¹ and tibia ²	= ^{1a,b} , = ^{2a} , ↓ ^{2b}		= ^{1a,b} , = ^{2a,b}	= ^{1a,b} , = ^{2a} , ↑ ^{2b}	= ^{1a} , ↑ ^{1b} , = ^{2a} , ↑ ^{2b}	= ^{1a,b} , = ^{2a,b}				= ^{1a,b} , = ^{2a,b}	= ^{1a} , ↑ ^{1b} , = ^{2a,b}			
Karim et al. 2018	Male and female (63.8 ± 9.7)	Femoral neck (cort) ¹ and head (trab) ²		= ¹		= ¹			= ²	= ²	= ²	= ²	= ²	= ²		
Hunt et al. 2019	Male (64.8 ± 8.1)	Femoral neck (trab)							=	=	↓	↑ [#]	↑ [#]			
Wölfel et al. 2020	Male and female (T2DM ^a : 73 ± 7; T2DMwHP ^b : 76 ± 8)	Femoral midshaft (cort)		= ^a , ↓ ^{#b}		= ^a , ↑ ^b										
Parle et al. 2020^s	Male and female (67.1 ± 7.4)	Femoral head (trab)							=	=	=	=	=			
Piccoli et al. 2020	Postmenopausal women (75.2 ± 8.5)	Femoral head (trab)							=	=	=	=	=	=	=	

	Gender (Age)	Tissue type	Cortical					Trabecular							
			BMD	TMD	Ct.Th	Ct.Po	Ct.Po.V	BMD	TMD	BV/TV	Tb.Th	Tb.N	Tb.Sp	SMI	Conn.D
Rodic et al. 2021 ^{&}	Male (70.6 ± 4.5)	Mandible				↓			↑	↑					
Sihota et al. 2021	Female (69.7 ± 10)	Femoral head (trab)							↓	↓	↓	↑ [#]	↑		
Cirovic et al. 2022	Postmenopausal women (77.1 ± 9.8)	Femoral neck (trab)							=	=	=	=	↑	=	
Yadav et al. 2022	Male and female (67.1 ± 7.4)	Femoral head (trab)						=	↓	↓					
Wölfel et al. 2022	Male and female (T2DM ^a : 77.2 ± 5.5; T2DMwHP ^b : 76 ± 8.7)	Tibial midshaft (cort)	=a, b	=a, b	=a, b	=a, ↑ ^b									
Wölfel et al. 2022 ^{&}	Male (74.3 ± 7.9)	Femoral midshaft (cort)	=		=	=									

[§]compared to OA controls samples; [&]only focusing on T2D group; [#]trending significance; Cort, cortical; Trab, trabecular; BMD, bone mineral density; TMD, tissue mineral density; BV/TV, bone volume per total volume; Ct.Th, cortical thickness; Ct.Po, cortical porosity; Ct.Po.V, cortical pore volume; Tb.Th, trabecular thickness; Tb.N, trabecular number; Tb.Sp, trabecular spacing; SMI, structural model index; Conn.D, connectivity density.

Table 2.13: Summary of cortical and trabecular microarchitecture from animal studies of T2D.

	Animal (Strain) Gender	Age (Duration of T2D)	Tissue type	Cortical					Trabecular							
				BMD	TMD	Ct.Th	Ct.Po	Ct.Po.N	BMD	TMD	BV/TV	Tb.Th	Tb.N	Tb.Sp	SMI	Conn.D
Saito et al. 2006*	Rat (WBN/Kob) Male	1, 2, 4, 6, 8, 10, 12, 14, 16 & 18 months (24-28 weeks*)	Femur	=												
Prisby et al. 2008*	Rat (ZDF (fa/fa)) Male	7, 13 & 20 weeks (8 weeks*)	Femur (midshaft) ^{1a} , (neck) ^{1b} , vertebra ² , tibia ³	↓ ^{1,3}					↓ ^{1a, 1b, 2, 3}							
Reinwald et al. 2009	Rat (ZDF (fa/fa), ZDSD) Male	33 weeks (ZDF: 21 weeks, ZDSD: 12- 18 weeks)	Femur (midshaft) ¹ , vertebra ²	↓ ^{1,2} ZDF, ↓ ^{1,2} ZDSD		↓ ¹ ZDF, ↓ ¹ ZDSD			↓ ^{1,2} ZDF, ↓ ^{1,2} ZDSD	↓ ² ZDF, ↓ ² ZDSD	↓ ² ZDF, ↓ ² ZDSD	= ² ZDF, = ² ZDSD	= ² ZDF, = ² ZDSD	↑ ² ZDF, ↑ ² ZDSD		
Hamann et al. 2011	Rat (ZDF (fa/fa)) Male	21 weeks (9 weeks)	Femur (dm, midshaft) ¹ , vertebra ²	↓ ^{1,2}		↓ ¹			↓ ^{1,2}	↓ ¹	↓ ¹	↓ ¹				
Hamann et al. 2013⁺	Rat (ZDF (fa/fa)) Male	23 weeks (11 weeks)	Femur (dm, midshaft) ^{1a} , (neck) ^{1b} , vertebra ²			↓ ^{1a}			↓ ^{1a, 2}	↓ ^{1a, 2}	↓ ^{1,=2}	= ^{1, 2}				
Devlin et al. 2014*	Mouse (Tallyho /JngJ (TH)) Male	8 & 17 weeks (~7 weeks*)	Femur1 (dm) ^{1a} , (midshaft) ^{1b} , vertebra ² , tibia ³			= ^{1a} , ↓ ^{1b}	↓ ^{1a}			↓ ²	= ^{1a, 2}	↓ ^{1a, =2}	↑ ^{1a, =2}	↑ ^{1a, 2}	↓ ²	

	Animal (Strain) Gender	Age (Duration of T2D)	Tissue type	Cortical					Trabecular							
				BMD	TMD	Ct.Th	Ct.Po	Ct.Po.N	BMD	TMD	BV/TV	Tb.Th	Tb.N	Tb.Sp	SMI	Conn.D
Hamann <i>et al.</i> 2014⁺	Rat (ZDF (fa/fa)) Male	23 weeks (11 weeks)	Femur (dm) ^{1a} (midshaft) ^{1b} , vertebra ²	↓ ^{1b}	↓ ^{1b}	↓ ^{1b}			↓ ^{1a, =2}	= ^{1a, 2}	↓ ^{1a, 2}					
Stabley <i>et al.</i> 2015*	Rat (ZDF (fa/fa)) Male	7, 13 & 20 weeks (8 weeks*)	Femur	↓					↓							
Picke <i>et al.</i> 2016⁺	Rat (ZDF (fa/fa)) Male	23 weeks (11 weeks)	Femur (dm) ^{1a} (midshaft) ^{1b}	↓ ^{1b}		↓ ^{1b}			↓ ^{1a}		↓ ^{1a}	↓ ^{1a}	↓ ^{1a}			
Creecy <i>et al.</i> 2016*	Rat (ZDSD) Male	16, 22 & 29 weeks (8-14 weeks*)	Femur (dm) ^{1a} (midshaft) ^{1b} , vertebra ² , radius ³		= ^{1b} , 3	↓ ^{1b, =3}	↑ ^{1b}	↑ ^{1b}			↓ ^{1a, 2}	↓ ^{1a, 2}	= ^{1a} , ↓ ²			= ^{1a, 2}
Creecy <i>et al.</i> 2018*	Mouse (Tallyho /JngJ (TH)) Male	16 & 34 weeks (~24 weeks)	Femur (dm) ^{1a} (midshaft) ^{1b} , vertebra ²		↑ ^{1b}	↑ ^{1b}	= ^{1b}	↓ ^{1b}		= ^{1a} , ↑ ²	↓ ^{1a} , = ²	= ^{1a} , ↑ ²	↓ ^{1a} , = ²	↑ ^{1a} , = ²	↑ ^{1a, 2}	↓ ^{1a, 2}
Zeitoun <i>et al.</i> 2019	Rat (ZDF (fa/fa)) Male	24 weeks (12 weeks)	Femur (head) ^a (neck) ^b (midshaft) ^c (dm) ^d	= ^{b, d}		= ^{b, d}	↑ ^{b, c}		= ^b , ↓ ^d		↓ ^{a, b, d}	↓ ^{a, d#} , = ^b	↓ ^{a, b, d}	↑ ^{a, b, d}	↑ ^{a, b, d}	↑ ^{a, =b} , ↓ ^d
Acevedo <i>et al.</i> 2018⁺	Rat (UCD- T2DM) Male	6 months (9.9 ± 1 weeks)	Ulnae ¹ , vertebra ²		↓ ¹					↓ ²	↓ ²	↓ ²	↓ ²	↑ ²	↑ ²	↑ ²

	Animal (Strain) Gender	Age (Duration of T2D)	Tissue type	Cortical					Trabecular							
				BMD	TMD	Ct.Th	Ct.Po	Ct.Po.N	BMD	TMD	BV/TV	Tb.Th	Tb.N	Tb.Sp	SMI	Conn.D
Sihota et al. 2020	Rat (HFD STZ Sprague Dawley)	21-22 weeks (8 weeks)	Femur		=	↓				=	↓	=	=	=	=	=
Tice et al. 2022	Female Mouse (MKR)	15 weeks (14 weeks)	Femur	=		↓										
Llabre et al. 2022	Male Mouse (C57BL/6J)	32 weeks (~9 weeks)	Femur		=	=			↑		↑	↑	=	=		
Micheletti et al. 2023	Male Rat (LepR -/- Lund MetS)	20 weeks (~4 weeks)	Femur ¹ , Calvaria ²		=	↓ ¹				=	↓ ¹	= ¹	↓ ¹	↑ ¹		
Woolley et al. 2023	Male Rat (ZDSD)	19 weeks (~4 weeks)	Femur		=	↓	↓ [#]									

*only focusing on oldest age group; +only comparing to vehicle group; #trending significance; ↑, increase; ↓, decrease; =, no difference; BMD, bone mineral density; TMD, tissue mineral density; BV/TV, bone volume per total volume; Ct.Th, cortical thickness; Ct.Po, cortical porosity; Ct.Po.V, cortical pore volume; Tb.Th, trabecular thickness; Tb.N, trabecular number; Tb.Sp, trabecular spacing; SMI, structural model index; Conn.D, connectivity density.

2.7.3 T2D and Tissue Mechanical Integrity

In Vitro Glycation and Mechanical Properties

Whilst it is understood that patients with T2D can present with an impaired cellular metabolism and alterations to their bone matrix, it has been widely hypothesised that the excess accumulation of AGEs the main contributing factor to the increased risk of fracture of T2 diabetic bone. In fact, there have been multiple *in-vitro* glycation studies that have tried to establish the relationship between AGE levels and bone fragility, whereby a bone samples was immersed in a ribose solution to facilitate the formation of non-enzymatic glycation AGEs (Vashishth et al., 2001). The earliest *in-vitro* glycation study was carried out by Vashishth and colleagues on cortical bovine bone, where they found an greater levels of fAGEs in the ribosylated group versus the non-ribosylated controls ($\uparrow 1,576\%$) and whilst they found the collagen network stiffened in the ribosylated group they ultimately saw no major different in the mechanical properties measured via compression or tension (Vashishth et al., 2001). Another study by Willet *et al.* (2013) investigated the influence of AGEs on the mechanical integrity of bovine cortical bone via three-point bend testing and found pentosidine was higher in the ribosylated groups than the controls and also reported an increase in secant modulus and decrease in ultimate strain, post-yield strain, toughness and damage fraction in the ribosylated groups. A human study by Merlo *et al.* (2020) found fAGEs to be higher in the ribosylated cortical bone ($\uparrow 236\%$), which coincided with reductions in stress intensity factor (K_c) and fracture toughness initiation load and time, as well as a reduced elastic modulus from micro-indentation testing but found no differences between groups from cyclic RPI testing. Conversely, another study found no difference in mechanical properties of cortical bovine bone at all despite increases in pentosidine (Viguet-Carrin et al., 2008). With this in mind, the overall data from *in-vitro* glycation studies has been contradictory, making it difficult to completely understand the relationship between AGEs and bone fragility. In addition, it is understood that *in-vitro* glycation generates AGE levels in bone higher than what occurs physiologically, and these models are not capable of capturing other complex physiological and biological nuances of the disease.

Human Studies

Table 2.14 summarises results from various *in-vivo* human studies that have examined mechanical properties of patients with T2D. Much of the current human research of bone fragility in T2D has been carried out on trabecular bone and the majority of these studies have

reported no difference in the mechanical properties of trabecular bone from femoral heads of patients with T2D when compared to controls (Parle et al., 2020; Piccoli et al., 2020; Yadav et al., 2022), despite seeing changes in mineral heterogeneity (Parle et al., 2020), altered gene expression of RUNX2 (bone formation) and Sost (Piccoli et al., 2020) and alterations to the biochemistry of the tissue (\downarrow mineral: matrix ratio, \uparrow CML, \uparrow fAGEs, \downarrow E-xLR, \uparrow NE-xLR) (Yadav et al., 2022).

Karim *et al.* (2018b) present one of the few studies that show impaired mechanical properties in T2D bone, where they found a reduction in yield stress of trabecular bone from the femoral head despite no difference in elastic modulus, yield strain and fAGEs. When examining the cortical component from the femoral neck, they reported an increased indentation distance, creep indentation distance and cortical fAGEs in the diabetic samples compared to the non-diabetic. Wölfel *et al.* (2022b) reported similar results in their type-2 diabetic cohort with high porosity (T2DwHP), where cortical bone samples were taken from the tibial midshaft of control, T2D patients with normal porosity (T2DM) and T2DMwHP, and were mechanically tested using RPI and nanoindentation. While it was reported that the T2DM group had no change in mechanical properties in comparison to controls, it was found that the T2DMwHP had an higher 1st cycle indentation distance (depth of probe into tissue in first cycle), 1st cycle creep indentation distance (depth of probe into bone tissue during holding phase of first cycle) and total indentation distance (distance travelled during entire cycle) than controls and T2DM groups and a higher indentation distance increase than controls, all indicative of a lower tissue hardness in the T2DMwHP group (Wölfel et al., 2022a). Furthermore, this cohort was also reported to have a lower average loading slope than control and T2DM groups, suggesting a lower tissue stiffness (Wölfel et al., 2022a). These changes were observed despite no difference found in the levels of fAGEs. Another study by Wölfel and colleagues (2022c) on cortical bone from femoral midshaft of patients with T2D reported a reduced elastic modulus and fibril strain in the elastic and inelastic region from small angle x-ray scattering with tensile testing and also reported a trending increase in CML and MG-H1. However, there are some limitations to human studies of bone fragility in T2D since it is often not possible to indicate the precise duration or severity of the disease that a patient is experiencing and human tissue and patient information regarding BMI, glucose levels and sex can be difficult to obtain, making it hard to control for possible confounding factors. Taken together, in general it has been found that the trabecular bone is unaffected by T2D or in fact stiffened or strengthened. Whilst the cortical tissue has also been shown to be stiffer in some studies of patients with T2D, there is evidence

to suggest that the cortical component may be adversely affected, particularly in cohorts with high porosity where indentation distances have been found to be greater than controls or diabetic patients with normal porosity.

Animal Studies

Table 2.15 summarises the results from various *ex-vivo* animal studies of T2D that have evaluated mechanical properties. Generally, earlier animal studies of T2D characterised macro-level mechanical properties of bone and, despite reporting a general reduction in the structural properties, the tissue-level mechanical properties are rarely reported (Hamann et al., 2014; Picke et al., 2016b; Saito et al., 2006). Earlier studies by Reinwald *et al.* (2009) and Hamann *et al.* (2014b) examined tissue-level properties of femora (three-point bend test) and vertebrae (compression) samples from ZDF (fa/fa) rats. Reinwald *et al.* (2009) found no difference in the tissue-level properties of the femora despite a lower femoral BMD but did find that elastic modulus and ultimate stress was lower in the vertebrae of ZDF (fa/fa) groups than the controls but no difference in toughness. Conversely, Hamann *et al.* (2014b) found that the femora of that ZDF (fa/fa) rats had a lower elastic modulus and ultimate stress but similar toughness when compared to controls. However, out of all of the above-mentioned studies, only Saito *et al.* (2006) assessed bone composition, and this made it difficult to fully how alterations at a cellular level may affect tissue mechanics in T2D. A longitudinal study by Creecy *et al.* (2016b) investigated how tissue composition and mechanics are altered with disease duration in ZDSD rats. Although toughness was reduced, no other tissue-level differences were found in the femoral midshaft or radius of the ZDSD rats with the longest term of diabetes compared to controls (29-weeks). There was also no change in levels of pentosidine or cortical tissue mineral density. Interestingly, stress intensity factor at crack initiation and cracking toughness was found to significantly reduce with age within the diabetic strain when no difference was observed with age for the controls (Creecy et al., 2016). More recently, Acevedo *et al.* (2018) examined AGEs and tissue-level mechanics from ulnar samples of UCD-T2DM rats and reported lower elastic modulus, yield and ultimate stress in the T2 diabetic tested in a three-point bend configuration than controls. Additionally, they reported a 40% reduction in the ultimate strain of the collagen fibril during ulna tensile testing measured via SAXS and a 27% increase in fAGEs (Acevedo et al., 2018). Interestingly, a study by Tice *et al.* (2022) investigated skeletal alterations in a non-obese mouse model of T2D (MKR mouse) and found that these mice presented with an increase in fracture toughness at crack initiation but a reduction in cracking toughness and toughening effect in comparison to the control mice. These

changes coincided with compositional changes, such as an increase in bulk fAGEs, pentosidine and CML. However, alterations were also found in the mineral component of the matrix such as an increase in crystal thickness, c-axis length and trending increase in carbonate: phosphate ratio in the MKR diabetic rats than controls, mineral: matrix and crystal orientation however were not different (Tice et al., 2022). They concluded that the increased fragility experienced in the non-obese T2D mice was attributed to altered mineral quality as well as undesired modifications to the organic component of the tissue. Llabre *et al.* (2022b) also reported similar alterations to the mineral component of the matrix in the T2D HFD mouse model, such as increased crystal size and d-spacing, which coincided with a reduced initiation and maximum toughness and increase in fAGEs, pentosidine and CML in the diabetic groups versus the controls. In fact, Llabre *et al.* (2022) found initiation toughness was negatively associated with fAGEs, CML, pentosidine and crystal d-spacing, whilst Tice *et al.* (2022) reported a negative correlation between cracking toughness and fAGEs, and a positive correlation between c-axis length, CML and pentosidine. Another very recent study by Mehta *et al.* (2023b) explored the viscoelastic properties of vertebral bone in a rat model of T2D, they found a significant reduction in creep strain, creep rate and stress relaxation in the T2D rats versus the controls and they also reported a negative correlation between NE-xLR, creep rate and stress relaxation. There are some drawbacks to the animal studies of bone fragility in T2D listed in Table 2.15 whereby many of these studies are limited by disease duration with some rodents in these studies being overtly diabetic for as little as ~4-weeks (Micheletti et al., 2023; Woolley et al., 2023) and with the average duration being 12.3-weeks. Taken together, most animal studies report a lower tissue-level stiffness in the T2D subjects versus the controls which often coincide with reduced tissue strength and similar to human studies some research has shown that indentation distances may be great in the rodents with T2D in comparison to their healthy counterpart. Understanding how fracture toughness is affected is more ambiguous since some studies have shown reductions in stress intensity and crack initiation and cracking toughness while others have shown no changes or increases, this might be due to the strain of animal used, the duration of the disease the animals have experience or not being able to detect any changes might be a functions of having a lower powered study.

Table 2.14: Summary of tissue-mechanical properties from human studies of T2D.

	Gender (age)	Tissue type										Fibril strain		Viscoelastic		Stress relaxed		Modulus	
			E	Hardness	σ_u / σ_y	ϵ_u / ϵ_y	PY- ϵ	Toughness	1 st InD	InD Increase	Total InD	Creep InD	EI/InEI	G1	G2	Short	Long	Mean Storage	Mean Loss
Burghardt et al. 2010	Postmenopausal women (62.9 ± 7.7)	Radius ¹ and tibia ² (cortical ^a , trabecular ^b)	= ¹ , ↑ ² , ↑ ^{1a} , =2 ^a				=												
Karim et al. 2018	Male and female (63.8 ± 9.7)	Femoral neck (cortical) ¹ and head (trabecular) ²	= ²		σ_u = ² σ_y ↓ ²	ϵ_y = ²		= ¹	↑ ¹	= ¹	↑ ¹								
Hunt et al. 2019	Male (64.8 ± 8.1)	Femoral neck (trabecular)	↑		σ_u ↑ σ_y ↑	ϵ_y = ϵ_u =	=	=											
Wölfel et al. 2020	Male and female (T2DMa: 73 ± 7; T2DMwHPb: 76 ± 8)	Femoral midshaft (cortical)	= ^{a,b}	= ^a , = ^b															
Parle et al. 2020^s	Male and female (67.1 ± 7.4)	Femoral head (trabecular)			σ_u =														
Piccoli et al. 2020	Postmenopausal women (75.2 ± 8.5)	Femoral head (trabecular)	=		σ_u = σ_y =														
Cirovic et al. 2022	Postmenopausal women (77.1 ± 9.8)	Femoral neck (trabecular)		↓															

Table 2.15: Summary of tissue-mechanical properties from animal studies of T2D.

	Animal (Strain) Gender	Age (duration of T2D)	Tissue type	E	Hardness	σ_u / σ_y	ϵ_u / ϵ_y	PY- ϵ	Toughness	InD			$K_{c, \text{init}}$	Cracking toughness	Viscoelastic properties (0.2 & 0.4% strain)					
										1 st	InD Increase	Total			Loading modulus	Unloading modulus	Creep strain	Recovery strain	Creep rate	Stress relaxation
Saito <i>et al.</i> 2006*	Rat (WBN/Kob) Male	1, 2, 4, 6, 8, 10, 12, 14, 16 & 18 months (24-28 weeks*)	Femur	↓																
Prisby <i>et al.</i> 2008*	Rat (ZDF (fa/fa)) Male	7, 13 & 20 weeks (8 weeks*)	Femur (midshaft) ^{1a} , (neck) ^{1b} , vertebra ² , tibia ³	= ^{1,3}		σ_u = ^{1,3}														
Reinwald <i>et al.</i> 2009	Rat ZDF (fa/fa), Male	21 weeks	Femur (midshaft) ¹ , vertebra ²	↓ ²		σ_u = ¹ ↓ ² σ_y = ¹	ϵ_u = ¹													
	Rat ZDSD Male	33 weeks		12-18 weeks	↓ ²		σ_u = ¹ ↓ ² σ_y = ¹	ϵ_u = ¹												
Hamann <i>et al.</i> 2013+	Rat ZDF (fa/fa), Male	23 weeks (11 weeks)	Femur (dm, midshaft) ^{1a} , (neck) ^{1b} , vertebra ²	↓ ^{1a}		σ_u ↓ ^{1a}		= ^{1a}												
Gallant <i>et al.</i> 2013	Rat (ZDSD) Male	32 weeks (10 weeks)	Femur (midshaft) ¹ , vertebra ²	= ¹		σ_u ↓ ^{1,2}		↓ ^{1,2}	↑ ^{1,2}											
Devlin <i>et al.</i> 2014*	Mouse (Tallyho/Jn gJ (TH)) Male	8 & 17 weeks (~7 weeks*)	Femur ¹ (dm) ^{1a} , (midshaft) ^{1b} , vertebra ² , tibia ³	= ¹					↑ ³	= ³										

	Animal (Strain) Gender	Age (duration of T2D)	Tissue type									Viscoelastic properties (0.2 & 0.4% strain)								
				E	Hardness	σ_u / σ_y	ϵ_u / ϵ_y	PY- ϵ	Toughness	1 st InD	InD Increase	Total InD	$K_{c, \text{init}}$	Cracking toughness	Loading modulus	Unloading modulus	Creep strain	Recovery strain	Creep rate	Stress relaxation
Hammond et al. 2014	Rat (ZSDS) Male	30 weeks (~12 weeks)	Tibia							=	↓	=								
Creecy et al. 2016*	Rat (ZSDS) Male	16, 22 & 29 weeks (8-14 weeks*)	Femur (dm) ^{1a} , (midshaft) ^{1b} , vertebra ² , radius ³	= ^{1b}		$\sigma_u = 1b, 3$			= ^{1b} , ↓ ³				= ^{1b}	= ^{1b}						
Creecy et al. 2018*	Mouse (Tallyho/JngJ (TH)) Male	16 & 34 weeks (~24 weeks)	Femur (dm) ^{1a} , (midshaft) ^{1b} , vertebra ²	= ^{1b}		$\sigma_u = 1b$, ↑ ²			= ^{1b}				↓ ^{1b#}	= ^{1b}						
Acevedo et al. 2018+	Rat (UCD-T2DM) Male	6 months (9.9 ± 1 weeks)	Ulnae ¹ , vertebra ²	↓ ¹		σ_u ↓ ¹ , σ_y ↓ ¹	ϵ_y ↓ ¹ , ϵ_u ↓ ¹													
Ay et al. 2020	Rat (STZ Wistar Albino) Male	1 and 3 months (~12 weeks*)	Femur (dm)	↓	↓															
Sihota et al. 2020	Rat (HFD STZ Sprague Dawley) Female	21-22 weeks (8 weeks)	Femur	↓	↓					↑	↑	↑								
Tice et al. 2022	Mouse (MKR) Male	15 weeks (14 weeks)	Femur										↑	↓						

	Animal (Strain) Gender	Age (duration of T2D)	Tissue type									Viscoelastic properties (0.2 & 0.4% strain)								
				E	Hardness	σ_u / σ_y	ϵ_u / ϵ_y	PY- ϵ	Toughness	1 st InD	InD Increase	Total InD	$K_{c, init}$	Cracking toughness	Loading modulus	Unloading modulus	Creep strain	Recovery strain	Creep rate	Stress relaxation
Llabre et al. 2022	Mouse (C57BL/6J) Male	32 weeks (~9 weeks)	Femur																	
Micheletti et al. 2023	Rat (LepR -/- Lund MetS) Male	20 weeks (~4 weeks)	Femur ¹ , Calvaria ²						=	=	=									
Woolley et al. 2023	Rat (ZDSD) Male	19 weeks (~4 weeks)	Femur	=	=	$\epsilon_y =$														
Mehta et al. 2023	Rat (Sprague-Dawley) Female	21-22 weeks (8 weeks)	Vertebra			$\sigma_u \uparrow$														

*only focusing on oldest age group; +only comparing to vehicle group; #trending significance; \uparrow , increase; \downarrow , decrease; =, no difference; E, Elastic modulus; σ_u , Ultimate stress; σ_y , Yield stress; ϵ_u , Ultimate strain; ϵ_y , Yield strain; PY- ϵ , Post-yield strain; InD, Indentation distance; El, Elastic region; InEl, Inelastic region.

2.8 Summary

In summary, T2D is a metabolic disease that can have deleterious effects at various levels throughout the body such as impairing cellular metabolism to altering the bone matrix and ultimately impairing the bone biomechanics. While patients with T2D are at an increased risk of bone fracture, the mechanisms that ultimately lead to this are not fully understood. Much of the current focus has been on the collagen component, particularly the accumulation of non-enzymatic AGEs, which have been proposed to stiffen the collagen matrix and impair the mechanical integrity of the tissue. However, to date in literature there has been no clear causal link found being AGEs and bone fragility in T2D. This highlights that other mechanisms must be responsible for the increased fragility, but the current data is limited since often the collagen and mineral components are studied in isolation. Additionally, the implications of disease duration and severity on bone fracture risk in patients has been difficult to properly examine in human studies since it is difficult to know the exact timepoint when a patient became diabetic. It is also difficult to control for different confounding factors such as sex and BMI. Hence, this thesis is a longitudinal investigation of the multiscale mechanics of bone fragility in T2D using a Zucker Diabetic Fatty (ZDF (*fa/fa*)) rat.

2.9 References

- Acevedo, C., Sylvia, M., Schaible, E., Graham, J.L., Stanhope, K.L., Metz, L.N., Gludovatz, B., Schwartz, A. V., Ritchie, R.O., Alliston, T.N., Havel, P.J., Fields, A.J., 2018. Contributions of Material Properties and Structure to Increased Bone Fragility for a Given Bone Mass in the UCD-T2DM Rat Model of Type 2 Diabetes. *J. Bone Miner. Res.* 33, 1066–1075. <https://doi.org/10.1002/jbmr.3393>
- Akbari, M., Hassan-Zadeh, V., 2018. IL-6 signalling pathways and the development of type 2 diabetes. *Inflammopharmacology* 26, 685–698. <https://doi.org/10.1007/s10787-018-0458-0>
- Ali, S., Rao, N.L., 2020. Correlation of serum fluorescence of advanced glycation end products with diabetes duration and glycemic control in type 2 diabetic patients. *Biomed. Res. Ther.* 7, 3933–3938. <https://doi.org/10.15419/bmrat.v7i8.623>
- Alikhani, M., Alikhani, Z., Boyd, C., Maclellan, C.M., Raptis, M., Liu, R., Pischon, N., Trackman, P.C., Gerstenfeld, L., Graves, D.T., 2007. Advanced glycation end products stimulate osteoblast apoptosis via the MAP kinase and cytosolic apoptotic pathways 40, 345–353. <https://doi.org/10.1016/j.bone.2006.09.011>
- Allen, M.R., Burr, D.B., 2013. Bone Modeling and Remodeling. *Basic Appl. Bone Biol.* 75–90. <https://doi.org/10.1016/B978-0-12-416015-6.00004-6>
- Amrein, K., Dobnig, H., Wagner, D., Piswanger-Sölkner, C., Pieber, T.R., Pilz, S., Tomaschitz, A., Dimai, H.P., Fahrleitner-Pammer, A., 2014. Sclerostin in institutionalized elderly women: Associations with quantitative bone ultrasound, bone turnover, fractures, and mortality. *J. Am. Geriatr. Soc.* 62, 1023–1029. <https://doi.org/10.1111/jgs.12791>
- Arakawa, S., Suzuki, R., Kurosaka, D., Ikeda, R., Hayashi, H., Kayama, T., Ohno, R. ichi, Nagai, R., Marumo, K., Saito, M., 2020. Mass spectrometric quantitation of AGEs and enzymatic crosslinks in human cancellous bone. *Sci. Rep.* 10, 1–12. <https://doi.org/10.1038/s41598-020-75923-8>
- Ascenzi, A., Bonucci, E., 1976. Relationship between ultrastructure and “pin test” in osteons. *Clin. Orthop. Relat. Res.* 275–94.
- ASTM E-399, 2014. Standard Test Method for Linear-Elastic Plane-Strain Fracture Toughness K_{Ic} of 1–33. <https://doi.org/10.1520/E0399-12E02.2>

- ASTM E1820, 2012. Standard Test Method for Measurement of Fracture Toughness i, 1–56.
<https://doi.org/10.1520/E1820-11.2>
- Augat, P., Schorlemmer, S., 2006. The role of cortical bone and its microstructure in bone strength. *Age Ageing* 35, 27–31. <https://doi.org/10.1093/ageing/afl081>
- Awonusi, A., Morris, M.D., Tecklenburg, M.M.J., 2007. Carbonate assignment and calibration in the Raman spectrum of apatite. *Calcif. Tissue Int.* 81, 46–52.
<https://doi.org/10.1007/s00223-007-9034-0>
- Ay, B., Parolia, K., Liddell, R.S., Qiu, Y., Grasselli, G., Cooper, D.M.L., Davies, J.E., 2020. Hyperglycemia compromises Rat Cortical Bone by Increasing Osteocyte Lacunar Density and Decreasing Vascular Canal Volume. *Commun. Biol.* 3, 1–9.
<https://doi.org/10.1038/s42003-019-0747-1>
- Bach-Gansmo, F.L., Irvine, S.C., Brüel, A., Thomsen, J.S., Birkedal, H., 2013. Calcified cartilage islands in rat cortical bone. *Calcif. Tissue Int.* 92, 330–338.
<https://doi.org/10.1007/s00223-012-9682-6>
- Bach-Gansmo, F.L., Weaver, J.C., Jensen, M.H., Leemreize, H., Mader, K.S., Stampanoni, M., Brüel, A., Thomsen, J.S., Birkedal, H., 2015. Osteocyte lacunar properties in rat cortical bone: Differences between lamellar and central bone. *J. Struct. Biol.* 191, 59–67.
<https://doi.org/10.1016/j.jsb.2015.05.005>
- Bagi, C.M., Wilkie, D., Georgelos, K., Williams, D., Bertolini, D., 1997. Morphological and structural characteristics of the proximal femur in human and rat. *Bone* 21, 261–267.
[https://doi.org/10.1016/S8756-3282\(97\)00121-X](https://doi.org/10.1016/S8756-3282(97)00121-X)
- Baron, R., Kneissel, M., 2013. WNT signaling in bone homeostasis and disease: from human mutations to treatments. *Nat. Med.* 19, 179–192. <https://doi.org/10.1038/nm.3074>
- Bartoli, E., Fra, G.P., Schianca, G.P.C., 2011. The oral glucose tolerance test (OGTT) revisited. *Eur. J. Intern. Med.* 22, 8–12. <https://doi.org/10.1016/j.ejim.2010.07.008>
- Bastard, J.P., Maachi, M., Van Nhieu, J.T., Jardel, C., Bruckert, E., Grimaldi, A., Robert, J.J., Capeau, J., Hainque, B., 2002. Adipose tissue IL-6 content correlates with resistance to insulin activation of glucose uptake both in vivo and in vitro. *J. Clin. Endocrinol. Metab.* 87, 2084–2089. <https://doi.org/10.1210/jcem.87.5.8450>
- Bažant, Z.P., 2004. Scaling theory for quasibrittle structural failure. *Proc. Natl. Acad. Sci. U.*

- S. A. 101, 13400–13407. <https://doi.org/10.1073/pnas.0404096101>
- Beck-Nielsen, H., Groop, L.C., 1994. Metabolic and genetic characterization of prediabetic states. Sequence of events leading to non-insulin-dependent diabetes mellitus. *J. Clin. Invest.* 94, 1714–1721. <https://doi.org/10.1172/JCI117518>
- Bellido, T., Borba, V.Z.C., Roberson, P., Manolagas, S.C., 1997. Activation of the Janus kinase/STAT (signal transducer and activator of transcription) signal transduction pathway by interleukin-6-type cytokines promotes osteoblast differentiation. *Endocrinology* 138, 3666–3676. <https://doi.org/10.1210/endo.138.9.5364>
- Bennett, C.M., Guo, M., Dharmage, S.C., 2007. HbA1c as a screening tool for detection of Type 2 diabetes: A systematic review. *Diabet. Med.* 24, 333–343. <https://doi.org/10.1111/j.1464-5491.2007.02106.x>
- Bilezikian, J.P., Bouillon, R., Clemens, T., Compston, J., Bauer, D.C., Ebeling, P.R., Engelke, K., Goltzman, D., Guise, T., Jan De Beur, S.M., Jüppner, H., Lyons, K., McCauley, L., McClung, M.R., Miller, P.D., Papapoulos, S.E., Roodman, G.D., Rosen, C.J., Seeman, E., Thakker, R. V., Whyte, M.P., Zaidi, M., 2018. Primer on the Metabolic Bone Diseases and Disorders of Mineral Metabolism, Primer on the Metabolic Bone Diseases and Disorders of Mineral Metabolism. Wiley. <https://doi.org/10.1002/9781119266594>
- Birkhold, A.I., Razi, H., Duda, G.N., Weinkamer, R., Checa, S., Willie, B.M., 2016. The Periosteal Bone Surface is Less Mechano-Responsive than the Endocortical. *Sci. Rep.* 6, 1–11. <https://doi.org/10.1038/srep23480>
- Blair, H.C., Larrouture, Q.C., Li, Y., Lin, H., Beer-Stoltz, D., Liu, L., Tuan, R.S., Robinson, L.J., Schlesinger, P.H., Nelson, D.J., 2017. Osteoblast differentiation and bone matrix formation in vivo and in vitro. *Tissue Eng. - Part B Rev.* 23, 268–280. <https://doi.org/10.1089/ten.teb.2016.0454>
- Blanchard, F., Duplomb, L., Baud’huin, M., Brounais, B., 2009. The dual role of IL-6-type cytokines on bone remodeling and bone tumors. *Cytokine Growth Factor Rev.* 20, 19–28. <https://doi.org/10.1016/j.cytogfr.2008.11.004>
- Bonds, D.E., Larson, J.C., Schwartz, A. V., Strotmeyer, E.S., Robbins, J., Rodriguez, B.L., Johnson, K.C., Margolis, K.L., 2006. Risk of fracture in women with type 2 diabetes: The women’s health initiative observational study. *J. Clin. Endocrinol. Metab.* 91, 3404–3410.

<https://doi.org/10.1210/jc.2006-0614>

- Bonucci, E., 1999. *Mechanical Testing of Bone and the Bone-Implant Interface*, CRC Press. CRC Press. <https://doi.org/10.1201/9781420073560>
- Boskey, A.L., 2013. Bone composition: relationship to bone fragility and antiosteoporotic drug effects. *Bonekey Rep.* 2, 1–11. <https://doi.org/10.1038/bonekey.2013.181>
- Boskey, A.L., 2006. Mineralization, Structure and Function of Bone, in: *Dynamics of Bone and Cartilage Metabolism*. Elsevier, pp. 201–212. <https://doi.org/10.1016/B978-012088562-6/50013-3>
- Boskey, A.L., Donnelly, E., Boskey, E., Spevak, L., Ma, Y., Zhang, W., Lappe, J., Recker, R.R., 2016. Examining the Relationships Between Bone Tissue Composition, Compositional Heterogeneity, and Fragility Fracture: A Matched Case-Controlled FTIR Study. *J. Bone Miner. Res.* 31, 1070–1081. <https://doi.org/10.1002/jbmr.2759>
- Boskey, A.L., Imbert, L., 2017. Bone quality changes associated with aging and disease: a review. *Ann. N. Y. Acad. Sci.* 1410, 93–106. <https://doi.org/10.1111/nyas.13572>
- Boskey, A.L., Marks, S.C., 1985. Mineral and matrix alterations in the bones of incisors-absent (ia/ia) osteopetrotic rats. *Calcif. Tissue Int.* 37, 287–292. <https://doi.org/10.1007/BF02554876>
- Boskey, A.L., Pleshko, N., Doty, S., Mendelsohn, R., 1992. Applications of Fourier Transform Infrared (FT-IR) Microscopy to the Study of Mineralization in Bone and Cartilage. *Cells Mater.* 2, 4.
- Botella Martínez, S., Varo Cenarruzabeitia, N., Escalada San Martín, J., Calleja Canelas, A., 2016. The diabetic paradox: Bone mineral density and fracture in type 2 diabetes. *Endocrinol. y Nutr.* (English Ed. 63, 495–501. <https://doi.org/10.1016/j.endoen.2016.10.010>
- Bouxsein, M.L., Boyd, S.K., Christiansen, B.A., Guldberg, R.E., Jepsen, K.J., Müller, R., 2010. Guidelines for assessment of bone microstructure in rodents using micro-computed tomography. *J. Bone Miner. Res.* 25, 1468–1486. <https://doi.org/10.1002/jbmr.141>
- Briot, K., Geusens, P., Em Bultink, I., Lems, W.F., Roux, C., 2017. Inflammatory diseases and bone fragility. *Osteoporos. Int.* 28, 3301–3314. <https://doi.org/10.1007/s00198-017-4189-7>

- Bucay, N., Sarosi, I., Dunstan, C.R., Morony, S., Tarpley, J., Capparelli, C., Scully, S., Tan, H.L., Xu, W., Lacey, D.L., Boyle, W.J., Simonet, W.S., 1998. osteoprotegerin-deficient mice develop early onset osteoporosis and arterial calcification. *Genes Dev.* 12, 1260–1268. <https://doi.org/10.1101/gad.12.9.1260>
- Buehler, M.J., 2007. Molecular nanomechanics of nascent bone: Fibrillar toughening by mineralization. *Nanotechnology* 18. <https://doi.org/10.1088/0957-4484/18/29/295102>
- Burger, E.H., Klein-Nulend, J., 1999. Mechanotransduction in bone—role of the lacunocanalicular network. *FASEB J.* 13, 101–112. <https://doi.org/10.1096/fasebj.13.9001.s101>
- Burghardt, A.J., Issever, A.S., Schwartz, A. V., Davis, K.A., Masharani, U., Majumdar, S., Link, T.M., 2010. High-resolution peripheral quantitative computed tomographic imaging of cortical and trabecular bone microarchitecture in patients with type 2 diabetes mellitus. *J. Clin. Endocrinol. Metab.* 95, 5045–5055. <https://doi.org/10.1210/jc.2010-0226>
- Burghardt, A.J., Kazakia, G.J., Laib, A., Majumdar, S., 2008. Quantitative Assessment of Bone Tissue Mineralization with Polychromatic Micro-Computed Tomography. *Calcif. Tissue Int.* 83, 129–138. <https://doi.org/10.1007/s00223-008-9158-x>
- Busa, B., Miller, L.M., Rubin, C.T., Qin, Y.X., Judex, S., 2005. Rapid establishment of chemical and mechanical properties during lamellar bone formation. *Calcif. Tissue Int.* 77, 386–394. <https://doi.org/10.1007/s00223-005-0148-y>
- Carriero, A., Carriero, A., Bruse, J.L., Oldknow, K.J., Luis, J., Farquharson, C., Shefelbine, S.J., 2014. Reference point indentation is not indicative of whole bone stress intensity fracture toughness Reference point indentation is not indicative of whole mouse bone measures of stress intensity fracture toughness. *Bone* 69. <https://doi.org/10.1016/j.bone.2014.09.020>
- Casanova, M., Balmelli, A., Carnelli, D., Courty, D., Schneider, P., Müller, R., 2017. Nanoindentation analysis of the micromechanical anisotropy in mouse cortical bone. *R. Soc. Open Sci.* 4, 160971. <https://doi.org/10.1098/rsos.160971>
- Cassidy, F.C., Shortiss, C., Murphy, C.G., Kearns, S.R., Curtin, W., De Buitléir, C., O’Brien, T., Coleman, C.M., 2020. Impact of type 2 diabetes mellitus on human bone marrow stromal cell number and phenotypic characteristics. *Int. J. Mol. Sci.* 21, 1–20.

<https://doi.org/10.3390/ijms21072476>

- Catalfamo, D.L., Britten, T.M., Storch, D.I., Calderon, N.L., Sorenson, H.L., Wallet, S.M., 2014. Hyperglycemia Induced and Intrinsic Alterations in Type 2 Diabetes-Derived Osteoclast Function. *Bone* 23, 1–7. <https://doi.org/10.1111/odi.12002>.Hyperglycemia
- CDC, 2023. Type 2 Diabetes [WWW Document]. Centers Dis. Control Prev. URL <https://www.cdc.gov/diabetes/basics/type2.html#:~:text=Type 2 diabetes most often,adults are also developing it.> (accessed 1.8.23).
- Chen, D., Wang, M., 2005. Development and application of rodent models for type 2 diabetes 307–317. <https://doi.org/10.1111/j.1463-1326.2004.00392.x>
- Christiansen, B.A., 2016. Effect of micro-computed tomography voxel size and segmentation method on trabecular bone microstructure measures in mice. *Bone Reports* 5, 136–140. <https://doi.org/10.1016/j.bonr.2016.05.006>
- Christodoulou, C., Cooper, C., 2003. What is osteoporosis? *Postgrad. Med. J.* 79, 133–138. <https://doi.org/10.1136/pmj.79.929.133>
- Cirovic, A., Cirovic, A., Djukic, D., Djonic, D., Zivkovic, V., Nikolic, S., Djuric, M., Milovanovic, P., 2022. Three-dimensional mapping of cortical porosity and thickness along the superolateral femoral neck in older women. *Sci. Rep.* 12, 1–8. <https://doi.org/10.1038/s41598-022-19866-2>
- Clark, J.B., Palmer, C.J., Shaw, W.N., 1983. The Diabetic Zucker Fatty Rat. *Proc. Soc. Exp. Biol. Med.* 173, 68–75. <https://doi.org/10.3181/00379727-173-41611>
- Clee, S.M., Attie, A.D., 2007. The genetic landscape of type 2 diabetes in mice. *Endocr. Rev.* 28, 48–83. <https://doi.org/10.1210/er.2006-0035>
- Cory, E., Nazarian, A., Entezari, V., Vartanians, V., Ralph, M., Snyder, B.D., 2010. Compressive axial mechanical properties of rat bone as functions of bone volume fraction , apparent density and micro-ct based mineral density 43, 953–960. <https://doi.org/10.1016/j.jbiomech.2009.10.047>
- Cowin, S., 2001. *Bone Mechanics Handbook*. *Lancet* 240, 43. [https://doi.org/10.1016/S0140-6736\(00\)62141-4](https://doi.org/10.1016/S0140-6736(00)62141-4)
- Creecy, A., Uppuganti, S., Merkel, A.R., O’Neal, D., Makowski, A.J., Granke, M., Voziyan,

- P., Nyman, J.S., 2016. Changes in the Fracture Resistance of Bone with the Progression of Type 2 Diabetes in the ZDSD Rat. *Calcif. Tissue Int.* 99, 289–301. <https://doi.org/10.1007/s00223-016-0149-z>
- Creecy, A., Uppuganti, S., Unal, M., Clay Bunn, R., Voziyan, P., Nyman, J.S., 2018a. Low bone toughness in the TallyHO model of juvenile type 2 diabetes does not worsen with age. *Bone* 110, 204–214. <https://doi.org/10.1016/j.bone.2018.02.005>
- Creecy, A., Uppuganti, S., Unal, M., Clay Bunn, R., Voziyan, P., Nyman, J.S., 2018b. Low bone toughness in the TallyHO model of juvenile type 2 diabetes does not worsen with age. *Bone* 110, 204–214. <https://doi.org/10.1016/j.bone.2018.02.005>
- Crockett, J.C., Rogers, M.J., Coxon, F.P., Hocking, L.J., Helfrich, M.H., 2011. Bone remodelling at a glance. *J. Cell Sci.* 124, 991–998. <https://doi.org/10.1242/jcs.063032>
- Currey, J.D., 2012. The structure and mechanics of bone. *J. Mater. Sci.* 47, 41–54. <https://doi.org/10.1007/s10853-011-5914-9>
- Currey, J.D., 2003. Role of collagen and other organics in the mechanical properties of bone. *Osteoporos. Int.* 14 Suppl 5, 29–36. <https://doi.org/10.1007/s00198-003-1470-8>
- Currey, J.D., 1984. Effects of differences in mineralization on the mechanical properties of bone. *Philos. Trans. R. Soc. Lond. B. Biol. Sci.* 304, 509–518. <https://doi.org/10.1098/rstb.1984.0042>
- Czaplicki, S., 2013. Chromatography in Bioactivity Analysis of Compounds, in: *Column Chromatography*. InTech, pp. 99–122. <https://doi.org/10.5772/55620>
- Dailey, H.L., Kersh, M.E., Collins, C.J., Troy, K.L., 2023. Mechanical Biomarkers in Bone Using Image-Based Finite Element Analysis. *Curr. Osteoporos. Rep.* 21, 266–277. <https://doi.org/10.1007/s11914-023-00784-9>
- Daniele, G., Winnier, D., Mari, A., Bruder, J., Fourcaudot, M., Pengou, Z., Tripathy, D., Jenkinson, C., Folli, F., 2015. Sclerostin and insulin resistance in prediabetes: Evidence of a cross talk between bone and glucose metabolism. *Diabetes Care* 38, 1509–1517. <https://doi.org/10.2337/dc14-2989>
- Danielsson, P.E., 1980. Euclidean distance mapping. *Comput. Graph. Image Process.* 14, 227–248. [https://doi.org/10.1016/0146-664X\(80\)90054-4](https://doi.org/10.1016/0146-664X(80)90054-4)

- Day, T.F., Guo, X., Garrett-Beal, L., Yang, Y., 2005. Wnt/ β -catenin signaling in mesenchymal progenitors controls osteoblast and chondrocyte differentiation during vertebrate skeletogenesis. *Dev. Cell* 8, 739–750. <https://doi.org/10.1016/j.devcel.2005.03.016>
- De Benedetti, F., Alonzi, T., Moretta, A., Lazzaro, D., Costa, P., Poli, V., Martini, A., Ciliberto, G., Fattori, E., 1997. Interleukin 6 causes growth impairment in transgenic mice through a decrease in insulin-like growth factor-I. A model for stunted growth in children with chronic inflammation. *J. Clin. Invest.* 99, 643–650. <https://doi.org/10.1172/JCI119207>
- De Benedetti, F., Meazza, C., Oliveri, M., Pignatti, P., Vivarelli, M., Alonzi, T., Fattori, E., Garrone, S., Barreca, A., Martini, A., 2001. Effect of IL-6 on IGF binding protein-3: A study in IL-6 transgenic mice and in patients with systemic juvenile idiopathic arthritis. *Endocrinology* 142, 4818–4826. <https://doi.org/10.1210/endo.142.11.8511>
- Delgado-Calle, J., Sato, A.Y., Bellido, T., 2017. Role and mechanism of action of sclerostin in bone. *Bone* 96, 29–37. <https://doi.org/10.1016/j.bone.2016.10.007>
- Delmas, P.D., Tracy, R.P., Riggs, B.L., Mann, K.G., 1984. Identification of the noncollagenous proteins of bovine bone by two-dimensional gel electrophoresis. *Calcif. Tissue Int.* 36, 308–316. <https://doi.org/10.1007/BF02405335>
- Devlin, Van Vliet, M., Motyl, K., Karim, L., Brooks, D.J., Louis, L., Conlon, C., Rosen, C.J., Bouxsein, M.L., 2014. Early-onset type 2 diabetes impairs skeletal acquisition in the male TALLYHO/JngJ mouse. *Endocrinol. (United States)* 155, 3806–3816. <https://doi.org/10.1210/en.2014-1041>
- Díaz, A., López-Grueso, R., Gambini, J., Monleón, D., Mas-Bargues, C., Abdelaziz, K.M., Viña, J., Borrás, C., 2019. Sex Differences in Age-Associated Type 2 Diabetes in Rats—Role of Estrogens and Oxidative Stress. *Oxid. Med. Cell. Longev.* 2019, 1–13. <https://doi.org/10.1155/2019/6734836>
- Donath, M.Y., Shoelson, S.E., 2011. Type 2 diabetes as an inflammatory disease. *Nat. Publ. Gr.* 11, 98–107. <https://doi.org/10.1038/nri2925>
- Donnelly, E., 2011. Methods for assessing bone quality: A review. *Clin. Orthop. Relat. Res.* 469, 2128–2138. <https://doi.org/10.1007/s11999-010-1702-0>
- Donnelly, E., Chen, D.X., Boskey, A.L., Baker, S.P., Van Der Meulen, M.C.H., 2010. Contribution of mineral to bone structural behavior and tissue mechanical properties.

- Calcif. Tissue Int. 87, 450–460. <https://doi.org/10.1007/s00223-010-9404-x>
- Donneys, A., Nelson, N.S., Deshpande, S.S., Boguslawski, M.J., Tchanque-Fossuo, C.N., Farberg, A.S., Buchman, S.R., 2012. Quantifying mineralization using bone mineral density distribution in the mandible. *J. Craniofac. Surg.* 23, 1502–1506. <https://doi.org/10.1097/SCS.0b013e3182519a76>
- Doube, M., 2015. The ellipsoid factor for quantification of rods, plates, and intermediate forms in 3D geometries. *Front. Endocrinol. (Lausanne)*. 6, 1–5. <https://doi.org/10.3389/fendo.2015.00015>
- Dragomir-Daescu, D., Op Den Buijs, Jorn Mceligot McEligot, S., Dai, Y., Entwistle, R.C., Salas, C., Melton, L.J., Bennet, K.E., Khosla, S., Amin, S., 2011. Robust QCT / FEA Models of Proximal Femur Stiffness and Fracture Load During a Sideways Fall on the Hip. *Ann. of Biomed. Eng.* 39, 742–755. <https://doi.org/10.1007/s10439-010-0196-y>
- Duckworth, W.C., 2001. Hyperglycemia and Cardiovascular Disease. *Curr. Atheroscler. Rep.* 3, 383–391.
- Einhorn, T.A., 1998. The cell and molecular biology of fracture healing. *Clin. Orthop. Relat. Res.* S7-21. <https://doi.org/10.1097/00003086-199810001-00003>
- Einhorn, T.A., Boskey, A.L., Gundberg, C.M., Vigorita, V.J., Devlin, V.J., Beyer, M.M., 1988. The mineral and mechanical properties of bone in chronic experimental diabetes. *J. Orthop. Res.* 6, 317–323. <https://doi.org/10.1002/jor.1100060303>
- Etgen, G.J., Oldham, B.A., 2000. Profiling of Zucker diabetic fatty rats in their progression to the overt diabetic state. *Metabolism*. 49, 684–688. [https://doi.org/10.1016/S0026-0495\(00\)80049-9](https://doi.org/10.1016/S0026-0495(00)80049-9)
- Eyre, D.R., Dickson, I.R., Van Ness, K., 1988. Collagen cross-linking in human bone and articular cartilage. Age-related changes in the content of mature hydroxypyridinium residues. *Biochem. J.* 252, 495–500. <https://doi.org/10.1042/bj2520495>
- Fajardo, R.J., Karim, L., Calley, V.I., Bouxsein, M.L., 2014. A Review of Rodent Models of Type 2 Diabetic Skeletal Fragility. *J. Bone Miner. Res.* 29, 1025–1040. <https://doi.org/10.1002/jbmr.2210>
- Fan, J., Abedi-Dorcheh, K., Sadat Vaziri, A., Kazemi-Aghdam, F., Rafieyan, S., Sohrabinejad, M., Ghorbani, M., Rastegar Adib, F., Ghasemi, Z., Klavins, K., Jahed, V., 2022. A Review

- of Recent Advances in Natural Polymer-Based Scaffolds for Musculoskeletal Tissue Engineering. *Polymers (Basel)*. 14, 2097. <https://doi.org/10.3390/polym14102097>
- Fantner, G.E., Hassenkam, T., Kindt, J.H., Weaver, J.C., Birkedal, H., Pechenik, L., Cutroni, J.A., Cidade, G.A.G., Stucky, G.D., Morse, D.E., Hansma, P.K., 2005. Sacrificial bonds and hidden length dissipate energy as mineralized fibrils separate during bone fracture. *Nat. Mater.* 4, 612–616. <https://doi.org/10.1038/nmat1428>
- Farlay, D., Duclos, M.-E., Gineyts, E., Bertholon, C., Viguet-Carrin, S., Nallala, J., Sockalingum, G.D., Bertrand, D., Roger, T., Hartmann, D.J., Chapurlat, R., Boivin, G., 2011. The Ratio 1660/1690 cm^{-1} Measured by Infrared Microspectroscopy Is Not Specific of Enzymatic Collagen Cross-Links in Bone Tissue. *PLoS One* 6, e28736. <https://doi.org/10.1371/journal.pone.0028736>
- Farlay, D., Panczer, G., Rey, C., Delmas, P.D., Boivin, G., 2010. Mineral maturity and crystallinity index are distinct characteristics of bone mineral. *J. Bone Miner. Metab.* 28, 433–445. <https://doi.org/10.1007/s00774-009-0146-7>
- Faselis, C., Katsimardou, A., Imprialos, K., Deligkaris, P., Kallistratos, M., Dimitriadis, K., 2019. Microvascular Complications of Type 2 Diabetes Mellitus. *Curr. Vasc. Pharmacol.* 18, 117–124. <https://doi.org/10.2174/1570161117666190502103733>
- Ferris, B.D., Klenerman, L., Dodds, R.A., Bitensky, L., Chayen, J., 1987. Altered organization of non-collagenous bone matrix in osteoporosis. *Bone* 8, 285–288. [https://doi.org/10.1016/8756-3282\(87\)90003-2](https://doi.org/10.1016/8756-3282(87)90003-2)
- Fonseca, J.E., Santos, M.J., Canhão, H., Choy, E., 2009. Interleukin-6 as a key player in systemic inflammation and joint destruction. *Autoimmun. Rev.* 8, 538–542. <https://doi.org/10.1016/j.autrev.2009.01.012>
- Franz-Odendaal, T.A., Hall, B.K., Witten, P.E., 2006. Buried alive: How osteoblasts become osteocytes. *Dev. Dyn.* 235, 176–190. <https://doi.org/10.1002/dvdy.20603>
- Fratzl, P., Gupta, H.S., Paschalis, E.P., Roschger, P., 2004. Structure and mechanical quality of the collagen-mineral nano-composite in bone. *J. Mater. Chem.* 14, 2115–2123. <https://doi.org/10.1039/b402005g>
- Frost, H.M., 1997. On our age-related bone loss: Insights from a new paradigm. *J. Bone Miner. Res.* 12, 1539–1546. <https://doi.org/10.1359/jbmr.1997.12.10.1539>

- Frost, H.M., 1994. Wolff's Law and bone's structural adaptations to mechanical usage: an overview for clinicians. *Angle Orthod.* 64, 175–88. <https://doi.org/10.1043/0003-3219>
- Frost, H.M., 1964. Bone remodeling dynamics. *Arthritis Rheum.* 7, 545. <https://doi.org/https://doi.org/10.1002/art.1780070512>
- Frost, H.M., 1960. In vivo osteocyte death. *J. Bone Joint Surg. Am.* 42-A, 138–43.
- Gallagher, J.C., 1990. The pathogenesis of osteoporosis. *Bone Miner.* 9, 215–227. [https://doi.org/10.1016/0169-6009\(90\)90039-I](https://doi.org/10.1016/0169-6009(90)90039-I)
- Gamsjaeger, S., Brozek, W., Recker, R., Klaushofer, K., Paschalis, E.P., 2014. Transmenopausal changes in trabecular bone quality. *J. Bone Miner. Res.* 29, 608–617. <https://doi.org/10.1002/jbmr.2073>
- Gamsjaeger, S., Masic, A., Roschger, P., Kazanci, M., Dunlop, J.W.C., Klaushofer, K., Paschalis, E.P., Fratzl, P., 2010. Cortical bone composition and orientation as a function of animal and tissue age in mice by Raman spectroscopy. *Bone* 47, 392–399. <https://doi.org/10.1016/j.bone.2010.04.608>
- Gamsjaeger, S., Mendelsohn, R., Boskey, A.L., Gourion-Arsiquaud, S., Klaushofer, K., Paschalis, E.P., 2017a. Vibrational Spectroscopic Imaging for the Evaluation of Matrix and Mineral Chemistry. *Curr Osteoporos Rep* 176, 139–148. <https://doi.org/doi:10.1007/s11914-014-0238-8>
- Gamsjaeger, S., Robins, S.P., Tatakis, D.N., Klaushofer, K., Paschalis, E.P., 2017b. Identification of Pyridinoline Trivalent Collagen Cross-Links by Raman Microspectroscopy. *Calcif. Tissue Int.* 100, 565–574. <https://doi.org/10.1007/s00223-016-0232-5>
- García-Martín, A., Rozas-Moreno, P., Reyes-García, R., Morales-Santana, S., García-Fontana, B., García-Salcedo, J.A., Muñoz-Torres, M., 2012. Circulating levels of sclerostin are increased in patients with type 2 diabetes mellitus. *J. Clin. Endocrinol. Metab.* 97, 234–241. <https://doi.org/10.1210/jc.2011-2186>
- García, I., Chiodo, V., Ma, Y., Boskey, A., 2016. Evidence of altered matrix composition in iliac crest biopsies from patients with idiopathic juvenile osteoporosis. *Connect. Tissue Res.* 57, 28–37. <https://doi.org/10.3109/03008207.2015.1088531>
- Gasser, J.A., Kneissel, M., 2017. Chapter 2 Bone physiology and biology, *Bone Toxicology*.

<https://doi.org/10.1007/978-3-319-56192-9>

Glass, D.A., Bialek, P., Ahn, J.D., Starbuck, M., Patel, M.S., Clevers, H., Taketo, M.M., Long, F., McMahon, A.P., Lang, R.A., Karsenty, G., 2005. Canonical Wnt signaling in differentiated osteoblasts controls osteoclast differentiation. *Dev. Cell* 8, 751–764. <https://doi.org/10.1016/j.devcel.2005.02.017>

Glimcher, M.J., 1989. Mechanism of calcification: Role of collagen fibrils and collagen-phosphoprotein complexes in vitro and in vivo. *Anat. Rec.* 224, 139–153. <https://doi.org/10.1002/ar.1092240205>

Gorski, J.P., 2011. Biomineralization of bone: A fresh view of the roles of non-collagenous proteins. *Front. Biosci.* 16, 2598–2621. <https://doi.org/10.2741/3875>

Gourion-Arsiquaud, S., Faibish, D., Myers, E., Spevak, L., Compston, J., Hodsman, A., Shane, E., Recker, R.R., Boskey, E.R., Boskey, A.L., 2009. Use of FTIR spectroscopic imaging to identify parameters associated with fragility fracture. *J. Bone Miner. Res.* 24, 1565–1571. <https://doi.org/10.1359/jbmr.090414>

Grey, A., Beckley, V., Doyle, A., Fenwick, S., Horne, A., Gamble, G., Bolland, M., 2012. Pioglitazone increases bone marrow fat in type 2 diabetes: Results from a randomized controlled trial. *Eur. J. Endocrinol.* 166, 1087–1091. <https://doi.org/10.1530/EJE-11-1075>

Grynblas, M.D., Tupy, J.H., Sodek, J., 1994. The distribution of soluble, mineral-bound, and matrix-bound proteins in osteoporotic and normal bones. *Bone* 15, 505–513. [https://doi.org/10.1016/8756-3282\(94\)90274-7](https://doi.org/10.1016/8756-3282(94)90274-7)

Gupta, H.S., Wagermaier, W., Zickler, G.A., Hartmann, J., Funari, S.S., Roschger, P., Wagner, D.H., Fratzl, P., 2006. Fibrillar level fracture in bone beyond the yield point. *Int. J. Fract.* 139, 425–436. <https://doi.org/10.1007/s10704-006-6635-y>

Hale, L. V., Galvin, R.J.S., Risteli, J., Ma, Y.L., Harvey, A.K., Yang, X., Cain, R.L., Zeng, Q., Frolik, C.A., Sato, M., Schmidt, A.L., Geiser, A.G., 2007. PINP: A serum biomarker of bone formation in the rat. *Bone* 40, 1103–1109. <https://doi.org/10.1016/j.bone.2006.11.027>

Hamann, C., Goettsch, C., Mettelsiefen, J., Henkenjohann, V., Rauner, M., Hempel, U., Bernhardt, R., Fratzl-Zelman, N., Roschger, P., Rammelt, S., Günther, K.-P., Hofbauer, L.C., 2011. Delayed bone regeneration and low bone mass in a rat model of insulin-

- resistant type 2 diabetes mellitus is due to impaired osteoblast function. *Am. J. Physiol. Metab.* 301, 1220–1228. <https://doi.org/10.1152/ajpendo.00378.2011>
- Hamann, C., Picke, A.K., Campbell, G.M., Balyura, M., Rauner, M., Bernhardt, R., Huber, G., Morlock, M.M., Günther, K.P., Bornstein, S.R., Glüer, C.C., Ludwig, B., Hofbauer, L.C., 2014. Effects of parathyroid hormone on bone mass, bone strength, and bone regeneration in male rats with type 2 diabetes mellitus. *Endocrinology* 155, 1197–1206. <https://doi.org/10.1210/en.2013-1960>
- Hamann, C., Rauner, M., Hohna, Y., Bernhardt, R., Mettelsiefen, J., Goettsch, C., Gunther, K.-P., Stolina, M., Han, C.-Y., Asuncion, F.J., Ominsky, M.S., Hofbauer, L.C., 2013. Sclerostin Antibody Treatment Improves Bone Mass, Bone Strength, and Bone Defect Regeneration in Rats With Type 2 Diabetes Mellitus 28, 627–638. <https://doi.org/10.1002/jbmr.1803>
- Handschin, R.G., Stern, W.B., 1995. X-ray diffraction studies on the lattice perfection of human bone apatite (Crista Iliaca). *Bone* 16, S355–S363. [https://doi.org/10.1016/S8756-3282\(95\)80385-8](https://doi.org/10.1016/S8756-3282(95)80385-8)
- Harrigan, T.P., Mann, R.W., 1985. Characterization of microstructural anisotropy in cancellous bone using a second rank tensor. *J. Mater. Sci.* 19, 761–767.
- Hernandez, C.J., Keaveny, T.M., 2006. A biomechanical perspective on bone quality. *Bone* 39, 1173–1181. <https://doi.org/10.1016/j.bone.2006.06.001>
- Herrmann, M., Seibel, M., 2008. The amino- and carboxyterminal cross-linked telopeptides of collagen type I, NTX-I and CTX-I: A comparative review. *Clin. Chim. Acta* 393, 57–75. <https://doi.org/10.1016/j.cca.2008.03.020>
- Hildebrand, T., Rüeegsegger, P., 1997. A new method for the model-independent assessment of thickness in three-dimensional images. *J. Microsc.* 185, 67–75. <https://doi.org/10.1046/j.1365-2818.1997.1340694.x>
- Hildebrand, Tor, Rüeegsegger, P., 1997. Quantification of bone microarchitecture with the structure model index. *Comput. Methods Biomech. Biomed. Engin.* 1, 15–23. <https://doi.org/10.1080/01495739708936692>
- Hill, T.P., Später, D., Taketo, M.M., Birchmeier, W., Hartmann, C., 2005. Canonical Wnt/ β -catenin signaling prevents osteoblasts from differentiating into chondrocytes. *Dev. Cell* 8,

727–738. <https://doi.org/10.1016/j.devcel.2005.02.013>

Hofbauer, L., Lacey, D., Dunstan, C., Spelsberg, T., Riggs, B., Khosla, S., 1999. Interleukin-1 β and tumor necrosis factor- α , but not interleukin-6, stimulate osteoprotegerin ligand gene expression in human osteoblastic cells. *Bone* 25, 255–259. [https://doi.org/10.1016/S8756-3282\(99\)00162-3](https://doi.org/10.1016/S8756-3282(99)00162-3)

Hofmann, T., Heyroth, F., Meinhard, H., Fränzel, W., Raum, K., 2006. Assessment of composition and anisotropic elastic properties of secondary osteon lamellae. *J. Biomech.* 39, 2282–2294. <https://doi.org/10.1016/j.jbiomech.2005.07.009>

Horwood, N.J., Elliott, J., Martin, T.J., Gillespie, M.T., 1998. Osteotropic Agents Regulate the Expression of Osteoclast Differentiation Factor and Osteoprotegerin in Osteoblastic Stromal Cells. *Endocrinology* 139, 4743–4743. <https://doi.org/10.1210/endo.139.11.6433>

Houillier, P., Froissart, M., Maruani, G., Blanchard, A., 2006. What serum calcium can tell us and what it can't. *Nephrol. Dial. Transplant.* 21, 29–32. <https://doi.org/10.1093/ndt/gfi268>

Hughes, P.C., Tanner, J.M., 1970. The assessment of skeletal maturity in the growing rat. *J. Anat.* 106, 371–402.

Hunt, H.B., Miller, N.A., Hemmerling, K.J., Koga, M., Lopez, K.A., Taylor, E.A., Sellmeyer, D.E., Moseley, K.F., Donnelly, E., 2021. Bone Tissue Composition in Postmenopausal Women Varies With Glycemic Control From Normal Glucose Tolerance to Type 2 Diabetes Mellitus. *J. Bone Miner. Res.* 36, 334–346. <https://doi.org/10.1002/jbmr.4186>

Hunt, H.B., Pearl, J.C., Diaz, D.R., King, K.B., Donnelly, E., 2018. Bone Tissue Collagen Maturity and Mineral Content Increase With Sustained Hyperglycemia in the KK-Ay Murine Model of Type 2 Diabetes. *J. Bone Miner. Res.* 33, 921–929. <https://doi.org/10.1002/jbmr.3365>

Hunt, H.B., Torres, A.M., Palomino, P.M., Marty, E., Saiyed, R., Cohn, M., Jo, J., Warner, S., Sroga, G.E., King, K.B., Lane, J.M., Vashishth, D., Hernandez, C.J., Donnelly, E., 2019. Altered Tissue Composition, Microarchitecture, and Mechanical Performance in Cancellous Bone From Men With Type 2 Diabetes Mellitus. *J. Bone Miner. Res.* 34, 1191–1206. <https://doi.org/10.1002/jbmr.3711>

Hygum, K., Starup-Linde, J., Harsløf, T., Vestergaard, P., Langdahl, B.L., 2017. Diabetes mellitus, a state of low bone turnover—a systematic review and meta-analysis. *Eur. J.*

- Endocrinol. 176, R137–R157. <https://doi.org/10.1530/EJE-16-0652>
- Indermaur, M., Casari, D., Kochetkova, T., Peruzzi, C., Zimmermann, E., Rauch, F., Willie, B., Michler, J., Schwiedrzik, J., Zysset, P., 2021. Compressive Strength of Iliac Bone ECM Is Not Reduced in Osteogenesis Imperfecta and Increases With Mineralization. *J. Bone Miner. Res.* 36, 1364–1375. <https://doi.org/10.1002/jbmr.4286>
- Ip, V., Toth, Z., Chibnall, J., McBride-Gagy, S., 2016. Remnant woven bone and calcified cartilage in mouse bone: Differences between ages/sex and effects on bone strength. *PLoS One* 11, 1–15. <https://doi.org/10.1371/journal.pone.0166476>
- Isojima, T., Sims, N.A., 2021. Cortical bone development, maintenance and porosity: genetic alterations in humans and mice influencing chondrocytes, osteoclasts, osteoblasts and osteocytes. *Cell. Mol. Life Sci.* 78, 5755–5773. <https://doi.org/10.1007/s00018-021-03884-w>
- Itoh, S., Udagawa, N., Takahashi, N., Yoshitake, F., Narita, H., Ebisu, S., Ishihara, K., 2006. A critical role for interleukin-6 family-mediated Stat3 activation in osteoblast differentiation and bone formation. *Bone* 39, 505–512. <https://doi.org/10.1016/j.bone.2006.02.074>
- Janghorbani, M., Feskanich, D., Willett, W.C., Hu, F., 2006. Prospective Study of Diabetes and Risk of Hip Fracture. *Diabetes Care* 29, 1573–1578. <https://doi.org/10.2337/dc06-0440>
- Janghorbani, M., Van Dam, R.M., Willett, W.C., Hu, F.B., 2007. Systematic review of type 1 and type 2 diabetes mellitus and risk of fracture. *Am. J. Epidemiol.* 166, 495–505. <https://doi.org/10.1093/aje/kwm106>
- Jee, W.S.S., 1983. *The Skeletal Tissues*.
- Jeon, U.S., 2008. Kidney and calcium homeostasis. *Electrolyte Blood Press.* 6, 68–76. <https://doi.org/10.5049/EBP.2008.6.2.68>
- Jepsen, Silva, M.J., Vashishth, D., Guo, X.E., van der Meulen, M.C., 2015. Establishing Biomechanical Mechanisms in Mouse Models: Practical Guidelines for Systematically Evaluating Phenotypic Changes in the Diaphyses of Long Bones. *J. Bone Miner. Res.* 30, 951–966. <https://doi.org/10.1002/jbmr.2539>
- Kahn, C.R., 1994. Insulin Action, Diabetogenes, and the Cause of Type II Diabetes. *Diabetes*

- 43, 1066–1085. <https://doi.org/10.2337/diab.43.8.1066>
- Kamml, J., Acevedo, C., Kammer, D.S., 2023. Advanced-Glycation Endproducts: How cross-linking properties affect the collagen fibril behavior. *J. Mech. Behav. Biomed. Mater.* 148, 106198. <https://doi.org/10.1016/j.jmbbm.2023.106198>
- Kanis, J.A., McCloskey, E. V., Johansson, H., Oden, A., Ström, O., Borgström, F., 2010. Development and use of FRAX® in osteoporosis. *Osteoporos. Int.* 21, 407–413. <https://doi.org/10.1007/s00198-010-1253-y>
- Karim, L., Moulton, J., Van Vliet, M., Velie, K., Robbins, A., Malekipour, F., Abdeen, A., Ayres, D., Bouxsein, M.L., 2018. Bone microarchitecture, biomechanical properties, and advanced glycation end-products in the proximal femur of adults with type 2 diabetes. *Bone* 114, 32–39. <https://doi.org/10.1016/j.bone.2018.05.030>
- Karim, L., Rezaee, T., Vaidya, R., 2019. The Effect of Type 2 Diabetes on Bone Biomechanics. *Curr. Osteoporos. Rep.* 17, 291–300. <https://doi.org/10.1007/s11914-019-00526-w>
- Karim, L., Tang, S.Y., Sroga, G.E., Vashishth, D., 2013. Differences in non-enzymatic glycation and collagen cross-links between human cortical and cancellous bone. *Osteoporos. Int.* 24, 2441–2447. <https://doi.org/10.1007/s00198-013-2319-4>
- Kartsogiannis, V., Ng, K.W., 2004. Cell lines and primary cell cultures in the study of bone cell biology. *Mol. Cell. Endocrinol.* 228, 79–102. <https://doi.org/10.1016/j.mce.2003.06.002>
- Kay, A.M., Simpson, C.L., Stewart, J.A., 2016. The Role of AGE/RAGE Signaling in Diabetes-Mediated Vascular Calcification. *J. Diabetes Res.* 2016, 1–8. <https://doi.org/10.1155/2016/6809703>
- Kazanci, M., Roschger, P., Paschalis, E.P., Klaushofer, K., Fratzl, P., 2006. Bone osteonal tissues by Raman spectral mapping: Orientation-composition. *J. Struct. Biol.* 156, 489–496. <https://doi.org/10.1016/j.jsb.2006.06.011>
- Kenkre, J.S., Bassett, J.H.D., 2018. The bone remodelling cycle. *Ann. Clin. Biochem.* 55, 308–327. <https://doi.org/10.1177/0004563218759371>
- Kerschnitzki, M., Wagermaier, W., Roschger, P., Seto, J., Shahar, R., Duda, G.N., Mundlos, S., Fratzl, P., 2011. The organization of the osteocyte network mirrors the extracellular matrix orientation in bone. *J. Struct. Biol.* 173, 303–311.

<https://doi.org/10.1016/j.jsb.2010.11.014>

Keysight Technologies Inc., 2017. Keysight Technologies Nano Indenter G200 Precise mechanical testing for micro-to-nano range of loads and displacements. Data Sheet.

Kim, T.Y., Schafer, A.L., 2016. Diabetes and Bone Marrow Adiposity. *Curr. Osteoporos. Rep.* 337–344. <https://doi.org/10.1007/s11914-016-0336-x>

Knothe Tate, M.L., Adamson, J.R., Tami, A.E., Bauer, T.W., 2004. The osteocyte. *Int. J. Biochem. Cell Biol.* 36, 1–8. [https://doi.org/10.1016/S1357-2725\(03\)00241-3](https://doi.org/10.1016/S1357-2725(03)00241-3)

Kochetkova, T., Groetsch, A., Indermaur, M., Peruzzi, C., Remund, S., Neuenschwander, B., Bellon, B., Michler, J., Zysset, P., Schwiedrzik, J., 2022. Assessing minipig compact jawbone quality at the microscale. *J. Mech. Behav. Biomed. Mater.* 134, 105405. <https://doi.org/10.1016/j.jmbbm.2022.105405>

Kochetkova, T., Peruzzi, C., Braun, O., Overbeck, J., Maurya, A.K., Neels, A., Calame, M., Michler, J., Zysset, P., Schwiedrzik, J., 2021. Combining polarized Raman spectroscopy and micropillar compression to study microscale structure-property relationships in mineralized tissues. *Acta Biomater.* 119, 390–404. <https://doi.org/10.1016/j.actbio.2020.10.034>

Koester, K.J., Ager, J.W., Ritchie, R.O., 2008. The true toughness of human cortical bone measured with realistically short cracks. *Nat. Mater.* 7, 672–677. <https://doi.org/10.1038/nmat2221>

Kontopoulos, I., Presslee, S., Penkman, K., Collins, M.J., 2018. Preparation of bone powder for FTIR-ATR analysis: The particle size effect. *Vib. Spectrosc.* 99, 167–177. <https://doi.org/10.1016/j.vibspec.2018.09.004>

Kourkoumelis, N., Zhang, X., Lin, Z., Wang, J., 2019. Fourier Transform Infrared Spectroscopy of Bone Tissue: Bone Quality Assessment in Preclinical and Clinical Applications of Osteoporosis and Fragility Fracture. *Clin. Rev. Bone Miner. Metab.* 17, 24–39. <https://doi.org/10.1007/s12018-018-9255-y>

Kume, S., Kato, S., Yamagishi, S., Inagaki, Y., Ueda, S., Arima, N., Okawa, T., Kojiro, M., Nagata, K., 2005. Advanced Glycation End-Products Attenuate Human Mesenchymal Stem Cells and Prevent Cognate Differentiation Into Adipose Tissue, Cartilage, and Bone. *J. Bone Miner. Res.* 20, 1647–1658. <https://doi.org/10.1359/JBMR.050514>

- Laakso, M., 1999. Hyperglycemia and cardiovascular disease in type 2 diabetes. *Diabetes* 48, 937–942. <https://doi.org/10.2337/diabetes.48.5.937>
- Lacroix, D., 2019. Biomechanical aspects of bone repair, in: *Bone Repair Biomaterials*. Elsevier, pp. 53–64. <https://doi.org/10.1016/B978-0-08-102451-5.00003-2>
- Lash, R.W., Nicholson, J.M., Velez, L., Van Harrison, R., McCort, J., 2009. Diagnosis and Management of Osteoporosis. *Prim. Care - Clin. Off. Pract.* 36, 181–198. <https://doi.org/10.1016/j.pop.2008.10.009>
- Launey, M.E., Buehler, M.J., Ritchie, R.O., 2010. On the mechanistic origins of toughness in bone, *Annual Review of Materials Research*. <https://doi.org/10.1146/annurev-matsci-070909-104427>
- Lekkala, S., Sacher, S.E., Taylor, E.A., Williams, R.M., Moseley, K.F., Donnelly, E., 2023. Increased Advanced Glycation Endproducts, Stiffness, and Hardness in Iliac Crest Bone From Postmenopausal Women With Type 2 Diabetes Mellitus on Insulin. *J. Bone Miner. Res.* 38, 261–277. <https://doi.org/10.1002/jbmr.4757>
- Li, D., Inouye, J., Davis, J., Arakaki, R.F., 2013. Associations between Psychosocial and Physiological Factors and Diabetes Health Indicators in Asian and Pacific Islander Adults with Type 2 Diabetes. *Nurs. Res. Pract.* 2013, 1–7. <https://doi.org/10.1155/2013/703520>
- Li, X., Ominsky, M.S., Niu, Q.T., Sun, N., Daugherty, B., D’Agostin, D., Kurahara, C., Gao, Y., Cao, J., Gong, J., Asuncion, F., Barrero, M., Warmington, K., Dwyer, D., Stolina, M., Morony, S., Sarosi, I., Kostenuik, P.J., Lacey, D.L., Simonet, W.S., Hua, Z.K., Paszty, C., 2008. Targeted deletion of the sclerostin gene in mice results in increased bone formation and bone strength. *J. Bone Miner. Res.* 23, 860–869. <https://doi.org/10.1359/jbmr.080216>
- Lievers, W.B., Poljsak, A.S., Waldman, S.D., Pilkey, A.K., 2010. Effects of dehydration-induced structural and material changes on the apparent modulus of cancellous bone. *Med. Eng. Phys.* 32, 921–925. <https://doi.org/10.1016/j.medengphy.2010.06.001>
- Liu, J., Kim, E.K., Ni, A., Kim, Y.R., Zheng, F., Lee, B.S., Kim, D.G., 2021. Multiscale characterization of ovariectomized rat femur. *J. Biomech.* 122. <https://doi.org/10.1016/j.jbiomech.2021.110462>
- LLabre, J.E., Sroga, G.E., Tice, M.J.L., Vashishth, D., 2022. Induction and rescue of skeletal fragility in a high-fat diet mouse model of type 2 diabetes: An in vivo and in vitro

- approach. *Bone* 156. <https://doi.org/10.1016/j.bone.2021.116302>
- López-Herradón, A., Portal-Núñez, S., García-Martín, A., Lozano, D., Pérez-Martínez, F.C., Ceña, V., Esbrit, P., 2013. Inhibition of the canonical Wnt pathway by high glucose can be reversed by parathyroid hormone-related protein in osteoblastic cells. *J. Cell. Biochem.* 114, 1908–1916. <https://doi.org/10.1002/jcb.24535>
- Lorensen, W.E., Cline, H.E., 1987. Marching cubes: A high resolution 3D surface construction algorithm. *ACM SIGGRAPH Comput. Graph.* 21, 163–169. <https://doi.org/10.1145/37402.37422>
- Maghsoudi-Ganjeh, M., Samuel, J., Ahsan, A.S., Wang, X., Zeng, X., 2021. Intrafibrillar mineralization deficiency and osteogenesis imperfecta mouse bone fragility. *J. Mech. Behav. Biomed. Mater.* 117, 104377. <https://doi.org/10.1016/j.jmbbm.2021.104377>
- Makki, K., Froguel, P., Wolowczuk, I., 2013. Adipose Tissue in Obesity-Related Inflammation and Insulin Resistance: Cells, Cytokines, and Chemokines. *ISRN Inflamm.* 2013, 1–12. <https://doi.org/10.1155/2013/139239>
- Makowski, A.J., Patil, C.A., Mahadevan-Jansen, A., Nyman, J.S., 2013. Polarization control of Raman spectroscopy optimizes the assessment of bone tissue. *J. Biomed. Opt.* 18, 055005. <https://doi.org/10.1117/1.jbo.18.5.055005>
- Manolagas, S.C., 2000. Birth and Death of Bone Cells: Basic Regulatory Mechanisms and Implications for the Pathogenesis and Treatment of Osteoporosis*. *Endocr. Rev.* 21, 115–137. <https://doi.org/10.1210/edrv.21.2.0395>
- Marcocci, C., Cetani, F., 2019. Primary Hyperparathyroidism, in: *Encyclopedia of Endocrine Diseases*. Elsevier, pp. 128–138. <https://doi.org/10.1016/B978-0-12-801238-3.65217-0>
- Marin, C., Luyten, F.P., Van der Schueren, B., Kerckhofs, G., Vandamme, K., 2018. The Impact of Type 2 Diabetes on Bone Fracture Healing. *Front. Endocrinol. (Lausanne)*. 9, 1–15. <https://doi.org/10.3389/fendo.2018.00006>
- Martini, F., Bartholomew, E.F., Garrison, C.W., Hutchings, R.T., Nath, J.L., Ober, W.C., Welch, K., 2012. *Fundamentals of anatomy & physiology*, 9th ed. ed, *Fundamentals of anatomy and physiology*. Pearson/Benjamin Cummings, San Francisco, Calif.
- Mashiatulla, M., Ross, R.D., Sumner, D.R., 2017. Validation of cortical bone mineral density distribution using micro-computed tomography. *Bone* 99, 53–61.

<https://doi.org/10.1016/j.bone.2017.03.049>

- McCarthy, Etcheverry, S.B., Cortizo, A.M., 2001. Effect of advanced glycation endproducts on the secretion of insulin-like growth factor-I and its binding proteins: role in osteoblast development. *Acta Diabetol.* 38, 113–122. <https://doi.org/10.1007/s005920170007>
- McCarthy, Uemura, T., Etcheverry, S.B., Cortizo, A.M., 2004. Advanced glycation endproducts interfere with integrin-mediated osteoblastic attachment to a type-I collagen matrix. *Int. J. Biochem. Cell Biol.* 36, 840–848. <https://doi.org/10.1016/j.biocel.2003.09.006>
- McConnell, D., 1962. The Crystal Structure of Bone. *Clin. Orthop.* 23, 253–268.
- Mehta, D., Sihota, P., Tikoo, K., Kumar, S., Kumar, N., 2023. Type 2 diabetes alters the viscoelastic behavior and macromolecular composition of vertebra. *Bone Reports* 18, 101680. <https://doi.org/10.1016/j.bonr.2023.101680>
- Merlo, K., Aaronson, J., Vaidya, R., Rezaee, T., Chalivendra, V., Karim, L., 2020. In Vitro-Induced High Sugar Environments Deteriorate Human Cortical Bone Elastic Modulus and Fracture Toughness. *J. Orthop. Res.* 38, 972–983. <https://doi.org/10.1002/jor.24543>
- Micheletti, C., Jolic, M., Grandfield, K., Shah, F.A., Palmquist, A., 2023. Bone structure and composition in a hyperglycemic, obese, and leptin receptor-deficient rat: Microscale characterization of femur and calvarium. *Bone* 172, 116747. <https://doi.org/10.1016/j.bone.2023.116747>
- Mihara, M., Hashizume, M., Yoshida, H., Suzuki, M., Shiina, M., 2012. IL-6/IL-6 receptor system and its role in physiological and pathological conditions. *Clin. Sci.* 122, 143–159. <https://doi.org/10.1042/CS20110340>
- Milat, F., Ng, K.W., 2009. Is Wnt signalling the final common pathway leading to bone formation? *Mol. Cell. Endocrinol.* 310, 52–62. <https://doi.org/10.1016/j.mce.2009.06.002>
- Miyata, T., Notoya, K., Yoshida, K., Horie, K., Maeda, K., Kurokawa, K., Taketomi, S., 1997. Advanced Glycation End Products Enhance Osteoclast-Induced Bone Resorption in Cultured Mouse Unfractionated Bone Cells and in Rats Implanted Subcutaneously with Devitalized Bone Particles. *J. Am. Soc. Nephrol.* 8, 260–270. <https://doi.org/10.1681/asn.v82260>
- Mizuno, A., Amizuka, N., Irie, K., Murakami, A., Fujise, N., Kanno, T., Sato, Y., Nakagawa,

- N., Yasuda, H., Mochizuki, S., Gomibuchi, T., Yano, K., Shima, N., Washida, N., Tsuda, E., Morinaga, T., Higashio, K., Ozawa, H., 1998. Severe Osteoporosis in Mice Lacking Osteoclastogenesis Inhibitory Factor/Osteoprotegerin. *Biochem. Biophys. Res. Commun.* 247, 610–615. <https://doi.org/10.1006/bbrc.1998.8697>
- Mohamed, A.M., 2008. An overview of bone cells and their regulating factors of differentiation. *Malays. J. Med. Sci.* 15, 4–12.
- Mohsin, S., Kaimala, S., Sunny, J.J., Adeghate, E., Brown, E.M., 2019. Type 2 Diabetes Mellitus Increases the Risk to Hip Fracture in Postmenopausal Osteoporosis by Deteriorating the Trabecular Bone Microarchitecture and Bone Mass. *J. Diabetes Res.* 2019, 1–10. <https://doi.org/10.1155/2019/3876957>
- Morgan, E.F., Gerstenfeld, L.C., 2020. The bone organ system: Form and function, Marcus and Feldman's Osteoporosis. INC. <https://doi.org/10.1016/B978-0-12-813073-5.00002-2>
- Morgan, E.F., Unnikrisnan, G.U., Hussein, A.I., 2018. Bone Mechanical Properties in Healthy and Diseased States. *Annu. Rev. Biomed. Eng.* 20, 119–143. <https://doi.org/10.1146/annurev-bioeng-062117-121139>
- Morgan, S., Poundarik, A.A., Vashishth, D., 2015. Do Non-collagenous Proteins Affect Skeletal Mechanical Properties? *Calcif. Tissue Int.* 97, 281–291. <https://doi.org/10.1007/s00223-015-0016-3>
- Morris, M.D., Mandair, G.S., 2011. Raman Assessment of Bone Quality. *Clin. Orthop. Relat. Res.* 469, 2160–2169. <https://doi.org/10.1007/s11999-010-1692-y>
- Müller, R., Koller, B., Hildebrand, T., Laib, A., Gianolini, S., Rügsegger, P., 1996. Resolution dependency of microstructural properties of cancellous bone based on three-dimensional μ -tomography. *Technol. Heal. Care* 4, 113–119. <https://doi.org/10.3233/thc-1996-4112>
- Murray, Coleman, 2019. Impact of Diabetes Mellitus on Bone Health. *Int. J. Mol. Sci.* 20, 4873. <https://doi.org/10.3390/ijms20194873>
- Nagai, R., Shirakawa, J., Fujiwara, Y., Ohno, R., Moroishi, N., Sakata, N., 2014. Detection of AGEs as markers for carbohydrate metabolism and protein denaturation 55, 1–6. <https://doi.org/10.3164/jcbrn.13>
- Napoli, N., Strollo, R., Paladini, A., Briganti, S.I., Pozzilli, P., Epstein, S., 2014. The alliance of mesenchymal stem cells, bone, and diabetes. *Int. J. Endocrinol.* 2014, 1–26.

- Nathan, D.M., Turgeon, H., Regan, S., 2007. Relationship between glycated haemoglobin levels and mean glucose levels over time. *Diabetologia* 50, 2239–2244. <https://doi.org/10.1007/s00125-007-0803-0>
- Nianogo, R.A., Arah, O.A., 2022. Forecasting Obesity and Type 2 Diabetes Incidence and Burden: The ViLA-Obesity Simulation Model. *Front. Public Heal.* 10, 1–13. <https://doi.org/10.3389/fpubh.2022.818816>
- Nishida, T., Hanaki, Y., Pezzotti, G., 1994. Effect of Notch-Root Radius on the Fracture Toughness of a Fine-Grained Alumina. *J. Am. Ceram. Soc.* 77, 606–608. <https://doi.org/10.1111/j.1151-2916.1994.tb07038.x>
- Nyman, J.S., 2013. Effect of diabetes on the fracture resistance of bone. *Clin. Rev. Bone Miner. Metab.* 11, 38–48. <https://doi.org/10.1007/s12018-012-9124-z>
- Nyman, J.S., Makowski, A.J., 2012. The contribution of the extracellular matrix to the fracture resistance of bone. *Curr. Osteoporos. Rep.* 10, 169–177. <https://doi.org/10.1007/s11914-012-0101-8>
- Nyman, J.S., Roy, A., Tyler, J.H., Acuna, R.L., Gayle, H.J., Wang, X., 2007. Age-related factors affecting the postyield energy dissipation of human cortical bone. *J. Orthop. Res.* 25, 646–655. <https://doi.org/10.1002/jor.20337>
- O’Hearn, M., Lara-Castor, L., Cudhea, F., Miller, V., Reedy, J., Shi, P., Zhang, J., Wong, J.B., Economos, C.D., Micha, R., Mozaffarian, D., Bas, M., Ali, J.H., Abumweis, S., Krishnan, A., Misra, P., Hwalla, N.C., Janakiram, C., Liputo, N.I., Musaiger, A., Pourfarzi, F., Alam, I., DeRidder, K., Termote, C., Memon, A., Turrini, A., Lupotto, E., Piccinelli, R., Sette, S., Anzid, K., Vossenaar, M., Mazumdar, P., Rached, I., Rovirosa, A., Zapata, M.E., Asayehu, T.T., Oduor, F., Boedecker, J., Aluso, L., Ortiz-Ulloa, J., Meenakshi, J. V., Castro, M., Grosso, G., Waskiewicz, A., Khan, U.S., Thanopoulou, A., Malekzadeh, R., Calleja, N., Ocke, M., Etemad, Z., Nsour, M. Al, Waswa, L.M., Nurk, E., Arsenault, J., Lopez-Jaramillo, P., Sibai, A.M., Damasceno, A., Arambepola, C., Lopes, C., Severo, M., Lunet, N., Torres, D., Tapanainen, H., Lindstrom, J., Virtanen, S., Palacios, C., Roos, E., Agdeppa, I.A., Desnacido, J., Capanzana, M., Misra, A., Khouw, I., Ng, S.A., Delgado, E.G., Caballero, M., Otero, J., Lee, H.J., Koksai, E., Guessous, I., Lachat, C., De Henauw, S., Rahbar, A.R., Tedstone, A., Naska, A., Mathee, A., Ling, A., Tedla, B., Hopping, B., Ginnela, B., Leclercq, C., Duante, C., Haerpfer, C., Hotz, C., Pitsavos, C., Rehm, C., van

Oosterhout, C., Cerdana, C., Bradshaw, D., Trichopoulos, D., Gauci, D., Fernando, D., Sygnowska, E., Vartiainen, E., Farzadfar, F., Zajkas, G., Swan, G., Ma, G., Pekcan, G., Ibrahim, H.M., Sinkko, H., Barbieri, H.E., Sioen, I., Myhre, J., Gaspoz, J.M., Odenkirk, J., Bundhamcharoen, K., Nelis, K., Zarina, K., Biro, L., Johansson, L., Steingrimsdottir, L., Riley, L., Yap, M., Inoue, M., Szabo, M., Ovaskainen, M.L., Lee, M.S., Chan, M.F., Cowan, M., Kandiah, M., Kally, O., Jonsdottir, O., Palmer, P., Vollenweider, P., Orfanos, P., Asciak, R., Templeton, R., Don, R., Yaakub, R., Selamat, R., Yusof, S., Al-Zenki, S., Hung, S.Y., Beer-Borst, S., Wu, S., Lukito, W., Hadden, W., Becker, W., Cao, X., Ma, Y., Lai, Y., Hjadaud, Z., Ali, J., Gravel, R., Tao, T., Veerman, J.L., Chiplonkar, S., Arici, M., Ngoan, L.T., Panagiotakos, D., Li, Y., Trichopoulou, A., Barengo, N., Khadilkar, A., Ekbote, V., Mohammadifard, N., Kovalskys, I., Laxmaiah, A., Rachakulla, H., Rajkumar, H., Meshram, I., Avula, L., Arlappa, N., Hemalatha, R., Iacoviello, L., Bonaccio, M., Costanzo, S., Martin-Prevel, Y., Castetbon, K., Jitnarin, N., Hsieh, Y. Te, Olivares, S., Tejada, G., Hadziomeragic, A., de Moura Souza, A., Pan, W.H., Huybrechts, I., de Brauw, A., Moursi, M., Maghroun, M., Zeba, A.N., Sarrafzadegan, N., Keinan-Boker, L., Goldsmith, R., Shimony, T., Jordan, I., Mastiholi, S.C., Mwangi, M., Kombe, Y., Bukania, Z., Alissa, E., Al-Daghri, N., Sabico, S., Gulliford, M., Diba, T.S., Oh, K., Kweon, S., Park, S., Cho, Y., Al-Hooti, S., Luangphaxay, C., Douangvichit, D., Siengsounthone, L., Marques-Vidal, P., Rybak, C., Luke, A., Piaseu, N., Rojroongwasinkul, N., Sundram, K., Baykova, D., Abedi, P., Sandjaja, S., Fadzil, F., Bukhary, N.B.I., Bovet, P., Chen, Y., Sawada, N., Tsugane, S., Rangelova, L., Petrova, S., Duleva, V., Lindroos, A.K., Sipinen, J.P., Moraesus, L., Bergman, P., Siamusantu, W., Szponar, L., Chang, H.Y., Sekiyama, M., Le Nguyen Bao, K., Nagalla, B., Polasa, K., Boindala, S., El Ati, J., Silva, I.R., Dommarco, J.R., Barquera, S., Rodríguez-Ramírez, S., Illescas-Zarate, D., Sanchez-Romero, L.M., Ikeda, N., Zaghoul, S., Houshiar-rad, A., Mohammadi-Nasrabadi, F., Abdollahi, M., Chuah, K.A., Mahdy, Z.A., Eldridge, A., Ding, E.L., Kruger, H., Henjum, S., Fernandez, A., Suarez-Ortegon, M.F., Al-Hamad, N., Janská, V., Tayyem, R., Mirmiran, P., Kelishadi, R., Lemming, E.W., Richter, A., Mensink, G., Wieler, L., Hoffman, D., Salanave, B., Kim, C. il, Kuriyan-Raj, R., Swaminathan, S., Garriguet, D., Dastgiri, S., Vaask, S., Karupaiah, T., Zohoori, F.V., Esteghamati, A., Hashemian, M., Noshad, S., Mwaniki, E., Yakes-Jimenez, E., Chileshe, J., Mwanza, S., Marques, L.L., Preston, A.M., Aguero, S.D., Oleas, M., Posada, L., Ochoa, A., Shamsuddin, K., Shariff, Z.M., Jan Bin Jan Mohamed, H., Manan, W., Nicolau, A., Tudorie, C., Poh, B.K., Abbott, P., Pakseresht, M., Sharma, S., Strand, T.,

- Alexy, U., Nöthlings, U., Carmikle, J., Brown, K., Koster, J., Waidyatilaka, I., Lanerolle, P., Jayawardena, R., Long, J.M., Hambidge, K.M., Krebs, N.F., Haque, A., Keding, G.B., Korkalo, L., Erkkola, M., Freese, R., Eleraky, L., Stuetz, W., Thorsdottir, I., Gunnarsdottir, I., Serra-Majem, L., Moy, F.M., Anderson, S., Jeewon, R., Zugravu, C.A., Adair, L., Ng, S.W., Skeaff, S., Marchioni, D., Fisberg, R., Henry, C., Ersino, G., Zello, G., Meyer, A., Elmadfa, I., Mitchell, C., Balfour, D., Geleijnse, J.M., Manary, M., Elkour, T., Nikiema, L., Mirzaei, M., Hakeem, R., 2023. Incident type 2 diabetes attributable to suboptimal diet in 184 countries. *Nat. Med.* 29, 982–995. <https://doi.org/10.1038/s41591-023-02278-8>
- O’Sullivan, L.M., Allison, H., Parle, E.E., Schiavi, J., McNamara, L.M., 2020. Secondary alterations in bone mineralisation and trabecular thickening occur after long-term estrogen deficiency in ovariectomised rat tibiae, which do not coincide with initial rapid bone loss. *Osteoporos. Int.* 31, 587–599. <https://doi.org/10.1007/s00198-019-05239-5>
- Odetti, P., Rossi, S., Monacelli, F., Poggi, A., Ciriigliaro, M., Federici, M., Federici, A., 2005. Advanced Glycation End Products and Bone Loss during Aging. *Ann. N. Y. Acad. Sci.* 1043, 710–717. <https://doi.org/10.1196/annals.1333.082>
- Odgaard, A., Gundersen, H.J., 1993. Quantification of connectivity in cancellous bone, with special emphasis on 3-D reconstructions. *Bone* 14, 173–182. [https://doi.org/10.1016/8756-3282\(93\)90245-6](https://doi.org/10.1016/8756-3282(93)90245-6)
- Oftadeh, R., Perez-Viloria, M., Villa-Camacho, J.C., Vaziri, A., Nazarian, A., 2015. Biomechanics and Mechanobiology of Trabecular Bone: A Review. *J. Biomech. Eng.* 137, 1–15. <https://doi.org/10.1115/1.4029176>
- Oliver, W.C., Pharr, G.M., 2004. Measurement of hardness and elastic modulus by instrumented indentation: Advances in understanding and refinements to methodology. *J. Mater. Res.* 19, 3–20. <https://doi.org/10.1557/jmr.2004.19.1.3>
- Oliver, W.C., Pharr, G.M., 1992. An improved technique for determining hardness and elastic modulus using load and displacement sensing indentation experiments. *J. Mater. Res.* 7, 1564–1583. <https://doi.org/10.1557/JMR.1992.1564>
- Olszta, M.J., Cheng, X., Jee, S.S., Kumar, R., Kim, Y.Y., Kaufman, M.J., Douglas, E.P., Gower, L.B., 2007. Bone structure and formation: A new perspective. *Mater. Sci. Eng. R Reports* 58, 77–116. <https://doi.org/10.1016/j.mser.2007.05.001>

- Ortega, N., Behonick, D.J., Werb, Z., 2004. Matrix remodeling during endochondral ossification. *Trends Cell Biol.* 14, 86–93. <https://doi.org/10.1016/j.tcb.2003.12.003>
- Ou-Yang, H., Paschalis, E.P., Mayo, W.E., Boskey, A.L., Mendelsohn, R., 2001. Infrared microscopic imaging of bone: Spatial distribution of CO₃-2-. *J. Bone Miner. Res.* 16, 893–900. <https://doi.org/10.1359/jbmr.2001.16.5.893>
- Paccou, J., Ward, K.A., Jameson, K.A., Dennison, E.M., Cooper, C., Edwards, M.H., Cooper, C., 2016. Bone Microarchitecture in Men and Women with Diabetes : The Importance of Cortical Porosity. *Calcif. Tissue Int.* 98, 465–473. <https://doi.org/10.1007/s00223-015-0100-8>
- Parle, E., Tio, S., Behre, A., Carey, J.J., Murphy, C.G., O'Brien, T.F., Curtin, W.A., Kearns, S.R., McCabe, J.P., Coleman, C.M., Vaughan, T.J., McNamara, L.M., 2020. Bone Mineral Is More Heterogeneously Distributed in the Femoral Heads of Osteoporotic and Diabetic Patients: A Pilot Study. *JBMR Plus* 4, 1–10. <https://doi.org/10.1002/jbm4.10253>
- Paschalis, E.P., Gamsjaeger, S., Klaushofer, K., 2017. Vibrational spectroscopic techniques to assess bone quality. *Osteoporos. Int.* 28, 2275–2291. <https://doi.org/10.1007/s00198-017-4019-y>
- Paschalis, E.P., Verdelis, K., Doty, S.B., Boskey, A.L., Mendelsohn, R., Yamauchi, M., 2001. Spectroscopic characterization of collagen cross-links in bone. *J. Bone Miner. Res.* 16, 1821–1828. <https://doi.org/10.1359/jbmr.2001.16.10.1821>
- Pass, C., MacRae, V.E., Ahmed, S.F., Farquharson, C., 2009. Inflammatory cytokines and the GH/IGF-I axis: Novel actions on bone growth. *Cell Biochem. Funct.* 27, 119–127. <https://doi.org/10.1002/cbf.1551>
- Patsch, J.M., Burghardt, A.J., Yap, S.P., Baum, T., Schwartz, A. V., Joseph, G.B., Link, T.M., 2013. Increased cortical porosity in type 2 diabetic postmenopausal women with fragility fractures. *J. Bone Miner. Res.* 28, 313–324. <https://doi.org/10.1002/jbmr.1763>
- Peacock, M., 2010. Calcium metabolism in health and disease. *Clin. J. Am. Soc. Nephrol.* 5, 23–30. <https://doi.org/10.2215/CJN.05910809>
- Pelletier, S., Dubourg, L., Carlier, M.C., Hadj-Aissa, A., Fouque, D., 2013. The relation between renal function and serum sclerostin in adult patients with CKD. *Clin. J. Am. Soc. Nephrol.* 8, 819–823. <https://doi.org/10.2215/CJN.07670712>

- Peterson, R.G., Shaw, W.N., Neel, M., Little, L.A., Eichberg, J., 1990. Zucker Diabetic Fatty Rat as a Model for Non-insulin-dependent Diabetes Mellitus. *ILAR J.* 32, 16–19. <https://doi.org/10.1093/ilar.32.3.16>
- Piccoli, A., Cannata, F., Strollo, R., Pedone, C., Leanza, G., Russo, F., Greto, V., Isgrò, C., Quattrocchi, C.C., Massaroni, C., Silvestri, S., Vadalà, G., Bisogno, T., Denaro, V., Pozzilli, P., Tang, S.Y., Silva, M.J., Conte, C., Papalia, R., Maccarrone, M., Napoli, N., 2020. Sclerostin Regulation, Microarchitecture, and Advanced Glycation End-Products in the Bone of Elderly Women With Type 2 Diabetes. *J. Bone Miner. Res.* 35, 2415–2422. <https://doi.org/10.1002/jbmr.4153>
- Picke, A., Campbell, G., Napoli, N., Hofbauer, L.C., Rauner, M., 2019. Update on the impact of type 2 diabetes mellitus on bone metabolism and material properties. *Endocr. Connect.* 8, R55–R70. <https://doi.org/10.1530/EC-18-0456>
- Picke, Alaguero, I.G., Campbell, G.M., Glüer, C., Salbach-hirsch, J., Rauner, M., Hofbauer, L.C., Hofbauer, C., 2016a. Bone defect regeneration and cortical bone parameters of type 2 diabetic rats are improved by insulin therapy ☆. *Bone* 82, 108–115. <https://doi.org/10.1016/j.bone.2015.06.001>
- Picke, Salbach-Hirsch, J., Hintze, V., Rother, S., Rauner, M., Kascholke, C., Möller, S., Bernhardt, R., Rammelt, S., Pisabarro, M.T., Ruiz-Gómez, G., Schnabelrauch, M., Schulz-Siegmund, M., Hacker, M.C., Scharnweber, D., Hofbauer, C., Hofbauer, L.C., 2016b. Sulfated hyaluronan improves bone regeneration of diabetic rats by binding sclerostin and enhancing osteoblast function. *Biomaterials* 96, 11–23. <https://doi.org/10.1016/j.biomaterials.2016.04.013>
- Prisby, R.D., Swift, J.M., Bloomfield, S.A., Hogan, H.A., Delp, M.D., 2008. Altered bone mass, geometry and mechanical properties during the development and progression of type 2 diabetes in the Zucker diabetic fatty rat. *J. Endocrinol.* 199, 379–388. <https://doi.org/10.1677/JOE-08-0046>
- Pritchard, J.M., Papaioannou, A., Tomowich, C., Giangregorio, L.M., Atkinson, S.A., Beattie, K.A., Adachi, J.D., DeBeer, J., Winemaker, M., Avram, V., Schwarcz, H.P., 2013. Bone mineralization is elevated and less heterogeneous in adults with type 2 diabetes and osteoarthritis compared to controls with osteoarthritis alone. *Bone* 54, 76–82. <https://doi.org/10.1016/j.bone.2013.01.032>

- Reinwald, S., Peterson, R.G., Allen, M.R., Burr, D.B., 2009. Skeletal changes associated with the onset of type 2 diabetes in the ZDF and ZDSD rodent models. *Am. J. Physiol. Metab.* 296, E765–E774. <https://doi.org/10.1152/ajpendo.90937.2008>
- Rey, C., Renugopalakrishnan, V., Shimizu, M., Collins, B., Glimcher, M.J., 1991. A resolution-enhanced Fourier Transform Infrared spectroscopic study of the environment of the CO₃²⁻ ion in the mineral phase of enamel during its formation and maturation. *Calcif. Tissue Int.* 49, 259–268. <https://doi.org/10.1007/BF02556215>
- Rezaee, T., Bouxsein, M.L., Karim, L., 2020. Increasing fluoride content deteriorates rat bone mechanical properties. *Bone* 136, 115369. <https://doi.org/10.1016/j.bone.2020.115369>
- Reznikov, N., Shahar, R., Weiner, S., 2014a. Three-dimensional structure of human lamellar bone: The presence of two different materials and new insights into the hierarchical organization. *Bone* 59, 93–104. <https://doi.org/10.1016/j.bone.2013.10.023>
- Reznikov, N., Shahar, R., Weiner, S., 2014b. Bone hierarchical structure in three dimensions, in: *Acta Biomaterialia*. Elsevier Ltd, pp. 3815–3826. <https://doi.org/10.1016/j.actbio.2014.05.024>
- Rho, J.-Y., Kuhn-Spearing, L., Zioupos, P., 1998. Mechanical properties and the hierarchical structure of bone. *Med. Eng. Phys.* 20, 92–102. [https://doi.org/10.1016/S1350-4533\(98\)00007-1](https://doi.org/10.1016/S1350-4533(98)00007-1)
- Rho, J.Y., Tsui, T.Y., Pharr, G.M., 1997. Elastic properties of human cortical and trabecular lamellar bone measured by nanoindentation. *Biomaterials* 18, 1325–1330. [https://doi.org/10.1016/S0142-9612\(97\)00073-2](https://doi.org/10.1016/S0142-9612(97)00073-2)
- Richard, H.A., Sander, M., 2016. Fundamentals of Fracture Mechanics, in: *Solid Mechanics and Its Applications*. pp. 55–112. https://doi.org/10.1007/978-3-319-32534-7_3
- Ritchie, R.O., 2011. The conflicts between strength and toughness. *Nat. Mater.* 10, 817–822. <https://doi.org/10.1038/nmat3115>
- Ritchie, R.O., 2010. How does human bone resist fracture? *Ann. N. Y. Acad. Sci.* 1192, 72–80. <https://doi.org/10.1111/j.1749-6632.2009.05232.x>
- Ritchie, R.O., Koester, K.J., Ionova, S., Yao, W., Lane, N.E., Iii, J.W.A., 2008. Measurement of the toughness of bone : A tutorial with special reference to small animal studies ☆. *Bone* 43, 798–812. <https://doi.org/10.1016/j.bone.2008.04.027>

- Roach, H.I., 1994. WHY DOES BONE MATRIX CONTAIN NON-COLLAGENOUS PROTEINS? THE POSSIBLE ROLES OF OSTEOCALCIN, OSTEONECTIN, OSTEOPONTIN AND BONE SIALOPROTEIN IN BONE MINERALISATION AND RESORPTION. *Cell Biol. Int.* 18, 617–628. <https://doi.org/10.1006/cbir.1994.1088>
- Rodic, T., Wölfel, E.M., Milovanovic, P., Fiedler, I.A.K., Cvetkovic, D., Jähn, K., Amling, M., Sopta, J., Nikolic, S., Zivkovic, V., Busse, B., Djuric, M., 2021. Bone quality analysis of jaw bones in individuals with type 2 diabetes mellitus—post mortem anatomical and microstructural evaluation. *Clin. Oral Investig.* 25, 4377–4400. <https://doi.org/10.1007/s00784-020-03751-1>
- Romanowicz, G.E., Terhune, A.H., Bielajew, B.J., Sexton, B., Lynch, M., Mandair, G.S., McNerny, E.M.B., Kohn, D.H., 2022. Collagen cross-link profiles and mineral are different between the mandible and femur with site specific response to perturbed collagen. *Bone Reports* 17, 101629. <https://doi.org/10.1016/j.bonr.2022.101629>
- Romero-Díaz, C., Duarte-Montero, D., Gutiérrez-Romero, S.A., Mendivil, C.O., 2021. Diabetes and Bone Fragility. *Diabetes Ther.* 12, 71–86. <https://doi.org/10.1007/s13300-020-00964-1>
- Roodman, G.D., 1996. Advances in bone biology: the osteoclast. *Endocr. Rev.* 17, 308–332. <https://doi.org/10.1210/er.17.4.308>
- Rosa, N., Moura, M.F.S.F., Olhero, S., Simoes, R., Magalhães, F.D., Marques, A.T., Ferreira, J.P.S., Reis, A.R., Carvalho, M., Parente, M., 2022. Bone: An Outstanding Composite Material. *Appl. Sci.* 12, 1–16. <https://doi.org/10.3390/app12073381>
- Roschger, P., Gupta, H.S., Berzlanovich, A., Ittner, G., Dempster, D.W., Fratzl, P., Cosman, F., Parisien, M., Lindsay, R., Nieves, J.W., Klaushofer, K., 2003. Constant mineralization density distribution in cancellous human bone. *Bone* 32, 316–323. [https://doi.org/10.1016/S8756-3282\(02\)00973-0](https://doi.org/10.1016/S8756-3282(02)00973-0)
- Roschger, P., Paschalis, E.P., Fratzl, P., Klaushofer, K., 2008. Bone mineralization density distribution in health and disease 42, 456–466. <https://doi.org/10.1016/j.bone.2007.10.021>
- Roschger, P., Rinnerthaler, S., Yates, J., Rodan, G.A., Fratzl, P., Klaushofer, K., 2001. Alendronate increases degree and uniformity of mineralization in cancellous bone and

- decreases the porosity in cortical bone of osteoporotic women. *Bone* 29, 185–191. [https://doi.org/10.1016/S8756-3282\(01\)00485-9](https://doi.org/10.1016/S8756-3282(01)00485-9)
- Rose-John, S., 2012. Il-6 trans-signaling via the soluble IL-6 receptor: Importance for the proinflammatory activities of IL-6. *Int. J. Biol. Sci.* 8, 1237–1247. <https://doi.org/10.7150/ijbs.4989>
- Rotter, V., Nagaev, I., Smith, U., 2003. Interleukin-6 (IL-6) Induces Insulin Resistance in 3T3-L1 Adipocytes and Is, Like IL-8 and Tumor Necrosis Factor- α , Overexpressed in Human Fat Cells from Insulin-resistant Subjects. *J. Biol. Chem.* 278, 45777–45784. <https://doi.org/10.1074/jbc.M301977200>
- Rubin, M.R., Paschalis, E.P., Poundarik, A., Sroga, G.E., McMahon, D.J., Gamsjaeger, S., Klaushofer, K., Vashishth, D., 2016. Advanced glycation endproducts and bone material properties in type 1 diabetic mice. *PLoS One* 11, 1–14. <https://doi.org/10.1371/journal.pone.0154700>
- Saito, M., Fujii, K., Mori, Y., Marumo, K., 2006. Role of collagen enzymatic and glycation induced cross-links as a determinant of bone quality in spontaneously diabetic WBN/Kob rats. *Osteoporos. Int.* 17, 1514–1523. <https://doi.org/10.1007/s00198-006-0155-5>
- Saito, M., Kida, Y., Kato, S., Marumo, K., 2014. Diabetes, collagen, and bone quality. *Curr. Osteoporos. Rep.* 12, 181–188. <https://doi.org/10.1007/s11914-014-0202-7>
- Saito, M., Marumo, K., 2013. Bone Quality in Diabetes. *Front. Endocrinol. (Lausanne)*. 4, 1–9. <https://doi.org/10.3389/fendo.2013.00072>
- Saito, M., Marumo, K., 2010. Collagen cross-links as a determinant of bone quality: A possible explanation for bone fragility in aging, osteoporosis, and diabetes mellitus. *Osteoporos. Int.* 21, 195–214. <https://doi.org/10.1007/s00198-009-1066-z>
- Saito, M., Marumo, K., Fujii, K., Ishioka, N., 1997. Single-Column High-Performance Liquid Chromatographic–Fluorescence Detection of Immature, Mature, and Senescent Cross-Links of Collagen. *Anal. Biochem.* 253, 26–32. <https://doi.org/10.1006/abio.1997.2350>
- Salmon, P.L., Ohlsson, C., Shefelbine, S.J., Doube, M., 2015. Structure model index does not measure rods and plates in trabecular bone. *Front. Endocrinol. (Lausanne)*. 6, 1–10. <https://doi.org/10.3389/fendo.2015.00162>
- Sanches, C.P., Vianna, A.G.D., Barreto, F.D.C., 2017. The impact of type 2 diabetes on bone

- metabolism. *Diabetol. Metab. Syndr.* 9, 1–7. <https://doi.org/10.1186/s13098-017-0278-1>
- Sanz-Nogués, C., Mustafa, M., Burke, H., O'Brien, T., Coleman, C.M., 2020. Knowledge, perceptions and concerns of diabetes-associated complications among individuals living with type 1 and type 2 diabetes mellitus. *Healthc.* 8, 1–12. <https://doi.org/10.3390/healthcare8010025>
- Sawyer, A., Lott, P., Titrud, J., McDonald, J., 2003. Quantification of tartrate resistant acid phosphatase distribution in mouse tibiae using image analysis. *Biotech. Histochem.* 78, 271–278. <https://doi.org/10.1080/10520290310001646668>
- Scanco Medical, 2023. SCANCO Medical FAQ [WWW Document]. Scanco Med. URL <https://www.scanco.ch/faq-customers.php> (accessed 6.13.23).
- Schaffler, M.B., Choi, K., Milgrom, C., 1995. Aging and matrix microdamage accumulation in human compact bone. *Bone* 17, 521–525. [https://doi.org/10.1016/8756-3282\(95\)00370-3](https://doi.org/10.1016/8756-3282(95)00370-3)
- Schaper, F., Rose-John, S., 2015. Interleukin-6: Biology, signaling and strategies of blockade. *Cytokine Growth Factor Rev.* 26, 475–487. <https://doi.org/10.1016/j.cytogfr.2015.07.004>
- Schileo, E., Dall'Ara, E., Taddei, F., Malandrino, A., Schotkamp, T., Baleani, M., Viceconti, M., 2008. An accurate estimation of bone density improves the accuracy of subject-specific finite element models. *J. Biomech.* 41, 2483–2491. <https://doi.org/10.1016/j.jbiomech.2008.05.017>
- Schmidt, F.N., Zimmermann, E.A., Campbell, G.M., Sroga, G.E., Püschel, K., Amling, M., Tang, S.Y., Vashishth, D., Busse, B., 2017. Assessment of collagen quality associated with non-enzymatic cross-links in human bone using Fourier-transform infrared imaging. *Bone* 97, 243–251. <https://doi.org/10.1016/j.bone.2017.01.015>
- Schriefer, J.L., Robling, A.G., Warden, S.J., Fournier, A.J., Mason, J.J., Turner, C.H., 2005. A comparison of mechanical properties derived from multiple skeletal sites in mice. *J. Biomech.* 38, 467–475. <https://doi.org/10.1016/j.jbiomech.2004.04.020>
- Schultz, M., 2001. Paleohistopathology of bone: A new approach to the study of ancient diseases. *Yearb. Phys. Anthropol.* 44, 106–147. <https://doi.org/10.1002/ajpa.10024>
- Schwartz, A. V., Ewing, S.K., Porzig, A.M., McCulloch, C.E., Resnick, H.E., Hillier, T.A., Ensrud, K.E., Black, D.M., Nevitt, M.C., Cummings, S.R., Sellmeyer, D.E., 2013.

- Diabetes and change in bone mineral density at the hip, calcaneus, spine, and radius in older women. *Front. Endocrinol. (Lausanne)*. 4, 1–9. <https://doi.org/10.3389/fendo.2013.00062>
- Schwartz, A. V., Vittinghoff, E., Bauer, D.C., Hillier, T.A., Strotmeyer, E.S., Ensrud, K.E., Donaldson, M.G., Cauley, J.A., Harris, T.B., Koster, A., Womack, C.R., Palermo, L., Black, D.M., 2011. Association of BMD and FRAX score with risk of fracture in older adults with type 2 diabetes. *JAMA - J. Am. Med. Assoc.* 305, 2184–2192. <https://doi.org/10.1001/jama.2011.715>
- Schwartz, A. V., Garnero, P., Hillier, T.A., Sellmeyer, D.E., Strotmeyer, E.S., Feingold, K.R., Resnick, H.E., Tykavsky, F.A., Black, D.M., Cummings, S.R., Harris, T.B., Bauer, D.C., 2009. Pentosidine and Increased Fracture Risk in Older Adults with Type 2 Diabetes 94, 2380–2386. <https://doi.org/10.1210/jc.2008-2498>
- Schwiedrzik, J., Raghavan, R., Bürki, A., Lenader, V., Wolfram, U., Michler, J., Zysset, P., 2014. In situ micropillar compression reveals superior strength and ductility but an absence of damage in lamellar bone. *Nat. Mater.* 13, 740–747. <https://doi.org/10.1038/nmat3959>
- Seeman, E., 2008. Bone quality: The material and structural basis of bone strength. *J. Bone Miner. Metab.* 26, 1–8. <https://doi.org/10.1007/s00774-007-0793-5>
- Sell, D.R., 1997. Ageing promotes the increase of early glycation Amadori product as assessed by ϵ -N-(2-furoylmethyl)-L-lysine (furosine) levels in rodent skin collagen. The relationship to dietary restriction and glycooxidation. *Mech. Ageing Dev.* 95, 81–99. [https://doi.org/10.1016/S0047-6374\(97\)01863-0](https://doi.org/10.1016/S0047-6374(97)01863-0)
- Sell, D.R., Monnier, V.M., 1989. Isolation, purification and partial characterization of novel fluorophores from aging human insoluble collagen-rich tissue. *Connect. Tissue Res.* 19, 77–92. <https://doi.org/10.3109/03008208909016816>
- Sell, D.R., Nagaraj, R.H., Grandhee, S.K., Odetti, P., Lapolla, A., Fogarty, J., Monnier, V.M., 1991. Pentosidine: A molecular marker for the cumulative damage to proteins in diabetes, aging, and uremia. *Diabetes. Metab. Rev.* 7, 239–251. <https://doi.org/10.1002/dmr.5610070404>
- Sheng, Z., Tong, D., Ou, Y., Zhang, H., Zhang, Z., Li, S., Zhou, J., Zhang, J., Liao, E., 2012.

- Serum sclerostin levels were positively correlated with fat mass and bone mineral density in Central South Chinese postmenopausal women. *Clin. Endocrinol. (Oxf)*. 76, 797–801. <https://doi.org/10.1111/j.1365-2265.2011.04315.x>
- Shipov, A., Zaslansky, P., Riesemeier, H., Segev, G., Atkins, A., Shahar, R., 2013. Unremodeled endochondral bone is a major architectural component of the cortical bone of the rat (*Rattus norvegicus*). *J. Struct. Biol.* 183, 132–140. <https://doi.org/10.1016/j.jsb.2013.04.010>
- Siegmund, T., Allen, M.R., Burr, D.B., 2008. Failure of mineralized collagen fibrils : Modeling the role of collagen cross-linking 41, 1427–1435. <https://doi.org/10.1016/j.jbiomech.2008.02.017>
- Sihota, P., Yadav, R.N., Dhaliwal, R., Bose, J.C., Dhiman, V., Neradi, D., Karn, S., Sharma, S., Aggarwal, S., Goni, V.G., Mehandia, V., Vashishth, D., Bhadada, S.K., Kumar, N., 2021. Investigation of Mechanical, Material, and Compositional Determinants of Human Trabecular Bone Quality in Type 2 Diabetes. *J. Clin. Endocrinol. Metab.* 106, E2271–E2289. <https://doi.org/10.1210/clinem/dgab027>
- Sihota, P., Yadav, R.N., Poleboina, S., Mehandia, V., Bhadada, S.K., Tikoo, K., Kumar, N., 2020a. Development of HFD-Fed /Low-DoseSTZ-Treated Female Sprague-Dawley Rat Model to Investigate Diabetic Bone Fragility at Different Organization Levels. *JBMR Plus* 4, 1–12. <https://doi.org/10.1002/jbm4.10379>
- Sihota, P., Yadav, R.N., Poleboina, S., Mehandia, V., Bhadada, S.K., Tikoo, K., Kumar, N., 2020b. Development of HFD-Fed/Low-Dose STZ-Treated Female Sprague-Dawley Rat Model to Investigate Diabetic Bone Fragility at Different Organization Levels. *JBMR Plus* 4, 1–12. <https://doi.org/10.1002/jbm4.10379>
- Sims, N.A., 2021. Influences of the IL-6 cytokine family on bone structure and function. *Cytokine* 146, 155655. <https://doi.org/10.1016/j.cyto.2021.155655>
- Song, L., 2017. Calcium and Bone Metabolism Indices, in: *Advances in Clinical Chemistry*. Elsevier Inc., pp. 1–46. <https://doi.org/10.1016/bs.acc.2017.06.005>
- Spencer, G.J., Utting, J.C., Etheridge, S.L., Arnett, T.R., Genever, P.G., 2006. Wnt signalling in osteoblasts regulates expression of the receptor activator of NFκB ligand and inhibits osteoclastogenesis in vitro. *J. Cell Sci.* 119, 1283–1296. <https://doi.org/10.1242/jcs.02883>

- Spevak, L., Flach, C.R., Hunter, T., Mendelsohn, R., Boskey, A., 2013. Fourier Transform Infrared Spectroscopic Imaging Parameters Describing Acid Phosphate Substitution in Biologic Hydroxyapatite. *Calcif. Tissue Int.* 92, 418–428. <https://doi.org/10.1007/s00223-013-9695-9>
- Starup-Linde, J., Vestergaard, P., 2016. Biochemical bone turnover markers in diabetes mellitus - A systematic review. *Bone* 82, 69–78. <https://doi.org/10.1016/j.bone.2015.02.019>
- Stauber, M., Müller, R., 2008. Micro-computed tomography: A method for the non-destructive evaluation of the three-dimensional structure of biological specimens. *Methods Mol. Biol.* 455, 273–292. https://doi.org/10.1007/978-1-59745-104-8_19
- Stefan, U., Michael, B., Werner, S., 2010. Effects of three different preservation methods on the mechanical properties of human and bovine cortical bone. *Bone* 47, 1048–1053. <https://doi.org/10.1016/j.bone.2010.08.012>
- Steiner, M., Volkheimer, D., Meyers, N., Wehner, T., Wilke, H.J., Claes, L., Ignatius, A., 2015. Comparison between different methods for biomechanical assessment of ex vivo fracture callus stiffness in small animal bone healing studies. *PLoS One* 10, 1–16. <https://doi.org/10.1371/journal.pone.0119603>
- Steppan, C.M., Crawford, D.T., Chidsey-Frink, K.L., Ke, H., Swick, A.G., 2000. Leptin is a potent stimulator of bone growth in ob/ob mice. *Regul. Pept.* 92, 73–78. [https://doi.org/10.1016/S0167-0115\(00\)00152-X](https://doi.org/10.1016/S0167-0115(00)00152-X)
- Strotmeyer, E.S., Cauley, J.A., Schwartz, A. V., Nevitt, M.C., Resnick, H.E., Bauer, D.C., Tylavsky, F.A., De Rekeneire, N., Harris, T.B., Newman, A.B., 2005. Nontraumatic fracture risk with diabetes mellitus and impaired fasting glucose in older white and black adults: The health, aging, and body composition study. *Arch. Intern. Med.* 165, 1612–1617. <https://doi.org/10.1001/archinte.165.14.1612>
- Suda, T., Takashi, N., Martin, T.J., 1992. Modulation of Osteoclast Differentiation. *Endocr. Rev.* 13, 66–80. <https://doi.org/10.1210/edrv-13-1-66>
- Sun, H., Saeedi, P., Karuranga, S., Pinkepank, M., Ogurtsova, K., Duncan, B.B., Stein, C., Basit, A., Chan, J.C.N., Mbanya, J.C., Pavkov, M.E., Ramachandaran, A., Wild, S.H., James, S., Herman, W.H., Zhang, P., Bommer, C., Kuo, S., Boyko, E.J., Magliano, D.J.,

2022. IDF Diabetes Atlas: Global, regional and country-level diabetes prevalence estimates for 2021 and projections for 2045. *Diabetes Res. Clin. Pract.* 183, 109119. <https://doi.org/10.1016/j.diabres.2021.109119>
- Svenson, K.L., Von Smith, R., Magnani, P.A., Suetin, H.R., Paigen, B., Naggert, J.K., Li, R., Churchill, G.A., Peters, L.L., 2007. Multiple trait measurements in 43 inbred mouse strains capture the phenotypic diversity characteristic of human populations. *J. Appl. Physiol.* 102, 2369–2378. <https://doi.org/10.1152/jappphysiol.01077.2006>
- Takagi, M., Kasayama, S., Yamamoto, T., Motomura, T., Hashimoto, K., Yamamoto, H., Sato, B., Okada, S., Kishimoto, T., 1997. Advanced glycation endproducts stimulate interleukin-6 production by human bone-derived cells. *J. Bone Miner. Res.* 12, 439–446. <https://doi.org/10.1359/jbmr.1997.12.3.439>
- Takahashi, M., Oikawa, M., Nagano, A., 2000. Effect of age and menopause on serum concentrations of pentosidine, an advanced glycation end product. *Journals Gerontol. - Ser. A Biol. Sci. Med. Sci.* 55, 137–140. <https://doi.org/10.1093/gerona/55.3.M137>
- Tanaka, K., Yamaguchi, T., Kanazawa, I., Sugimoto, T., 2015. Effects of high glucose and advanced glycation end products on the expressions of sclerostin and RANKL as well as apoptosis in osteocyte-like MLO-Y4-A2 cells. *Biochem. Biophys. Res. Commun.* 461, 193–199. <https://doi.org/10.1016/j.bbrc.2015.02.091>
- Tang, S.Y., Zeenath, U., Vashishth, D., 2007. Effects of non-enzymatic glycation on cancellous bone fragility. *Bone* 40, 1144–1151. <https://doi.org/10.1016/j.bone.2006.12.056>
- Taylor, E.A., Donnelly, E., 2020. Raman and Fourier transform infrared imaging for characterization of bone material properties. *Bone* 139, 115490. <https://doi.org/10.1016/j.bone.2020.115490>
- Taylor, E.A., Lloyd, A.A., Salazar-Lara, C., Donnelly, E., 2017. Raman and Fourier Transform Infrared (FT-IR) Mineral to Matrix Ratios Correlate with Physical Chemical Properties of Model Compounds and Native Bone Tissue. *Appl. Spectrosc.* 71, 2404–2410. <https://doi.org/10.1177/0003702817709286>
- Terada, M., Inaba, M., Yano, Y., Hasuma, T., Nishizawa, Y., Morii, H., Otani, S., 1998. Growth-Inhibitory Effect of a High Glucose Concentration on Osteoblast-like Cells. *Bone* 22, 17–23. [https://doi.org/10.1016/S8756-3282\(97\)00220-2](https://doi.org/10.1016/S8756-3282(97)00220-2)

- Thorpe, S.R., Baynes, J.W., 2003. Maillard reaction products in tissue proteins : New products and new perspectives Review Article 275–281. <https://doi.org/10.1007/s00726-003-0017-9>
- Tice, M.J.L., Bailey, S., Sroga, G.E., Gallagher, E.J., Vashishth, D., 2022. Non-Obese MKR Mouse Model of Type 2 Diabetes Reveals Skeletal Alterations in Mineralization and Material Properties. *JBMR Plus* 6, 1–14. <https://doi.org/10.1002/jbm4.10583>
- Trammell, L.H., Kroman, A.M., 2012. Bone and Dental Histology, Research Methods in Human Skeletal Biology. Elsevier Inc. <https://doi.org/10.1016/B978-0-12-385189-5.00013-3>
- Tsai, S.W., Wu, E.M., 1971. A General Theory of Strength for Anisotropic Materials. *J. Compos. Mater.* 5, 58–80. <https://doi.org/10.1177/002199837100500106>
- Tsuda, H., Arends, J., 1994. Orientational Micro-Raman Spectroscopy on Hydroxyapatite Single Crystals and Human Enamel Crystallites. *J. Dent. Res.* 73, 1703–1710. <https://doi.org/10.1177/00220345940730110501>
- Turner, C.H., 2006. Bone strength: Current concepts. *Ann. N. Y. Acad. Sci.* 1068, 429–446. <https://doi.org/10.1196/annals.1346.039>
- Turner, C.H., Rho, J., Takano, Y., Tsui, T.Y., Pharr, G.M., 1999. The elastic properties of trabecular and cortical bone tissues are similar: Results from two microscopic measurement techniques. *J. Biomech.* 32, 437–441. [https://doi.org/10.1016/S0021-9290\(98\)00177-8](https://doi.org/10.1016/S0021-9290(98)00177-8)
- Tzaphlidou, M., 2005. The role of collagen in bone structure: An image processing approach. *Micron* 36, 593–601. <https://doi.org/10.1016/j.micron.2005.05.009>
- Unnanuntana, A., Rebolledo, B.J., Michael Khair, M., Dicarlo, E.F., Lane, J.M., 2011. Diseases affecting bone quality: Beyond osteoporosis. *Clin. Orthop. Relat. Res.* 469, 2194–2206. <https://doi.org/10.1007/s11999-010-1694-9>
- Uppuganti, S., Granke, M., Makowski, A.J., Does, M.D., Nyman, J.S., 2016. Age-related changes in the fracture resistance of male Fischer F344 rat bone. *Bone* 83, 220–232. <https://doi.org/10.1016/j.bone.2015.11.009>
- Valderrábano, R.J., Linares, M.I., 2018. Diabetes mellitus and bone health: epidemiology, etiology and implications for fracture risk stratification. *Clin. Diabetes Endocrinol.* 4, 9.

<https://doi.org/10.1186/s40842-018-0060-9>

- Vallet-Regi, M., Navarrete, D.A., 2015. CHAPTER 1. Biological Apatites in Bone and Teeth, in: RSC Nanoscience and Nanotechnology. pp. 1–29. <https://doi.org/10.1039/9781782622550-00001>
- van Lenthe, G.H., Voide, R., Boyd, S.K., Müller, R., 2008. Tissue modulus calculated from beam theory is biased by bone size and geometry: Implications for the use of three-point bending tests to determine bone tissue modulus. *Bone* 43, 717–723. <https://doi.org/10.1016/j.bone.2008.06.008>
- Vanleene, M., Rey, C., Ho Ba Tho, M.C., 2008. Relationships between density and Young's modulus with microporosity and physico-chemical properties of Wistar rat cortical bone from growth to senescence. *Med. Eng. Phys.* 30, 1049–1056. <https://doi.org/10.1016/j.medengphy.2007.12.010>
- Vashishth, D., 2009. Small animal bone biomechanics. *Bone* 43, 794–797. <https://doi.org/10.1016/j.bone.2008.06.013.Small>
- Vashishth, D., 2007. The Role of the Collagen Matrix in Skeletal Fragility. *Curr. Osteoporos. Rep.* 5, 62–66.
- Vashishth, D., Gibson, G., Khoury, J., Schaffler, M., Kimura, J., Fyhrie, D., 2001. Influence of nonenzymatic glycation on biomechanical properties of cortical bone. *Bone* 28, 195–201. [https://doi.org/10.1016/S8756-3282\(00\)00434-8](https://doi.org/10.1016/S8756-3282(00)00434-8)
- Verbruggen, A.S.K., McNamara, L.M., 2023. Mechanoregulation may drive osteolysis during bone metastasis: A finite element analysis of the mechanical environment within bone tissue during bone metastasis and osteolytic resorption. *J. Mech. Behav. Biomed. Mater.* 138, 105662. <https://doi.org/10.1016/j.jmbbm.2023.105662>
- Vestergaard, P., 2007. Discrepancies in bone mineral density and fracture risk in patients with type 1 and type 2 diabetes—a meta-analysis. *Osteoporos. Int.* 18, 427–444. <https://doi.org/10.1007/s00198-006-0253-4>
- Viguet-Carrin, S., Farlay, D., Bala, Y., Munoz, F., Bouxsein, M.L., Delmas, P.D., 2008. An in vitro model to test the contribution of advanced glycation end products to bone biomechanical properties. *Bone* 42, 139–149. <https://doi.org/10.1016/j.bone.2007.08.046>
- Viguet-Carrin, S., Garnero, P., Delmas, P.D., 2006. The role of collagen in bone strength 319–

336. <https://doi.org/10.1007/s00198-005-2035-9>
- Von Euw, S., Wang, Y., Laurent, G., Drouet, C., Babonneau, F., Nassif, N., Azaïs, T., 2019. Bone mineral: new insights into its chemical composition. *Sci. Rep.* 9, 1–11. <https://doi.org/10.1038/s41598-019-44620-6>
- Wang, X., Shen, X., Li, X., Mauli Agrawal, C., 2002. Age-related changes in the collagen network and toughness of bone. *Bone* 31, 1–7. [https://doi.org/10.1016/S8756-3282\(01\)00697-4](https://doi.org/10.1016/S8756-3282(01)00697-4)
- Wang, Y.W., Sun, G.D., Sun, J., Liu, S.J., Wang, J., Xu, X.H., Miao, L.N., 2013. Spontaneous type 2 diabetic rodent models. *J. Diabetes Res.* 2013. <https://doi.org/10.1155/2013/401723>
- Wei, J., Shimazu, J., Makinistoglu, M.P., Maurizi, A., Kajimura, D., Zong, H., Takarada, T., Lezaki, T., Pessin, J.E., Hinoi, E., Karsenty, G., 2015. Glucose Uptake and Runx2 Synergize to Orchestrate Osteoblast Differentiation and Bone Formation. *Cell* 161, 1576–1591. <https://doi.org/10.1016/j.cell.2015.05.029>
- Weiner, S., Wagner, H.D., 1998. THE MATERIAL BONE: Structure-Mechanical Function Relations. *Annu. Rev. Mater. Sci.* 28, 271–298. <https://doi.org/10.1146/annurev.matsci.28.1.271>
- Whitehouse, W.J., 1974. The quantitative morphology of anisotropic trabecular bone. *J. Microsc.* 101, 153–168. <https://doi.org/10.1111/j.1365-2818.1974.tb03878.x>
- Whyte, M.P., 2006. Paget ' s Disease of Bone. *Evaluation* 593–600.
- Willett, T.L., Dapaah, D.Y., Uppuganti, S., Granke, M., Nyman, J.S., 2019. Bone collagen network integrity and transverse fracture toughness of human cortical bone. *Bone* 120, 187–193. <https://doi.org/10.1016/j.bone.2018.10.024>
- Willett, T.L., Suttly, S., Gaspar, A., Avery, N., Grynepas, M., 2013. In vitro non-enzymatic ribation reduces post-yield strain accommodation in cortical bone. *Bone* 52, 611–622. <https://doi.org/10.1016/j.bone.2012.11.014>
- Willett, T.L., Voziyan, P., Nyman, J.S., 2022. Causative or associative: A critical review of the role of advanced glycation end-products in bone fragility. *Bone* 163, 116485. <https://doi.org/10.1016/j.bone.2022.116485>

- Wittig, N.K., Birkedal, H., 2022. Bone hierarchical structure: spatial variation across length scales. *Acta Crystallogr. Sect. B Struct. Sci. Cryst. Eng. Mater.* 78, 305–311. <https://doi.org/10.1107/S2052520622001524>
- Wölfel, E.M., Fiedler, I.A.K., Dragoun Kolibova, S., Krug, J., Lin, M.-C., Yazigi, B., Siebels, A.K., Mushumba, H., Wulff, B., Ondruschka, B., Püschel, K., Glüer, C.C., Jähn-Rickert, K., Busse, B., 2022a. Human tibial cortical bone with high porosity in type 2 diabetes mellitus is accompanied by distinctive bone material properties. *Bone* 165, 116546. <https://doi.org/10.1016/j.bone.2022.116546>
- Wölfel, E.M., Jähn-Rickert, K., Schmidt, F.N., Wulff, B., Mushumba, H., Sroga, G.E., Püschel, K., Milovanovic, P., Amling, M., Campbell, G.M., Vashishth, D., Busse, B., 2020. Individuals with type 2 diabetes mellitus show dimorphic and heterogeneous patterns of loss in femoral bone quality. *Bone* 140, 115556. <https://doi.org/10.1016/j.bone.2020.115556>
- Wölfel, E.M., Schmidt, F.N., vom Scheidt, A., Siebels, A.K., Wulff, B., Mushumba, H., Ondruschka, B., Püschel, K., Scheijen, J., Schalkwijk, C.G., Vettorazzi, E., Jähn-Rickert, K., Gludovatz, B., Schaible, E., Amling, M., Rauner, M., Hofbauer, L.C., Zimmermann, E.A., Busse, B., 2022b. Dimorphic Mechanisms of Fragility in Diabetes Mellitus: the Role of Reduced Collagen Fibril Deformation. *J. Bone Miner. Res.* 37, 2259–2276. <https://doi.org/10.1002/jbmr.4706>
- Wolff, J., 1986. Concept of the Law of Bone Remodelling, in: *The Law of Bone Remodelling*. Springer Berlin Heidelberg, Berlin, Heidelberg, pp. 1–1. https://doi.org/10.1007/978-3-642-71031-5_1
- Wolfram, U., Schwiedrzik, J., 2016. Post-yield and failure properties of cortical bone. *Bonekey Rep.* 5, 1–10. <https://doi.org/10.1038/bonekey.2016.60>
- Woolley, W., Obata, Y., Martin, K., Acevedo, C., 2023. Whole-Bone Toughness Is Linked to Canal and Osteocyte Lacunae Deficits in the ZDSD Type 2 Diabetic Rat Model. *Jom* 20–24. <https://doi.org/10.1007/s11837-023-05882-8>
- Wu, H., Patterson, C.C., Zhang, X., Ghani, R.B.A., Magliano, D.J., Boyko, E.J., Ogle, G.D., Luk, A.O.Y., 2022. Worldwide estimates of incidence of type 2 diabetes in children and adolescents in 2021. *Diabetes Res. Clin. Pract.* 185, 109785. <https://doi.org/10.1016/j.diabres.2022.109785>

- Wu, Z., Baker, T.A., Ovaert, T.C., Niebur, G.L., 2011. The Effect of Holding Time on Nanoindentation Measurements of Creep in Bone. *J Biomech* 44, 1066–1072. <https://doi.org/10.1016/j.jbiomech.2011.01.039>.The
- Yadav, R.N., Sihota, P., Neradi, D., Bose, J.C., Dhiman, V., Karn, S., Sharma, S., Aggarwal, S., Goni, V.G., Bhadada, S.K., Kumar, N., 2022. Effects of type 2 diabetes on the viscoelastic behavior of human trabecular bone. *Med. Eng. Phys.* 104, 103810. <https://doi.org/10.1016/j.medengphy.2022.103810>
- Yamako, G., Tokunaga, K., Takano, R., Endo, N., 2006. Morphological and Mechanical Evaluation of the Cancellous Bone in the Rat Femoral Head 1, 195–203. <https://doi.org/10.1299/jbse.1.195>
- Yamauchi, M., Young, D.R., Chandler, G.S., Mechanic, G.L., 1988. Cross-linking and new bone collagen synthesis in immobilized and recovering primate osteoporosis. *Bone* 9, 415–418. [https://doi.org/10.1016/8756-3282\(88\)90124-X](https://doi.org/10.1016/8756-3282(88)90124-X)
- Yan, J., Mecholsky, J.J., Clifton, K.B., 2007. How tough is bone? Application of elastic-plastic fracture mechanics to bone. *Bone* 40, 479–484. <https://doi.org/10.1016/j.bone.2006.08.013>
- Yasuda, H., Shima, N., Nakagawa, N., Yamaguchi, K., Kinosaki, M., Mochizuki, S., Tomoyasu, A., Yano, K., Goto, M., Murakami, A., Tsuda, E., Morinaga, T., Higashio, K., Udagawa, N., Takahashi, N., Suda, T., 1998. Osteoclast differentiation factor is a ligand for osteoprotegerin/osteoclastogenesis-inhibitory factor and is identical to TRANCE/RANKL. *Proc. Natl. Acad. Sci.* 95, 3597–3602. <https://doi.org/10.1073/pnas.95.7.3597>
- Yoshitake, F., Itoh, S., Narita, H., Ishihara, K., Ebisu, S., 2008. Interleukin-6 directly inhibits osteoclast differentiation by suppressing receptor activator of NF- κ B signaling pathways. *J. Biol. Chem.* 283, 11535–11540. <https://doi.org/10.1074/jbc.M607999200>
- Zákány, J., Duboule, D., 1993. Correlation of expression of Wnt-1 in developing limbs with abnormalities in growth and skeletal patterning. *Nature* 362, 546–549. <https://doi.org/10.1038/362546a0>
- Zeitoun, D., Caliaperoumal, G., Bensidhoum, M., Constans, J.M., Anagnostou, F., Bousson, V., 2019. Microcomputed tomography of the femur of diabetic rats: alterations of

- trabecular and cortical bone microarchitecture and vasculature—a feasibility study. *Eur. Radiol. Exp.* 3, 17. <https://doi.org/10.1186/s41747-019-0094-5>
- Zhang, G., Xu, S., Yang, J., Guan, F., Cao, L., Mao, H., 2018. Combining specimen-specific finite-element models and optimization in cortical-bone material characterization improves prediction accuracy in three-point bending tests. *J. Biomech.* 76, 103–111. <https://doi.org/10.1016/j.jbiomech.2018.05.042>
- Zhang, H., Schuster, B.E., Wei, Q., Ramesh, K.T., 2006. The design of accurate micro-compression experiments. *Scr. Mater.* 54, 181–186. <https://doi.org/10.1016/j.scriptamat.2005.06.043>
- Zhang, J.-M., An, J., 2007. Cytokines, Inflammation, and Pain. *Int. Anesthesiol. Clin.* 45, 27–37. <https://doi.org/10.1097/AIA.0b013e318034194e>
- Zimmermann, E.A., Busse, B., Ritchie, R.O., 2015. The fracture mechanics of human bone: influence of disease and treatment. *Bonekey Rep.* 4, 1–13. <https://doi.org/10.1038/bonekey.2015.112>
- Zimmermann, E.A., Ritchie, R.O., 2015. Bone as a Structural Material. *Adv. Healthc. Mater.* 4, 1287–1304. <https://doi.org/10.1002/adhm.201500070>
- Zimmermann, E.A., Schaible, E., Bale, H., Barth, H.D., Tang, S.Y., Reichert, P., Busse, B., Alliston, T., Ager III, J.W., Ritchie, R.O., 2011. Age-related changes in the plasticity and toughness of human cortical bone at multiple length scales. *Proc Natl Acad Sci* 35, 14416–14421. <https://doi.org/10.1073/pnas.1107966108>
- Zysset, P.K., Edward Guo, X., Edward Hoffler, C., Moore, K.E., Goldstein, S.A., 1999. Elastic modulus and hardness of cortical and trabecular bone lamellae measured by nanoindentation in the human femur. *J. Biomech.* 32, 1005–1012. [https://doi.org/10.1016/S0021-9290\(99\)00111-6](https://doi.org/10.1016/S0021-9290(99)00111-6)

CHAPTER 3

Longitudinal Alterations in Bone Morphometry, Mechanical Integrity and Composition in Type-2 Diabetes in a Zucker Diabetic Fatty (ZDF) Rat

This Chapter has been adapted from a published article, 'Monahan GE, Schiavi-Tritz J, Britton M, Vaughan TJ. Longitudinal alterations in bone morphometry, mechanical integrity and composition in Type-2 diabetes in a Zucker diabetic fatty (ZDF) rat. Bone. 2023 May;170:116672. doi: 10.1016/j.bone.2023.116672. Epub 2023 Jan 13. PMID: 36646266'.

3.1 Introduction

Type-2 Diabetes (T2D) mellitus is a metabolic disorder that accounts for 90 - 95% of overall diabetic cases (Valderrábano and Linares, 2018). Skeletal fragility is a major complication of T2D. Recently, it has been identified that T2D patients can have up to a 3-fold increased risk of bone fracture (Janghorbani et al., 2006; Karim and Bouxsein, 2016). Moreover, disease duration may play a role, where individuals with long-term diabetes have a higher incidence of fracture than short-term diabetes (Folk et al., 1999; Retzepi and Donos, 2010). Paradoxically, T2D is not accompanied by a reduction in bone mineral density (BMD), which is highly implicated in other bone diseases such as osteoporosis (Parfitt et al., 1983). In fact, it has been found that patients with T2D can present with higher bone mass, compared to non-diabetic controls (Vestergaard, 2007). This implies that T2D is associated with reduced bone *quality*, with recent studies indicating that sub-tissue alterations to the organic constituents of the bone matrix contribute to impaired biomechanical behaviour (Dhaliwal et al., 2014; Karim and Bouxsein, 2016; Rubin and Patsch, 2016; Saito and Marumo, 2013). During T2D, elevated

levels of glucose, results in a hyperglycaemic environment, which has been proposed to increase the accumulation of non-enzymatic cross-links in the form of Advanced Glycated End-products (AGEs) (Furst et al., 2016; Goldin et al., 2006). AGEs are thought to stiffen the collagen leading to a more brittle behaviour. While it has been widely hypothesised that AGEs are the primary cause of bone fragility in T2D (Karim and Bouxsein, 2016; Saito and Marumo, 2010; Willett et al., 2022; Yamamoto and Sugimoto, 2016), there remains limited experimental evidence that provides a mechanistic link between AGE accumulation and tissue mechanics in T2D.

Much of the current understanding of the mechanics of bone fragility in T2D has been generated using *in-vitro* glycation models (Catanese et al., 1999; Poundarik et al., 2015; Vashishth et al., 2001; Viguet-Carrin et al., 2008; Zimmermann et al., 2011), whereby animal or human tissue was immersed in a ribose solution to facilitate non-enzymatic glycation of the protein network. In some cases, studies have found only subtle changes in mechanical properties (Vashishth et al., 2001; Viguet-Carrin et al., 2008) despite significant increases in AGE accumulation. Other studies have found that AGE accumulation primarily affects the post-yield and toughness properties of the tissue (Catanese et al., 1999; Zimmermann et al., 2011). In particular, Poundarik *et al* (2015) investigated *in-vitro* glycated human cortical bone and found that fluorescent Advanced Glycation End-products (fAGE) accumulation was two-times greater and fracture toughness was reduced in the *in-vitro* glycated tissue versus the controls. However, these *in-vitro* glycation models are severely limited by the fact that they generate AGEs levels in the tissue much higher than occurs physiologically. Meanwhile, the difficulty in obtaining direct measurements *in-vivo* means that quantitative data describing precisely how bone tissue properties are impaired in patients with T2D is limited. To date, most human studies have focused on compression of trabecular cores (Karim et al., 2018; Karim and Vashishth, 2012), where it is difficult to decouple structural and material properties (Karim et al., 2018; Karim and Vashishth, 2012). Notably, it has been found that cortical indentation distances of bone from the femoral neck has a negative correlation between serum total AGEs, but trabecular bone AGEs showed a positive correlation between compressive yield stress and strain (Karim et al., 2018). Alternatively, animal studies can provide a wider understanding of the aetiology of skeletal fragility in diabetes since confounding factors such as disease duration and gender can be controlled. There is currently no single animal model that can represent all features of T2D in humans. Hence, further animal studies are required to further understand each strain and get an idea of which strains closely mimic T2D in humans. Moreover, the

advantage of the Zucker Diabetic Fatty (ZDF) strain is that it is a well-established animal model of T2D, and the onset and progression of the disease is well understood (Chen et al., 1996; Etgen and Oldham, 2000; Farooqi et al., 2007; Hansson et al., 1972; Hughes and Tanner, 1970; Lee et al., 1994; Peterson et al., 1990; Steppan et al., 2000; Yokoi et al., 2013). Moreover, these rats develop T2D between 9- to 11-weeks of age before they have become skeletally mature (occurring at ~16-weeks). This animal model may provide a wider understanding of the progression of the disease in a population that develops T2D during puberty. Many studies of animals with diabetes have examined bone mechanical properties. Yet, there is a lack of animal research that has examined how AGE accumulation actually relates to bone fragility as the disease progresses.

Reinwald *et al.* (2009b) investigated skeletal fragility of the femoral and L4 vertebral bone in ZDF and Zucker Diabetic Sprague Dawley (ZDSD) rats at 33-weeks of age. Both strains had a lower bone mineral content than controls, which coincided with the structural deficits found for femoral and vertebral bone after monotonic loading. Both strains showed no difference in material properties for femoral bone in comparison to controls, however, ZDF rats had a lower vertebral ultimate stress and modulus than controls. While the ZDSD rats showed similar results and had a lower bone toughness than controls, this study did not evaluate AGE content in tissue. The University of California, Davis (UCD)-T2DM rat has also been used, where it has been found that diabetic rats had a higher concentration of cortical bone AGEs than controls at 6-months of age (Acevedo et al., 2018). Under monotonic loading, ulnar bone from diabetic rats had a significant reduction in bending rigidity, yield moment, elastic modulus, yield and ultimate stress. Conversely, Prisby *et al.* (2008) explored mechanical properties of ZDF femoral and tibial bone at 7- (short-term), 12- and 20- (long-term) weeks of age and found that, although structural deficits were observed in the long-term diabetic femora and tibia, there were no material-level differences observed. While AGE content was again not measured in this study, other studies have investigated, in detail, changes in bone composition during T2D. Creecy *et al.* (2016) have used Raman spectroscopy and high performance liquid chromatography (HPLC) on ZDSD rat femoral bone to quantify cortical tissue composition at 16-, 22- and 29-weeks. Raman spectroscopy results showed that ZDSD rats at 29-weeks had higher mineral: matrix ratio and crystallinity. HPLC results demonstrated no difference in levels of pentosidine (a non-enzymatic crosslink) between strains at any ages, although a significant increase with age was seen in the diabetic cohort. They found ultimate stress and fracture toughness of femurs at 16- and 22-weeks old ZDSD rats was higher than controls but

showed no difference between strains at 29-weeks; ZDSD radius bone had reduced toughness at 29-weeks. While alterations at the sub-tissue level of the bone matrix likely plays a role in diabetic bone fragility, there are a lack of combined studies that investigate in detail how such sub-tissue properties are related to the mechanical properties of T2 diabetic tissue (Hunt et al., 2021, 2019, 2018; Schmidt et al., 2017; Sihota et al., 2020a; Wölfel et al., 2020). Furthermore, longitudinal animal studies that consider older long-term diabetic time-points are required to understand how disease duration affects AGE accumulation and skeletal fragility.

This Chapter conducts a longitudinal investigation on the geometrical, structural and material properties of T2D bone using a Zucker Diabetic Fatty (ZDF) rat model over a 46-week period (~ one year old). Specifically, in this Chapter it is hypothesized that cortical bone of the Zucker Diabetic Fatty (*fa/fa*) rats will have an impaired mechanical integrity, particularly as the duration of the disease increases which will be related to an accumulation of AGEs in cortical tissue of the ZDF (*fa/fa*) rats in comparison to the Zucker Lean (*fa/+*) control rats. The objectives of this Chapter are to (i) examine geometrical alterations in T2 diabetic and control cortical bone at various ages using micro-computed tomography; (ii) assess the fracture mechanics of cortical bone at the structural- and tissue-levels using a three-point bend test; (iii) explore the composition of T2D cortical bone tissue and skin using Fourier Transform Infrared (FTIR) Spectroscopy and fluorescence AGE (fAGE) analysis; and (iv) investigate a correlation between cortical bone tissue composition and its fragility in T2D.

3.2 Materials and Methods

3.2.1 Animal model and tissues

Animal Model

A longitudinal 46-week study using male Zucker Diabetic Fatty [(ZDF: *fa/fa*) (T2D) and Zucker Lean (ZL: *fa/+*) (Control)] (Charles River, France) rats at 12-, 26- and 46-weeks of age (n = 7 - 9, per age, per condition) was conducted to investigate the geometrical, structural and material properties of bone in T2D at various metabolic stages throughout the life of the animal. Animals arrived at approximately 8- to 10-weeks old and were maintained under standard environmental conditions, with temperature maintained at 20 - 24°C, humidity maintained at 45 - 50%, and a 12 h light/dark cycle with food and water *ad libitum*. At 10-weeks old, ZDF and ZL rats were switched from a normal to a high fat diet (HFD) to induce a hyperglycaemic state in these rats, which accelerates the progression of the disease into overt diabetes (Formulab Diet 5008, LabDiet, St. Louis, USA (17% kcal from Fat)). The animals were

handled in accordance with the European Guidelines for Care and Use of Laboratory Animals (Directive 2010/63/EU). The Animal Care Research Ethics Committee (ACREC) in the University of Galway, Ireland approved this project. In total, three rats died or were euthanized due to weight loss > 10% of their body weight or health issues. ZDF rats which exhibited Lean rat characteristics were excluded from the dataset and *vice versa*. See Appendix Figure S3.1 for a detailed timeline of the animal study over a 14-month period.

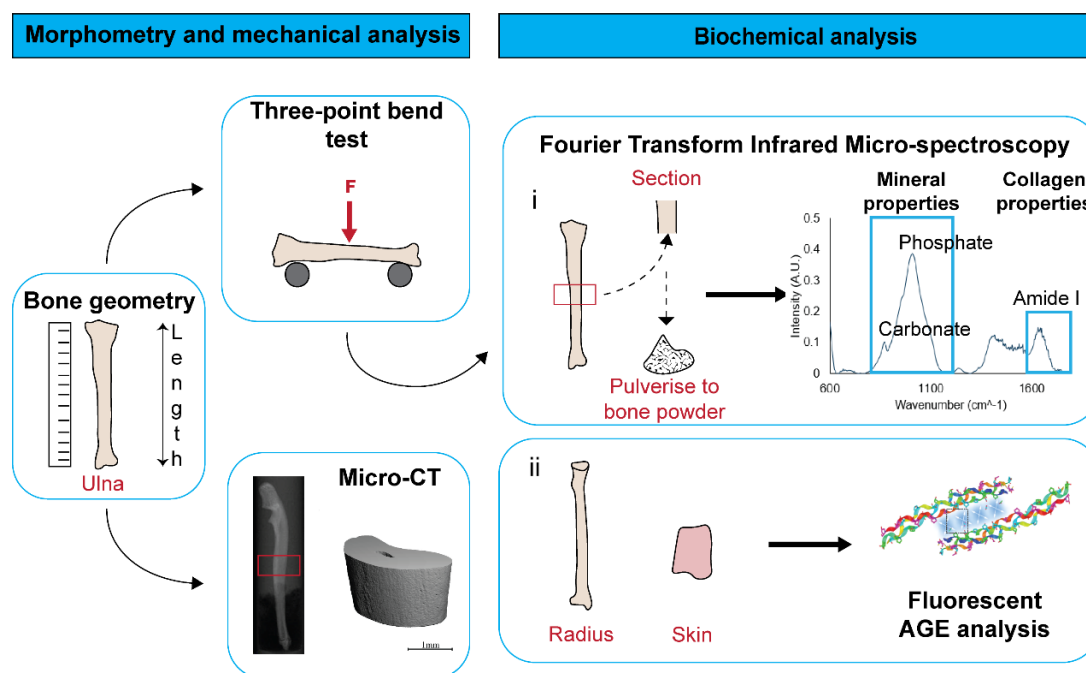


Figure 3.1: Workflow of sample preparation methods and the tissue type used for each characterization technique; microarchitectural and biomechanical analysis using ulnae and compositional analysis, such as, (i) FTIR, (ii) fAGE analysis for demineralised cortical bone and skin sections.

Rats were euthanized at 12- (Early-stage diabetes), 26- (Established diabetes) and 46-weeks (Long-term diabetes) of age. The blood glucose levels were recorded on the day of sacrifice with a glucometer to check the diabetic state of the animals. However, data recorded from the glucometer are not reported here as the glucometer could not accurately measure blood glucose values > 33 mmol/L. After measuring their weight, right ulnae, radius bone and skin samples were dissected, wrapped in PBS-soaked gauze (ulnae, radius) or soaked in PBS (skin) then frozen at -20°C. In this Chapter, the ulna was used for biomechanical and compositional analysis as they had a slender and flat shape, reducing the effect of slipping during three-point bend testing. Moreover, it is understood that the most common fracture regions for T2D patients are the hip (Janghorbani et al., 2007), vertebrae (Koh et al., 2010) and wrist (Vestergaard, 2007). Although femurs are commonly used in assessing fracture probability in

the femoral and hip region, there are a lack of studies that explore fracture risk in bones associated with the wrist region in diabetes. The radius was used for fAGE analysis to measure AGE accumulation from cortical bone in a region approximate to the ulna. Blood serum was collected on the day of euthanasia and frozen at -80°C until analysis. Before experimentation, bones were defrosted for approximately 12 h. Microarchitectural, biomechanical and compositional analysis were carried out to analyse local and systemic factors influenced by T2D. Right ulnae underwent X-Ray Micro-computed Tomography (micro-CT) scanning to determine geometric and morphometric properties, followed by a mechanical characterisation through three-point bend testing, after which, a biochemical analysis was carried out. Cortical bone samples were sectioned from the mid-diaphysis and milled into a bone powder for FTIR analysis to measure various mineral- and collagen-properties, while skin and cortical bone sections were used to quantify AGE content through fAGE analysis (Figure 3.1).

Serum Analysis

Serum glucose levels were also measured to compare the hyperglycaemic state of the animals. Serum levels of insulin-like growth factor hormone I (IGF-I) were measured to explore the homeostasis of longitudinal bone growth and osteoblast function in T2D rats. On the day of euthanasia, blood samples were collected by cardiac puncture from the rats and samples were left to clot at room temperature for 1-2 h. Blood samples were then centrifuged (Eppendorf 5424R microcentrifuge, Hamburg, Germany) at 2,000 g for 15 min. Once the serum was separated from the clotted blood, the serum was aliquot into 1.5 mL Eppendorf tubes. Serum levels of glucose were measured using a quantitative glucose assay kit from Abcam (ab272532, Abcam, Cambridge, England) following the manufacturer's protocol. Briefly, the serum was diluted in sample dilution buffer provide with the kit by $4\times$ and $2\times$ for the ZDF and ZL, respectively. Samples and standards were added with 200 μL /well in duplicate to a 96-well plate. The absorbance was read at 630 nm using a SynergyTM HT multi-mode microplate reader (BioTek). Serum levels of IGF-I were measured using an ELISA kit from AssayGenie (RTEB0037, AssayGenie, Dublin, Ireland) according to the manufacturer's protocol. Samples were diluted 1:100 and the micro-plate was read at 450 nm.

3.2.2 Geometric and Morphometric Properties

Bone Size and Shape

To compare the growth of lean and ZDF (*fa/fa*) rats, basic measurements of the ulna were taken using a Vernier Callipers before testing, which included bone length (L), anterior-posterior (AP) and medial-lateral (ML) diameters.

X-Ray Micro-Computed Tomography (μ -CT)

Right ulnae were imaged using a high-resolution micro-CT scanner (μ CT100, Scanco Medical, Brüttisellen, Switzerland) at an isotropic voxel size of 5 μ m. Scan settings used an X-Ray tube potential of 70 kVp, a current of 57 μ A, an integration time of 500 ms at 1,070 projections per 180° and a 0.5 mm thick aluminium filter was used to reduce beam-hardening artefacts. A 1.5 mm (300 slices, 62.4 minutes per bone) cortical bone volume of interest (VOI) from the mid-diaphysis of the ulnae was scanned. Each slice was fitted with a contour around the periosteal and endosteal surface and segmented with a threshold of 710 mg HA/ cm³ (Rezaee et al., 2020).

Using Scanco Image Processing Language, a series of structural and compositional parameters, which included polar moment of inertia (pMOI), medial-lateral and anterior-posterior moment of inertia (I_{ml} and I_{ap}), cross-sectional distance from the centroid to outermost point (C_{ml}), cortical area (Ct.Area) cortical tissue material density (TMD), could be measured using previously published guidelines (Bouxsein et al., 2010).

3.2.3 Structural and Material Properties

Quasi-static Flexural Testing

Following micro-CT imaging, mechanical testing of right ulnae samples was carried out until failure using a three-point bend test to measure whole-bone mechanical and material properties using a compression testing instrument with a 2.5 kN load cell (Zwick/Roell, Ulm, Germany). Bones were kept hydrated at room temperature before testing. One sample was excluded from the 12-week old ZDF (*fa/fa*) group, as it was accidentally fractured during dissection. Load was applied to the medial aspect of the mid-diaphysis, with a pre-load of 0.4 N at a crosshead speed of 0.03 mm/s, over a support span of $L = 7 \times$ AP diameter. Force-displacement (F vs. d) curves were converted to moment-normalised displacement (M vs. d') curves, according to Equations 3.1 and 3.2 and used to quantify bending rigidity (k) (slope of linear portion of curve), yield (found using 0.2% offset method) and ultimate moment (maximum load

experienced), post-yield displacement (PYD) (displacement that occurs between the yield and failure point) and energy-to-failure (area under the curve) (Figure 3.2).

$$M = \frac{FL}{4} \quad (3.1)$$

$$d' = \frac{12d}{L^2} \quad (3.2)$$

Material properties (e.g., Elastic modulus (E), Yield stress and strain, Ultimate stress (σ) and strain (ϵ) and toughness) were determined based on the Equations below. Beam theory was used to convert M vs d' curves to stress-strain curves (Equations (3.3) - (3.5)) (Acevedo et al., 2018; Farr et al., 2014). Micro-CT derived images were used to quantify geometric parameters of I_{ml} and C_{ml} , based on the cross-sectional geometries obtained for each bone scan. These were determined using evaluation scripts in the Scanco Image Processing Language according to previously published guidelines (Jepsen et al., 2015). In addition to reporting the estimated material properties using Equations (3.3) - (3.5), linear regression analysis was carried out to examine the intercept term and slope of ultimate moment versus section modulus (I_{ml}/C_{ml}) and compare variations between T2D (fa/fa) and control ($fa/+$) rats (see Appendix Section 3.2).

$$E = \frac{kL^3}{48I_{ml}} \quad (3.3)$$

$$\sigma = \frac{FLC_{ml}}{4I_{ml}} \quad (3.4)$$

$$(\epsilon) = \frac{12c_{mL}d}{L^2} \quad (3.5)$$

Where, F = force; L = span length; k = bending rigidity; d = displacement.

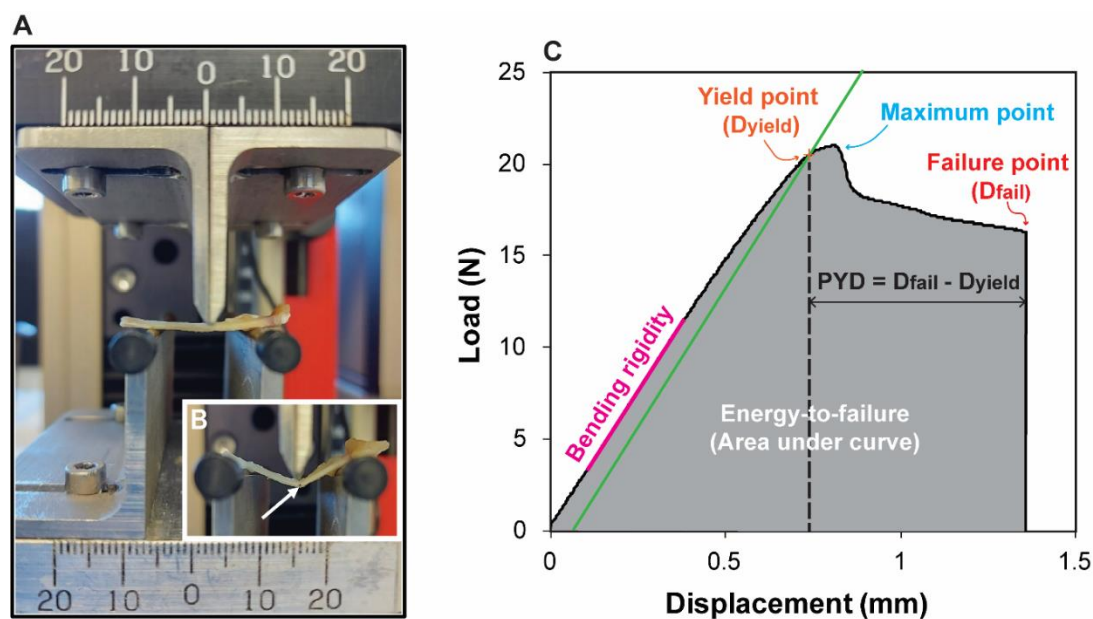


Figure 3.2: (A) Initial set-up of the three-point bend test, (B) failure point reached and (C) a moment-normalised displacement curve from loading the right ulnae from rats until failure.

3.2.4 Biochemical Analysis

Fourier transform-infrared spectroscopy (FTIR) analysis

Attenuated Total Reflective (ATR) FTIR analysis was used to assess bone quality by examining mineral and collagen properties, such as, (1) mineral: matrix ratio, (2) carbonate: phosphate ratio, (3) mineral crystallinity, (4) acid phosphate content and (5) collagen maturity. A Spectral analysis protocol was developed using OriginPro 8 (OriginLab, Northampton, MA, USA) software and measure properties. Approximately 60 mg of cortical bone sectioned from the ulnar mid-shaft was used for ATR-FTIR after biomechanical testing. Bones were cleaned of surrounding tissue, bone marrow was removed, and bones were sectioned using a low-speed saw (Buehler Inc., Lake Bluff, IL). Bone sections were placed inside a sterile cryotube, 700 μL of distilled water (dH_2O) was added and bones were pulverised using a disperser (T10 Basic ULTRA-TURREX, IKA, Sigma Aldrich).

The powder-water mixture in the tubes were centrifuged (Eppendorf 5424R microcentrifuge, Hamburg, Germany) at 5,000 g for 15 min to separate the powder from water. The water was pipetted out of the tube and discarded. The powders were left to dry in the tubes overnight on a hot plate at 37 $^{\circ}\text{C}$. ATR-FTIR spectra were obtained (Spectral region: 600 to 4,000 cm^{-1} , Resolution: 4 cm^{-1} , Number of scans: 20, Mode: absorbance) (FTIR-8300 spectrometer, Shimadzu) from bone powders and three separate measurements were taken to get an average spectrum for each sample. Spectra were baseline corrected and the mineral parameters included

the mineral: matrix ratio (area ratio of the phosphate ν_1 to ν_3 peak [916 to 1180 cm^{-1}] to amide I peak [1596 to 1712 cm^{-1}]) (Boskey and Imbert, 2017) and the carbonate: phosphate ratio (area ratio of the carbonate ν_2 peak [852 to 890 cm^{-1}] to the phosphate ν_1 to ν_3 peak [916 to 1,180 cm^{-1}]) (Beasley et al., 2014; Kourkoumelis et al., 2019; McCreadie et al., 2006). Phosphate hidden sub-bands were determined in a 900 – 1,200 cm^{-1} wavenumber range using second derivative hidden peaks and Savitzky-Golay smoothing method (Gardegaront et al., 2018; Kourkoumelis et al., 2019). The sub-bands were Gaussian curve fit to the phosphate distribution (Farlay et al., 2010; Gadaleta et al., 1996), where mineral crystallinity (Ratio of areas at the peak of $\approx 1,020$ and $\approx 1,030$ cm^{-1}) (Boskey et al., 2016; Ou-Yang et al., 2001; Querido et al., 2018; Yerramshetty and Akkus, 2008) and acid phosphate content (Ratio of areas at the peak of $\approx 1,096$ and 1,127 cm^{-1}) (Boskey and Mendelsohn, 2005; Farlay et al., 2010; Ou-Yang et al., 2001; Spevak et al., 2013) could be measured.

Finally, collagen-parameters were quantified by using second derivative analysis to fit the amide I band with seven Gaussian peaks ($\approx 1,610, 1,630, 1,645, 1,661, 1,678, 1,692$ and 1,702 cm^{-1}) (Schmidt et al., 2017). The area under each sub-peak was recorded and collagen maturity (Ratio of areas 1,660 and 1,692 cm^{-1}) – a proposed measurement pyridinoline to divalent cross-links (Boskey and Pleshkocamacho, 2007; Gieroba et al., 2021; Paschalis et al., 2001; Schmidt et al., 2017).

3.2.5 Fluorescence Advanced Glycated End-Products (fAGE) Analysis

AGEs accumulate in the bone as well as in various connective tissues throughout the body (Gkogkolou and Böhm, 2012; Goldin et al., 2006). Total fAGEs were measured from skin and radius cortical bone sections using a fluorometric assay to quantify the level of AGEs present. Skin and bone sections were demineralised in 45% formic acid for 8 - 10 days. Activated Papain Enzyme Digestion Solution (APEDS) was made up on the day of digestion by adding a papain enzyme from papaya latex at a final concentration of 7.76 units/mL (P3125, Sigma Aldrich, St. Louis, MO) to 40 mL of papain buffer extract (100 mM sodium Phosphate Buffer/ 500 mM Na_2EDTA , pH 6.5) and 63 mg L-cysteine hydrochloride (C7477, Sigma Aldrich, St. Louis, MO). Skin and cortical bone sections of similar weight were placed into 1.5 mL black O-ringed micro-centrifuge tubes and 1 mL of APEDS solution as added to each tube and rotated overnight at 10 rpm in an oven at 60°C. Once fully digested, vortexed and quickly spun using a table-top centrifuge. Samples (100 μL of sample per tube) were lyophilised, then hydrolysed by adding 100 μL of 38% HCl and then incubated in the oven at 110°C for 20 h in the black O-ring tubes. Samples were then centrifuged at $>5,000g$ for 5 min and then left to dry on a hot

plate for 48 h at 50°C under a fume hood. Once the HCl had fully evaporated, 200 µL of ultra-pure water was added and samples were centrifuged at 15,000 *g* for 10 min and only the supernatant was used for analysis. A quinine assay was carried out to quantify the level of AGEs. Quinine standards were made up (serially dilution, 0, 0.5, 1, 2, 3.5, 5, 10 µg/mL, Stock: 10 µg/mL quinine per 1 mL of 0.1 N H₂SO₄) and 50 µL of the standards and 80 µL of the samples were added in duplicate to a black flat-bottomed 96-well plate. The fluorescence was measured using a plate reader (Synergy HT BioTek, Germany) at 360/460 nm excitation/emission. Fluorescence of the samples was normalised against quinine standards.

Collagen content was measured from a hydroxyproline absorbance assay. A 1 mg/mL hydroxyproline solution was made up by adding 40 mg trans-4-Hydroxy-L-proline (H54409, Sigma Aldrich, St. Louis, MO) to 40 mL ultra-pure H₂O and was later used to create the hydroxyproline stock solution to make up the standards. Hydroxyproline standards were made up (0, 0.1, 0.25, 0.5, 1, 2, 5, 10 µg/mL, Stock: 50 µg/mL hydroxyproline per 1 mL of papain buffer extract). Skin and bone samples were diluted 50X with dH₂O for each age group, 60 µL of the samples and standards was added to a clear 96-well plate and absorbance was measured (570 nm excitation/ emission). The absorbance of samples was normalised against serially diluted hydroxyproline standards. The collagen content was derived based on prior knowledge that collagen consists of 14% hydroxyproline (Ignat'eva et al., 2007; Kafienah and Sims, 2004). Total fAGEs are reported in units of ng quinine/ mg collagen.

3.3 Statistical Analysis

Normality and homogeneity of variances for all geometrical, biomechanical and compositional data were analysed using a Shapiro-Wilk test and homogeneity of variance was analysed with Levene's test using R statistical software (version R-4.1.0). Where normality and variance were not a concern, two-way ANOVA tests were carried out to (1) compare differences between each strain, followed by a multiple comparisons Bonferroni test and (2) compare differences within each strain across the different ages (12-, 26- and 46-weeks), followed by a multiple comparisons Tukey test (GraphPad Software, Inc., La Jolla, CA). If normality and variance was a concern, a Kruskal-Wallis test was used followed by the non-parametric Dunn's test to provide the adjusted *p*-value. Alpha levels of $p \leq 0.05$ were considered significant for a 95% confidence interval. Data was pooled for all strains and ages when measuring correlation coefficients. The coefficients of correlation were calculated by Pearson's method. Data are represented as mean \pm standard deviation.

3.4 Results

To assess the health of the animal, body mass and blood glucose levels were measured on the day of the euthanasia. In addition, IGF-I, one of the major growth factors involved in bone formation and development, was quantified in the serum in order to understand the differentiating function of the osteoblasts in T2D diabetic bone. Body mass was higher in T2D rats compared to age-matched controls at 12- and 26-weeks of age (Table 3.1). However, some diabetic rats showed signs of poor-health as the disease progressed. This was highlighted in various ways, through a decrease in movement, development of cataracts and a decreased food intake resulting in a loss of body mass. Long-term diabetic rats (46-weeks) as a result had a $11.4\% \pm 2.8\%$ ($p = 0.001$) reduction in body mass compared to 26-week diabetic rats and were, on average, 62.9 g (95% CI: 29.28, 96.47, $p < 0.001$) lighter than age-matched controls (Appendix Figure S3.2).

Serum glucose levels were higher in diabetic rats at all ages in comparison to controls (Table 3.1). Like the reduction in body mass of diabetic rats from 26- to 46-weeks, serum glucose levels decreased, on average, by 38.8% ($p < 0.001$) in long-term compared to established diabetic (*fa/fa*) rats as evidenced by a loss of appetite. Insulin growth factor hormone-I (IGF-I) levels of controls naturally declined by 38.7% ($p = 0.03$) with age (12- to 46-weeks) in lean rats until there was no significant difference between T2D (*fa/fa*) and control IGF-I levels at 46-weeks. However, this natural decline with age did not occur in T2D (*fa/fa*) rats. In fact, diabetic rats IGF-I levels tended ($p = 0.06$) to be lower than controls at 12-weeks of age and these levels did not change throughout any stage of diabetes in this ZDF (*fa/fa*) strain. There was a trending interaction between age and strain on IGF-I (Variation = 5.17%, $p = 0.05$).

3.4.1 Geometric and Morphometric Properties

TMD between diabetic (fa/fa) and control (fa/+) rats did not change as the disease progressed

Since T2D is not often accompanied by a reduction in mineral density, the material tissue mineral density of cortical bone (Ct.TMD) was measured. Ct.TMD increased with age for control and ZDF (*fa/fa*) rats (Table 3.1). Ct.TMD of early stage (12-weeks) diabetic rats with 1134 ± 18.8 mg HA/cm³ was lower than age-matched controls with 1155.9 ± 22.3 mg HA/cm³ ($p = 0.04$). As the disease progressed, there was no difference in Ct.TMD between strains.

Cortical bone geometrical deficits related to rat strain

To further understand longitudinal bone growth and development during T2D, bone geometry was examined. Bone geometry was also required for beam theory analysis after mechanical testing. Ulnae from ZDF (*fa/fa*) rats were shorter in length and smaller in diameter compared to healthy controls at every stage of diabetes (Table 3.1). Similarly, geometrical properties, such as, polar moment of inertia (pMOI), medial-lateral moment of inertia (I_{ml}) and cortical bone area (Ct.Ar), measured from micro-CT data showed declines in bone size for diabetic rats versus controls (Table 3.1). From 26- to 46-weeks of age, pMOI (+26.3%), I_{ml} (+26.9%) and Ct.Ar (+12.8%) significantly ($p < 0.001$) increased for control rats. However, there was no difference in pMOI, I_{ml} and Ct.Ar of diabetic rats, indicating that bone growth slowed between the established and long-term diabetic phase in this ZDF (*fa/fa*) strain.

Table 3.1. Animal body mass, serum, bone geometry and composition from μ CT data.

	Control (<i>fa/+</i>)			T2D (<i>fa/fa</i>)		
	12 weeks ^a (n = 8-9)	26 weeks ^b (n = 8)	46 weeks (n = 7-9)	12 weeks ^a (n = 8-9)	26 weeks ^b (n = 8)	46 weeks (n = 7-9)
Body mass, g	293 ± 12.5	421 ± 27.9	466 ± 31.6	368 ± 19.4***	455 ± 32.2*	403 ± 33.1***
Serum glucose, mmol/L	12 ± 4.1	18 ± 4.9	12 ± 2.2	33.2 ± 6.9***	31 ± 5.9***	19 ± 2.6*, a, b
IGF-I, ng/mL	168 ± 72.7	155 ± 26.3	103 ± 31.9	105 ± 56.8 ⁺	76 ± 28.4**	81 ± 31.5
Geometry						
Length, mm	31 ± 0.9	32 ± 1.1 ^a	34 ± 0.8 ^a	29 ± 1.1**	30.3 ± 0.9***	31 ± 1.0***, a
ML Diameter, mm	1.17 ± 0.02	1.20 ± 0.09	1.42 ± 0.1 ^{a, b}	1.07 ± 0.02*	1.09 ± 0.06*	1.13 ± 0.08***
AP Diameter, mm	2.63 ± 0.2	2.65 ± 0.2	2.82 ± 0.2 ^a	2.45 ± 0.05*	2.48 ± 0.13*	2.62 ± 0.13*, a
Aspect ratio	15.80 ± 1	15.57 ± 0.98	14 ± 1.13 ^{a, b}	15.96 ± 0.49	15.89 ± 0.69	16.25 ± 1.14***
pMOI, mm ⁴	1.06 ± 0.21	1.71 ± 0.3 ^a	2.16 ± 0.3 ^{a, b}	0.82 ± 0.1*	1.16 ± 0.14***, a	1.255 ± 0.1***, a
I _{ml} , mm ⁴	0.14 ± 0.02	0.26 ± 0.03 ^a	0.33 ± 0.04 ^{a, b}	0.10 ± 0.01**	0.15 ± 0.01***, a	0.16 ± 0.01***, a
Ct.Ar, mm ²	1.99 ± 0.16	2.58 ± 0.13 ^a	2.91 ± 0.16 ^{a, b}	1.72 ± 0.08***	2.06 ± 0.1***, a	2.11 ± 0.07***, a
Composition (μCT)						
Ct.TMD, mgHA/cm ³	1155.9 ± 22.3	1250.5 ± 19.3 ^a	1289 ± 4.1 ^{a, b}	1134 ± 18.8*	1246.5 ± 16.4 ^a	1285.3 ± 15.1 ^{a, b}

Values are mean ± SD. T2D, Type-2 diabetic; IGF-I, Insulin growth factor hormone I; ML, Medial-lateral, AP, Anterior-posterior; pMOI, Polar moment of inertia; I_{ml}, Medial-lateral moment of inertia; Ct.Ar, Cortical area, Ct.TMD, Cortical Tissue mineral density. Difference from aged matched lean control (*fa/+*) rats with * ($p < 0.05$), ** ($p < 0.01$), *** ($p < 0.001$) and ⁺ ($p = 0.06$) significance.

^a significantly different from 12-weeks determined by a multiple comparisons Tukey test

^b significantly different from 26-weeks determined by a multiple comparisons Tukey test

3.4.2 Structural and Material Properties

Resistance to deformation and fracture and reduced ductility in diabetic (fa/fa) rat tissue

The structural properties of ulnar cortical bone were measured via three-point bend testing at all time-points (Figure 3.3). Ultimate moment and whole bone strength of ZDF (fa/fa) rats were also significantly lower than age-matched controls at 12- (-20.4%), 26- (-31.8%) and 46-weeks (-43.8%) old (Figure 3.3 (B)). Energy-to-failure increased 1.5-fold ($p = 0.007$) in control rats from 12- to 46-weeks, while diabetic rats showed no increase in energy-to-failure with age. Conversely, from 26- to 46-weeks, energy-to-failure tended towards a decrease (Figure 3.3 (C)) and long-term diabetic rats had a significantly reduced ability to resist fracture in comparison to controls ($p < 0.01$). Rats with earlier stages of diabetes had a more ductile behaviour compared to controls at 12- ($p < 0.01$) and 26-weeks ($p < 0.05$) (Figure 3.3 (D)). Yet, as these rats aged and the disease progressed, post-yield displacement reduced and was no longer greater than control bones, indicating that bone ductility significantly reduced with long-term diabetes (Figure 3.3 (D)).

Tissue material strength of diabetic (fa/fa) rats impaired as the disease progressed

Figure 3.4 shows the tissue-level material properties, where bone geometry was considered to explore the tissue itself. Although the mean elastic modulus of diabetic rats reduced by 7% from 26- to 46-weeks, this was not significant ($p = 0.52$) (Figure 3.4 (A)). Although disease duration did not affect tissue level modulus, it was found that tissue material strength was affected. Yield and ultimate stress increased with age from 12- to 46-weeks for control rats by 24.7% and 20.6% ($p < 0.001$), respectively (Figure 3.4 (B) & (D)).

Furthermore, when examining strain-related differences, tissue yield and ultimate strength of rats with earlier stages of diabetes at 12- and 26-weeks were not different to those of the age-matched controls. Despite this, by 46-weeks of age, long-term diabetic rats had a significantly lower tissue yield (-11.4%) and ultimate (-11.3%) ($p < 0.05$) strength in comparison to their age-matched controls (Figure 3.4 (B) & (D)). This indicates that, at a material level, the tissue itself was impaired as the disease progressed, ultimately leading to a reduced bone strength. The toughness represents the area under the stress-strain curve and no differences were found between strains at each age. It was demonstrated that diabetic rats showed a trend towards a decrease in toughness from 12- to 46-weeks of age (-25.5%) ($p = 0.08$), while there was no difference in toughness with age for controls. Additionally, a significant statistical interaction

between strain and age on bone toughness was found (15.75% of total variation, $p = 0.02$). A linear regression analysis was used to further explore the material strength by analysing ultimate modulus versus section modulus between strains at each age (see Appendix Figure S3.5). It was found that ultimate moment varies between strains at the various ages when section modulus is considered at 26 and 46-weeks. Control ($fa/+$) rats had a significantly higher material strength at 26- ($p < 0.05$) and 46-weeks ($p < 0.001$) in comparison to T2D (fa/fa) rats.

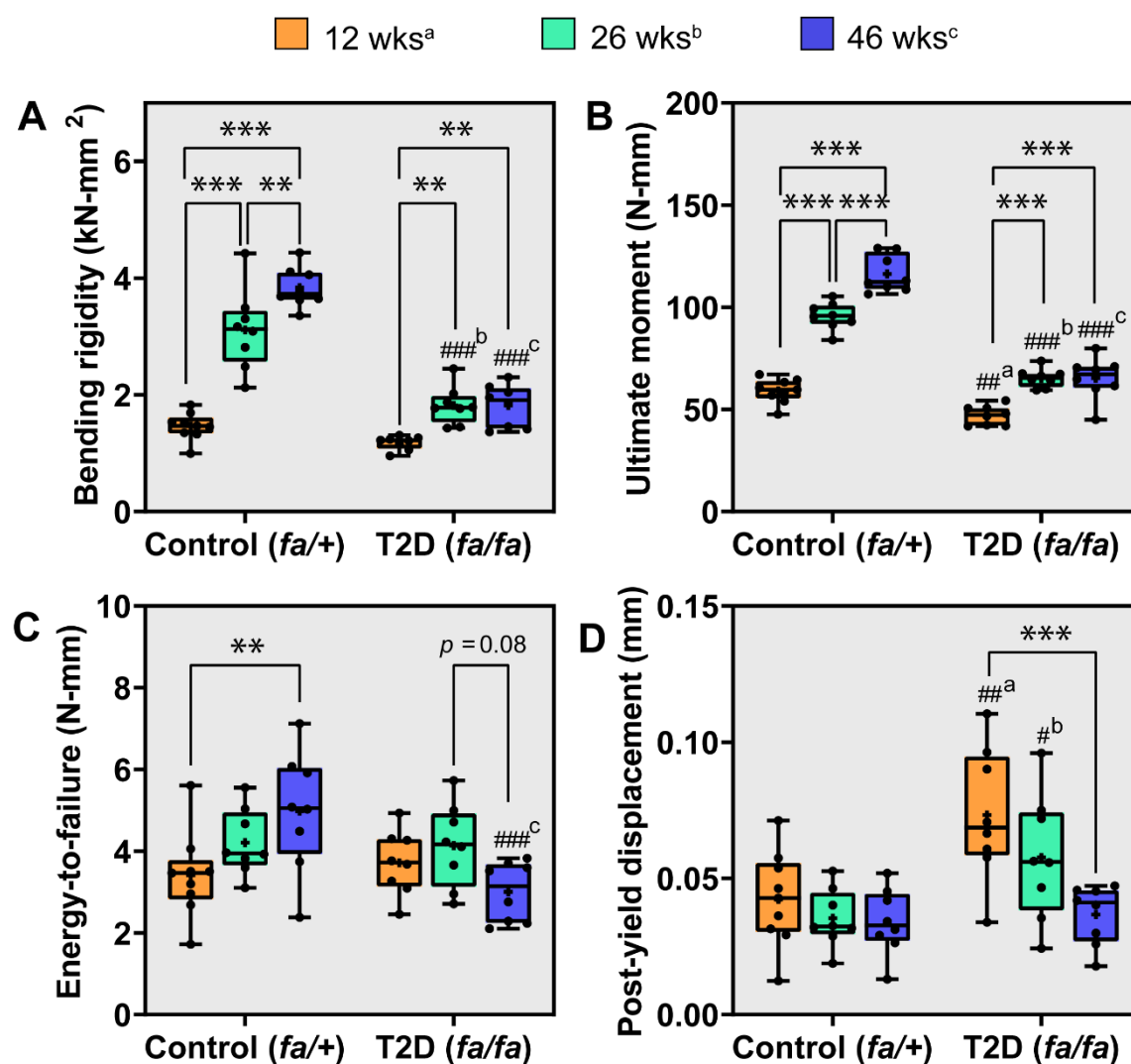


Figure 3.3: Structural properties (A) bending rigidity, (B) ultimate moment, (C) energy-to-failure and (D) post-yield displacement measured from loading cortical ulnar rat bone until failure in a three-point bend configuration. * ($p < 0.05$), ** ($p < 0.01$) and *** ($p < 0.001$) significance within strain, # ($p < 0.05$), ## ($p < 0.01$) and ### ($p < 0.001$) significance between strain at 12^a, 26^b, and 46^c weeks.

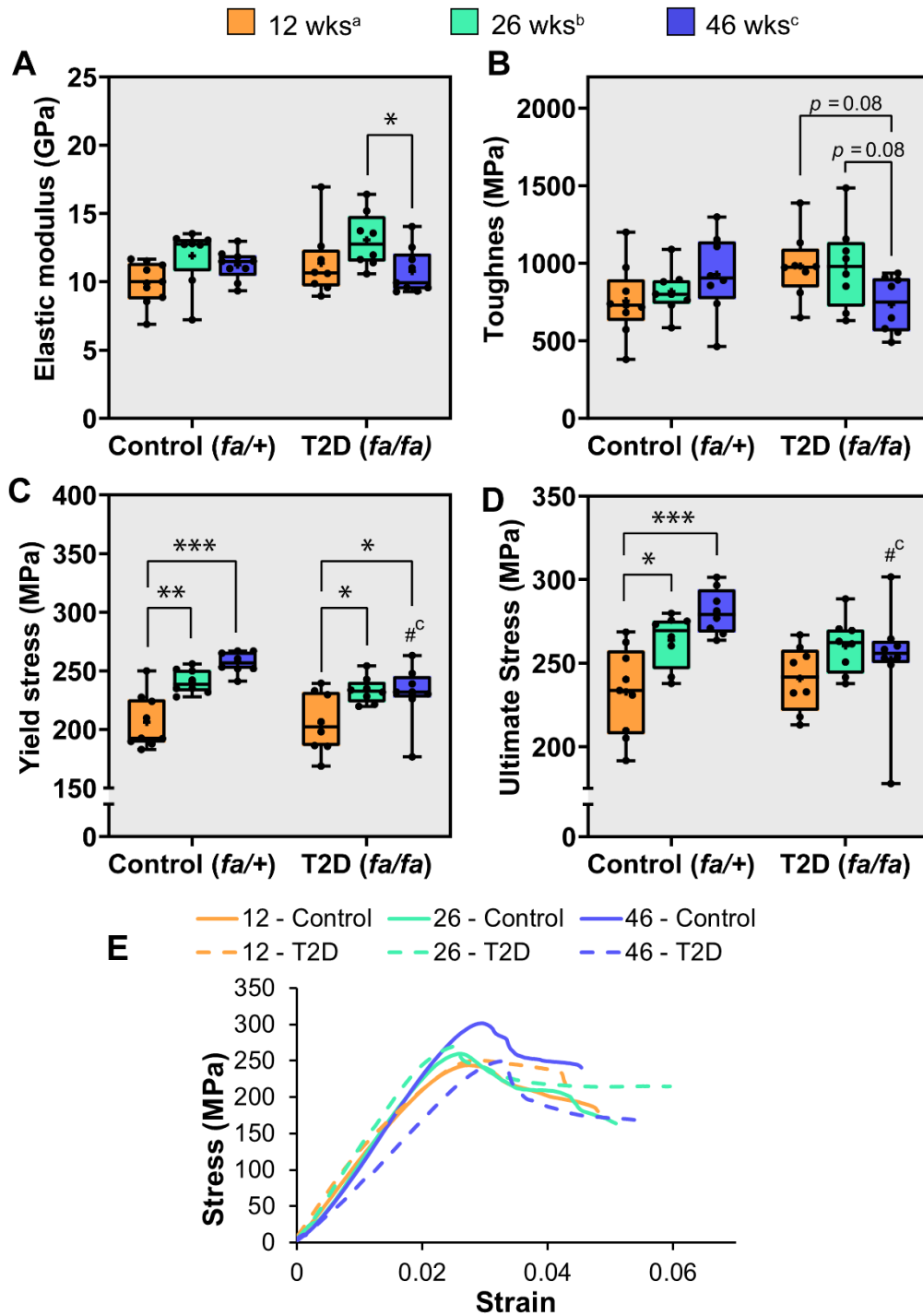


Figure 3.4. Material properties: (A) elastic modulus, (B) yield stress, (C) toughness and (D) ultimate stress measured from a three-point bend test considering bone geometry. (E) Sample stress-strain curves per group. * ($p < 0.05$), ** ($p < 0.01$) and *** ($p < 0.001$) significance within rat strains, # ($p < 0.05$), ## ($p < 0.01$) and ### ($p < 0.001$) significance between rat strains at 12^a, 26^b, and 46^c weeks.

3.4.3 Biochemical Analysis

Individual mineral constituents altered in long-term diabetic (fa/fa) rat bone

FTIR was used to assess bone quality by examining various mineral- and collagen-properties. Carbonate: phosphate ratio increased from 12- to 46-weeks of age for ZDF (*fa/fa*) rats (+12.5%, $p < 0.05$) and control (+25%, $p < 0.001$) rats (Figure 3.5 (B)). As the disease progressed, long-term diabetic rats had a 10% reduction in carbonate: phosphate ratio in comparison to age-matched controls ($p < 0.05$). Acid phosphate content reduced significantly from 12- to 26-weeks of age (-34%, $p < 0.05$) but there was no difference in acid phosphate content from 26- to 46-weeks. On average, ZDF (*fa/fa*) rats had 13% (95% CI: 4%, 21%, $p < 0.01$) and 10% (95% CI: 1%, 19%, $p < 0.05$) more acid phosphate content than controls at 12- and 46-weeks of age, respectively (Figure 3.5 (D)). There was no significant difference in mineral: matrix ratio, mineral crystallinity and collagen maturity between control and ZDF (*fa/fa*) rats at all ages (Table 3.2). However, collagen maturity exhibited a significant interaction on strain (Variation = 20.75%, $p = 0.002$).

Table 3.2. Compositional properties measured from ulnar cortical tissue obtained from rats as determined from Fourier transform-infrared spectroscopy (FTIR) analysis.

	Control (<i>fa/+</i>)			T2D (<i>fa/fa</i>)		
	12 weeks ^a (n = 8-9)	26 weeks ^b (n = 8)	46 weeks (n = 7-9)	12 weeks ^a (n = 8-9)	26 weeks ^b (n = 8)	46 weeks (n = 7-9)
Mineral: Matrix ratio	5.129 ± 0.94	4.83 ± 0.88	5.12 ± 0.86	5.68 ± 0.93	4.75 ± 0.86	5.40 ± 0.39
Carbonate: Phosphate ratio ⁺⁺	0.016 ± 0.0007	0.017 ± 0.002	0.020 ± 0.002 ^{a, b}	0.016 ± 0.0011	0.017 ± 0.001	0.018 ± 0.0005*
Mineral Crystallinity	0.94 ± 0.23	1.07 ± 0.23	1.26 ± 0.57	1.00 ± 0.27	1.22 ± 0.31	1.02 ± 0.21
Acid Phosphate Content ^{+, ++}	0.17 ± 0.06	0.15 ± 0.07	0.12 ± 0.06	0.29 ± 0.09**	0.19 ± 0.06 ^a	0.22 ± 0.06*
Collagen Maturity ⁺	2.79 ± 0.41	3.14 ± 0.82	3.41 ± 0.83	3.75 ± 0.72	4.00 ± 1.19	4.09 ± 1.11

Values are mean ± SD. T2D, Type-2 diabetic; Difference from aged matched lean control (*fa/+*) rats with * ($p < 0.05$), ** ($p < 0.01$) and *** ($p < 0.001$) significance. ^a significantly different from 12-weeks determined by a multiple comparisons Tukey test. ^b significantly different from 26-weeks determined by a multiple comparisons Tukey test. ⁺ Significant ANOVA interaction between strain. ⁺⁺ Significant ANOVA interaction between age.

3.4.4 Fluorescence Advanced Glycated End-Products (fAGE) Analysis

AGE accumulation increased in skin of long-term diabetic (fa/fa) rats but not bone

AGEs were measured from two tissue types: bone, to directly compare AGE-levels to the tissues' mechanical integrity and skin, to explore a surrogate marker of AGEs. Figure 3.5 shows diabetic (*fa/fa*) rats at 46-weeks of age had 2-fold ($p < 0.001$) more AGEs present in the skin than controls (Figure 3.5 (A)). There was no difference in the concentration of AGEs in the cortical bone between ZDF (*fa/fa*) and control rats at any age (Figure 3.5 (C)). Skin AGEs exhibited a significant interaction between strain and age (Variation = 10.51%, $p = 0.02$). Whereas bone AGEs only showed a trending interaction on age (Variation = 11%, $p = 0.07$).

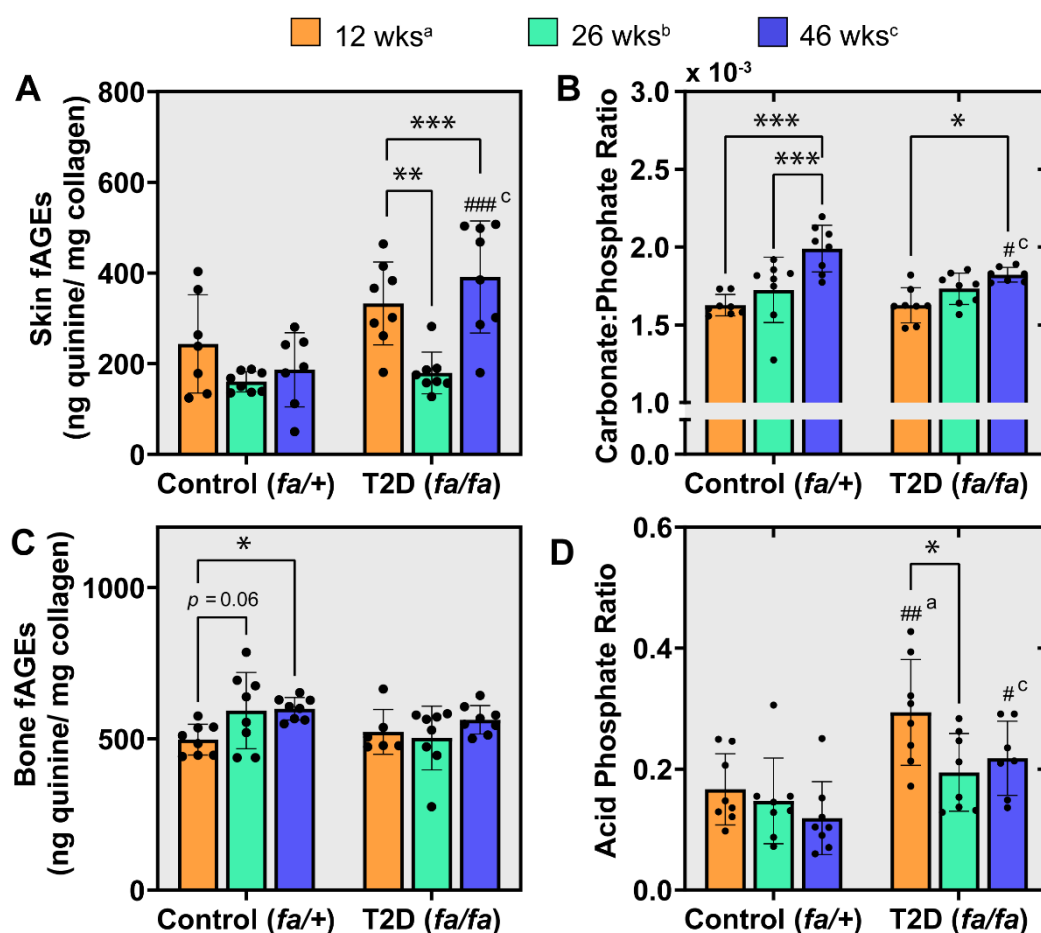


Figure 3.5. Various compositional results from (A, C) fAGE analysis of cortical bone and skin sections from rats and (B, D) FTIR analysis of cortical ulnar bone measuring carbonate:phosphate ratio and acid phosphate content. * ($p < 0.05$), ** ($p < 0.01$) and *** ($p < 0.001$) significance within rat strains, # ($p < 0.05$), ## ($p < 0.01$) and ### ($p < 0.001$) significance between rat strains at 12^a, 26^b, and 46^c weeks.

3.4.5 Correlation results among serum levels, skin and bone composition

All correlation results described in this Section are shown in Appendix Table S3.1. Mineral-properties measured via FTIR such as, carbonate: phosphate ratio and acid phosphate content were associated with serum glucose levels ($r = -0.33, p < 0.05$ and $r = 0.37, p < 0.05$, respectively). However, serum glucose levels and TMD showed no correlation. Fluorescent AGEs measured from skin and bone samples did not have a significant correlation with blood glucose levels. Interestingly, TMD and acid phosphate content were negatively correlated ($r = -0.46, p < 0.01$) (Appendix Table S3.1). TMD was also positively correlated with the mineral-property, carbonate: phosphate ratio ($r = 0.35, p < 0.01$) (Appendix Table S3.1). AGEs from bone tissue correlated positively with TMD (Bone $r = 0.33, p = 0.025$), yet skin AGEs did not (Appendix Table S3.1).

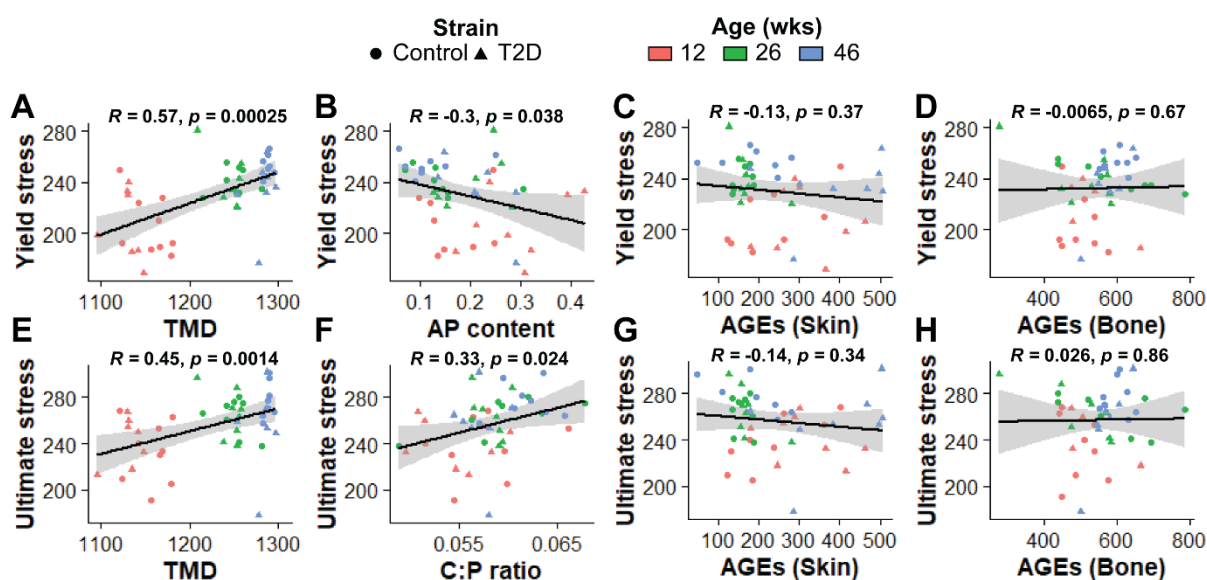


Figure 3.6. Correlation results showing the association of the material properties yield stress with (A) tissue mineral density (TMD), (B) acid phosphate (AP) content, (C) AGEs in rat skin and (D) AGEs in rat bone; and ultimate stress with (E) tissue mineral density (TMD), (F) Carbonate:phosphate ratio (C:P), (G) AGEs in rat skin and (H) AGEs in rat bone.

3.4.6 Correlation results for biomechanical properties

Correlation results shown in this Section were carried out to investigate if there was an association between AGEs and bone composition with the tissues mechanical integrity. Collagen maturity was positively associated with AGEs in the skin ($r = 0.33, p = 0.029$), but had no correlation with AGEs in bone (Appendix Table S3.1). Yield and ultimate stress were not associated with AGEs in skin (Yield stress: $r = -0.13, p = 0.37$; Ultimate stress: $r = -0.14, p = 0.34$), or bone (Yield stress: $r = 0.021, p = 0.89$; Ultimate stress: $r = 0.017, p = 0.92$) (Figure

3.6 (C) & (G)). Yield and ultimate stress were positively correlated with TMD (Figure 3.6 (A) & (E)) ($r = 0.57, p < 0.001$ and $r = 0.45, p < 0.01$). However, it is clear that age has an influence on this correlation where at 12-weeks lower TMD levels correlate with lower yield and ultimate stresses and as rat's age and bones get bigger, TMD levels have increased and correlate to higher yield and ultimate stresses. Interestingly, Yield stress was negatively correlated with acid phosphate content ($r = -0.3, p < 0.05$) Figure 3.6 (B)). Ultimate stress was positively associated with, the carbonate: phosphate ratio ($r = 0.33, p < 0.05$) (Figure 3.6 (F)). Both carbonate: phosphate ratio and acid phosphate content were properties associated with the mineral component of the bone tissue. Bones extracellular matrix is made up of an organic (collagenous and non-collagenous proteins) and inorganic (hydroxyapatite and other minerals) component which affects bones toughness and strength, respectively (An et al., 2016; Ma et al., 2022). This further explains the significant correlation between bone strength and the mineral properties measured via FTIR and lack of correlation with the non-collagenous AGEs.

3.5 Discussion

In this Chapter, it was shown that the accumulation of fluorescent AGEs was not the main contributing factor to bone fragility in long-term ZDF (*fa/fa*) rats and suggest that diabetic bone disease occurs through a multifactorial mechanism, possibly arising from an altered bone turnover process. For this, a factor-by-factor approach was used to investigate the (i) geometrical, (ii) structural, (iii) material and (iv) compositional properties of tissue in the presence of diabetes through a ZDF (*fa/fa*) rat model at different stages of the diseases: at 12- (Early-stage diabetes), 26- (Established diabetes) and 46-weeks (Long-term diabetes) old. To the authors' knowledge, this is the first ZDF (*fa/fa*) longitudinal animal study investigating long-term diabetic bone fragility in rats up to 46-weeks of age. This Chapter demonstrated that longitudinal diabetic bone growth was impaired as early as 12-weeks of age and by 46-weeks, bone size was significantly lower than healthy controls. The geometrical deficits were reflected in the structural properties. In particular, long-term (46-weeks) diabetic rats were structurally compromised with a lower bending rigidity and energy-to-failure than controls. Importantly, it was found that, independently of the structural deficits, the material tissue-level properties of T2D bone were impaired. Long-term diabetic rats had a significant reduction in yield and ultimate stress in comparison to their age-matched controls. Interestingly, post-yield displacement (structural property) and toughness (material property) was negatively affected by disease duration within the diabetic strain. Compositional differences were also found in long-term diabetic subjects, with higher AGE accumulation in skin samples in T2D subjects,

as mineral alterations observed through FTIR analysis, with a reduction in carbonate: phosphate ratio and an increase in acid phosphate content. Importantly, it was found that AGEs measured from both bone and skin sections had no correlation with tissue-level strength. Other distinct alterations such as carbonate: phosphate ratio and acid phosphate content were associated with tissue level strength.

Individuals with T2D have a greater risk of fracture than non-diabetic (Janghorbani et al., 2006) and it is understood that the duration of the disease plays a role in fracture risk (Creecy et al., 2016; Folk et al., 1999; Prisby et al., 2008; Retzepe and Donos, 2010). The effects of T2D on bone strength has been explored through various *in-vitro* (Catanese et al., 1999; Poundarik et al., 2015; Vashishth et al., 2001; Viguet-Carrin et al., 2008; Zimmermann et al., 2011) and *in-vivo* studies (Karim et al., 2018; Wölfel et al., 2020). However, T2D is a complex disease that *in-vitro* studies are not yet able to adequately mimic and there is limited availability of human tissue for testing and a large variability in intensity and length of the disorder, which implies a lack of quantitative tissue-level data on T2D bone for the same stage of the disease. This Chapter is a longitudinal investigation of bone fragility in ZDF (*fa/fa*) and control rats at 12- (Early-stage diabetes), 26- (Established diabetes) and 46-weeks (Long-term diabetes). To the investigator's knowledge, this is the first T2 diabetic longitudinal animal study aging ZDF (*fa/fa*) rats up to 46-weeks of age. Saito *et al.* (2006) explored bone fragility in diabetic WBN/Kob rats aged up to 72-weeks (18 months), however, this strain of diabetic rat becomes spontaneously diabetic between 48- to 52-weeks of age, meaning these rats were only diabetic for approximately 24- to 28-weeks. However, in this Chapter, these ZDF (*fa/fa*) rats become spontaneously diabetic between 9-to 11-weeks old, meaning these rats were overtly diabetic for approximately 35- to 37-weeks. These results have shown that, ZDF (*fa/fa*) rats experienced a reduction in bone strength in comparison to controls and that disease duration played a role in this. Moreover, post-yield displacement results demonstrated that long-term diabetic rats had reduced ductility in comparison to younger diabetic rats. This highlights that, as the disease progressed, long-term diabetic bones fractured in a more brittle manner than short-term diabetic bones. No difference in post-yield displacement between strains at 46-weeks was seen. However, in comparison to controls, diabetic rats had a reduced ability to resist deformation due to deficits in bending rigidity, a reduced ability to resist fracture due to reduced energy-to-failure and could not withstand as high a load due to lower ultimate moments. This is similar to what has been previously reported in work by Prisby *et al.* (2008) where ZDF (*fa/fa*) (T2D) rats showed no changes in post-yield displacement but did see differences in the

energy-to-failure. Similarly, work by Creecy *et al.* (2016), which used ZDSR rats, found no difference in post-yield displacement between strains at any age but did find differences in Energy-to-failure of radius bone at all ages. Nevertheless, the negative effects on the structural properties of the diabetic rats in this Chapter can, for the most part, be attributed to the geometrical deficits of these ZDF (*fa/fa*) diabetic rats. This is further shown by the IGF-I levels of the diabetic rats which indicates the dysfunction of their bone growth. The short bone phenotype has also been reported in other studies that have used the ZDF (*fa/fa*) strain as their T2D subjects, where the smaller sized bones have been proposed as a phenotype of the ZDF (*fa/fa*) strain (Prisby *et al.*, 2008; Reinwald *et al.*, 2009).

Despite the variety of animal studies that have investigated the fracture mechanics of T2 diabetic bone (Devlin *et al.*, 2014; Hamann *et al.*, 2014; Reinwald *et al.*, 2009; Sihota *et al.*, 2020a), few studies have explored tissue material properties and often bones with a less favourable geometry for bending or measuring tissue properties are examined, according to their aspect ratio (span length: bone width). Where Jepsen *et al.* (2015) states that using a slender bone such as the radius, can increase the aspect ratio leading to a more accurate estimation of the elastic modulus. Similarly, the ulnar is also considered a slender bone. Importantly, this study highlighted that both structural- and tissue-level properties of ZDF (*fa/fa*) rats were impaired. Indeed, rats with long-term (46-weeks) T2D showed a reduction in tissue yield and ultimate stress. Although the elastic modulus of T2 diabetic bone tended towards being lower than controls, this was not significant due to greater variability which is expected in *in vivo* studies. This is similar to a previous study, which found no differences in modulus of elasticity but did find reductions in bone strength between T2D rats and controls (Prisby *et al.*, 2008). This may also be due to the significant difference in aspect ratio between diabetic and controls at 46-weeks due to significant difference in bone length growth. However, some studies did not go as far as to measure the material-properties following a structural analysis (Devlin *et al.*, 2014a; Saito *et al.*, 2006; Sihota *et al.*, 2020a). Several other studies have found some material level differences, whereby yield and/or ultimate strength of diabetic ulnar (Acevedo *et al.*, 2018) or vertebral (Gallant *et al.*, 2013; Reinwald *et al.*, 2009) bone was found to be lower than their healthy counterparts. The results from this Chapter reveal that as the disease progressed the tissue itself, regardless of bone geometry, became impaired with reductions in bone strength observed.

A novel contribution of this study is that tissue composition was measured through FTIR and fAGE analysis at 12-, 26- and 46-weeks. The extent to which bone quality may be affected

during T2D is not fully understood and there is a lack of understanding of the sub-tissue alterations that take place during T2D. This Chapter demonstrated that in long-term (46-weeks) ZDF (*fa/fa*) rats, skin AGE concentration was higher than controls, but there was no difference in cortical bone AGE levels between strains at any age. Studies have suggested that elevated levels of non-enzymatic glycated cross-links leads to a deterioration in tissue properties (Karim et al., 2018; Saito et al., 2006). However, to date, there is still no causal relationship between AGE accumulation and T2D, since previous work measuring bulk fAGEs have shown that diabetic subjects have higher (Acevedo et al., 2018; LLabre et al., 2022; Sihota et al., 2020a; Tice et al., 2022) or unchanged levels (Creedy et al., 2016; Devlin et al., 2014a; Karim et al., 2018; Wölfel et al., 2020b) in comparison to controls. Indeed, increased blood glucose levels can interfere with bone homeostasis (Ogawa et al., 2007; Picke et al., 2019; Tanaka et al., 2015). Recent work by Entz *et al.* (2022) found that when the extracellular matrix was produced by human bone marrow adipocytes osteoblastogenesis was not affected, but disruption to the mineralisation phase of osteoblasts was observed. Furthermore, when a high glucose environment was introduced they found differential alterations in mineralisation quality (Entz et al., 2022).

Interestingly, through FTIR analysis it was demonstrated that some mineral constituents at the sub-tissue level, such as carbonate: phosphate ratio and acid phosphate content, were altered as a result of some possible metabolic impairment due to the hyperglycaemic environment. Both carbonate (CO_3^{2-}) and acid phosphate (HPO_4^{2-}) are the main ions that substitute into the apatite mineral lattice during the modelling and remodelling of bone. However, it is important to note that rodent cortical bone does not remodel in the same way human bone would remodel due to their lack of a well-developed Haversian system like humans. Instead, it is thought that rat bones continue to grow in their outer cortex and the marrow side continues to be resorbed throughout life. Conversely, there has been some evidence to suggest that rodent bone may also be remodelled on intracortical surfaces after maturation, since it is highly vascularised with transcortical vessels containing both osteoclast and osteoblast progenitors (Grüneboom et al., 2019; Isojima and Sims, 2021; Root et al., 2020; Walker et al., 2020), similar to how Haversian systems continue to be remodelled, with intracortical blood vessels in human bone during adulthood (Enlow, 1985; Sims and Martin, 2020). Both properties were associated with tissue strength across both groups. Long-term diabetic rats had a 10% ($p < 0.05$) reduction in carbonate: phosphate ratio in comparison to controls. Interestingly, previous studies have found that a reduction in carbonate: phosphate ratio has been linked to an increased risk of fracture

(McCreadie et al., 2006) as well as an accumulation of bone micro-damage (Ruppel et al., 2006). In addition, a reduced carbonate: phosphate ratio has also been seen in patients presenting with low or high bone turnover (Isaksson et al., 2010; Malluche et al., 2012) and in fact may convey a lack in type-B carbonate substitutions and thus resulting in a lack of bone maturation during the mineralisation process (Velraj et al., 2020). Long-term diabetic bone had 10% (95% CI: 1%, 19%, $p < 0.05$) more acid phosphate content than controls. Acid phosphate content is usually present at high concentrations in young, immature bone, which explains the elevated levels of AP content in 12-week old rats while the young bones are still modelling (Gadaleta et al., 1996; Huang et al., 2002). However, higher levels of acid phosphate content in 12-week T2D rats than controls may indicate that bone modelling was altered in early stages of bone growth and development. By 46-weeks it is possible that a high acid phosphate content may be indicating that secondary mineralisation is not proceeding correctly suggesting bone turnover is also affected (Sai et al., 2018; Spevak et al., 2013). Considering that a low carbonate: phosphate ratio could indicate a lack of bone maturation, the latter argument is supported in this data from the 46-week old diabetic rats with a long-term exposure to a high glucose environment. This may also suggest further secondary health complications that might be affecting the bone turnover process such as, chronic renal dysregulation, kidney disease, reduced bone vascularisation or metabolic acidosis, which should be explored further in future studies. Therefore, this Chapter indicates that AGE accumulation is not a main contributing factor to bone fragility in these ZDF (*fa/fa*) rats. Instead, results from the FTIR analysis indicates that the impaired mechanical integrity of the bone tissue is a multifactorial mechanism influenced by an altered bone turnover process that reduces bone quality and impairs biomechanical properties as the disease progresses.

The basic building block of the ordered material, bone, majorly consists of mineralised collagen fibrils, which are found at the nanoscale. These mineralised organic collagen fibrils are composed of hydroxyapatite mineral crystals and non-collagenous proteins, representing the reinforcement and compliant matrix phase, respectively (Ascenzi and Bonucci, 1976; Currey, 1984; Hofmann et al., 2006). These hydroxyapatite mineral crystals and collagen fibrils give bone its stiffness, strength and ductility, respectively, during loading. The correlation results reveal that the mineral properties were altered, with a reduction in carbonate: phosphate ratio and increase in acid phosphate content in long-term diabetic rats which may play a role in reducing the ultimate strength and yield strength of the bone tissue, respectively. Hence, it can be hypothesised that the weakness of the long-term diabetic bone in these ZDF (*fa/fa*) rats is

related to the mineralisation process, whereby the apatite lattice structure is distorted or not maturing into stable hydroxyapatite. It is worth noting that the disruption of the mineral properties occurs in long-term diabetic rats after a prolonged duration with the disease where the rats have not been administered any insulin, medications or a diet or lifestyle change; it is unlikely for patients with long-term T2D to never have some form of intervention throughout the duration of their disease.

There are several limitations and future recommendations that should be noted. The ZDF (*fa/fa*) rat model has a leptin receptor deficiency due to an amino acid substitution, which has been observed in children that possess congenital leptin receptor deficiencies (Fajardo et al., 2014; Farooqi et al., 2007). As a result, these rats experience an insatiable appetite, causing them to become overtly diabetic and obese at approximately 9-weeks of age (Fajardo et al., 2014). These rats reach skeletal maturity when they are around 12-weeks old, at which point they also develop a frank-like diabetic condition (Reinwald et al., 2009). In this Chapter, the high fat diet was started at approximately 10-weeks of age, before these rats reached skeletal maturity. It is thought that loss of function of their leptin-receptors may influence the bone size. However, it is also likely that the early onset of T2D before they reached puberty may have influenced their longitudinal stunt in growth. Although there is currently no single animal model that represents all features of T2D in humans; with a rise in the incidence of T2D in children and adolescents in the United States, Australia, China, Canada and United Kingdom (Candler et al., 2018; Divers et al., 2002; Haynes et al., 2016; Slater et al., 2019; Tung et al., 2022; Wu et al., 2022) and a great lack of data that explores the ramifications of long-term diabetes in patients with youth-onset type-2 diabetes (Y. Fan et al., 2022), it is possible that this ZDF (*fa/fa*) strain may be a suitable animal model to mimic the progression of T2D when developed during childhood or adolescence. Especially since the exact time-point of the onset of diabetes in this strain is known. Additionally, this model is also representative of the small, but still existent, population of humans that develop T2D as a result of a leptin or leptin receptor deficiency (DePaoli, 2014).

In addition, at approximately 44-weeks of age diabetic rats began to lose body mass, due to a loss of appetite and/ or a worsening of their illness. This loss in weight has been observed in both ZDF (*fa/fa*) and ZDSD rats (Creecy et al., 2016; Prisby et al., 2008; Reinwald et al., 2009) with disease progression and may be a limitation of these rat strains in modelling long-term diabetes without some form of intervention (e.g. insulin or medications). However, a similar study has not found body mass to be a significant explanatory variable for bending strength (Creecy et al., 2016) although it may present as a possible confounding effect. In this Chapter,

diabetic rats were switched from a high fat diet to a normal diet to help to mitigate their illness at approximately 42-weeks. Hence, at 46-weeks diabetic rats have lower blood-glucose levels than diabetic rats at 26-weeks, but this may be due to their loss of appetite. Nonetheless, diabetic rats at 46-weeks still have higher blood glucose levels in comparison to the age-matched controls. Interestingly, previous research has found accumulating evidence to suggest that a disruption of insulin and the growth hormone IGF-I homeostasis in diabetic subjects may be responsible for skeletal deficits (Fowlkes et al., 2008) and increased vertebral fracture risk (Sugimoto et al., 1997; Yamaguchi et al., 2006). In this Chapter, at 12- and 26-weeks controls demonstrated a trend towards and significantly higher serum IGF-I levels than age-matched diabetic rats, respectively. As growth and development slowed with age, IGF-I levels decreased for 46-weeks old controls. However, the levels of IGF-I remained low for diabetic rats, leading to a possible explanation for the stunt in growth for these ZDF (*fa/fa*) rats. Studies have also shown that high glucose concentrations or the presence of AGEs impair the stimulatory actions of IGF-I on osteoblasts (McCarthy et al., 2001b; Terada et al., 1998). Previous research investigating childhood obesity and T2D, found that during puberty IGF-I levels rose and fell in a pattern similar to the rise and fall of insulin resistance, suggesting that the growth hormone IGF-I axis contributes to the insulin resistance of puberty (Hannon et al., 2005). Thus, it may be useful for future studies to explore serum IGF-I levels in patients with T2D, to help understand bone growth, development and fragility in this disease. Additionally, results from this Chapter do not reflect the clear increase in bulk fAGEs with disease progression, as was seen in previous work on human bone (Dyer et al., 1993; Karim et al., 2013). Nor is a similar trend of results seen from surrogate measurements of AGE levels taken from the skin when compared to bone. This may be explained by the fact that the fAGE technique is a bulk measurement for AGEs, including pentosidine, crossline and vesperlysines A, B & C to name a few. However, the extent of how quantifiable each AGE is through this fluorescent assay is unknown and some AGEs are better correlated with bone than others, such as the non-fluorescent AGE, carboxymethyl-lysine (CML) (Thomas et al., 2018). Future work should explore different techniques such as high-performance liquid chromatography (HPLC) and mass spectrometry to quantify individual AGEs, in particular CML and pentosidine, rather than a bulk fAGE approach. A final limitation, is that when preparing the bone powder samples for ATR-FTIR the samples were left to dry overnight in air at 37°C. It is possible that exposing these samples to air for a long period of time could potentially allow the collagen to become oxidised and denatured. In future it might be better to reduce drying time or temperature when trying to remove water from the samples. Nevertheless, all samples underwent the same

preparation and therefore are comparable in this study. Additionally, it may be important to note that if samples to be used for FTIR analysis were stored in PBS this may affect the FTIR spectra. However, in this Chapter samples were not immersed in PBS, they were surrounded by gauze with PBS and immediately frozen before mechanical testing. Since the samples were immediately frozen it is unlikely the PBS would have greatly permeated into the bone tissue.

3.6 Concluding Remarks

This Chapter found that long-term ZDF (*fa/fa*) rats had a reduced tissue-level yield and ultimate strength in comparison to controls, regardless of the geometrical deficits of this rat strain. The reduced tissue material strength coincided with the mineral properties carbonate: phosphate ratio and acid phosphate content but was not associated with AGE content. This indicates that bone fragility in these ZDF (*fa/fa*) rats occurs through a multifactorial mechanism influenced initially by impaired bone growth and development and proceeding to an altered bone turnover process that reduces bone quality and impairs biomechanical properties with a long-term duration of the disease. However, further work is required to uncover these contributing factors.

Appendix 3.1

Details of animal study

Figure S3.1 shows a detailed timeline of the animal study from when animals arrived to when the high fat diet (HFD) began and endpoints for each age group. This Figure also details when animals from a specific cohort died due to illness in control ($fa/+$) and Zucker Diabetic Fatty (ZDF) (fa/fa) rats.

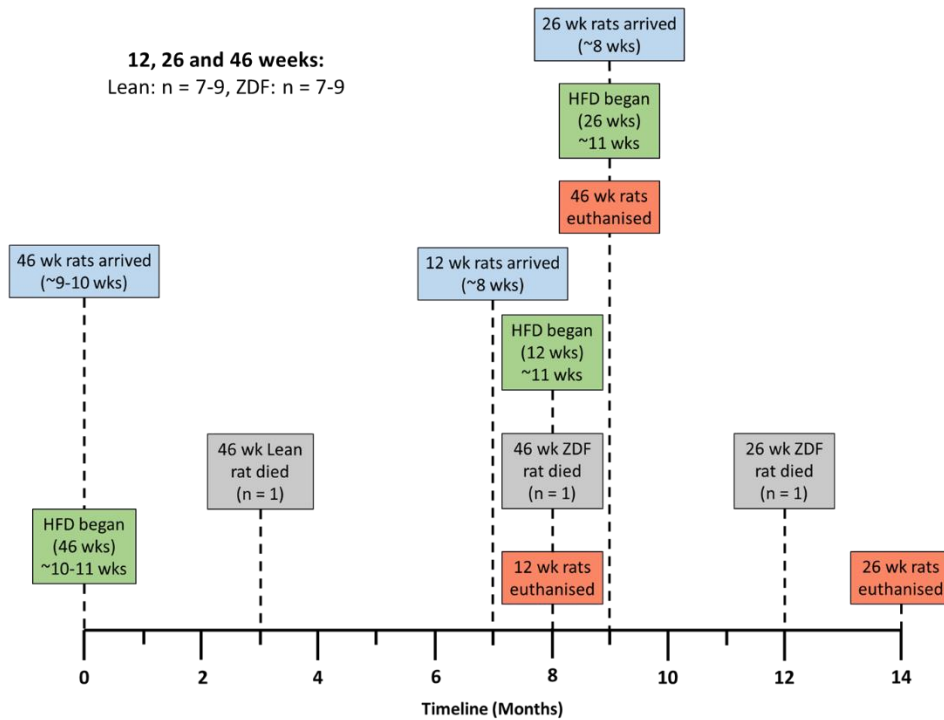


Figure S3.1. Timeline of the animal study over a 14-month period.

Body mass loss of 46-week cohort with long-term diabetes

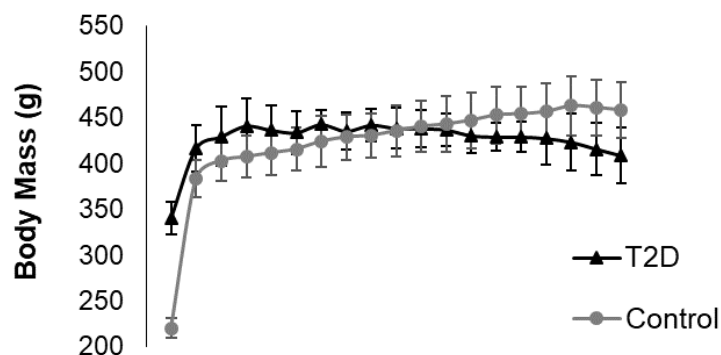


Figure S3.2. Evidence of weight loss as the disease progressed in long-term (46-week old) diabetic (fa/fa) rats in comparison to aging controls. Weight loss began at approximately 34 wks.

Table S3.1. Correlations for data from T2D (*fa/fa*) and control (*fa/+*) rats at all ages pooled. Significant correlations are written in bold.

Parameter	AGEs bone	Ultimate Stress	Yield Stress	C:P ratio	AP content	CM	TMD	Blood glucose
AGEs skin	-0.032 (ns)	-0.14 (ns)	-0.13 (ns)	-0.2 (ns)	0.26 (<i>p</i> = 0.08)	0.33 (<i>p</i> = 0.029)	-0.12 (ns)	0.17 (ns)
AGEs bone	-	0.017 (ns)	0.021 (ns)	0.17 (ns)	-0.18 (ns)	0.15 (ns)	0.33 (<i>p</i> = 0.025)	-0.15 (ns)
MC	0.063 (ns)	0.17 (ns)	0.21 (ns)	0.2 (ns)	-0.23 (ns)	-0.16 (ns)	0.2 (ns)	-0.013 (ns)
Min:Mat	-0.13 (ns)	-0.075 (ns)	-0.044 (ns)	-0.36 (<i>p</i> = 0.012)	0.037 (ns)	0.19 (ns)	-0.2 (ns)	0.12 (ns)
C:P ratio	0.17 (ns)	0.33 (<i>p</i> = 0.024)	0.24 (<i>p</i> = 0.1)	-	-0.35 (<i>p</i> = 0.017)	-0.23 (ns)	0.35 (<i>p</i> = 0.017)	-0.33 (<i>p</i> = 0.027)
AP content	-0.18 (ns)	-0.19 (ns)	-0.3 (<i>p</i> = 0.038)	-	-	0.08 (ns)	-0.46 (<i>p</i> = 0.0016)	0.37 (<i>p</i> = 0.012)
CM	0.15 (ns)	0.057 (ns)	0.098 (ns)	-	-	-	0.032 (ns)	0.33 (<i>p</i> = 0.025)
TMD	-	0.45 (<i>p</i> = 0.0014)	0.57 (<i>p</i> = 0.00025)	-	-	-	-	-0.12 (ns)
Blood glucose	-	-0.1 (ns)	-0.13 (ns)	-	-	-	-	-

Values are R-value (*p*-value), ns = *p*-value > 0.1, MC, Mineral Crystallinity; Min:Mat, Mineral: Matrix ratio; C:P ratio, Carbonate: Phosphate ratio; AP content, Acid Phosphate content; CM, Collagen Maturity; TMD, Tissue Mineral Density; AGEs, Advanced Glycated End-products.

Appendix 3.2

Linear regression analysis of ultimate moment vs. section modulus (I_{ml}/C_{ml}) between type-2 diabetic (fa/fa) and Control ($fa/+$) rats

In addition to reporting the estimated material properties, such as ultimate stress, shown in Figure 3.4, a linear regression analysis was also performed to see if the slope and intercept term of ultimate moment and the section modulus (I_{ml}/C_{ml}) varies between control ($fa/+$) and diabetic (fa/fa) rats at the various ages. The scatter plot in Figure S3.3 shows the linearity of each strain and in Figure S3.4, each strain is split up into age-groups to assess the linearity.

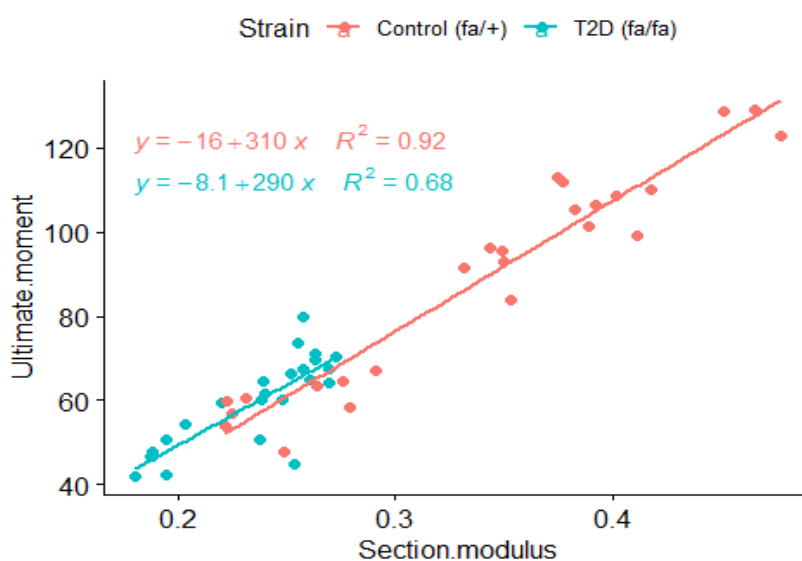


Figure S3.3. Scatter plot of ultimate moment vs. section modulus for control ($fa/+$) and T2D (fa/fa) rats to assess the linearity. All ages are represented within each strain in this plot. Slope and R-squared values for each strain are shown.

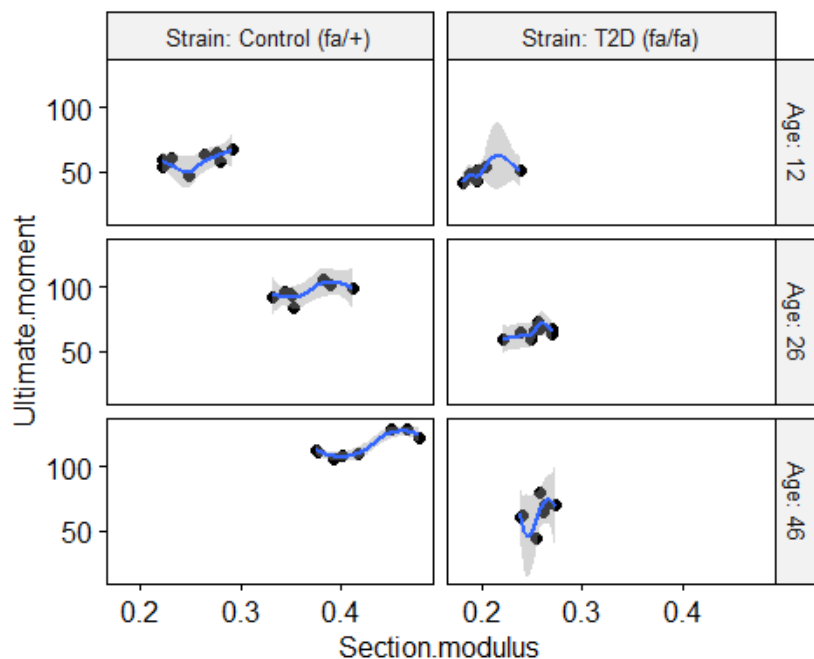


Figure S3.4. Scatter plot of ultimate moment vs. section modulus for Control (*fa/+*) and T2D (*fa/fa*) rats faceted by age to assess linearity.

A Type-II ANOVA test was carried out using R statistical software (version R-4.1.0) to investigate the interactions between the independent variables, strain and age, on ultimate modulus when section modulus was considered. After adjusting for section modulus, there was a significant interaction between Strain and Age on Ultimate moment, $F(2, 42) = 7.13$, $p = 0.002$. A pairwise comparisons test was then carried out using an Emmeans tests to estimate the marginal means and p-values were adjusted using a Bonferroni test. Alpha levels of $p \leq 0.05$ were considered significant for a 95% confidence interval. These results investigate the influence of section modulus and strain on ultimate moment between Controls (*fa/+*) and diabetic (*fa/fa*) groups. The pairwise comparisons between Controls (*fa/+*) and diabetic (*fa/fa*) groups was statistically significant in rats at 26- and 46-weeks of age ($p < 0.05$, $p < 0.001$, respectively). However, there was no significant interaction between strains on ultimate moment at 12-weeks of age ($p = 0.39$) (see Figure S3.5).

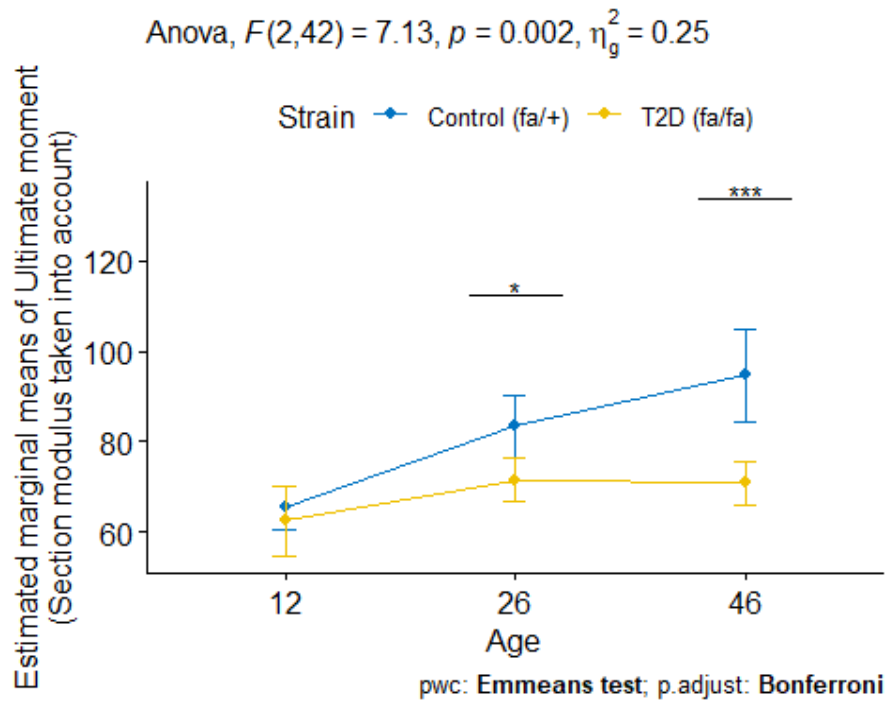


Figure S3.5. Line plot used to show how the estimated marginal means of ultimate moment varies between strains at the various ages when section modulus is considered. This graph displays * ($p < 0.05$), ** ($p < 0.01$), *** ($p < 0.001$) significance and the interaction between strain and age is displayed at the top of the graph.

3.7 References

- Acevedo, C., Sylvia, M., Schaible, E., Graham, J.L., Stanhope, K.L., Metz, L.N., Gludovatz, B., Schwartz, A. V., Ritchie, R.O., Alliston, T.N., Havel, P.J., Fields, A.J., 2018. Contributions of Material Properties and Structure to Increased Bone Fragility for a Given Bone Mass in the UCD-T2DM Rat Model of Type 2 Diabetes. *J. Bone Miner. Res.* 33, 1066–1075. <https://doi.org/10.1002/jbmr.3393>
- An, J., Leeuwenburgh, S., Wolke, J., Jansen, J., 2016. Mineralization Processes in Hard Tissue: Bone. *Biominer. Biomater. Fundam. Appl.* 129–146. <https://doi.org/10.1016/B978-1-78242-338-6.00005-3>
- Ascenzi, A., Bonucci, E., 1976. Relationship between ultrastructure and “pin test” in osteons. *Clin. Orthop. Relat. Res.* 275–94.
- Beasley, M.M., Bartelink, E.J., Taylor, L., Miller, R.M., 2014. Comparison of transmission FTIR, ATR, and DRIFT spectra: Implications for assessment of bone bioapatite diagenesis. *J. Archaeol. Sci.* 46, 16–22. <https://doi.org/10.1016/j.jas.2014.03.008>
- Boskey, A.L., Donnelly, E., Boskey, E., Spevak, L., Ma, Y., Zhang, W., Lappe, J., Recker, R.R., 2016. Examining the Relationships Between Bone Tissue Composition, Compositional Heterogeneity, and Fragility Fracture: A Matched Case-Controlled FTIRI Study. *J. Bone Miner. Res.* 31, 1070–1081. <https://doi.org/10.1002/jbmr.2759>
- Boskey, A.L., Imbert, L., 2017. Bone quality changes associated with aging and disease: a review. *Ann. N. Y. Acad. Sci.* 1410, 93–106. <https://doi.org/10.1111/nyas.13572>
- Boskey, A.L., Mendelsohn, R., 2005. Infrared analysis of bone in health and disease. *J. Biomed. Opt.* 10, 031102. <https://doi.org/10.1117/1.1922927>
- Boskey, A.L., Pleshkocamacho, N., 2007. FT-IR imaging of native and tissue-engineered bone and cartilage. *Biomaterials* 28, 2465–2478. <https://doi.org/10.1016/j.biomaterials.2006.11.043>
- Bouxsein, M.L., Boyd, S.K., Christiansen, B.A., Guldberg, R.E., Jepsen, K.J., Müller, R., 2010. Guidelines for assessment of bone microstructure in rodents using micro-computed tomography. *J. Bone Miner. Res.* 25, 1468–1486. <https://doi.org/10.1002/jbmr.141>
- Candler, T.P., Mahmoud, O., Lynn, R.M., Majbar, A.A., Barrett, T.G., Shield, J.P.H., 2018. Continuing rise of Type 2 diabetes incidence in children and young people in the UK.

- Diabet. Med. 35, 737–744. <https://doi.org/10.1111/dme.13609>
- Catanese, J., Bank, R., TeKoepple, J., Keaveny, T., 1999. Increased cross-linking by non-enzymatic glycation reduces the ductility of bone and bone collagen. *ASME-PUBLICATIONS-BED* 42, 267--268.
- Chen, H., Charlat, O., Tartaglia, L.A., Woolf, E.A., Weng, X., Ellis, S.J., Lakey, N.D., Culpepper, J., More, K.J., Breitbart, R.E., Duyk, G.M., Tepper, R.I., Morgenstern, J.P., 1996. Evidence That the Diabetes Gene Encodes the Leptin Receptor: Identification of a Mutation in the Leptin Receptor Gene in db/db Mice. *Cell* 84, 491–495. [https://doi.org/10.1016/S0092-8674\(00\)81294-5](https://doi.org/10.1016/S0092-8674(00)81294-5)
- Creecy, A., Uppuganti, S., Merkel, A.R., O’Neal, D., Makowski, A.J., Granke, M., Voziyan, P., Nyman, J.S., 2016. Changes in the Fracture Resistance of Bone with the Progression of Type 2 Diabetes in the ZDSD Rat. *Calcif. Tissue Int.* 99, 289–301. <https://doi.org/10.1007/s00223-016-0149-z>
- Currey, J.D., 1984. Effects of differences in mineralization on the mechanical properties of bone. *Philos. Trans. R. Soc. Lond. B. Biol. Sci.* 304, 509–518. <https://doi.org/10.1098/rstb.1984.0042>
- DePaoli, A.M., 2014. Leptin in common obesity and associated disorders of metabolism. *J. Endocrinol.* 223, T71–T81. <https://doi.org/10.1530/JOE-14-0258>
- Devlin, Van Vliet, M., Motyl, K., Karim, L., Brooks, D.J., Louis, L., Conlon, C., Rosen, C.J., Bouxsein, M.L., 2014. Early-onset type 2 diabetes impairs skeletal acquisition in the male TALLYHO/JngJ mouse. *Endocrinol. (United States)* 155, 3806–3816. <https://doi.org/10.1210/en.2014-1041>
- Dhaliwal, R., Cibula, D., Ghosh, C., Weinstock, R.S., Moses, A.M., 2014. Bone quality assessment in type 2 diabetes mellitus. *Osteoporos. Int.* 25, 1969–1973. <https://doi.org/10.1007/s00198-014-2704-7>
- Divers, J., Mayer-Davis, E.J., Lawrence, J., Isom, S., Dabelea, D., Dolan, L., Imperatore, G., Marcovina, S., David, P.J., Pihoker, C., Hamman, R.F., Saydah, S., Wagenknecht, L.E., 2002. Morbidity and Mortality Weekly Report Trends in Incidence of Type 1 and Type 2 Diabetes Among Youths-Selected Counties and Indian Reservations, United States, 2002-2015 69, 161–165.

- Dyer, D.G., Dunn, J.A., Thorpe, S.R., Bailie, K.E., Lyons, T.J., Mccance, D.R., Baynes, J.W., 1993. Accumulation of Maillard Reaction Products in Skin Collagen in Diabetes and Aging *CH20H* 91, 2463–2469.
- Enlow, D.H., 1985. A Study of the Post-Natal Growth and Remodeling of Bone 80, 270–278.
- Entz, L., Falgayrac, G., Chauveau, C., Pasquier, G., Lucas, S., 2022. The extracellular matrix of human bone marrow adipocytes and glucose concentration differentially alter mineralization quality without impairing osteoblastogenesis. *Bone Reports* 17, 101622. <https://doi.org/10.1016/j.bonr.2022.101622>
- Etgen, G.J., Oldham, B.A., 2000. Profiling of Zucker diabetic fatty rats in their progression to the overt diabetic state. *Metabolism*. 49, 684–688. [https://doi.org/10.1016/S0026-0495\(00\)80049-9](https://doi.org/10.1016/S0026-0495(00)80049-9)
- Fajardo, R.J., Karim, L., Calley, V.I., Bouxsein, M.L., 2014. A Review of Rodent Models of Type 2 Diabetic Skeletal Fragility. *J. Bone Miner. Res.* 29, 1025–1040. <https://doi.org/10.1002/jbmr.2210>
- Fan, Y., S.H Lau, E., Wu, H., Yang, A., Chow, E., So, W.-Y., P.S Kong, A., C.W Ma, R., C.N Chan, J., O.Y Luk, A., 2022. Incidence of long-term diabetes complications and mortality in youth-onset type 2 diabetes: a systematic review. *Diabetes Res. Clin. Pract.* 191, 110030. <https://doi.org/10.1016/j.diabres.2022.110030>
- Farlay, D., Panczer, G., Rey, C., Delmas, P.D., Boivin, G., 2010. Mineral maturity and crystallinity index are distinct characteristics of bone mineral. *J. Bone Miner. Metab.* 28, 433–445. <https://doi.org/10.1007/s00774-009-0146-7>
- Farooqi, I.S., Wangensteen, T., Collins, S., Kimber, W., Matarese, G., Keogh, J.M., Lank, E., Bottomley, B., Lopez-Fernandez, J., Ferraz-Amaro, I., Dattani, M.T., Ercan, O., Myhre, A.G., Retterstol, L., Stanhope, R., Edge, J.A., McKenzie, S., Lessan, N., Ghodsi, M., De Rosa, V., Perna, F., Fontana, S., Barroso, I., Undlien, D.E., O’Rahilly, S., 2007. Clinical and Molecular Genetic Spectrum of Congenital Deficiency of the Leptin Receptor. *N. Engl. J. Med.* 356, 237–247. <https://doi.org/10.1056/NEJMoa063988>
- Farr, J.N., Drake, M.T., Amin, S., Melton, L.J., McCready, L.K., Khosla, S., 2014. In Vivo Assessment of Bone Quality in Postmenopausal Women With Type 2 Diabetes. *J. Bone Miner. Res.* 29, 787–795. <https://doi.org/10.1002/jbmr.2106>

- Folk, J.W., Starr, A.J., Early, J.S., 1999. Early Wound Complications of Operative Treatment of Calcaneus Fractures: Analysis of 190 Fractures. *J. Orthop. Trauma* 13, 369–372.
- Fowlkes, J.L., Bunn, R.C., Thrailkill, K.M., 2008. Contributions of the Insulin/Insulin-Like Growth Factor-1 Axis to Diabetic Osteopathy. *J. Diabetes Metab.* 29, 1883–1889. <https://doi.org/10.4172/2155-6156.S1-003.Contributions>
- Furst, J.R., Bandeira, L.C., Fan, W., Agarwal, S., Nishiyama, K.K., McMahon, D.J., Dworakowski, E., Jiang, H., Silverberg, S.J., Rubin, M.R., 2016. Advanced Glycation Endproducts and Bone Material Strength in Type 2 Diabetes. *J. Clin. Endocrinol. Metab.* 101, 2502–2510. <https://doi.org/10.1210/jc.2016-1437>
- Gadaleta, S.J., Paschalis, E.P., Betts, F., Mendelsohn, R., Boskey, A.L., 1996. Fourier transform infrared spectroscopy of the solution-mediated conversion of amorphous calcium phosphate to hydroxyapatite: New correlations between X-ray diffraction and infrared data. *Calcif. Tissue Int.* 58, 9–16. <https://doi.org/10.1007/BF02509540>
- Gallant, M.A., Brown, D.M., Organ, J.M., Allen, M.R., Burr, D.B., 2013. Reference-point indentation correlates with bone toughness assessed using whole-bone traditional mechanical testing. *Bone* 53, 301–305. <https://doi.org/10.1016/j.bone.2012.12.015>
- Gardegaront, M., Farlay, D., Peyruchaud, O., Follet, H., 2018. Automation of the Peak Fitting Method in Bone FTIR Microspectroscopy Spectrum Analysis: Human and Mice Bone Study. *J. Spectrosc.* 2018, 1–11. <https://doi.org/10.1155/2018/4131029>
- Gieroba, B., Przekora, A., Kalisz, G., Kazimierzak, P., Song, C.L., Wojcik, M., Ginalska, G., Kazarian, S.G., Sroka-Bartnicka, A., 2021. Collagen maturity and mineralization in mesenchymal stem cells cultured on the hydroxyapatite-based bone scaffold analyzed by ATR-FTIR spectroscopic imaging. *Mater. Sci. Eng. C* 119, 111634. <https://doi.org/10.1016/j.msec.2020.111634>
- Gkogkolou, P., Böhm, M., 2012. Advanced glycation end products. *Dermatoendocrinol.* 4, 259–270. <https://doi.org/10.4161/derm.22028>
- Goldin, A., Beckman, J.A., Schmidt, A.M., Creager, M.A., 2006. Advanced Glycation End Products. *Circulation* 114, 597–605. <https://doi.org/10.1161/CIRCULATIONAHA.106.621854>
- Grüneboom, A., Hawwari, I., Weidner, D., Culemann, S., Henneberg, S., Brenzel, A., Merz,

- S., Bornemann, L., Wuelling, M., Kling, L., Hasenberg, M., Voortmann, S., Baum, W., Ohs, A., Kraff, O., Quick, H.H., Jäger, M., Landgraeber, S., Dudda, M., Danuser, R., Stein, J. V, Rohde, M., Gelse, K., Garbe, A.I., Adamczyk, A., Westendorf, A.M., Christiansen, S., Engel, D.R., Vortkamp, A., Herrmann, M., Kamradt, T., Schett, G., Hasenberg, A., 2019. A network of trans-cortical capillaries as mainstay for blood circulation in long bones. *Nat Metab.* 1, 236–250. <https://doi.org/10.1038/s42255-018-0016-5.A>
- Hamann, C., Picke, A.K., Campbell, G.M., Balyura, M., Rauner, M., Bernhardt, R., Huber, G., Morlock, M.M., Günther, K.P., Bornstein, S.R., Glüer, C.C., Ludwig, B., Hofbauer, L.C., 2014. Effects of parathyroid hormone on bone mass, bone strength, and bone regeneration in male rats with type 2 diabetes mellitus. *Endocrinology* 155, 1197–1206. <https://doi.org/10.1210/en.2013-1960>
- Hannon, T.S., Rao, G., Arslanian, S.A., 2005. Childhood Obesity and Type 2 Diabetes Mellitus. *Pediatrics* 116, 473–480. <https://doi.org/10.1542/peds.2004-2536>
- Hansson, L.I., Menander-Sellman, K., Stenström, A., Thorngren, K.G., 1972. Rate of normal longitudinal bone growth in the rat. *Calcif. Tissue Res.* 10, 238–251. <https://doi.org/10.1007/BF02012553>
- Haynes, A., Kalic, R., Cooper, M., K Hewitt, J., Davis, E.A., 2016. Increasing incidence of type 2 diabetes in Indigenous and non-Indigenous children in Western Australia, 1990–2012. *Med. J. Aust.* 204, 2–3. <https://doi.org/10.5694/MJA15.00958>
- Hofmann, T., Heyroth, F., Meinhard, H., Fränzel, W., Raum, K., 2006. Assessment of composition and anisotropic elastic properties of secondary osteon lamellae. *J. Biomech.* 39, 2282–2294. <https://doi.org/10.1016/j.jbiomech.2005.07.009>
- Huang, R., Miller, L., Carlson, C., Chance, M., 2002. Characterization of bone mineral composition in the proximal tibia of *Cynomolgus* monkeys: effect of ovariectomy and nandrolone decanoate treatment. *Bone* 30, 492–497. [https://doi.org/10.1016/S8756-3282\(01\)00691-3](https://doi.org/10.1016/S8756-3282(01)00691-3)
- Hughes, P.C., Tanner, J.M., 1970. The assessment of skeletal maturity in the growing rat. *J. Anat.* 106, 371–402.
- Hunt, H.B., Miller, N.A., Hemmerling, K.J., Koga, M., Lopez, K.A., Taylor, E.A., Sellmeyer,

- D.E., Moseley, K.F., Donnelly, E., 2021. Bone Tissue Composition in Postmenopausal Women Varies With Glycemic Control From Normal Glucose Tolerance to Type 2 Diabetes Mellitus. *J. Bone Miner. Res.* 36, 334–346. <https://doi.org/10.1002/jbmr.4186>
- Hunt, H.B., Pearl, J.C., Diaz, D.R., King, K.B., Donnelly, E., 2018. Bone Tissue Collagen Maturity and Mineral Content Increase With Sustained Hyperglycemia in the KK-Ay Murine Model of Type 2 Diabetes. *J. Bone Miner. Res.* 33, 921–929. <https://doi.org/10.1002/jbmr.3365>
- Hunt, H.B., Torres, A.M., Palomino, P.M., Marty, E., Saiyed, R., Cohn, M., Jo, J., Warner, S., Sroga, G.E., King, K.B., Lane, J.M., Vashishth, D., Hernandez, C.J., Donnelly, E., 2019. Altered Tissue Composition, Microarchitecture, and Mechanical Performance in Cancellous Bone From Men With Type 2 Diabetes Mellitus. *J. Bone Miner. Res.* 34, 1191–1206. <https://doi.org/10.1002/jbmr.3711>
- Ignat'eva, N.Y., Danilov, N.A., Averkiev, S. V., Obrezkova, M. V., Lunin, V. V., Sobol', E.N., 2007. Determination of hydroxyproline in tissues and the evaluation of the collagen content of the tissues. *J. Anal. Chem.* 62, 51–57. <https://doi.org/10.1134/S106193480701011X>
- Isaksson, H., Turunen, M.J., Rieppo, L., Saarakkala, S., Tamminen, I.S., Rieppo, J., Kröger, H., Jurvelin, J.S., 2010. Infrared spectroscopy indicates altered bone turnover and remodeling activity in renal osteodystrophy. *J. Bone Miner. Res.* 25, 1360–1366. <https://doi.org/10.1002/jbmr.10>
- Isojima, T., Sims, N.A., 2021. Cortical bone development, maintenance and porosity: genetic alterations in humans and mice influencing chondrocytes, osteoclasts, osteoblasts and osteocytes. *Cell. Mol. Life Sci.* 78, 5755–5773. <https://doi.org/10.1007/s00018-021-03884-w>
- Janghorbani, M., Feskanich, D., Willett, W.C., Hu, F., 2006. Prospective Study of Diabetes and Risk of Hip Fracture. *Diabetes Care* 29, 1573–1578. <https://doi.org/10.2337/dc06-0440>
- Janghorbani, M., Van Dam, R.M., Willett, W.C., Hu, F.B., 2007. Systematic review of type 1 and type 2 diabetes mellitus and risk of fracture. *Am. J. Epidemiol.* 166, 495–505. <https://doi.org/10.1093/aje/kwm106>

- Jepsen, Silva, M.J., Vashishth, D., Guo, X.E., van der Meulen, M.C., 2015. Establishing Biomechanical Mechanisms in Mouse Models: Practical Guidelines for Systematically Evaluating Phenotypic Changes in the Diaphyses of Long Bones. *J. Bone Miner. Res.* 30, 951–966. <https://doi.org/10.1002/jbmr.2539>
- Kafienah, W., Sims, T.J., 2004. Biochemical Methods for the Analysis of Tissue-Engineered Cartilage, in: Hollander, A.P., Hatton, P. V (Eds.), *Biopolymer Methods in Tissue Engineering*. Humana Press, New Jersey, pp. 217–230. <https://doi.org/10.1385/1-59259-428-X:217>
- Karim, L., Bouxsein, M.L., 2016. Effect of type 2 diabetes-related non-enzymatic glycation on bone biomechanical properties. *Bone* 82, 21–27. <https://doi.org/10.1016/j.bone.2015.07.028>
- Karim, L., Moulton, J., Van Vliet, M., Velie, K., Robbins, A., Malekipour, F., Abdeen, A., Ayres, D., Bouxsein, M.L., 2018. Bone microarchitecture, biomechanical properties, and advanced glycation end-products in the proximal femur of adults with type 2 diabetes. *Bone* 114, 32–39. <https://doi.org/10.1016/j.bone.2018.05.030>
- Karim, L., Tang, S.Y., Sroga, G.E., Vashishth, D., 2013. Differences in non-enzymatic glycation and collagen cross-links between human cortical and cancellous bone. *Osteoporos. Int.* 24, 2441–2447. <https://doi.org/10.1007/s00198-013-2319-4>
- Karim, L., Vashishth, D., 2012. Heterogeneous Glycation of Cancellous Bone and Its Association with Bone Quality and Fragility. *PLoS One* 7, e35047. <https://doi.org/10.1371/journal.pone.0035047>
- Koh, W.P., Wang, R., Ang, L.W., Heng, D., Yuan, J.M., Yu, M.C., 2010. Diabetes and risk of hip fracture in the Singapore Chinese Health Study. *Diabetes Care* 33, 1766–1770. <https://doi.org/10.2337/dc10-0067>
- Kourkoumelis, N., Zhang, X., Lin, Z., Wang, J., 2019. Fourier Transform Infrared Spectroscopy of Bone Tissue: Bone Quality Assessment in Preclinical and Clinical Applications of Osteoporosis and Fragility Fracture. *Clin. Rev. Bone Miner. Metab.* 17, 24–39. <https://doi.org/10.1007/s12018-018-9255-y>
- Lee, Y., Hirose, H., Ohneda, M., Johnson, J.H., McGarry, J.D., Unger, R.H., 1994. Beta-cell lipotoxicity in the pathogenesis of non-insulin-dependent diabetes mellitus of obese rats:

- impairment in adipocyte-beta-cell relationships. *Proc. Natl. Acad. Sci.* 91, 10878–10882. <https://doi.org/10.1073/pnas.91.23.10878>
- LLabre, J.E., Sroga, G.E., Tice, M.J.L., Vashishth, D., 2022. Induction and rescue of skeletal fragility in a high-fat diet mouse model of type 2 diabetes: An in vivo and in vitro approach. *Bone* 156. <https://doi.org/10.1016/j.bone.2021.116302>
- Ma, C., Du, T., Niu, X., Fan, Y., 2022. Biomechanics and mechanobiology of the bone matrix. *Bone Res.* 10. <https://doi.org/10.1038/s41413-022-00223-y>
- Malluche, H.H., Porter, D.S., Monier-Faugere, M.-C., Mawad, H., Pienkowski, D., 2012. Differences in Bone Quality in Low- and High-Turnover Renal Osteodystrophy. *J. Am. Soc. Nephrol.* 23, 525–532. <https://doi.org/10.1681/ASN.2010121253>
- McCarthy, Etcheverry, S.B., Cortizo, A.M., 2001. Effect of advanced glycation endproducts on the secretion of insulin-like growth factor-I and its binding proteins: role in osteoblast development. *Acta Diabetol.* 38, 113–122. <https://doi.org/10.1007/s005920170007>
- McCreadie, B.R., Morris, M.D., Chen, T., Sudhaker Rao, D., Finney, W.F., Widjaja, E., Goldstein, S.A., 2006. Bone tissue compositional differences in women with and without osteoporotic fracture. *Bone* 39, 1190–1195. <https://doi.org/10.1016/j.bone.2006.06.008>
- Ogawa, N., Yamaguchi, T., Yano, S., Yamauchi, M., Yamamoto, M., Sugimoto, T., 2007. The Combination of High Glucose and Advanced Glycation End-products (AGEs) Inhibits the Mineralization of Osteoblastic MC3T3-E1 Cells through Glucose-induced Increase in the Receptor for AGEs. *Horm. Metab. Res.* 39, 871–875. <https://doi.org/10.1055/s-2007-991157>
- Ou-Yang, H., Paschalis, E.P., Mayo, W.E., Boskey, A.L., Mendelsohn, R., 2001. Infrared microscopic imaging of bone: Spatial distribution of CO3²⁻. *J. Bone Miner. Res.* 16, 893–900. <https://doi.org/10.1359/jbmr.2001.16.5.893>
- Parfitt, A.M., Mathews, C.H.E., Villanueva, A.R., Kleerekoper, M., Frame, B., Rao, D.S., 1983. Relationships between surface, volume, and thickness of iliac trabecular bone in aging and in osteoporosis. Implications for the microanatomic and cellular mechanisms of bone loss. *J. Clin. Invest.* 72, 1396–1409. <https://doi.org/10.1172/JCI111096>
- Paschalis, E.P., Verdelis, K., Doty, S.B., Boskey, A.L., Mendelsohn, R., Yamauchi, M., 2001. Spectroscopic characterization of collagen cross-links in bone. *J. Bone Miner. Res.* 16,

- 1821–1828. <https://doi.org/10.1359/jbmr.2001.16.10.1821>
- Peterson, R.G., Shaw, W.N., Neel, M., Little, L.A., Eichberg, J., 1990. Zucker Diabetic Fatty Rat as a Model for Non-insulin-dependent Diabetes Mellitus. *ILAR J.* 32, 16–19. <https://doi.org/10.1093/ilar.32.3.16>
- Picke, A., Campbell, G., Napoli, N., Hofbauer, L.C., Rauner, M., 2019. Update on the impact of type 2 diabetes mellitus on bone metabolism and material properties. *Endocr. Connect.* 8, R55–R70. <https://doi.org/10.1530/EC-18-0456>
- Poundarik, A.A., Wu, P.-C., Evis, Z., Sroga, G.E., Ural, A., Rubin, M., Vashishth, D., 2015. A direct role of collagen glycation in bone fracture. *J. Mech. Behav. Biomed. Mater.* 52, 120–130. <https://doi.org/10.1016/j.jmbbm.2015.08.012>
- Prisby, R.D., Swift, J.M., Bloomfield, S.A., Hogan, H.A., Delp, M.D., 2008. Altered bone mass, geometry and mechanical properties during the development and progression of type 2 diabetes in the Zucker diabetic fatty rat. *J. Endocrinol.* 199, 379–388. <https://doi.org/10.1677/JOE-08-0046>
- Querido, W., Ailavajhala, R., Padalkar, M., Pleshko, N., 2018. Validated Approaches for Quantification of Bone Mineral Crystallinity Using Transmission Fourier Transform Infrared (FT-IR), Attenuated Total Reflection (ATR) FT-IR, and Raman Spectroscopy. *Appl. Spectrosc.* 72, 1581–1593. <https://doi.org/10.1177/0003702818789165>
- Reinwald, S., Peterson, R.G., Allen, M.R., Burr, D.B., 2009. Skeletal changes associated with the onset of type 2 diabetes in the ZDF and ZDSD rodent models. *Am. J. Physiol. Metab.* 296, E765–E774. <https://doi.org/10.1152/ajpendo.90937.2008>
- Retzepi, M., Donos, N., 2010. The effect of diabetes mellitus on osseous healing. *Clin. Oral Implants Res.* 21, 673–681. <https://doi.org/10.1111/j.1600-0501.2010.01923.x>
- Rezaee, T., Bouxsein, M.L., Karim, L., 2020. Increasing fluoride content deteriorates rat bone mechanical properties. *Bone* 136, 115369. <https://doi.org/10.1016/j.bone.2020.115369>
- Root, S.H., Wee, N.K., Novak, S., Rosen, C.J., Baron, R., Matthews, B.G., Kalajzic, I., 2020. Perivascular osteoprogenitors are associated with trans-cortical channels of long bones. *Stem Cells* 38, 769–781. <https://doi.org/10.1002/stem.3159>
- Rubin, M.R., Patsch, J.M., 2016. Assessment of bone turnover and bone quality in type 2

- diabetic bone disease: current concepts and future directions. *Bone Res.* 4, 16001. <https://doi.org/10.1038/boneres.2016.1>
- Ruppel, M.E., Burr, D.B., Miller, L.M., 2006. Chemical makeup of microdamaged bone differs from undamaged bone. *Bone* 39, 318–324. <https://doi.org/10.1016/j.bone.2006.02.052>
- Sai, Y., Shiwaku, Y., Anada, T., Tsuchiya, K., Takahashi, T., Suzuki, O., 2018. Capacity of octacalcium phosphate to promote osteoblastic differentiation toward osteocytes in vitro. *Acta Biomater.* 69, 362–371. <https://doi.org/10.1016/j.actbio.2018.01.026>
- Saito, M., Fujii, K., Mori, Y., Marumo, K., 2006. Role of collagen enzymatic and glycation induced cross-links as a determinant of bone quality in spontaneously diabetic WBN/Kob rats. *Osteoporos. Int.* 17, 1514–1523. <https://doi.org/10.1007/s00198-006-0155-5>
- Saito, M., Marumo, K., 2013. Bone Quality in Diabetes. *Front. Endocrinol. (Lausanne)*. 4, 1–9. <https://doi.org/10.3389/fendo.2013.00072>
- Saito, M., Marumo, K., 2010. Collagen cross-links as a determinant of bone quality: A possible explanation for bone fragility in aging, osteoporosis, and diabetes mellitus. *Osteoporos. Int.* 21, 195–214. <https://doi.org/10.1007/s00198-009-1066-z>
- Schmidt, F.N., Zimmermann, E.A., Campbell, G.M., Sroga, G.E., Püschel, K., Amling, M., Tang, S.Y., Vashishth, D., Busse, B., 2017. Assessment of collagen quality associated with non-enzymatic cross-links in human bone using Fourier-transform infrared imaging. *Bone* 97, 243–251. <https://doi.org/10.1016/j.bone.2017.01.015>
- Sihota, P., Yadav, R.N., Poleboina, S., Mehandia, V., Bhadada, S.K., Tikoo, K., Kumar, N., 2020. Development of HFD-Fed /Low-DoseSTZ-Treated Female Sprague-Dawley Rat Model to Investigate Diabetic Bone Fragility at Different Organization Levels. *JBMR Plus* 4, 1–12. <https://doi.org/10.1002/jbm4.10379>
- Sims, N.A., Martin, T.J., 2020. Osteoclasts Provide Coupling Signals to Osteoblast Lineage Cells through Multiple Mechanisms. *Annu. Rev. Physiol.* 82, 507–529. <https://doi.org/10.1146/annurev-physiol-021119-034425>
- Slater, M., Green, M.E., Shah, B., Khan, S., Jones, C.R., Sutherland, R., Jacklin, K., Walker, J.D., 2019. First Nations people with diabetes in Ontario: methods for a longitudinal population-based cohort study. *C. open* 7, E680–E688. <https://doi.org/10.9778/cmajo.20190096>

- Spevak, L., Flach, C.R., Hunter, T., Mendelsohn, R., Boskey, A., 2013. Fourier Transform Infrared Spectroscopic Imaging Parameters Describing Acid Phosphate Substitution in Biologic Hydroxyapatite. *Calcif. Tissue Int.* 92, 418–428. <https://doi.org/10.1007/s00223-013-9695-9>
- Steppan, C.M., Crawford, D.T., Chidsey-Frink, K.L., Ke, H., Swick, A.G., 2000. Leptin is a potent stimulator of bone growth in ob/ob mice. *Regul. Pept.* 92, 73–78. [https://doi.org/10.1016/S0167-0115\(00\)00152-X](https://doi.org/10.1016/S0167-0115(00)00152-X)
- Sugimoto, T., Nishiyama, K., Kuribayashi, F., Chihara, K., 1997. Serum levels of insulin-like growth factor (IGF) I, IGF-binding protein (IGFBP)-2, and IGFBP-3 in osteoporotic patients with and without spinal fractures. *J. Bone Miner. Res.* 12, 1272–1279. <https://doi.org/10.1359/jbmr.1997.12.8.1272>
- Tanaka, K., Yamaguchi, T., Kanazawa, I., Sugimoto, T., 2015. Effects of high glucose and advanced glycation end products on the expressions of sclerostin and RANKL as well as apoptosis in osteocyte-like MLO-Y4-A2 cells. *Biochem. Biophys. Res. Commun.* 461, 193–199. <https://doi.org/10.1016/j.bbrc.2015.02.091>
- Terada, M., Inaba, M., Yano, Y., Hasuma, T., Nishizawa, Y., Morii, H., Otani, S., 1998. Growth-Inhibitory Effect of a High Glucose Concentration on Osteoblast-like Cells. *Bone* 22, 17–23. [https://doi.org/10.1016/S8756-3282\(97\)00220-2](https://doi.org/10.1016/S8756-3282(97)00220-2)
- Thomas, C.J., Cleland, T.P., Sroga, G.E., Vashishth, D., 2018. Accumulation of carboxymethyl-lysine (CML) in human cortical bone. *Bone* 110, 128–133. <https://doi.org/10.1016/j.bone.2018.01.028>
- Tice, M.J.L., Bailey, S., Sroga, G.E., Gallagher, E.J., Vashishth, D., 2022. Non-Obese MKR Mouse Model of Type 2 Diabetes Reveals Skeletal Alterations in Mineralization and Material Properties. *JBMR Plus* 6, 1–14. <https://doi.org/10.1002/jbm4.10583>
- Tung, J.Y. ling, Kwan, E.Y. wah, But, B.W. man, Wong, W.H. sang, Fu, A.C. cheung, Pang, G., Tsang, J.W. yan, Yau, H. chung, Belaramani, K., Wong, L. ming, Wong, S.M. yee, Lo, P., Ng, K. leung, Yeung, W.K. yee, Chan, K. tat, Chan, A.M. kit, Wong, S.W. chun, Tay, M. kut, Chung, J., Lee, C. yin, Lam, Y. yu, Cheung, P. to, 2022. Incidence and clinical characteristics of pediatric-onset type 2 diabetes in Hong Kong: The Hong Kong childhood diabetes registry 2008 to 2017. *Pediatr. Diabetes* 23, 556–561. <https://doi.org/10.1111/pedi.13231>

- Valderrábano, R.J., Linares, M.I., 2018. Diabetes mellitus and bone health: epidemiology, etiology and implications for fracture risk stratification. *Clin. Diabetes Endocrinol.* 4, 9. <https://doi.org/10.1186/s40842-018-0060-9>
- Vashishth, D., Gibson, G., Khoury, J., Schaffler, M., Kimura, J., Fyhrie, D., 2001. Influence of nonenzymatic glycation on biomechanical properties of cortical bone. *Bone* 28, 195–201. [https://doi.org/10.1016/S8756-3282\(00\)00434-8](https://doi.org/10.1016/S8756-3282(00)00434-8)
- Velraj, G., Karthikeyan, S., Chitra, A., 2020. Mineralization changes substituted type b carbonate of Po43^- ion in the bone minerals of an archaeological sample studied using fourier self deconvolution technique. *Indian J. Biochem. Biophys.* 57, 277–282. <https://doi.org/10.56042/ijbb.v57i3.36490>
- Vestergaard, P., 2007. Discrepancies in bone mineral density and fracture risk in patients with type 1 and type 2 diabetes—a meta-analysis. *Osteoporos. Int.* 18, 427–444. <https://doi.org/10.1007/s00198-006-0253-4>
- Viguet-Carrin, S., Farlay, D., Bala, Y., Munoz, F., Bouxsein, M.L., Delmas, P.D., 2008. An in vitro model to test the contribution of advanced glycation end products to bone biomechanical properties. *Bone* 42, 139–149. <https://doi.org/10.1016/j.bone.2007.08.046>
- Walker, E.C., Truong, K., McGregor, N.E., Poulton, I.J., Isojima, T., Gooi, J.H., John Martin, T., Sims, N.A., 2020. Cortical bone maturation in mice requires SOCS3 suppression of gp130/STAT3 signalling in osteocytes. *Elife* 9, 1–27. <https://doi.org/10.7554/eLife.56666>
- Willett, T.L., Voziyan, P., Nyman, J.S., 2022. Causative or associative: A critical review of the role of advanced glycation end-products in bone fragility. *Bone* 163, 116485. <https://doi.org/10.1016/j.bone.2022.116485>
- Wölfel, E.M., Jähn-Rickert, K., Schmidt, F.N., Wulff, B., Mushumba, H., Sroga, G.E., Püschel, K., Milovanovic, P., Amling, M., Campbell, G.M., Vashishth, D., Busse, B., 2020. Individuals with type 2 diabetes mellitus show dimorphic and heterogeneous patterns of loss in femoral bone quality. *Bone* 140, 115556. <https://doi.org/10.1016/j.bone.2020.115556>
- Wu, H., Patterson, C.C., Zhang, X., Ghani, R.B.A., Magliano, D.J., Boyko, E.J., Ogle, G.D., Luk, A.O.Y., 2022. Worldwide estimates of incidence of type 2 diabetes in children and adolescents in 2021. *Diabetes Res. Clin. Pract.* 185, 109785.

<https://doi.org/10.1016/j.diabres.2022.109785>

- Yamaguchi, T., Kanatani, M., Yamauchi, M., Kaji, H., Sugishita, T., Baylink, D.J., Mohan, S., Chihara, K., Sugimoto, T., 2006. Serum Levels of Insulin-Like Growth Factor (IGF); IGF-Binding Proteins-3, -4, and -5; and Their Relationships to Bone Mineral Density and the Risk of Vertebral Fractures in Postmenopausal Women. *Calcif. Tissue Int.* 78, 18–24. <https://doi.org/10.1007/s00223-005-0163-z>
- Yamamoto, M., Sugimoto, T., 2016. Advanced Glycation End Products, Diabetes, and Bone Strength. *Curr. Osteoporos. Rep.* 14, 320–326. <https://doi.org/10.1007/s11914-016-0332-1>
- Yerramshetty, J.S., Akkus, O., 2008. The associations between mineral crystallinity and the mechanical properties of human cortical bone. *Bone* 42, 476–482. <https://doi.org/10.1016/j.bone.2007.12.001>
- Yokoi, N., Hoshino, M., Hidaka, S., Yoshida, E., Beppu, M., Hoshikawa, R., Sudo, K., Kawada, A., Takagi, S., Seino, S., 2013. A Novel Rat Model of Type 2 Diabetes: The Zucker Fatty Diabetes Mellitus ZFDM Rat. *J. Diabetes Res.* 2013, 1–9. <https://doi.org/10.1155/2013/103731>
- Zimmermann, E.A., Schaible, E., Bale, H., Barth, H.D., Tang, S.Y., Reichert, P., Busse, B., Alliston, T., Ager III, J.W., Ritchie, R.O., 2011. Age-related changes in the plasticity and toughness of human cortical bone at multiple length scales. *Proc Natl Acad Sci* 35, 14416–14421. <https://doi.org/10.1073/pnas.1107966108>

CHAPTER 4

Experimental and Computational Mechanics of Bone Fragility in Type-2 Diabetes: A Longitudinal Investigation Using Zucker Diabetic Fatty (ZDF) Rats

This Chapter has been adapted directly from a manuscript that is under review, 'Monahan et al., Experimental and Computational Mechanics of Bone Fragility in Type-2 Diabetes: A Longitudinal Investigation Using Zucker Diabetic Fatty (ZDF) Rats.

4.1 Introduction

Type-2 Diabetes (T2D) is associated with increased bone fragility, with patients having up to a 3-fold increase in hip fracture risk (Janghorbani et al., 2007). Unlike osteoporotic patients, a reduction in bone mineral density (BMD) is not responsible for this increase in bone fragility, since patients with T2D often present with a normal-to-high BMD (Parfitt et al., 1983). This suggests that the quality of the bone tissue itself is affected, whereby the intrinsic properties of the bone matrix are impaired. While recent studies have suggested that sub-tissue alterations to the organic constituents of the bone matrix contribute to impaired biomechanical behaviour (Karim et al., 2018; Poundarik et al., 2015; Saito et al., 2006), the precise pathophysiological factors that contribute to these abnormalities remain unknown. With the onset of T2D, metabolic and cellular functions throughout the body are altered (Hygum et al., 2017; Picke et al., 2019). It is proposed that these systemic changes disrupt normal bone metabolism, which impairs the normal maintenance of the bone tissue matrix, leading to deteriorated sub-tissue biomechanics and ultimately weakening the overall structure (Picke et al., 2019; Rubin and Patsch, 2016; Yamaguchi, 2010; Zhao et al., 2020). However, the precise sub-tissue alterations

that take place and mechanisms that impair whole-bone fracture mechanics in T2D remains poorly understood.

It has been widely proposed that the hyperglycaemic state in T2D forms an excess accumulation of non-enzymatic crosslinks and adducts, termed Advanced Glycated End-products (AGEs), in the organic matrix of bone (Karim and Bouxsein, 2016; Saito et al., 2006; Willett et al., 2022; Yamamoto and Sugimoto, 2016). AGE crosslinks are formed when proteins and lipids within the collagen structure bind together and are widely hypothesised to stiffen the collagen network, reducing ductility and fracture toughness (Delmas et al., 1984; Granke et al., 2015; Vashishth, 2007; Wang et al., 2002; Zimmermann et al., 2011). This is reportedly caused by a reduction in intra-fibrillar sliding (Siegmund et al., 2008) and leads to a more brittle tissue behaviour. Alternatively, non-crosslinking adducts are formed when the protein structure itself is modified, which can ultimately impair protein function (Nagai et al., 2014), yet there is a limited number of studies that have measured AGE adducts and their implications for bone fragility in T2D. Furthermore, much of the evidence supporting the role of AGEs in diabetic bone fragility has been derived from *in vitro* studies (Merlo et al., 2020; Vashishth et al., 2001; Willett et al., 2013), or in some cases animal studies, whereby increased pentosidine (PEN) (a non-enzymatic crosslink) and fluorescent AGEs (a bulk measurement of AGEs) have been associated with a reduction in bone toughness and fracture toughness (K_{Ic}) (LLabre et al., 2022; Tice et al., 2022). However, additional animal studies have found no differences in PEN or bulk fAGEs despite reporting reductions in post-yield displacement (Devlin et al., 2014), energy-to-failure and toughness (Creecy et al., 2016) and as seen in Chapter 3, bone strength. More importantly, the vast majority of human studies have found no significant differences between the amount of fAGEs in diabetic tissue, compared to healthy controls (Hunt et al., 2019; Karim et al., 2018; Wölfel et al., 2022a, 2022b, 2020). In particular, Wölfel *et al.* (2022b) found that cortical bone from the femoral midshaft of patients with T2D had a reduced elastic modulus and reduced inelastic and elastic region fibril/ tissue strain in comparison to controls, despite there being no observable differences in AGEs. This highlights that other mechanisms, aside from AGEs, must contribute to bone fragility in T2D.

In T2D, hyperglycaemia can disrupt cellular metabolism resulting in altered bone homeostasis, which may compromise the tissue structure, ultimately impairing bone quality and leading to an increased risk of fracture (Picke et al., 2019). Whilst there are various human studies that have explored the influence of altered bone microarchitecture and composition on the tissue biomechanical properties in T2D (Hunt et al., 2019; Karim et al., 2018; Lekkala et al., 2023;

Wölfel et al., 2022a, 2022b; Yadav et al., 2022), the majority of these studies do not consider cellular behaviour, or alterations in tissue or serum biochemical factors that arise during the onset of the disease. This is perhaps due to human tissue and serum being limited and difficult to obtain and, to date, only three human studies have examined pathophysiological factors contributing to bone fragility in cortical (Lekkala et al., 2023; Wölfel et al., 2020) and trabecular (Lekkala et al., 2023; Piccoli et al., 2020) tissue. Several of these studies found bone remodelling to be reduced as evidenced by reduced levels of bone formation and resorption markers, P1NP and CTX, respectively (Lekkala et al., 2023), impaired expression of the bone formation controlling genes, sclerostin (Sost) and RUNX2 (Piccoli et al., 2020) and lower osteon density, mineralisation and higher mineral heterogeneity in the diabetic cohorts than controls (Wölfel et al., 2020). However, despite the altered remodelling process (as evidence by serum markers, evaluation of gene expression and/ or histology), these studies did not find any reduction to any tissue-level properties of T2 diabetic bone (Lekkala et al., 2023; Piccoli et al., 2020; Wölfel et al., 2020). Apart from the difficulty in obtaining direct measurements from human bone tissue *in vivo*, human studies can be confounded by the analysis of different bone sites and the inability to control disease duration in T2 diabetic patients, which means that the precise parameters that are altered remain poorly understood.

Longitudinal animal studies of T2D provide a platform to understand how the pathophysiology of diabetes leads to impaired skeletal fragility. However, in various publications the cellular, compositional and biomechanical aspects of T2 diabetic bone fragility have been studied in isolation of one another (Caliaperoumal et al., 2018; Hamann et al., 2011; Hunt et al., 2018; Stabley et al., 2015; Zeitoun et al., 2019), meaning that the understanding of the key mechanisms responsible remains somewhat fragmented. For example, several studies have characterised structural properties of T2 diabetic tissue, and indeed observed impaired bone structural-level properties, but have failed to quantify material-level biomechanics (Hamann et al., 2011; Hunt et al., 2018; Picke et al., 2016a) or composition (Gallant et al., 2013; Prisby et al., 2008; Reinwald et al., 2009), with limited or no insight provided into cellular level behaviour. A study by Hamann *et al.* (2013) found alterations to cellular markers measured from serum such as, an increase in calcium, CTX and reductions in osteocalcin, indicating impaired bone cellular metabolism. This was further highlighted by an impaired bone micro-architecture and reduced stiffness, ultimate load, elastic modulus and ultimate strength in the cortical tissue, however, this study did not explore the role of AGEs or bone composition (Hamann et al., 2013). While Devlin *et al.* (2014) examined both cellular behaviour, bone

matrix composition and tissue-level biomechanics in a Tallyho/JngJ diabetic mouse, they found few significant differences in cellular markers (CTX and osteocalcin were unchanged), fAGE levels, or tissue-level properties. This was most likely attributed to the short disease duration, whereby the Tallyho/JngJ diabetic mice were only overtly T2 diabetic for approximately 7-weeks. Several other studies using rodent models of T2D have also been limited by a relatively short disease duration. In the previous Chapter a long-term 46-week longitudinal study using Zucker Diabetic Fatty (ZDF (*fa/fa*)) rats was conducted, and showed that in long term T2D (e.g. 46-weeks) the ulnar bone of the ZDF (*fa/fa*) rats had significantly reduced tissue strength in comparison to age-matched controls, whereas diabetic rats at 12-weeks showed no difference to controls. In addition, a correlation between tissue material strength and tissue carbonate:phosphate ratio and the acid phosphate content were found. However, it was not explored how disease duration leads to alterations at the cellular level. Together, the key findings across studies on cellular activity, tissue composition and tissue mechanics remain fragmented from one another, and more comprehensive study designs are required.

The objective of this Chapter was to investigate biological, biophysical and biomechanical factors that contribute to bone fragility in T2D. In particular, this study uses a Zucker Diabetic Fatty (ZDF) (*fa/fa*) rat model and conducts a 46-week longitudinal analysis that evaluates the (i) biological markers of cellular metabolism, (ii) sub-tissue properties of the organic components of the bone matrix, (iii) bone structure, morphometry and mineralisation, and (iv) tissue and whole-bone fracture mechanics in addition to tissue-biomechanics using Finite element (FE) modelling.

4.2 Material and Methods

4.2.1 Animal Model and Tissues

The animal model and details used in this Chapter are the same as was described previously in Chapter 3. Rats were euthanized at 12- (Early-stage diabetes), 26- (Established diabetes) and 46-weeks (Long-term diabetes) of age using male Zucker Diabetic Fatty [(ZDF: *fa/fa*) (T2D) and Zucker Lean (ZL: *fa/+*) (Control)] (Charles River, France) (n = 7 - 9, per age, per condition). Right femora were dissected, wrapped in PBS then frozen at -20°C. Right after the euthanasia, blood samples were collected by a cardiac puncture and samples were left to clot at room temperature for 1 - 2 h. Blood samples were then centrifuged (Eppendorf 5424R microcentrifuge, Hamburg, Germany) at 2,000g for 15 min. Once the serum was separated from the clotted blood, the serum was aliquoted into 1.5 mL Eppendorf tubes and frozen at -80°C until analysis. Before experimentation, bones were defrosted for approximately 12 h.

Figure 4.1 shows an outline of the techniques used in this Chapter. Serum markers were measured to assess glycaemic control, bone turnover and general health markers. Compositional, microarchitectural and biomechanical analysis was carried out for local factors influenced by T2D. Right femora bone geometry was measured. Bones were then notched and underwent X-Ray Micro-computed Tomography (micro-CT) scanning to determine bone microarchitecture and measure notch angle morphometric properties, followed by a mechanical characterisation through fracture toughness and sideways fall testing using a custom made rig. Following this, AGE accumulation in cortical bone was quantified through fluorescent AGE (fAGE) analysis and high performance liquid chromatography (HPLC) testing (Figure 4.1).

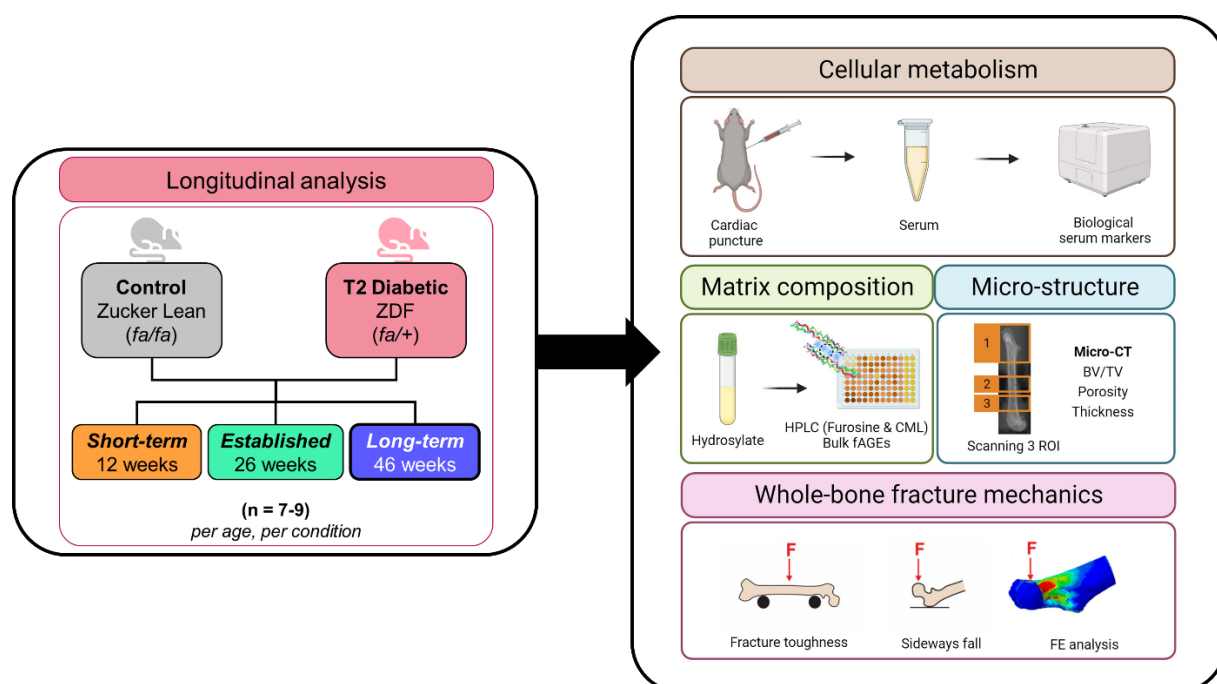


Figure 4.1. Schematic of longitudinal analyses carried out in this chapter to explore cellular metabolism, the organic matrix composition, bone structure and morphology and whole bone fracture mechanics in a ZDF rats model of T2D.

4.2.2 Bone Turnover and Metabolism

Serum Analysis

Serum from the blood was collected after euthanasia to assess cellular metabolism. Glycaemic control was assessed by measuring the ratio of glycated haemoglobin per the amount of normal haemoglobin (% HbA1c/ HbA1) from the serum. Bone turnover was examined by measuring markers of bone formation via procollagen type 1 amino terminal propeptide (P1NP) and bone resorption via C-telopeptide of collagen alpha-I (CTX-I) and Sclerostin (Sost), which is

produced by osteocytes and regulates the Wnt-pathway (Delgado-Calle et al., 2017). Interlukin-6 (IL-6) and calcium were measured to assess the inflammatory state and general health of the animals, respectively. All markers were measured via ELISA kits from AssayGenie (Dublin, Ireland), using a 96-well plate and absorbance was read at 450 nm, unless stated otherwise. Serum levels of HbA1c were measured (FTF100850, AssayGenie, Dublin, Ireland) following the manufacturer's protocol. Briefly, the serum was diluted in sample dilution buffer provide with the kit by 2X for the ZDF (*fa/fa*) and ZL (*fa/+*). Samples and standards were added with 100 μ L/well in duplicate. Haemoglobin subunit alpha-1/2 (HbA1) was also measured (RTEB0313, AssayGenie, Dublin, Ireland) to quantify the %HbA1c/ HbA1. Samples were diluted 4X with sample dilution buffer and added with 100 μ L/well. P1NP, CTX-I and Sost were measured (RTFI01061, RTFI00704 and RTFI00095, AssayGenie, Dublin, Ireland) according to the manufacturer's protocol. Samples were diluted 25X when measuring P1NP and CTX-I and 5X when measuring Sost. Samples and standards were added with 100 μ L/well in duplicate. IL-6 was measured (RTFI00034, AssayGenie, Dublin, Ireland), with samples diluted 2X and added with 100 μ L/well. The total calcium content of the serum was measured with Total Calcium LiquiColor® (0150, Stanbio). Wells were washed twice with PBS and the supernatant was removed. The well plates were kept at -80°C until analysis. Then 0.5 mL of a HCl solution at 0.5 M was added to each sample and these were placed on an orbital shaker overnight. Following, 20 μ L of samples or standard samples were added in triplicate, then 200 μ L of the working solution added to each well (1:1 Total Calcium colour reagent: Total Calcium Base). For this final assay, the absorbance was read at 590 nm and the calcium content in each sample was calculated according to the standard curve.

4.2.3 Organic Matrix Composition

Bulk Fluorescent AGEs (fAGEs)

Fluorescent AGE (fAGE) analysis is a common bulk measurement and measures a combination of non-enzymatic AGEs such as pentosidine, crossline and vesperlysines A, B & C. Once ready for sectioning, distal femurs were removed from PBS and a low-speed saw used to section a 4 mm cross-section of cortical bone from the diaphysis of the distal femur. Following sectioning, cortical samples were demineralised in 45% formic acid for 8 - 10 days. Samples were then papain digested and hydrolysed according to methods previously outlined in Chapter 3. Each sample had two tubes of hydrolysate samples, one used for the fAGE analysis and the other for HPLC. Hydrolysate samples for fAGE were rehydrated with distilled water (dH₂O) and

hydrolysate samples for HPLC were kept dried. AGE accumulation was quantified using a quinine assay and normalised against the amount of collagen using a hydroxyproline assay, (both protocols described previously in Chapter 3). Collagen content was derived based on prior knowledge that collagen consists of 14% hydroxyproline (Ignat'eva et al., 2007). Total fAGEs are reported in units of ng quinine/ mg collagen.

High performance liquid chromatography (HPLC)

These measurements were carried out as part of a collaboration with Prof. Halima Kerdjoudj at Université de Reims Champagne-Ardenne (Reims, France). As glycation reaction is a complex process involving early and late steps, two different glycation products were quantified to evaluate each phase of the process. Thus, furosine concentrations provided information about the formation of Amadori products (furosine is a by-product formed from fructose-lysine during acid hydrolysis) during the early stages of glycation, whereas carboxymethyl-lysine (CML) provided information about the later stage (formation of AGEs) involving oxidative reactions. At 12- and 46-weeks, hydrolysates were prepared using methods previously described in Chapter 3.

Furosine and CML quantification was performed using a LC20 chromatographic system equipped with a Kinetex XB-C18 column (100 × 3.0 mm, 2.6 μm - Phenomenex) with a gradient program composed of 5 mM ammonium formate (pH 2.9) as mobile phase A and 100% acetonitrile as mobile phase B. For Furosine the flow rate was constant at 0.3 mL/min during all separation steps. The gradient program was as follows: 0 – 0.1 min: 5% B; 0.1 – 4.1 min: gradient to 95% B; 4.1 – 6.1 min: 95% B; 6.1 – 7.1 min: gradient to 5% B; 7.1 – 13.1 min: 5% B (Injection volume: 3 μL; oven temperature: 40°C). Detection was performed (API4000 system, ABSciex, France) in positive-ion mode with an electrospray ionization (ESI) source. Multiple reaction monitoring (MRM) transitions used for quantification were as follows: 255.1 > 84.2 for furosine and 259.0 > 88.2 for d4-Furosine. For CML the flow rate was constant at 0.9 mL/min during all separation steps. The gradient program was as follows: 0 – 0.3 min: 90% B; 0.3 – 1.5 min: gradient to 50% B; 1.5 – 2.0 min: 50% B; 2.0 – 3.1 min: gradient to 40% B; 3.1 – 3.5 min: 40% B; 3.5 – 4.0 min: gradient to 90% B (Injection volume: 10 μL; oven temperature: 25°C). Detection was performed as mentioned above. MRM transitions used for quantification were as follows: 205.1 > 130.1 for CML and 207.1 > 84.1 for d2-CML. Calibration curves have been performed by preparing diluted serum solutions spiked with increased amounts of CML (ranging from 2.5 μM to 80 μM), which have been submitted to the

same pre-analytical treatments as rodent bone samples. In addition, lysine content in hydrolysates were quantified by HPLC in order to normalize the expression of results.

4.2.4 Microarchitecture and Mineralisation

Micro-computed tomography (Micro-CT) analysis

To assess the micro-architecture of cortical and trabecular bone, micro-CT (μ CT100, Scanco Medical) was used pre- and post-mechanical testing to scan the proximal femur (ROI: 33.5% of total femur length) and the notched diaphysis (ROI: 1.5 mm) to measure the notch angle and unnotched diaphysis (ROI: 2 mm). High resolution scans were taken using a voxel size of 7 μ m (proximal femur and notched region) and 5 μ m (midshaft), an X-Ray tube potential of 70 kVp, current of 114 μ A, energy of 8W and integration time of 600 ms. A 0.5 mm thick aluminium filter was used to reduce beam hardening artefacts and a 0.8 Gaussian filter and Support value of 1 was used. An evaluation script in the Scanco Image Processing language (IPL) was used to rotate the proximal femurs so that slices for evaluation were oriented along the femoral neck axis, allowing the femoral neck region of interest to be indicated easier and to ensure consistency across scans. To evaluate cortical and trabecular bone from the femoral neck region, the last slice of the femoral neck was determined distally and contours were then applied in the proximal direction every five slices until the VOI extended over 150 slices (Zeitoun et al., 2019). A global density threshold of 691.3 mg HA/cm³ (4000 HU) captured both cortical and trabecular tissue, whilst also eliminating interference of soft tissue (Bouxsein et al., 2010; Verbruggen et al., 2022). For the midshaft, the VOI extended over 409 slices. Post-mechanical testing, the proximal femurs were scanned to capture fracture patterns of the femoral neck following the sideways fall simulation (ROI: 11 mm, Voxel size: 10 μ m). DICOMS were collected for each post-fracture scan.

A series of structural (i.e., cortical bone area (Ct.Area)), compositional (i.e., Cortical and trabecular BMD, TMD) and morphological (i.e., Tb.Th, Tb.N, Tb.Sp, BV/TV, Conn.D, SMI and DA, cortical porosity (Ct.Po)) parameters could be measured from the femoral diaphysis, neck and head using established guidelines (Bouxsein et al., 2010). Grey-level histograms were obtained from the micro-CT images following published methodology (O'Sullivan et al., 2020). A custom MATLAB script was written to determine the weighted mean and most frequent mineral density (M_{mean} , M_{mode}). Tissue volume at low, high and medium mineral density were quantified below, above and between the 25th and 75th percentiles respectively (TV_{25} , TV_{50} , TV_{75}) (O'Sullivan et al., 2020; Verbruggen et al., 2022). The 25th, 50th and 75th

percentile mineral density baseline was taken as the average value of the controls at each age and compared against the diabetic groups.

4.2.5 Biomechanical Analysis

Fracture Toughness Testing

Notch Preparation

Basic geometric measurements of lean (*fa/+*) and ZDF (*fa/fa*) femora were recorded before preparing the notch to ensure the correct notch depth was created and to compare geometrical differences between groups. A notch of a known dimension was created to represent a dominant flaw to assess the bones' resistance to fracture when a defect is present. Using a Vernier Callipers the femoral length (L), midshaft and femoral neck anterior-posterior (AP), medial-lateral (ML) and femoral head diameters were recorded. Notches were prepared using previously published guidelines (Ritchie et al., 2008). An initial notch of a depth ~20% of the midshaft AP diameter was created on the posterior side of the bone using a low-speed saw (IsoMet™ Low Speed Precision Cutter, Buehler Inc., Lake Bluff, IL) with a diamond embedded blade (IsoMet™ with a 3 in. × 0.007 in. Diamond Wafering Blade, Buehler Inc., Lake Bluff, IL). The initial notch was sharpened with a small razor blade coated in 1 μm diamond suspension fluid moving back and forth over the notch approximately 15 times. Bones were sonicated for 3 min in distilled water for cleaning.

Mechanical Testing

After the micro-notch was prepared on the posterior of the mid-diaphysis, femurs were tested until failure in a three-point bend configuration to assess fracture resistance in the presence of a small defect. Femurs were loaded on the anterior side so that the notched posterior side was in tension (Zwick 2.5 kN load cell, 0.1 N pre-load, 0.06 mm/min crosshead speed) to measure the stress intensity factor (K_{Ic}) at crack initiation ($MPa\sqrt{m}$), work-to-fracture (%) and cracking toughness (MJ/m^3) (Figure 4.2 (A)). Force-displacement curves were recorded. The maximum load method of calculating K_{Ic} was used, whereby the maximum force measured during three-point-bend testing the femurs to failure along with the notch angle was used to calculate the critical stress intensity factor required to initiate the formation of a crack using Equation 4.1 (Figure 4.2 (B)) (Ritchie et al., 2008). Work-to-fracture (W_f) was measured from the area under the curve, which represents the energy required to propagate a crack until failure (Figure 4.2 (B)). Similarly, cracking toughness (T_{cr}) was calculated as the span-adjusted work-to-fracture normalised by cortical area (Ct.Ar) using Equation 4.2, where the notch angle (θ_c) was

measured from micro-CT scans. Distal femurs were kept following the fracture toughness testing and soaked in PBS until sectioning for fAGE and HPLC analysis.

$$K_{ic} = F_b \frac{P_{max} S R_o}{\pi(R_o^4 - R_i^4)} \sqrt{\pi R_m \theta_c} \quad (4.1)$$

$$Cracking\ toughness = \frac{W_f}{S C t . A r} \quad (4.2)$$

Where, F_b is calculated using Equations from (Ritchie et al., 2008); P_{max} = maximum force; S = span length; R_o = periosteal radius; R_i = Endosteal radius; R_m = mean radius; θ_c = notch angle, W_f = area under the force-displacement curve of notched femurs; $C t . A r$ = cortical area.

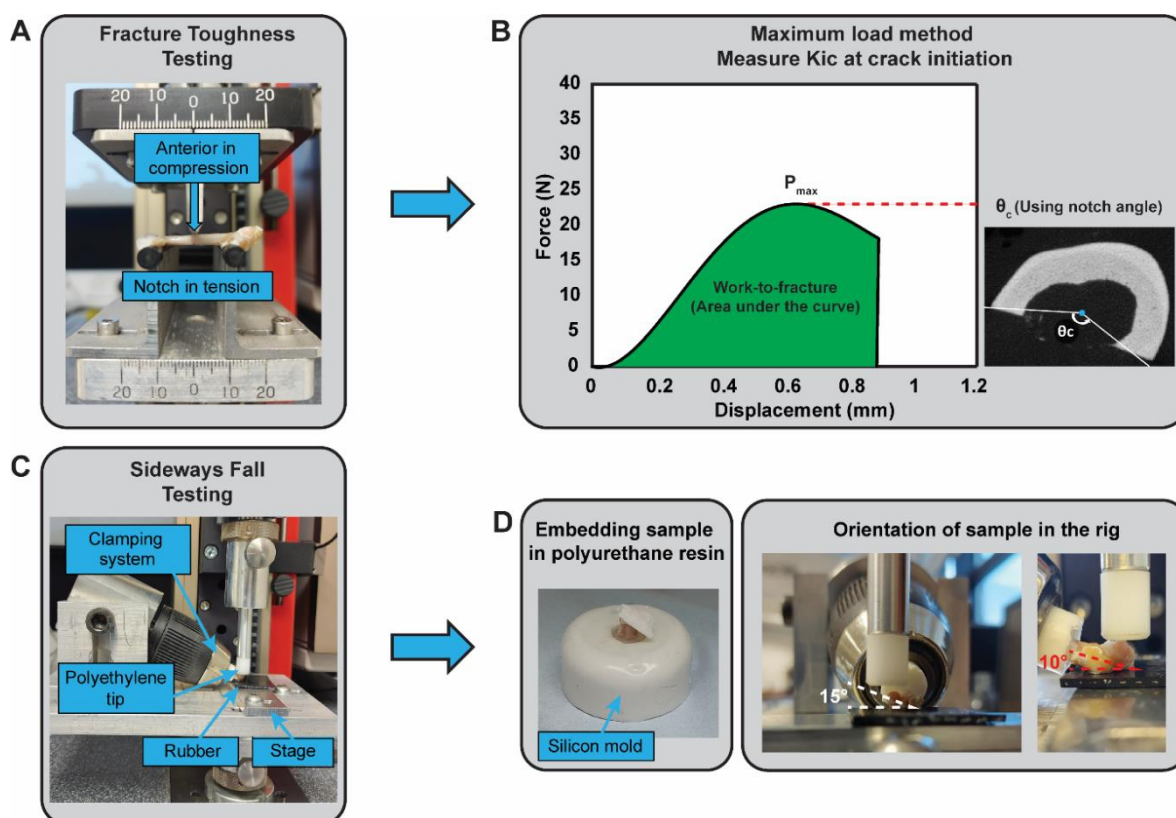


Figure 4.2. (A-B) Initial set-up used for the fracture toughness test with the notch in tension under the load and the resulting force-displacement curve obtained after testing until failure, where the maximum load method was used along with the notch angle to measure stress intensity factor for crack initiation; (C-D) Custom-made rig and set-up used to carry out the sideways fall test, where proximal femurs were embedded into a quick-drying polyurethane resin and oriented as shown in (D) in the rig before loading the femoral head.

Sideways Fall Testing

Immediately following fracture toughness testing, proximal femurs were kept and loaded in a sideways fall configuration test using a custom-build rig seen in Figure 4.2 (C), based on previous rig designs (Jämsä et al., 1998; Zhang and Qin, 2005). Proximal femurs were immediately set into a quick-drying polyurethane resin (Xencast P2 Fast Cast Polyurethane Resin, P2-1, Easy Composites Ltd., Stoke-on-Trent, UK) up to 40% of the total proximal height and were set into a custom-build silicon mold (Condensation Cure Silicone Rubber, CS25, Easy Composites Ltd., Stoke-on-Trent, UK) with a section of PBS soaked gauze wrapped around the femoral head and neck (Figure 4.2 (D)). The rig was created using aluminium and a drill head fixed the polyurethane base of the embedded sample in place to prevent rotation (Figure 4.2 (C)). The clamp system and sample stage were adjustable to ensure the femoral shaft was 10° to the horizontal plane and that the femoral neck was internally rotated at 15° , as in Figure 4.2 (D). A sheet of rubber (RS Pro black rubber sheet, 506-3078, RS Components, Dublin) was placed under the trochanter on the sample stage to prevent crushing of the femoral head during testing as previously suggested (Figure 4.2 (C)) (Backman, 1957). The compressor head was also created using aluminium with a polyethylene tip (Figure 4.2 (C)) to avoid sliding when in contact with the femoral head. Femoral heads were compressed until failure (Zwick 2.5 kN load cell, 5 N pre-load, 2 mm/min crosshead speed) and force-displacement curves were obtained. From the force-displacement curves maximum load, stiffness, toughness and post-yield displacement were measured. Notably, the displacement that occurs between yield and failure and can reflect whether a material behaved in a brittle or ductile manner (Jepsen et al., 2015).

Micro-CT derived finite element analysis (μ FEA)

Image-based finite element (FE) models were generated using methods taken from Verbruggen *et al.* (Verbruggen and McNamara, 2023), whereby DICOM images of a subset ($n = 5-6$, per condition, per age excluding 26-week cohort) of proximal femurs were imported to MIMICS (18.0, Materialise, Belgium). Femur geometry was separated from floating artefacts, a smoothing factor of 0.4 was applied. The models were discretised using $\sim 1,100,000$ 4-noded tetrahedral elements (C3D4) using 3matic software (10.0, Materialise, Belgium). A maximum edge length of 0.15 mm was applied. Models assigned voxel-specific material properties based on a power-law (Schileo et al., 2008) elastic-density relationship (Equation 4.3 – 4.5), with parameters calibrated based on experimental force-displacement data, enabling specimen-

specific predictions of tissue-level strain at failure. Each model was mapped with 100 materials, where the bone mineral density obtained via Micro-CT (ρ_{CT}) were converted to ash density (ρ_{Ash}) and then to Elastic modulus (E) (Keller, 1994; Lu et al., 2019; Schileo et al., 2008), with Poisson's ratio assumed as 0.3 (Cheong et al., 2020; Verbruggen and McNamara, 2023).

$$\rho_{CT} = -0.0056148 + 0.0007764 \text{ HU} \quad (4.3)$$

$$\rho_{Ash} = 0.079 + (0.8772 * \rho_{CT}) \quad (4.4)$$

$$E = 10.5 * (\rho_{Ash}^{2.29}) \quad (4.5)$$

A sideways fall test was simulated using Abaqus software (Dassault Systems, version 2017) through displacement-based loading of a rigid plate in contact with the femoral head, similar to the experimental test. Proximal femurs were fixed in all directions at the bottom and lesser trochanter (Figure 4.3) similar to the experimental set-up. The maximum principle strain at the 99th percentile was recorded to remove any singularity effects and contour plots of the strain distributions were analysed.

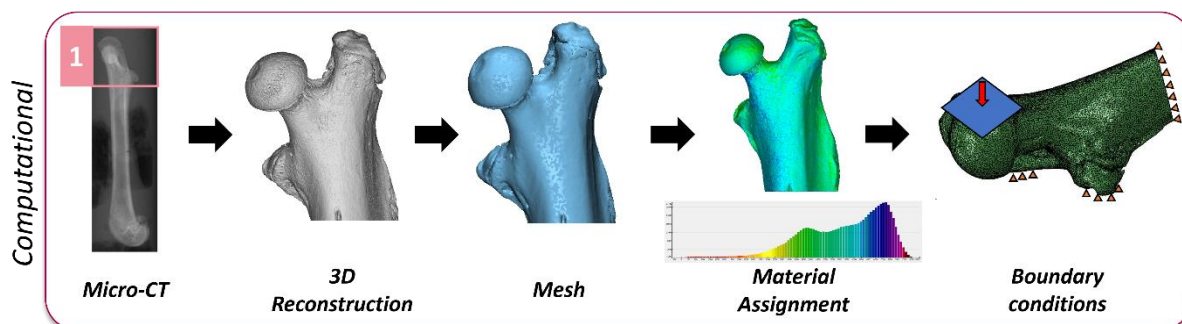


Figure.4 3. FE modelling pathway from micro-CT to sideways fall simulation in Abaqus. The proximal femur was CT-scanned, segmented and reconstructed to obtain a 3D solid model of the proximal femur. DICOMS were obtained and imported into MIMICS and 3-Matic software to process the femurs, apply a tetrahedral mesh and assign material properties to the elements (y-axis of material assignment graph) based on Hounsfield units (HU) (x-axis of material assignment graph). This model was imported into Abaqus, boundary conditions were applied, the femoral head was compressed to concentrate the stress at the femoral neck.

4.3 Statistical Analysis

Normality and homogeneity of variances for all geometrical, biomechanical and compositional data were analysed using a Shapiro-Wilk test and homogeneity of variance was analysed with Levene's test using R statistical software (version R-4.1.0). Where normality and variance were

not a concern, two-way ANOVA tests were carried out to (1) compare differences between each strain, followed by a multiple comparisons Bonferroni test and (2) compare differences within each strain across the different ages (12-, 26- and 46-weeks), followed by a multiple comparisons Tukey test (GraphPad Software, Inc., La Jolla, CA). If normality and variance was a concern, a Kruskal-Wallis test was used followed by the non-parametric Dunn's test to provide the adjusted p -value. Alpha levels of $p \leq 0.05$ were considered significant for a 95% confidence interval. The coefficients of correlation were calculated by Pearson's method. Data are represented as mean \pm standard deviation.

4.4 Results

4.4.1 Bone Turnover and Metabolism – Serum Analysis

Alterations at the cellular-level possibly indicative of systemic changes in the T2D (fa/fa) cohort

Bone turnover markers were measured from the serum to assess biological changes during long-term T2D, and results are shown in Figure 4.4 and Appendix Table S4.1. While there was no difference in the ratio of HbA1c/ HbA1 between strains at 12- and 26-weeks of age, the ratio of HbA1c/ HbA1 significantly increased with age in the T2D (*fa/fa*) cohort, but not the controls (Figure 4.1 (A)). This ratio was 2-fold ($p < 0.05$) greater in the 46-week diabetic rats than their age-matched healthy counterparts, highlighting that glycaemic control was considerably impaired with the long-term diabetic (*fa/fa*) cohort. There was no change in the levels of P1NP, a marker of bone formation, with age for the controls. However, P1NP levels declined (-58.9%, $p < 0.01$) with age from 12- to 46-weeks in the diabetic (*fa/fa*) cohort and were 36.3% and 43.4% ($p < 0.01$) lower than controls at 26- and 46-weeks, respectively (Figure 4.1 (D)). Similarly, levels of CTX-I, a marker of bone resorption, remained unchanged in the control rats, whilst in the T2D (*fa/fa*) cohort CTX-I levels increased 2-fold ($p < 0.001$) from 26- to 46-weeks and by 46-weeks diabetic (*fa/fa*) rats had 2-fold ($p < 0.01$) greater CTX-I than age-matched controls (Figure 4.1 (E)). Interestingly, the concentration of Sost in the serum was significantly higher at all ages in the T2D (*fa/fa*) rats than the controls ($p < 0.001$) and significantly increased with age whilst in the controls there was no change with age (Figure 4.1 (F)). Similarly, serum calcium levels were elevated at all ages in the T2D (*fa/fa*) rats in comparison to the controls (Figure 4.1 (B)). Lastly, the diabetic (*fa/fa*) rats at 26- and 46-weeks had 1.5- and 2-fold ($p < 0.05$) higher serum levels of IL-6 than age-matched controls,

respectively. Together these results provide evidence to suggest alterations in bone formation at the systemic level within the T2D (*fa/fa*) rats (Figure 4.1 (C)).

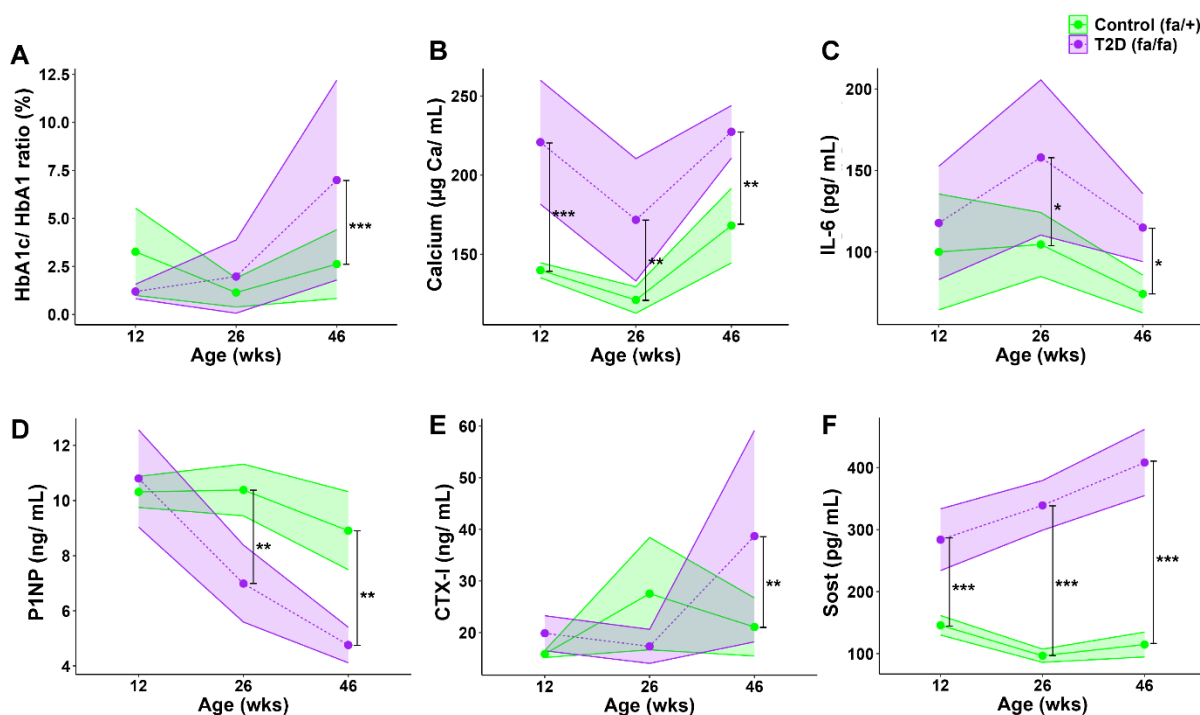


Figure 4.4. Cellular metabolism markers measured from serum to explore glycaemic control measuring (A) HbA1c/ HbA1 ratio, general health measuring (B) Calcium and (C) IL-6 and bone turnover by measuring (D) P1NP, (E) CTX-I and (F) Sost from control and T2D (*fa/fa*) rats. * ($p < 0.05$), ** ($p < 0.01$) and *** ($p < 0.001$) significance between strains.

4.4.2 Organic Matrix Composition – Bulk fAGEs and HPLC

Glycation markers, Furosine and CML were elevated in long-term diabetic (fa/fa) rats

Bulk fAGEs, furosine and CML were measured to assess the accumulation of AGE crosslinks, early-stage glycation and glycoxidative damage, respectively. There was no difference between strains at any age in the levels of cortical bulk fAGEs (Figure 4.5 (A)). The levels of Furosine were 1.3- and 2.1-fold higher in the diabetic (*fa/fa*) rats than the controls at 12- ($p = 0.005$) and 46-weeks ($p < 0.001$) of age, respectively. Furosine significantly increased by 82.13% ($p < 0.001$) from 12- to 46-weeks in the diabetic rats, but no change with age was observed in the controls (Figure 4.5 (B)). There was no difference in CML levels between strains at 12-weeks of age and at 46-weeks, there was a non-significant trend towards a 1.2-fold ($p = 0.06$) increase in the diabetic (*fa/fa*) cohort compared to age-matched controls. There was no change with age for both strains (Figure 4.5 (C)).

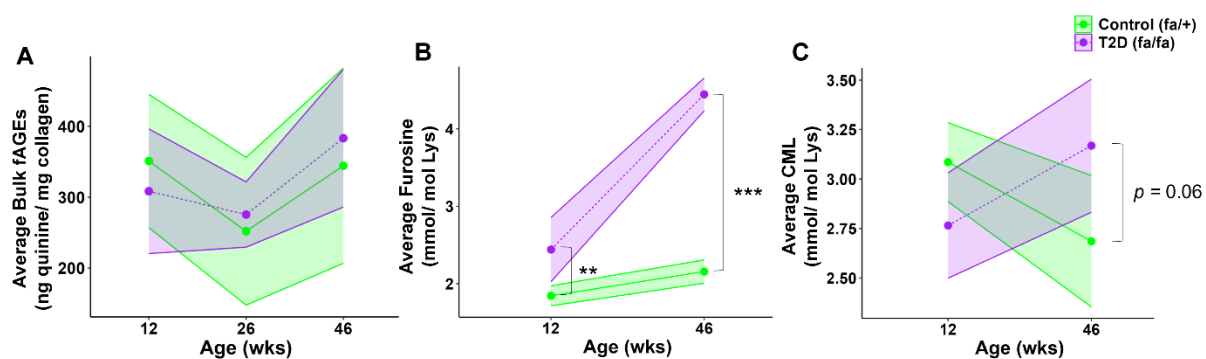


Figure 4.5: (A) No change in bulk fAGEs. (B and C) Furosine increased with age in T2D (fa/fa) rats. (B) Furosine levels elevated in these rats at all ages, while (C) CML showed a trend towards an increase in long-term T2D (fa/fa) rats. ** ($p < 0.01$) and *** ($p < 0.001$) significance between strains.

4.4.3 Bone Microarchitecture – Micro-CT Analysis

Trabecular bone quantity declined in diabetic (fa/fa) rats as the disease progressed and was particularly lower than controls in long-term diabetic (fa/fa) rats

Micro-CT was used to assess trabecular bone morphology and mineral density from the femoral neck region, with all results shown in Table 4.2. Trabecular bone mineral density (Tb.BMD), which is an apparent measure of density of the bone tissue and marrow, reduced from 12- to 46-weeks in the diabetic (fa/fa) rats reducing by 49.4% ($p < 0.001$). As expected, controls had no significant reduction from 12- to 46-weeks (-2.4%, $p = 0.85$). Although Tb.BMD was not different between strains at 12-weeks, diabetic (fa/fa) rats had significantly lower Tb.BMD at 26- (-25.1%, $p < 0.001$) and 46-weeks (-48%, $p < 0.001$) in comparison to the age-matched controls. Trabecular bone volume per the total volume (Tb.BV/TV) (Figure 4.6 (D)) also showed no difference with age from 12- to 46-weeks in controls, whereas diabetic (fa/fa) rats had significant differences (-55.1%, $p < 0.001$), being 34.2% and 52.2% ($p < 0.001$) lower than age-matched controls at 26- and 46-weeks, respectively. As for Tb.TMD, which is the material measure of density for just the bone tissue, control and diabetic (fa/fa) rats showed a 2.5% ($p < 0.001$) and a 1.5% ($p = 0.02$) increase from 12- to 46-weeks, respectively. Interestingly, there was no difference in Tb.TMD between strains, although diabetic (fa/fa) rats at 46-weeks showed a trend towards a lower (1.3%, $p = 0.05$) Tb.TMD than their age-matched controls. At 46-weeks, the reduction in Tb.BMD and Tb.BV/TV (and trending reduction in Tb.TMD) in the diabetic (fa/fa) cohort may in part be explained by a reduced amount of trabecular tissue present, as evidenced by a reduction in trabecular number (Tb.N) (-35.1%, $p < 0.001$)

(Figure 4.6 (A)), trabecular thickness (Tb.Th) (-16.2%, $p < 0.001$) (Figure 4.6 (B)), connectivity density (Conn.D) (44.4%, $p < 0.001$) (Figure 4.6 (E)) and an increase in trabecular spacing (Tb.Sp) (+45.1%, $p < 0.01$) (Figure 4.6 (C)) in comparison to age-matched healthy controls. Lastly, structural model index (SMI) was measured to quantify the plate- versus rod-like trabeculae structure (where 0 is for parallel plates and 3 is for cylindrical rods, positive SMI indicates a convex surface and negative indicates a concave surface). At 12-weeks both strains had negative SMI values that were not significantly different, with these negative values indicating a more concave plate-like shape. As the controls aged, SMI remained mainly negative at 12- and 46-weeks maintaining a robust plate-like, concave structure, yet, as the T2D (*fa/fa*) cohort aged their SMI increased and became more positive, indicating a more rod-like, convex shape (Figure 4.6 (F)).

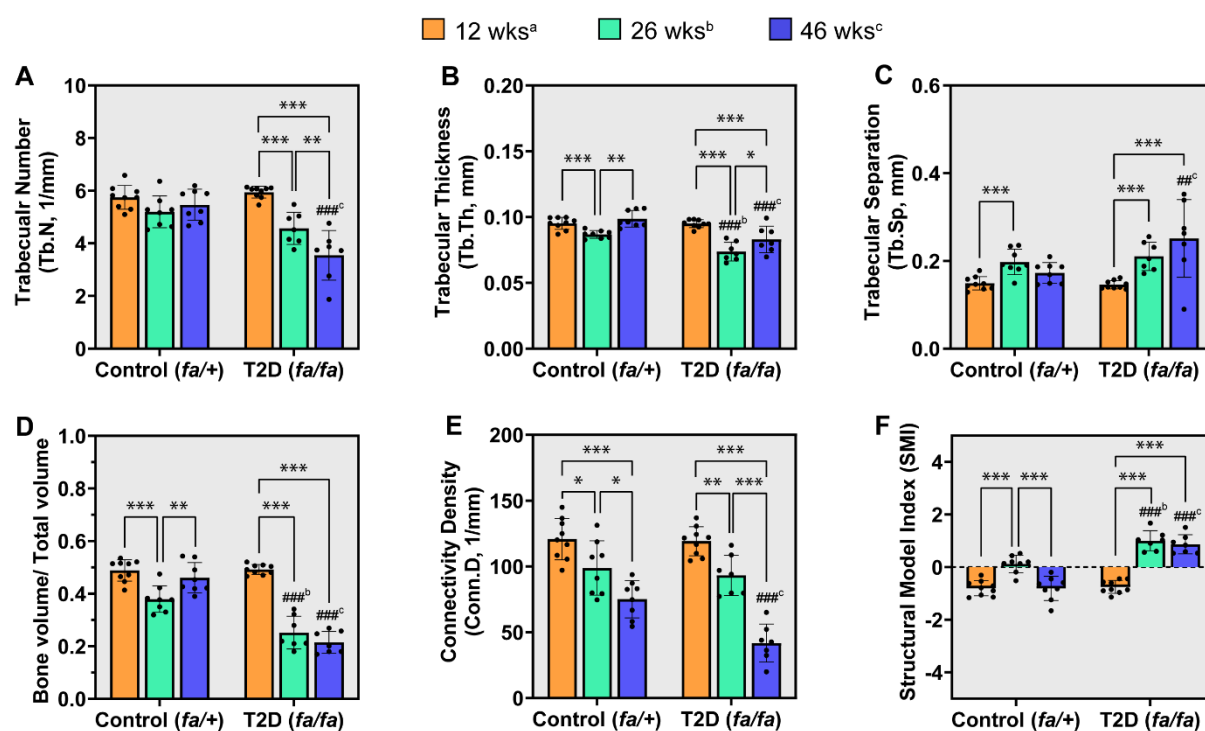


Figure 4.6. Morphological properties of trabecular bone from the femoral neck region such as (A) trabecular number, (B) trabecular thickness, (C) trabecular spacing, (D) bone volume/total volume, (E) connectivity density and (F) structural model index. * ($p < 0.05$), ** ($p < 0.01$) and *** ($p < 0.001$) significance within strain, # ($p < 0.05$), ## ($p < 0.01$) and ### ($p < 0.001$) significance between strain at 12^a, 26^b, and 46^c weeks.

Table 4.2. Trabecular and cortical bone morphological properties from the femoral neck and midshaft regions.

	Control (<i>fa/+</i>)			T2D (<i>fa/fa</i>)		
	12 weeks ^a (n = 9)	26 weeks ^b (n = 8)	46 weeks (n = 8)	12 weeks ^a (n = 9)	26 weeks ^b (n = 7)	46 weeks (n = 7)
<i>Femoral neck (trabecular)</i>						
Tb.BMD, mg HA/ cm ³	606.22 ± 42.28	515.36 ± 48.36 ^a	591.50 ± 67.87 ^b	607.27 ± 22.27	386.11 ± 74.29***, ^a	307.50 ± 67.77***, ^{a, b}
Tb.TMD, mg HA/ cm ³	1039.07 ± 9.74	1021.33 ± 18.19 ^a	1064.87 ± 9.58 ^{a, b}	1035.97 ± 6.44	1031.85 ± 6.22	1051.35 ± 11.25 ^{+, a, b}
Tb.BV/TV	0.49 ± 0.04	0.38 ± 0.05 ^a	0.46 ± 0.06 ^b	0.49 ± 0.02	0.25 ± 0.06***, ^a	0.22 ± 0.04***, ^a
Tb.N, 1/mm	5.75 ± 0.45	5.20 ± 0.60	5.47 ± 0.59	5.94 ± 0.22	4.57 ± 0.61 ^a	3.55 ± 0.95***, ^{a, b}
Tb.Th, mm	0.095 ± 0.005	0.087 ± 0.003 ^a	0.099 ± 0.006 ^b	0.095 ± 0.003	0.074 ± 0.007***, ^a	0.083 ± 0.01***, ^{a, b}
Tb.Sp, 1/mm	0.149 ± 0.015	0.197 ± 0.029 ^a	0.173 ± 0.024	0.145 ± 0.009	0.211 ± 0.033 ^a	0.251 ± 0.089***, ^a
Conn.D, 1/mm ³	120.77 ± 15.65	98.78 ± 20.66 ^a	75.08 ± 14.17 ^{a, b}	119.17 ± 11.02	93.23 ± 15.25 ^a	41.78 ± 14.42***, ^{a, b}
SMI	-0.80 ± 0.29	0.12 ± 0.33 ^a	-0.81 ± 0.46 ^b	-0.75 ± 0.25	1.01 ± 0.38***, ^a	0.87 ± 0.36***, ^a
<i>Femoral neck (cortical)</i>						
Ct.BMD, mg HA/ cm ³	970.67 ± 26.48	1079.47 ± 14.07 ^a	1106.66 ± 11.84 ^{a, b}	965.03 ± 18.12	1071.88 ± 7.67 ^a	1090.30 ± 9.33 ^a
Ct.TMD, mg HA/ cm ³	1060.35 ± 13.38	1121.62 ± 14.16 ^a	1147.29 ± 12.96 ^{a, b}	1058.65 ± 13.83	1122.18 ± 8.17 ^a	1150.40 ± 10.25 ^{a, b}
Ct.BV/TV, %	0.89 ± 0.023	0.95 ± 0.004 ^a	0.96 ± 0.002 ^a	0.88 ± 0.014	0.95 ± 0.006 ^a	0.94 ± 0.007*, ^a
Ct.Th, mm	0.29 ± 0.03	0.49 ± 0.02 ^a	0.48 ± 0.02 ^a	0.27 ± 0.02	0.41 ± 0.04***, ^a	0.35 ± 0.03***, ^{a, b}
Ct.Ar, mm ²	2.21 ± 0.14	2.92 ± 0.16 ^a	2.98 ± 0.17 ^a	2.19 ± 0.07	2.54 ± 0.07***, ^a	2.34 ± 0.14***, ^b
Ct.Po, %	4.8 ± 0.3	5.1 ± 0.3	5.0 ± 0.4	4.8 ± 0.3	5.5 ± 0.4	5.5 ± 0.4*, ^a
<i>Femoral midshaft (cortical)</i>						

Ct.BMD, mg HA/ cm ³	1114.95 ± 6.98	11.92.70 ± 11.04 ^a	1221.33 ± 11.11 ^{a, b}	1106.28 ± 14.51	1185.08 ± 11.78 ^a	1217.45 ± 8.49 ^{a, b}
Ct.TMD, mg HA/ cm ³	1144.87 ± 9.12	1214.31 ± 11.26	1240.95 ± 10.63	1136.78 ± 13.74	1211.57 ± 12.40 ^{**} , a, b	1246.65 ± 7.94 ^{a, b}
Ct.BV/TV, %	0.970 ± 0.007	0.982 ± 0.001 ^a	0.984 ± 0.003 ^a	0.969 ± 0.008	0.977 ± 0.002 ^a	0.977 ± 0.003 [*] , a
Ct.Th, mm	0.48 ± 0.05	0.72 ± 0.02	0.74 ± 0.10	0.43 ± 0.04	0.61 ± 0.04 ^{***} , a	0.56 ± 0.02 ^{***} , a
Ct.Ar, mm ²	5.09 ± 0.20	6.97 ± 0.40	8.28 ± 0.49	5.12 ± 0.24	5.96 ± 0.31 ^{***} , a	5.81 ± 0.31 ^{***} , a, b
Ct.Po, %	8.62 ± 0.68	8.36 ± 0.52	7.70 ± 0.52 ^a	8.19 ± 0.63	8.09 ± 0.54	8.67 ± 1.02 [*]

Values are mean ± SD. T2D, Type-2 diabetic; BMD, Bone mineral density; TMD, Tissue mineral density; BV/TV, Bone volume/ Total volume; Tb.N, Trabecular number; Tb.Th, Trabecular thickness; Tb.Sp, Trabecular spacing; Conn.D, Connectivity density; SMI, Structural model index; DA, Degree of Anisotropy; Ct.Ar, Cortical area; Ct.Po, Cortical porosity.

Difference from aged matched lean control (*fa*/+) rats with * ($p < 0.05$), ** ($p < 0.01$), *** ($p < 0.001$) and + (*trending influence*).

^a significantly different from 12-weeks determined by a multiple comparisons Tukey test

^b significantly different from 26-weeks determined by a multiple comparisons Tukey test

As the disease progressed, diabetic (fa/fa) rats demonstrated less cortical bone, with reduced thickness and increased porosity in comparison to the controls

Cortical bone micro-CT scans were analysed to assess microstructure and mineral density from the femoral neck and midshaft region (Table 4.2). There was no difference found in cortical bone mineral density (Ct.BMD) from the femoral neck and midshaft regions between strains at all ages. Whilst there was no difference between strains, cortical tissue mineral density (Ct.TMD) from the femoral neck and midshaft increased with age for both T2D (*fa/fa*) (neck: +8.7%, midshaft: +9.7%) ($p < 0.001$) and control rats (neck: +8.2%, midshaft: 8.4%) ($p < 0.001$). Femoral neck and midshaft cortical bone volume per total volume (Ct.BV/TV) were found to increase with age for both strains, however, by 46-weeks, T2D (*fa/fa*) rats had a 2.1% and 0.7% reduction in Ct.BV/TV in comparison to age-matched healthy controls ($p = 0.02$), respectively (Figure 4.7 (A) & (D)). This reduction in Ct.BV/TV also coincided with a 10% and 12.6% ($p = 0.03$) increase in cortical porosity (Ct.Po) in the long-term diabetic (*fa/fa*) rats in comparison to the age-matched controls within the femoral neck and midshaft region, respectively (Figure 4.7 (C) & (F)). Cortical bone was also thinner in the diabetic (*fa/fa*) rats at 26- and 46-weeks of age, with a 16.3% and a 27.1% reduction ($p < 0.001$) in cortical thickness (Ct.Th) at the femoral neck region (Figure 4.7 (B)) and a 15.3% and 24.3% ($p < 0.001$) reduction in midshaft thickness, respectively (Figure 4.7 (E)). Cortical area (Ct.Ar) was also smaller in the 26- and 46-week old diabetic (*fa/fa*) rats, with femoral neck Ct.Ar being 13% and 21.5% smaller (Figure 4.7 (C)) and midshaft Ct.Ar being 14.5% and 29.8% smaller in comparison to the age-matched controls, respectively.

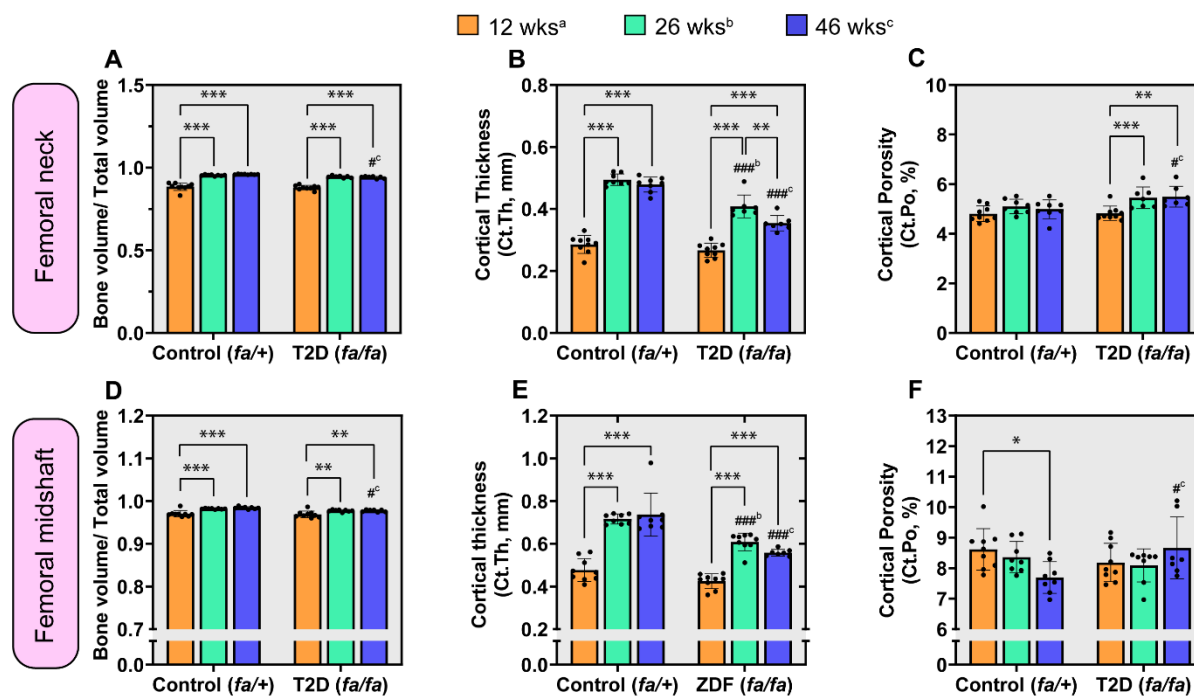


Figure 4.7. Microarchitectural properties measured from micro-CT of the cortical bone from the (A-C) femoral neck and (D-F) midshaft region, measuring (A & D) bone volume per total volume, (B & E) cortical thickness and (C & F) cortical porosity. * ($p < 0.05$), ** ($p < 0.01$) and *** ($p < 0.001$) significance within strain, # ($p < 0.05$), ## ($p < 0.01$) and ### ($p < 0.001$) significance between strain at 12^a, 26^b, and 46^c weeks.

4.4.4 Bone Mineralisation – BMDD Analysis

Although trabecular and cortical bone quantity was reduced, no change found in mineralisation of bone from the femoral neck region

Bone mineral density distribution (BMDD) analysis was carried out to examine bone mineralisation in the femoral neck and midshaft region (data in Appendix Table S4.1). Interestingly, although there was less trabecular (\downarrow Tb.BMD, \downarrow Tb.BV/TV) and cortical bone (\downarrow Ct.BV/TV, \downarrow Ct.Ar) present in the T2D (*fa/fa*) rats particularly at 46-weeks (as described in the previous Section), there was no difference in mineral distribution (TV₂₅, TV₅₀, TV₇₅) (Figure 4.8 & 4.9 (D-F)) or heterogeneity (FWHM) at any age (Figure 4.8 & 4.9 (C)). However, it was found that the T2D (*fa/fa*) cohort had a greater reduction with age in tissue volume at low mineral density of cortical bone from the femoral neck than the controls, reducing by 27.8% ($p < 0.05$) from 12- to 46-weeks in the controls and 40% ($p < 0.001$) in the diabetic (*fa/fa*) group (Figure 4.8 (D)).

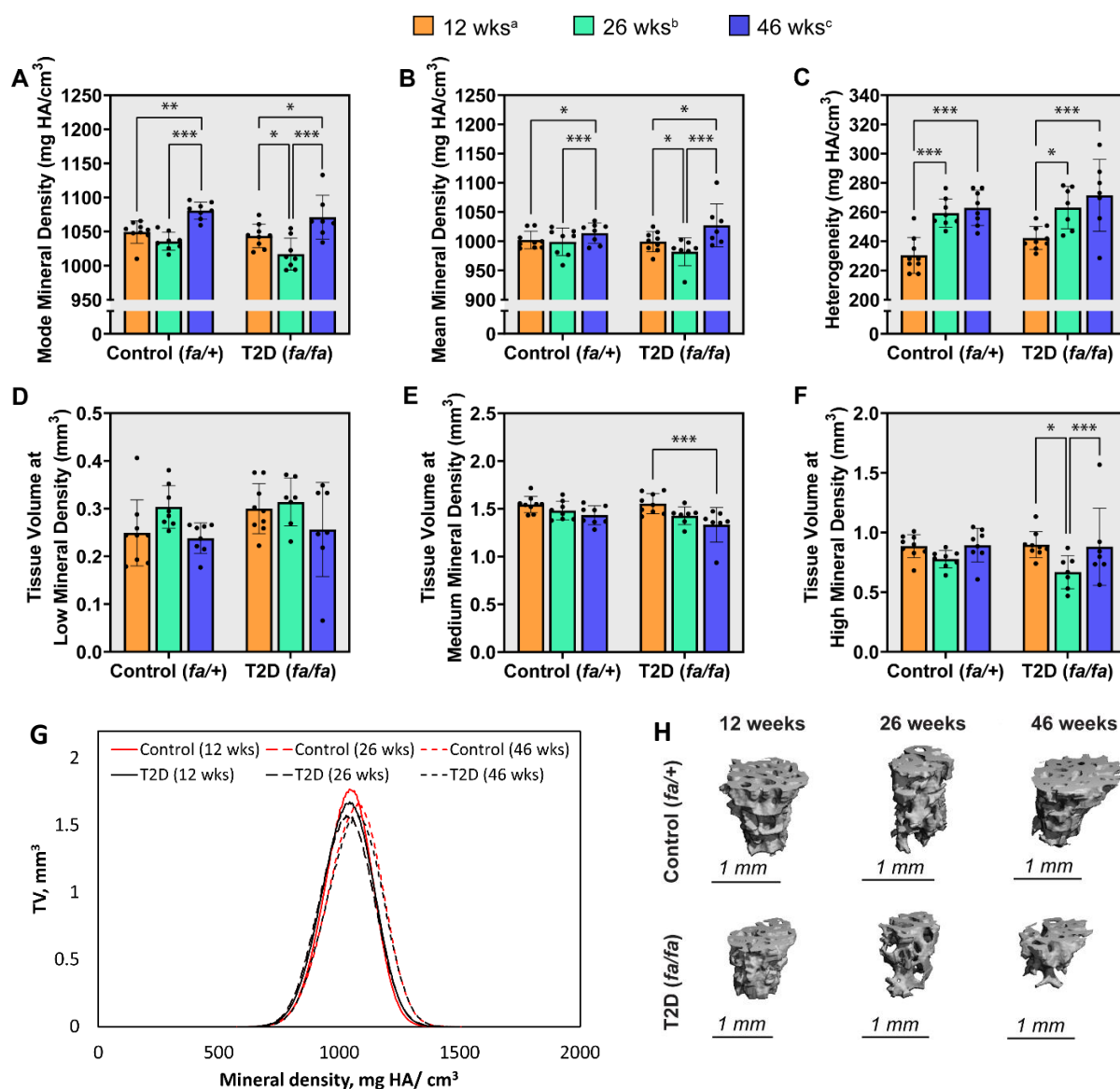


Figure 4.8. (A) Mode mineral density, (B) mean mineral density, (C) heterogeneity, (D) tissue volume at low mineral density, (E) tissue volume at medium mineral density and (F) tissue volume at high mineral density measured from the analysis of the (G) bone mineral density distribution of the (H) trabecular bone from the femoral neck region. * ($p < 0.05$), ** ($p < 0.01$) and *** ($p < 0.001$) significance within strain.

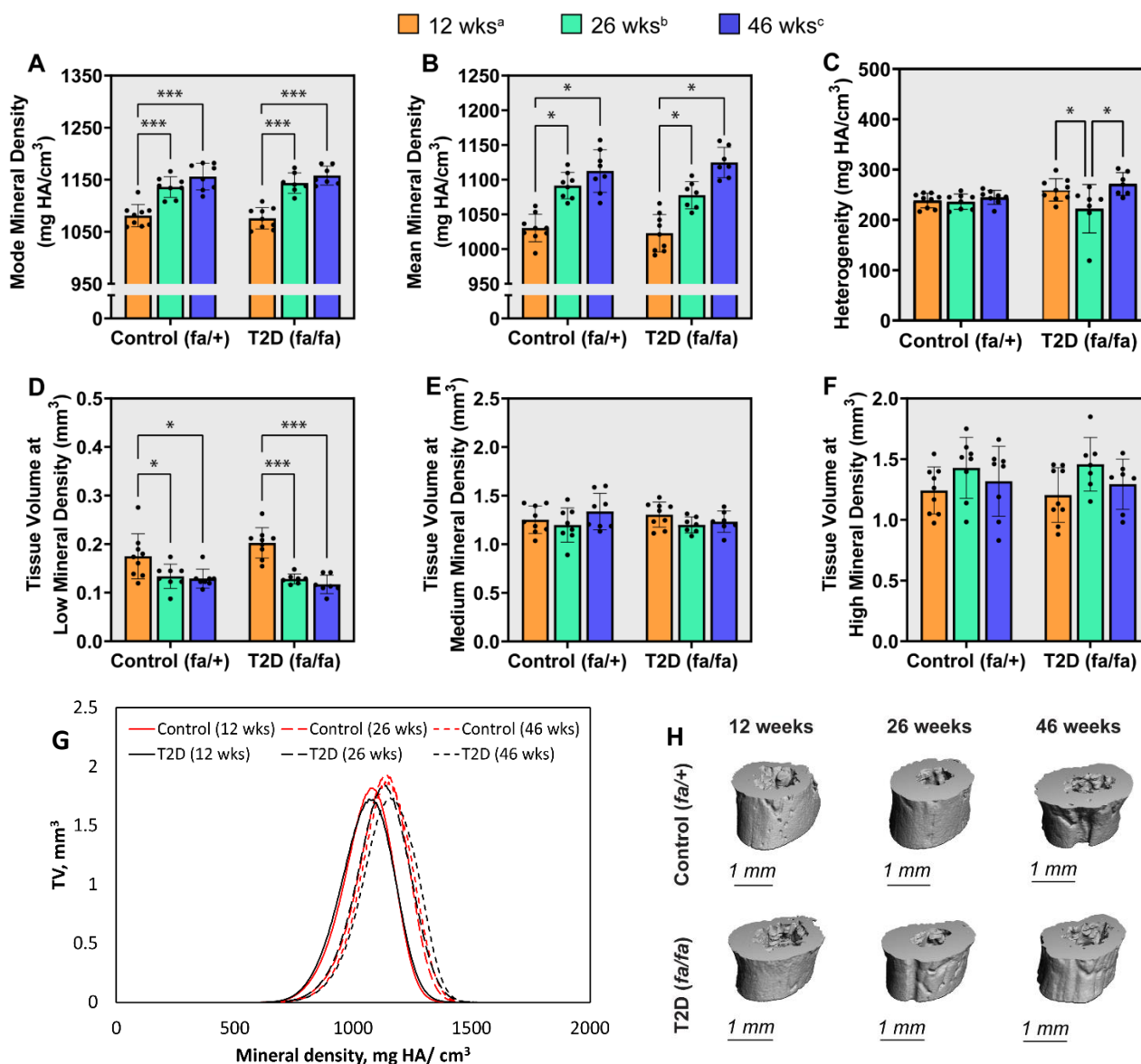


Figure 4.9. (A) Mode mineral density, (B) mean mineral density, (C) heterogeneity, (D) tissue volume at low mineral density, (E) tissue volume at medium mineral density and (F) tissue volume at high mineral density measured from the analysis of the (G) bone mineral density distribution of the (H) cortical bone from the femoral neck region. * ($p < 0.05$), ** ($p < 0.01$) and *** ($p < 0.001$) significance within strain.

BMDD analysis of cortical bone from the midshaft indicated altered mineral distribution and heterogeneity, particularly as the disease progressed

BMDD analysis of cortical bone from the femoral midshaft showed no difference in mode or mean mineral density between strains at any age (Figure 4.10 (A) & (B)), yet certain alterations to mineral distribution were found. At 12-weeks, T2D (fa/fa) rats had a 71.4% ($p < 0.05$) higher volume of tissue at low mineral density (TV₂₅) than age-matched controls. While there was no

change in TV₂₅ with age, the T2D (*fa/fa*) cohort showed a 50% ($p < 0.001$) reduction from 12- to 46-weeks (Figure 4.10 (D)). Similarly, the volume of tissue at high mineral density (TV₇₅) remained largely the same from 12- to 46-weeks for the controls, whereas the diabetic (*fa/fa*) rats exhibited a trend towards a reduction (-17.4%, $p = 0.09$) in TV₇₅ and by 46-weeks, diabetic (*fa/fa*) rats displayed a trending decrease (-19%, $p = 0.07$) in the volume of tissue present at high mineral density (Figure 4.10 (F)). Whilst there was no difference in tissue volume at medium mineral density (TV₅₀), it was found that TV₅₀ increased with age for the controls, whereas no difference with age was demonstrated for the diabetic (*fa/fa*) cohort (Figure 4.10 (E)). Interestingly, heterogeneity increased with age for the control cohort but not the diabetic, where diabetic (*fa/fa*) heterogeneity was 8.2% ($p < 0.05$) higher than controls at 12-weeks and 12% ($p < 0.001$) lower than controls at 46-weeks. (Figure 4.10 (C)).

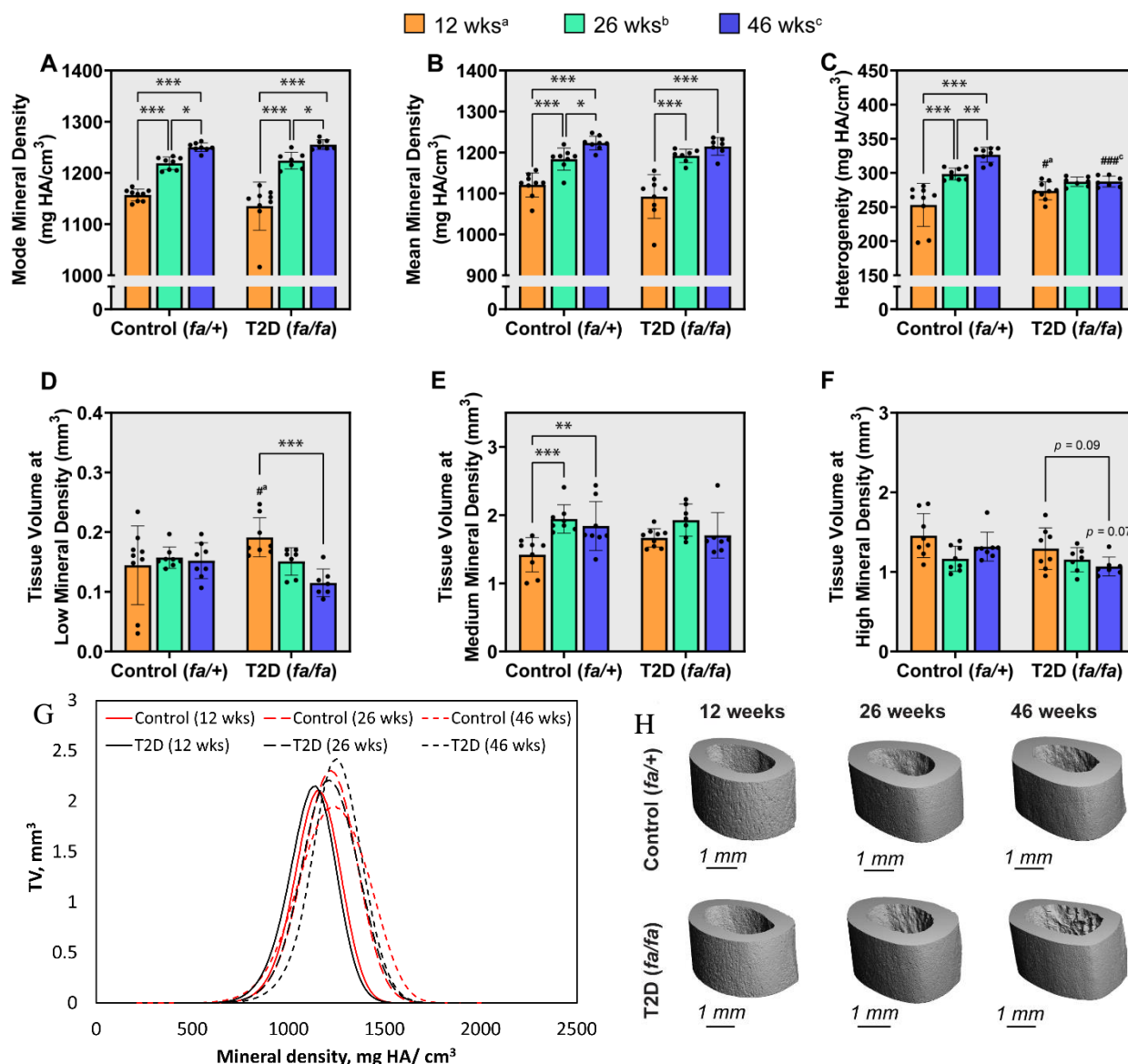


Figure 4.10. (A) Mode mineral density, (B) mean mineral density, (C) heterogeneity, (D) tissue volume at low mineral density, (E) tissue volume at medium mineral density and (F) tissue volume at high mineral density measured from the analysis of the (G) bone mineral density distribution of the (H) cortical bone from the midshaft region. * ($p < 0.05$), ** ($p < 0.01$) and *** ($p < 0.001$) significance within strain, # ($p < 0.05$), ## ($p < 0.01$) and ### ($p < 0.001$) significance between strain at 12^a, 26^b, and 46^c weeks.

4.4.5 Biomechanical Analysis

During fracture toughness testing, once a crack had been initiated, less energy was required to propagate the crack to failure in the long-term diabetic (fa/fa) rats

A fracture toughness test was carried out to assess critical stress intensity at crack initiation (K_{Ic}). Cracking toughness was also measured as a reflection of the energy to propagate a crack.

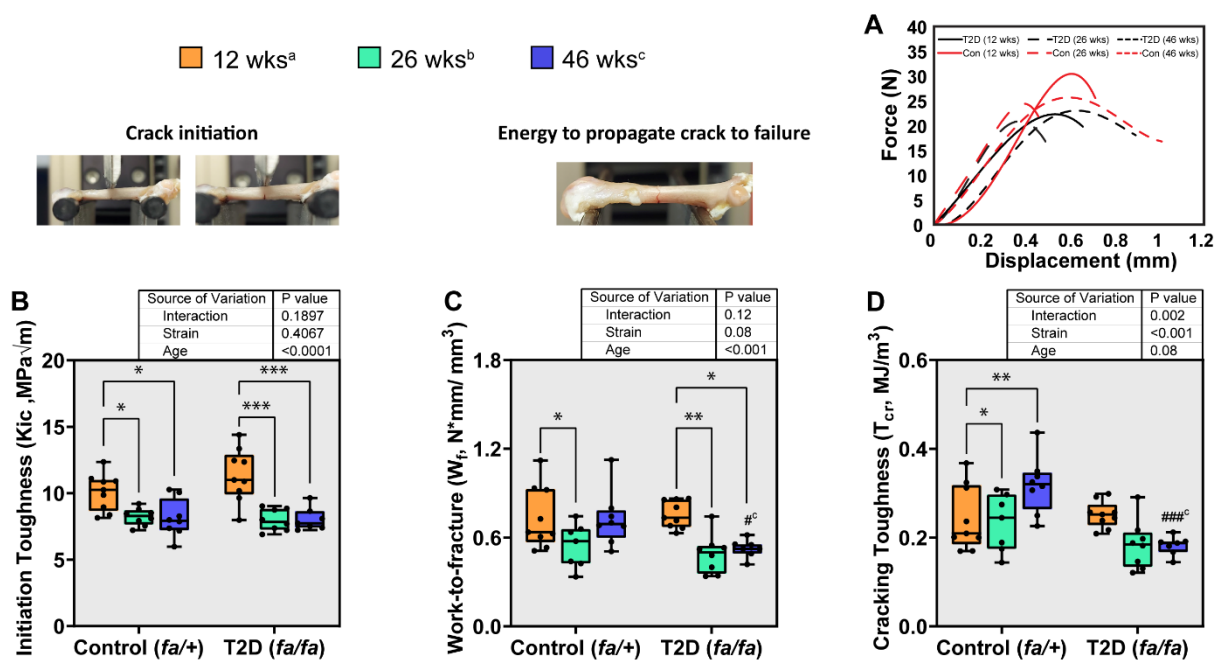


Figure 4.11. (A) Average load-displacement curves (per age, per strain) after fracture toughness testing used to measure (B) stress intensity factor at crack initiation, (C) work-to-fracture and (D) cracking toughness. * ($p < 0.05$), ** ($p < 0.01$) and *** ($p < 0.001$) significance within strain, # ($p < 0.05$), ## ($p < 0.01$) and ### ($p < 0.001$) significance between strain at 12^a, 26^b, and 46^c weeks.

There was no difference between strains at any age in initiation toughness (K_{Ic}), however, K_{Ic} significantly reduced with age from 12- to 46-weeks for both T2D (fa/fa) (-29.2%, $p < 0.001$) and control (-19.5%, $p = 0.02$) rats (Figure 4.11 (B)). Diabetic (fa/fa) rats demonstrated a 30.6% reduction ($p = 0.01$) in work-to-fracture (W_f) with age from 12- to 46-weeks, whereas controls did not (-1.4%, $p > 0.99$). At 46-weeks, W_f was 1.4-fold ($p = 0.04$) lower in the T2D (fa/fa) cohort than their age-matched healthy controls (Figure 4.11 (C)). At 46-weeks, T2D (fa/fa) rats had a significantly lower cracking toughness (T_{cr}) than age-matched controls, demonstrating a 42.8% reduction ($p < 0.001$) and a significant interaction between strain and age (Variation = 18.61%, $p = 0.002$) (Figure 4.11 (D)). This highlights that although the stress intensity factor required to form a crack was not different between strains at 46-weeks, once a crack had been initiated less energy was required to propagate the crack to failure in the long-term diabetic (fa/fa) rats with respect to the healthy controls.

During sideways fall testing, as the disease progressed in the diabetic (*fa/fa*) rats post-yield displacement became impaired, indicating more brittle tissue behaviour.

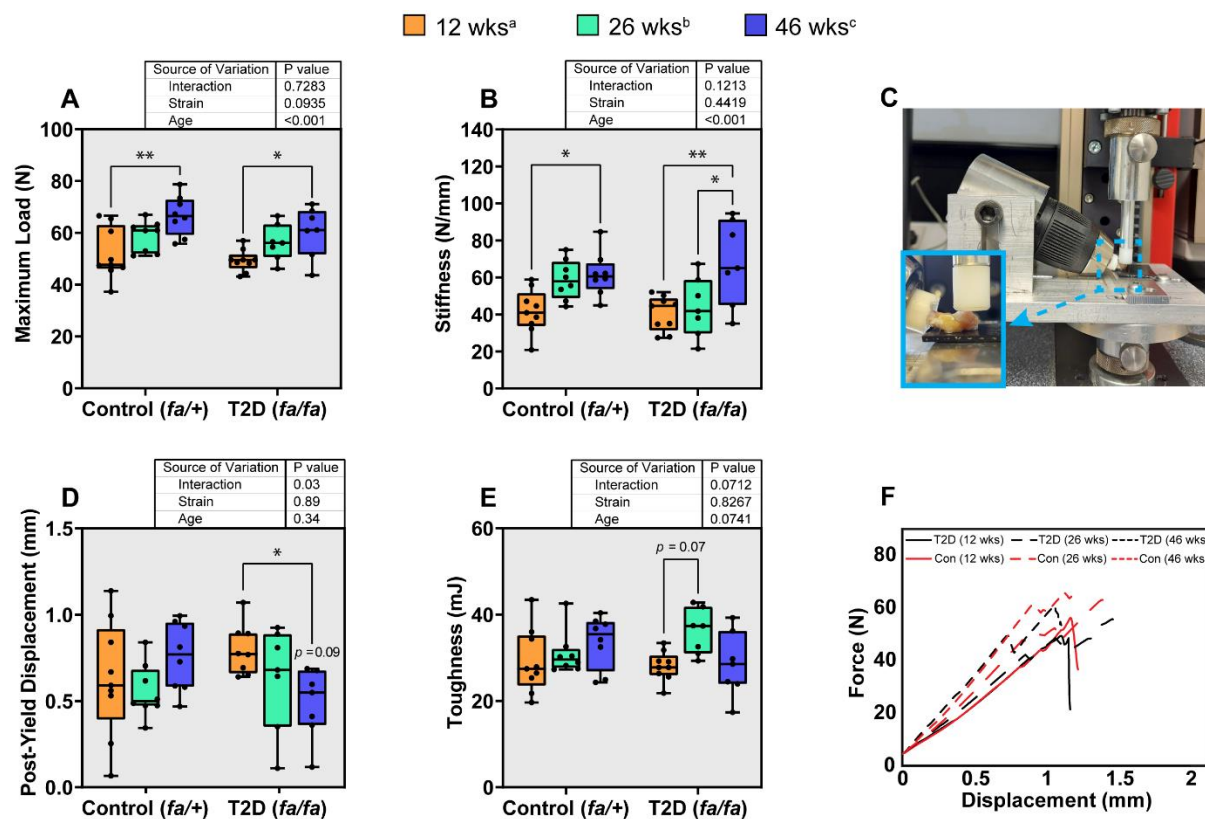


Figure 4.12. Sideways fall testing used to examine (A) maximum load, (B) stiffness, (D) post-yield displacement and (E) toughness of the femoral neck using a (C) custom-made rig where (F) average force-displacement curves were generated. * ($p < 0.05$), ** ($p < 0.01$) and *** ($p < 0.001$) significance within strain.

Femoral heads were compressed in a sideways configuration using a custom-made rig to simulate a fall scenario. Both strains showed an increase in maximum load with age. However, control rats had a 1.3-fold greater increase with age than the T2D (*fa/fa*) cohort, with the increased difference from 12- to 46-weeks being 14.86 ± 2.43 N ($p < 0.01$) for controls and 11.05 ± 5.5 N ($p = 0.03$) for T2D (*fa/fa*) rats (Figure 4.12 (A)). Stiffness also increased with age for both strains. Again, no difference was found between strains, however, T2D (*fa/fa*) rats had a 1.4-fold greater increase in stiffness with age than the controls, with the increase difference from 12- to 46-weeks being 20.1 ± 0.03 N ($p < 0.01$) for controls and 27.6 ± 13.4 N ($p = 0.03$) for T2D (*fa/fa*) rats (Figure 4.12 (B)). Interestingly, controls showed no difference in post-yield displacement (PYD) with age, yet T2D (*fa/fa*) rats demonstrated a 38.8% ($p = 0.04$) reduction in PYD from 12- to 46-weeks and at 46-weeks showed a 1.6-fold

($p = 0.09$) trending decrease in PYD when compared to age-matched controls with the interaction between strain and age showing significance (Variation = 14.85%, $p = 0.03$) (Figure 4.12 (D)). There was no difference in toughness between strains or with age (Figure 4.12 (E)).

4.4.6 Micro-FE Analysis

Decreased strain distribution with age in the proximal femurs of T2D (fa/fa) rats and no change with age for controls (fa/+)

Finite element models simulated the sideways fall test and predicted the maximum principle strain at the point of failure, according to each of the experimental load-displacement curves (Figure 4.13). Contour plots of the maximum principle strain in one sample from each group at 12- and 46-weeks of age were modelled where regions of high maximum principle strain were predominantly concentrated transcervically along the femoral neck region (Figure 4.13 (B)). These regions of high strain coincided with the observed fracture patterns observed in the experimental tests. The distributions of maximum principle strain at failure were quantitatively compared across disease groups and age groups, as in Figure 4.13 (A). This analysis revealed tissue failure strain was significantly reduced in the diabetic (*fa/fa*) cohort from 12- to 46-weeks, indicating a more brittle behaviour with disease progression. However, there was no significant differences detected with age for the controls. No overt differences in strain distribution were discernible between T2 diabetic (*fa/fa*) and healthy age-matched controls (*fa/+*), indicating the tissue-level failure strain was not different between groups.

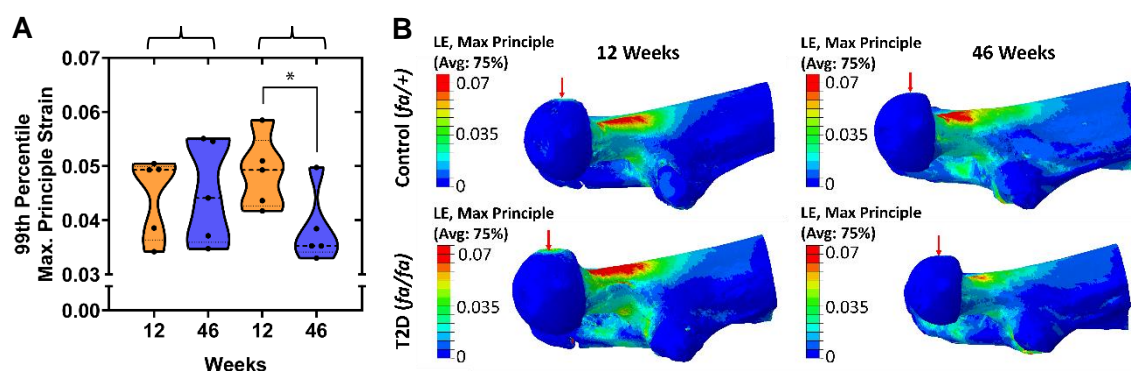


Figure 4.13. Micro-FE sideways fall simulation. (A) Maximum principle strain at the 99th percentile and (B) contour plots comparing the strain predictions for the proximal femurs of control (*fa/+*) and T2D (*fa/fa*) rats at 12- and 46-weeks. * ($p < 0.05$).

4.5 Discussion

This Chapter presents the first long-term longitudinal investigation of T2 diabetic bone fragility, revealing the sequence of biological, biophysical, and biomechanical events that could contribute to bone fragility in a ZDF (*fa/fa*) rat model for T2D. The full sequence of these observations is summarised in Figure 4.14, with further discussion of each stage presented below. Firstly, it was found that several cellular alterations took place within the diabetic (*fa/fa*) rat model over time. The diabetic (*fa/fa*) cohort had a lack of long-term glycaemic control, impaired homeostasis, and inflammation, particularly at 46-weeks, where this cohort had higher levels of HbA1c/HbA1 and IL-6 in comparison to controls. The diabetic state also disrupted bone metabolism and cell activity, with an increase in Sost levels with age and significantly higher levels of Sost than the controls at all ages, reduced serum P1NP levels at 26- and 46-weeks and higher CTX-I levels in the 46-week diabetic (*fa/fa*) rats. The disrupted cellular activity led to alterations in the organic bone matrix, especially in the late-stages (46-weeks) of the disease, where furosine, a marker for early-stage glycation, and CML, a non-fluorescing, non-crosslinking AGE and marker of glycoxidative damage, was higher than controls. Micro-CT analysis further revealed possible consequences to the diabetic bone morphology, evident by increased cortical porosity, thinner bone and reduced trabecular bone volume fraction. Cortical bone mineralisation was also affected, where heterogeneity was altered in the cortical femoral midshaft in addition to a reduction in TV_{low} and TV_{high} with age in the diabetic (*fa/fa*) cohort, but not controls. Together, these sub-tissue alterations coincided with deterioration of the fracture mechanics, with biomechanical testing showing significantly reduced cracking toughness and work-to-fracture in 46-week diabetic (*fa/fa*) rats, compared to controls. FEA revealed a reduction in maximum principle strain with age in the diabetic (*fa/fa*) cohort but not controls, which is notably similar to sideways fall test results, where reductions in PYD with age shown for the diabetic (*fa/fa*) rats but not controls from the sideways fall test. Overall, this Chapter provides novel insight into the pathophysiological mechanisms that lead to bone fragility in long-term T2D.

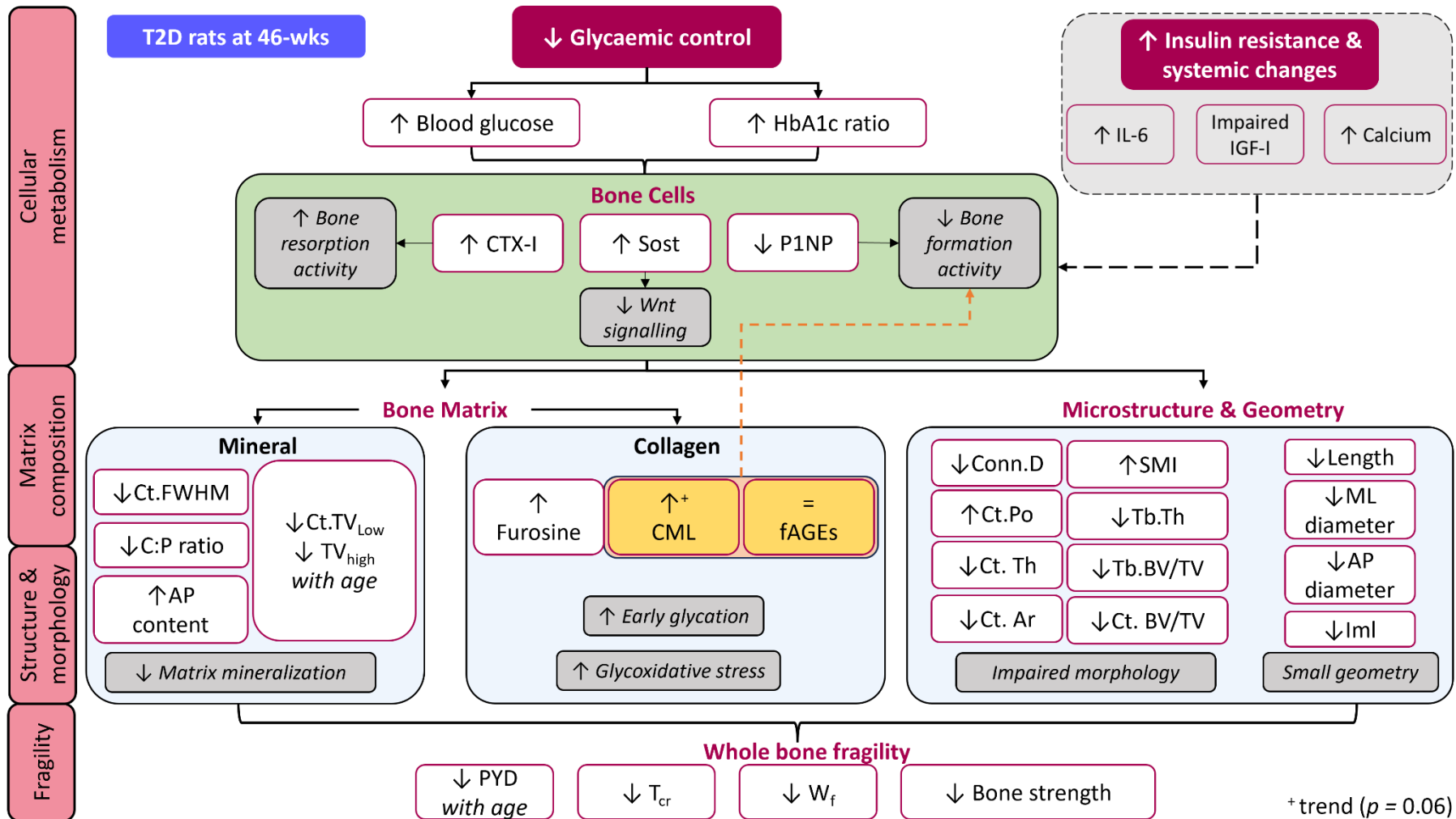


Figure 4.14. A combined summary results from Chapter 3 and 4 of the proposed sequence of alterations that occur from the cellular, to the sub-tissue, to the whole-bone biomechanical level that led to an increased fracture risk. Where ZDF (fa/fa) rat at 46-weeks of age presented with

impaired glycaemic control, impaired insulin resistance and a variety of systemic changes affected normal bone cell function. Particularly, SOST which was positively correlated to blood glucose levels and negatively correlated to serum PINP, ultimately indicating compromised osteoblast function. A reduction in heterogeneity, TV_{low} and TV_{high} with age in the diabetic (fa/fa) rats highlighted a reduction in bone forming cell activity as well as reduced matrix mineralisation which was also evident in the microstructure. It is less clear as to whether altered cellular metabolism led to increased glycoxidative damage or visa-versa. Altogether these factors are likely to have played a role in the diabetic whole bone fragility of these rats. However, CML and fAGEs are highlighted in yellow to show no significant difference between strains, making their role in the bigger picture of bone fragility in ZDF (fa/fa) rats questionable.

Bone turnover is tightly regulated by osteocytes and hormones to preserve the structural and compositional integrity of the tissue to ensure it can withstand high loads and optimally resist fracture. It is understood that T2D can have a direct effect on bone cells and disrupt bone maintenance, with human studies reporting reduced bone turnover in patients presenting with T2D (Lekkala et al., 2023; Piccoli et al., 2020; Purnamasari et al., 2017; Sassi et al., 2018; Wölfel et al., 2020). Whilst it is understood that an altered bone microarchitecture and composition could impair the mechanical integrity of the tissue, there is a limited understanding around the origins of microarchitectural and compositional changes in T2D to begin with. Moreover, altered bone turnover does not fully elucidate the physiological factors that contribute to bone fragility in this disease. A novel contribution of this work is that the downstream effects of an altered bone turnover and metabolism on the biomechanical properties of bone in diabetic (*fa/fa*) rats as the disease progresses with age was investigated, particularly, the influence it may have on bone microstructure and composition. In this Chapter, diabetic (*fa/fa*) rats develop a frank-like diabetic condition at 12-weeks of age and at this point they are deemed skeletally mature (Reinwald et al., 2009). At 12-weeks, diabetic (*fa/fa*) rats had similar serum levels of HbA1c/HbA1, P1NP, CTX-I and IL-6 as controls, however, serum sclerostin (Sost) and calcium were elevated. Calcium plays a pivotal role in insulin secretion and glucose homeostasis. It has been shown that increased circulating calcium is associated with impaired glucose metabolism and is involved in the development and maintenance of T2D (Lorenzo et al., 2014). Sost is a protein secreted by osteocytes that has an antagonistic effect on Wingless (Wnt) signalling and it is important in regulating bone cell functions (Delgado-Calle et al., 2017; Zákány and Duboule, 1993). Studies on patients with T2D reported increased level of Sost within the serum with both good and bad glycaemic control, and that it was correlated with increasing glycated haemoglobin (HbA1c) and insulin resistance (García-Martín et al., 2012; Piccoli et al., 2020). In this Chapter, Sost levels increased with age in the diabetic (*fa/fa*) cohort, and at 46-weeks glycaemic control was impaired. Pereira *et al* (2017) investigated the role of Sost in the pathogenesis of skeletal complications in ZDF (*fa/fa*) rats and concluded that the impaired microarchitecture and cellular turnover experienced in these rats was not correlated with changes in serum and bone sclerostin expression, however, this study was only carried out in ZDF (*fa/fa*) rats aged up to 14-weeks (diabetic for ~ 3 - 5 weeks). This Chapter explored serum Sost levels in ZDF (*fa/fa*) rats at 12- (at onset of frank diabetes), 26- (diabetic for ~15 - 17 weeks) and 46-weeks (diabetic for ~ 35 - 37 weeks). While no differences to Tb.BV/TV, Ct.BV/TV, Tb.Th, SMI or Ct.Ar were found between strains at 12-weeks, when faceted by age, it was found that these parameters were not correlated to serum

Sost (see Appendix Table S4.3). At 26- and 46-weeks, SOST was correlated negatively to Tb.BV/TV, Ct.BV/TV, Tb.Th, Ct.Ar and positively to SMI (see Appendix Table S4.3). In this Chapter, serum Sost was negatively correlated with serum P1NP (see Appendix Table S4.3). Hence, similar to Pereira *et al* (2017), results presented in this Chapter indicate that at 12-weeks or in the early stage of the disease, Sost does not play a major role in the pathogenesis of skeletal complications in ZDF (*fa/fa*) rats. However, as the disease progresses it is possible that Sost does begin to contribute to the alterations found in the cortical and trabecular microstructure, mainly by inhibiting osteoblastogenesis, as evidenced by a reduction in serum P1NP at 26- and 46-weeks. This is also confirmed in a study by Hamann *et al* (2011) which investigated bone regeneration *in-vivo* in ZDF (*fa/fa*) rats when a defect was created in the femoral midshaft. In their study, they reported a reduction in serum bone formation markers P1NP and osteocalcin as well as a reduced gene expression of Runt-related transcription factor 2 (RUNX2), osteopontin, bone morphogenic protein 2 (BMP-2) and osteocalcin in the diabetic (*fa/fa*) rats, which clearly indicates impaired osteoblast function, resulting in altered bone regeneration in the ZDF (*fa/fa*) rats.

It is thought that the hyperglycaemic state, increased inflammation, and oxidative stress leads to an increase in the formation of non-enzymatic AGEs in T2 diabetic bone. For the first time, the levels of furosine, CML and IL-6 were quantified from ZDF (*fa/fa*) rats at various stages of the disease. The levels of furosine were higher in the cortical bone from the femoral midshaft of T2D (*fa/fa*) rats at all ages in comparison to controls. While furosine is not an AGE, it is a product of the early stages of glycation that forms as a result of a series of non-enzymatic reactions between reducing sugars and amino acids or collagen proteins, known as the Maillard reaction. The exact role of IL-6 in the pathogenesis of T2D is not very clear since its effects on insulin sensitivity and glucose metabolism are quite tissue-dependent (Akbari and Hassan-Zadeh, 2018). However, elevated circulating levels of IL-6 have been shown to be indicative of chronic low-grade inflammation which is highly implicated with abdominal fat accumulation and obesity, a characteristic of the ZDF (*fa/fa*) strain (van Greevenbroek *et al.*, 2013). The role of IL-6 in the development of insulin resistance in T2D is yet to be elucidated, since literature to date has shown evidence of the deleterious effect of IL-6 on insulin activity (Lagathu *et al.*, 2003) while others have shown IL-6 to promote an anti-inflammatory effect and aid in glucose maintenance (Akbari and Hassan-Zadeh, 2018; Wallenius *et al.*, 2002). If one considers how T2D develops in the ZDF (*fa/fa*) rats, interestingly it is seen that these rats become obese at around 9-weeks of age and that from 7- to 10-weeks insulin levels are high

(Chen and Wang, 2005), which would explain why IL-6 levels were not different from controls at 12-weeks. However, it has been shown that by ~ 20-weeks, insulin levels fall (Peterson et al., 1990; Prisby et al., 2008) whereas in this Chapter, at 26-weeks, IL-6 levels are higher than controls. It is likely that in the ZDF (*fa/fa*) strain, obesity is driving a pro-inflammatory state evidenced by high circulating levels of IL-6, which may play a role leading to insulin resistance. Indeed, such circulating levels are found to be increased as insulin levels begin to decrease (Akbari and Hassan-Zadeh, 2018). Hence IL-6 may also be aiding in impaired glucose homeostasis, evidenced by a positive correlation to blood glucose and furosine within this study (see Appendix Figure S4.1 (A, B)).

In this Chapter, no differences in the levels of total fluorescent AGE crosslinks (fAGEs) between strains at any age were found. However, trending higher levels of CML, a non-crosslinking, non-fluorescent AGE, were observed in the T2D (*fa/fa*) rats at 46-weeks versus age-matched controls. This may be indicative of increased oxidative stress in the T2 diabetic cohort. This is similar to results from previous studies of T2D, where they reported no difference in the levels of fAGEs but did report greater pentosidine from trabecular bone of the femoral neck (Hunt et al., 2019) and greater CML and MG-H1 from cortical bone of the femoral midshaft (Wölfel et al., 2022b). A recent mass spectrometry study by Arakawa *et al* (2020) found that AGE adducts (such as MG-H1, CML and CEL) were considerably more abundant (by at least an order of magnitude) than AGE crosslinks. This highlights the importance of quantifying both types of AGEs, while also suggesting that AGE crosslinks may not play as big a role in altering the mechanical integrity of T2 diabetic bone as is hypothesised. The correlation of these results reveals that there was a strong interaction between early glycation and altered osteoblast activity, evidenced by furosine being positively correlated to blood glucose levels and Sost, while being negatively correlated to P1NP (see Appendix Figure S4.1 (C-E)). However, this may not reflect a causal relationship but instead describes that both furosine, blood glucose and SOST increase as the disease progresses. The relationship between CML and cellular metabolism was less clear. An *in vitro* study by McCarthy *et al* (2004) showed how AGEs could disrupt osteoblast activity in long-standing T2D by reducing osteoblast cell attachment to the type-I collagen matrix, inhibiting differentiation and proliferation, and suppressing ALP secretion which may lead to reduced osteoid mineralization. However, in this Chapter there was no correlation found between CML or any cellular metabolism markers such as SOST, P1NP and CTX-I (see Appendix Figure S4.1 (F)).

Interestingly, whilst the T2D (*fa/fa*) rats presented with a reduced trabecular bone quantity and altered trabecular structure from the femoral neck region, mineralization of the trabeculae did not seem to be impaired, evidenced by no change in Tb.TMD and no change to any parameters measured via BMDD analysis. The cortical bone from the femoral neck and midshaft of the T2D (*fa/fa*) rats were smaller in size (decrease of Ct.Th and Ct.Ar), had a greater porosity than controls but Ct.TMD was also unchanged. Like the trabecular bone, cortical bone from the femoral neck region did not appear to have altered mineralisation, whereas cortical bone from the midshaft did. Mineral heterogeneity of cortical bone from the femoral midshaft was compromised as the disease progressed in the T2D (*fa/fa*) rats, where these rats had a higher heterogeneity at 12-weeks in comparison to the controls. However, the heterogeneity of the diabetic (*fa/fa*) rats did not change with age, whereas the controls had increased and by 46-weeks T2D (*fa/fa*) rats presented with a lower mineral heterogeneity than controls. At 12 weeks, diabetic (*fa/fa*) rats exhibited a significantly higher volume of poorly mineralized tissue (TV_{low}) compared to the controls. However, as the rats with T2D (*fa/fa*) aged, the volume of TV_{low} decreased. This was not observed in the control group. Furthermore, the volume of highly mineralised tissue (TV_{high}) also trended towards a reduction with age ($p = 0.09$) and between strains at 46-weeks ($p = 0.07$) in the diabetic (*fa/fa*) cohort and not controls. Since newly formed bone is less mineralised than older tissue, the reduction in TV_{low} and TV_{high} with age in the diabetic (*fa/fa*) rats highlight a reduction in bone forming cell activity as well as a reduced matrix mineralisation. Normally, carbonate ions assimilate into bioapatite and aid in the formation of plate-like crystals, independent of collagen, which enhance bone strength at the nanoscale (Deymier et al., 2017). In the previous Chapter a reduced carbonate substitution was reported in cortical bone of diabetic (*fa/fa*) rats at 46-weeks in comparison to controls, which in addition to reduced heterogeneity and a reduction in TV_{low} and TV_{high} with age, could be indicative of an altered mineralization process.

This Chapter revealed that, although the stress intensity factor required to initiate a crack (K_{Ic}) was not different between strains at any age, once a crack had formed, less energy was required to propagate that crack to failure in the diabetic (*fa/fa*) rats at 46-weeks of age versus age-matched controls. It is likely that the reduced mineral heterogeneity and increased porosity of the diabetic (*fa/fa*) rats at 46-weeks have impaired the energy dissipation mechanisms of bone at the cortical midshaft leading to reduced cracking toughness and work-to-fracture. In healthy individuals with a normal bone turnover process, mineral heterogeneity is deemed at an optimal level that can allow for the healthy tissue to sustain microdamage, limit microdamage

propagation and continue this cycle by the removal of damaged tissue via turnover (Sereferlengez et al., 2015). Conversely, a more homogeneous tissue has a greater ability to prevent crack initiation but lacks the ability to control crack propagation. This was shown in a study on patients who presented with atypical fragility fractures where lower tissue heterogeneity was highly correlated with increased crack propagation (Granke et al., 2016; Lloyd et al., 2017). Resistance to crack initiation in this cohort did not change regardless of the fact that cortical porosity was increased. Similarly, Tice and colleagues (2022) found no reduction in initiation toughness of non-obese MKR mice with T2D, but did report reductions in cracking toughness and work-to-failure, which they attributed to the impact of mineralization.

It has been reported that T2D patients can have an increased risk of fracture, with the hip being a common sites for fracture in patients with T2D (Janghorbani et al., 2006). Hence, in this study, a sideways fall test was carried out to simulate a hip fracture. However, no difference in maximum load, stiffness or toughness from the sideways fall test was reported between strains at any age. Yet, post-yield displacement (PYD) decreased with age from 12- to 46-weeks in the diabetic (*fa/fa*) rats, while no change occurred with age in the lean, healthy controls. At 46-weeks it was reported that diabetic (*fa/fa*) rats had a trending lower PYD than age-matched controls and the interaction between strain and age was significant, suggesting that disease duration plays a significant role in the brittleness of the femoral neck. Furthermore, FE simulations of the sideways fall test demonstrated that tissue-level failure strain was significantly reduced with age from 12- to 46-weeks in the diabetic (*fa/fa*) rats. Overall, these findings are similar to Devlin *et al* (2014) who reported that the femoral midshaft from TALLYHO/JngJ mice with T2D showed no difference in stiffness or higher ultimate force under three-point bend in the T2 diabetic mice at 17-weeks compared to age matched controls, yet PYD was significantly lower. This indicates that at 46-weeks, the femoral neck of the diabetic (*fa/fa*) rats was not structurally weaker, but a longer exposure time to the disease brought about a more brittle behaviour. PYD is technically a structural property which may also reflect tissue-level matrix alterations (Jepsen et al., 2015). Hence, here the relationship between PYD and microstructural changes to the trabecular (SMI and Conn.D) and cortical bone (Ct.Ar and cortical porosity) and also to alterations in the organic matrix (CML) was examined. Interestingly, when faceted by strain, PYD correlated to SMI, Conn.D and Ct.Ar but not CML or cortical porosity in the diabetic rats, indicating that PYD in the femoral neck of ZDF (*fa/fa*) rats at 46-weeks was structurally altered by the trabecular microstructure and cortical bone quantity, which is likely a direct result of the altered cellular metabolism that

shown bone formation to be reduced (\downarrow P1NP at 26- and 46-weeks) and resorption to be increased (\uparrow CTX-I at 46-weeks) that influenced these structural properties (see Figure 4.14 and Appendix Figure S4.2)

There are several limitations to this study and future recommendations to be considered, in addition to those captured in Chapter 3 with the same animal model. Firstly, it is important to note that cortical bone from the femoral neck region and the midshaft region cannot be compared because both were scanned at different voxel sizes. The proximal femur was scanned at $7\ \mu\text{m}$ for these scans to be later used for FE analysis and to reduce the computational cost of the models, which may not be high enough resolution to fully capture differences in mineral quality and porosity for the trabecular and cortical bone in this region, whereas the femoral midshaft was scanned at a $5\ \mu\text{m}$ voxel size. However, the differences in the mineralisation of the midshaft region in comparison to the lack of differences observed in the femoral neck region may also be due to the fact that both the midshaft and femoral neck regions are exposed to different mechanical stresses. For example, a study by Wehner *et al.* (2010) reported internal forces and moments varied along the femoral axis (proximal, midshaft and distal femoral region), with the orientation of the bending moment (M_z) in the frontal plane shifted along the femoral axis. In this study, maximal values varied from -6 bodyweight by mm (BWmm) in the proximal femur to 4.1 BWmm in the distal femur, and the midshaft reflected a value in the middle of these two regions (Wehner *et al.*, 2010). Secondly, it is possible that sample size was not large enough to adequately capture significant changes in PYD for the sideways fall test seeing as PYD is understood to be influenced by a higher variance and since a trending difference between strains was found (Jepsen *et al.*, 2015). In addition, due to a limitation of sample numbers and not being normalised again cell number, some values from serum markers were found to be highly variable. Finally, this Chapter aimed to investigate the downstream effects of altered bone metabolism on the biomechanical properties of bone in diabetic (*fa/fa*) rats by assessing serum biological markers. A marker of interest for future work with ZDF (*fa/fa*) rats may be the receptor for AGEs, known as RAGE, which is thought interrupt several mechanisms of bone cell metabolism such as osteoblast formation, osteoclast activity and vascular calcification to name a few (Miranda *et al.*, 2017; Ogawa *et al.*, 2007; Valcourt *et al.*, 2007; Wang *et al.*, 2016). RAGE could also clarify whether an altered cellular metabolism led to increased glycoxidative damage or visa-versa. In addition, histological analysis of bone sections in future studies could accompany the examination of biological serum markers such

as trichrome mason staining to identify regions of immature or newly mineralised tissue from the more mature mineral directly from the tissue of the ZDF (*fa/fa*) rats.

4.6 Concluding Remarks

The present Chapter brings new insights into the factors that contribute to bone fragility in a ZDF (*fa/fa*) rat model of T2D. This Chapter highlights the downstream effects of an altered bone turnover and metabolism on the biomechanical properties of bone in diabetic (*fa/fa*) rats, which was shown to impair tissue microstructure and alter the organic matrix composition, which is depicted in Figure 4.14. It was shown that T2D had a regional impact on bone mineralisation, whereby heterogeneity and mineral distribution was affected in the cortical bone of the femoral midshaft but not in the femoral neck of the ZDF (*fa/fa*) rats. Additionally, it was uncovered that increased duration of the disease leads to impaired tissue properties, and a reduced capacity to dissipate energy during fracture events through a multifactorial process. Hence, AGEs are not the sole contributor to increased bone fragility in ZDF (*fa/fa*) rats.

Appendix 4.1

Table S4.1. Cellular metabolism markers measured from serum to explore glycaemic control, bone turnover and general health of the control and T2D (*fa/fa*) rats.

	Control (<i>fa/+</i>)			T2D (<i>fa/fa</i>)		
	12 weeks ^a (n = 6)	26 weeks ^b (n = 6-7)	46 weeks (n = 4-6)	12 weeks ^a (n = 6)	26 weeks ^b (n = 7)	46 weeks (n = 4-6)
Glycaemic control						
HbA1c/ HbA1, %	3.03 ± 2.09	1.14 ± 0.75	3.06 ± 2.22	1.30 ± 0.42	1.86 ± 1.64	6.55 ± 4.78 ^{**} , a, b
Bone cellular markers						
P1NP, ng/ mL	10.67 ± 1.11	10.44 ± 0.87	8.91 ± 1.42	12.25 ± 3.88	6.65 ± 1.34 ^{**} , a, b	5.04 ± 0.72 ^{**} , a
CTX-I, ng/ mL &	15.73 ± 0.63	23.59 ± 5.56	20.27 ± 5.56	19.87 ± 3.39	17.27 ± 2.95	45.11 ± 16.94 ^{**} , b
Sost, pg/ mL	138.34 ± 17.04	95.76 ± 10.03	115.60 ± 17.03	274.11 ± 50.38 ^{***}	335.44 ± 36.98 ^{***} , a	430.99 ± 73.32 ^{***} , a, b
General health markers						
Calcium, µg Ca/ mL serum &&	134.85 ± 11.48	121.68 ± 7.17	160.70 ± 24.82 ^b	217.23 ± 34.62 ^{***}	170.13 ± 31.17 ^{**} , a	213.78 ± 38.46 ^{**} , b
IL-6, pg/ mL	94.48 ± 31.44	98.41 ± 24.19	71.75 ± 21.21	127.67 ± 39.51	144.81 ± 49.33 [*]	116.08 ± 18.90 [*]

Values are mean ± SD. T2D, Type-2 diabetic; HbA1c/ HbA1, Ratio of glycated haemoglobin to normal haemoglobin; P1NP, procollagen type 1 amino terminal propeptide; CTX-I, C-telopeptide of collagen alpha-I; Sost, Sclerostin; IL-6, Interlukin-6.

Difference from aged matched lean control (*fa/+*) rats with * ($p < 0.05$), ** ($p < 0.01$), *** ($p < 0.001$) and + (*treanding influence*).

& n = 5, 5 and 7 at 12-, 26- and 46-weeks in controls and n = 5, 6 and 5 at 12-, 26- and 46-weeks in T2D

&& n = 9, 8 and 8 at 12-, 26- and 46-weeks in controls and n = 9, 8 and 7 at 12-, 26- and 46-weeks in T2D

^a significantly different from 12-weeks determined by a multiple comparisons Tukey test

^b significantly different from 26-weeks determined by a multiple comparisons Tukey test

Bone mineral density distribution data obtained for the femoral neck and midshaft

Table S4.2 shows provides additional values gotten from the bone mineral density distribution analysis on the femoral neck and midshaft region.

Table S4.2. Trabecular and cortical bone mineralisation properties from the evaluations of the bone mineral density distributions of the femoral neck and midshaft regions.

	Control (<i>fa/+</i>)			T2D (<i>fa/fa</i>)		
	12 weeks ^a (n = 9)	26 weeks ^b (n = 8)	46 weeks (n = 8)	12 weeks ^a (n = 9)	26 weeks ^b (n = 7)	46 weeks (n = 7)
<i>Femoral neck (trabecular)</i>						
M _{mode} , mg HA/ cm ³	1049.32 ± 16.24	1035.70 ± 13.13	1080.83 ± 12.28 ^{a, b}	1043.60 ± 17.26	1017.14 ± 23.21 ^a	1071.09 ± 32.15 ^{a, b}
M _{mean} , mg HA/ cm ³	1002.16 ± 15.18	999.03 ± 23.47	1014.03 ± 17.34 ^{a, b}	999.33 ± 17.09	982.13 ± 24.01 ^a	1027.20 ± 36.81 ^{a, b}
Heterogeneity, mg HA/ cm ³	230.42 ± 12.22	259.27 ± 9.70 ^a	262.87 ± 11.94 ^a	242.27 ± 7.90	263.13 ± 14.48 ^a	271.50 ± 24.55 ^a
TV ₂₅ , mm ³	0.25 ± 0.07	0.30 ± 0.04	0.24 ± 0.03	0.30 ± 0.05	0.31 ± 0.05	0.26 ± 0.10
TV ₅₀ , mm ³	1.55 ± 0.09	1.48 ± 0.10	1.43 ± 0.10	1.55 ± 0.11	1.43 ± 0.09	1.33 ± 0.18 ^a
TV ₇₅ , mm ³	0.89 ± 0.10	0.78 ± 0.07	0.89 ± 0.14	0.90 ± 0.11	0.67 ± 0.14 ^a	0.88 ± 0.32 ^b
<i>Femoral neck (cortical)</i>						
M _{mode} , mg HA/ cm ³	1080.92 ± 21.32	1135.90 ± 19.76 ^a	1155.96 ± 25.64 ^a	1075.94 ± 20.52	1143.50 ± 19.60 ^a	1157.87 ± 18.18 ^a
M _{mean} , mg HA/ cm ³	1030.27 ± 19.80	1091.48 ± 18.97 ^a	1112.46 ± 30.60 ^a	1022.97 ± 26.93	1077.71 ± 19.54 ^a	1124.84 ± 21.99 ^a
Heterogeneity, mg HA/ cm ³	238.50 ± 14.60	236.29 ± 15.26	244.94 ± 13.83	259.68 ± 22.03	222.32 ± 48.27 ^a	271.52 ± 22.58 ^b
TV ₂₅ , mm ³	0.18 ± 0.05	0.13 ± 0.03 ^a	0.13 ± 0.02 ^a	0.20 ± 0.03	0.13 ± 0.01 ^a	0.12 ± 0.02 ^a
TV ₅₀ , mm ³	1.25 ± 0.14	1.20 ± 0.18	1.34 ± 0.19	1.31 ± 0.13	1.20 ± 0.08	1.23 ± 0.11

TV75, mm ³ <i>Femoral midshaft</i> <i>(cortical)</i>	1.24 ± 0.19	1.43 ± 0.25	1.32 ± 0.29	1.20 ± 0.23	1.46 ± 0.22	1.29 ± 0.21
M _{mode} , mg HA/ cm ³	1156.74 ± 11.56	1218.89 ± 12.33 ^a	1250.23 ± 8.46 ^{a, b}	1135.22 ± 46.86	1223.97 ± 16.35 ^a	1255.29 ± 9.45 ^{a, b}
M _{mean} , mg HA/ cm ³	1120.82 ± 29.44	1183.69 ± 27.25 ^a	1223 ± 16.80 ^{a, b}	1092.41 ± 53.36	1191.83 ± 16.20 ^a	1214.67 ± 21.60 ^a
Heterogeneity, mg HA/ cm ³	252.98 ± 31.48	298.51 ± 8.74 ^a	326.66 ± 10.99 ^{a, b}	273.79 ± 13.08*	287.06 ± 6.77	287.39 ± 8.02***, b
TV25, mm ³	0.14 ± 0.07	0.16 ± 0.02	0.15 ± 0.03	0.24 ± 0.15*	0.15 ± 0.02	0.12 ± 0.02 ^b
TV50, mm ³	1.42 ± 0.25	1.94 ± 0.21 ^a	1.84 ± 0.36 ^a	1.67 ± 0.14	1.93 ± 0.24	1.70 ± 0.33 ^{a, b}
TV75, mm ³	1.38 ± 0.34	1.17 ± 0.16	1.29 ± 0.20	1.16 ± 0.46	1.15 ± 0.15	1.07 ± 0.12 ^{#, a, b}

Values are mean ± SD. T2D, Type-2 diabetic; M_{mode}, Mode Mineral Density; M_{mean}, Mean Mineral Density; TV25, Tissue Volume at Low Mineral Density (25th percentile); TV50, Tissue Volume at Medium Mineral Density (50th percentile); TV75, Tissue Volume at Medium Mineral Density (75th percentile).

Difference from aged matched lean control (*fa*+) rats with * ($p < 0.05$), ** ($p < 0.01$), *** ($p < 0.001$) and # (*trending influence*).

^a significantly different from 12-weeks determined by a multiple comparisons Tukey test

^b significantly different from 26-weeks determined by a multiple comparisons Tukey test

Appendix 4.2

Correlation analysis

Data was pooled for all strains and ages when measuring correlation coefficients in Figure S4.1. The coefficients of correlation were calculated by Pearson's method. There was a negative correlation between P1NP and the HbA1c ratio ($R = -0.33$, $p = 0.04$) and a trending positive correlation with Sost ($R = 0.29$, $p = 0.08$). The HbA1c ratio also correlated with several mineral and structural trabecular properties such as, trabecular TMD ($R = 0.41$, $p = 0.01$), trabecular BV/TV ($R = -0.36$, $p = 0.02$) and connectivity density ($R = -0.53$, $p = 0.0005$). However, the HbA1c ratio did not show a correlation to any mechanical testing properties such as, K_{ic}, cracking toughness or PYD or cortical bone structural and mineral properties such as, TMD ($R = 0.28$, $p = 0.09$), BV/TV, porosity and area.

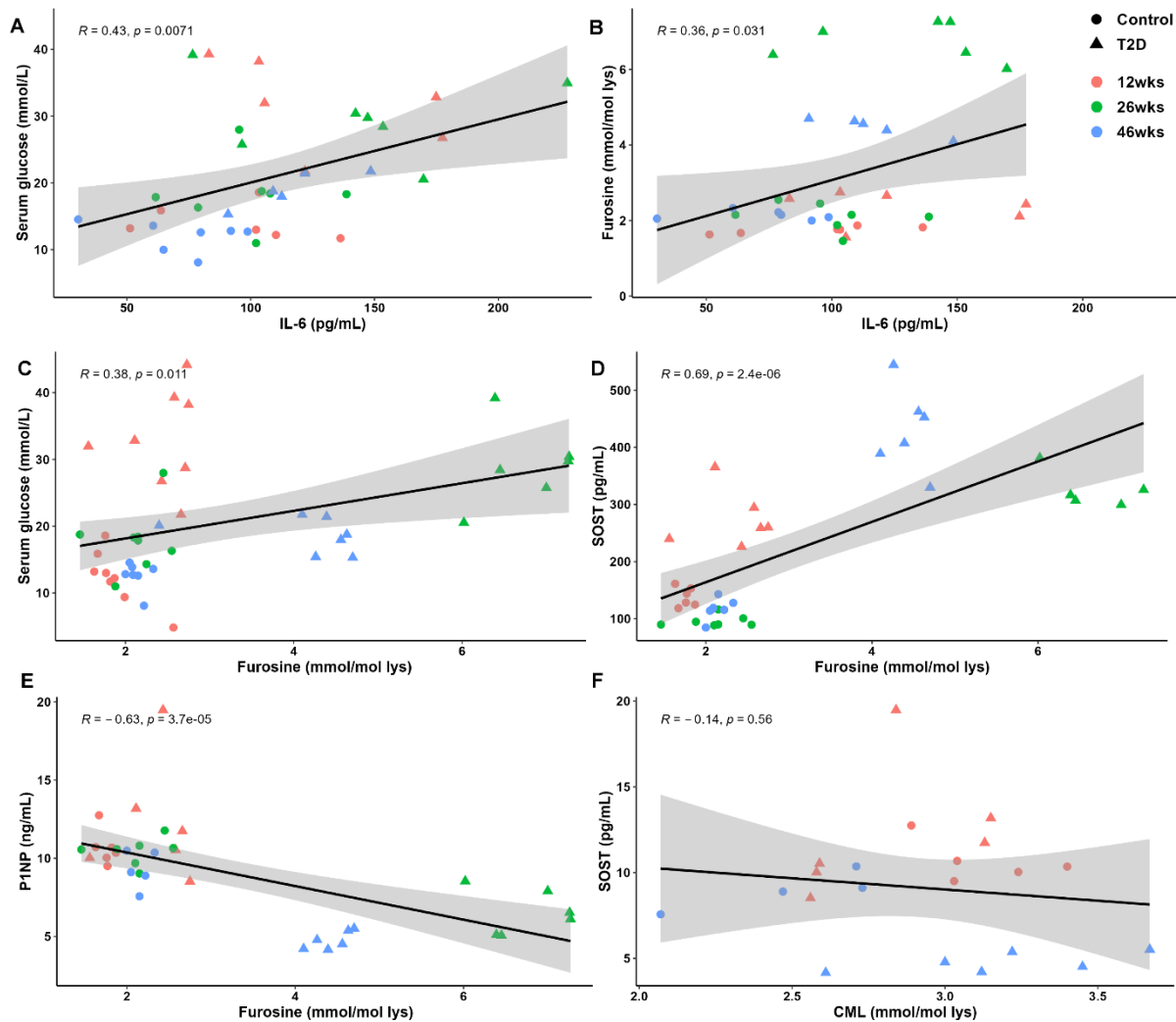


Figure S4.1. Correlations between parameters of (A-C) glycaemic control (serum glucose and furosine) and inflammation (IL-6) and (D-F) glycation control, oxidative stress (CML) and cellular metabolism (Sost, P1NP). Data for all strains and ages are pooled.

Data was pooled for all ages and faceted by strain to examine the different relationship microstructure and alterations to the organic matrix on the T2D (*fa/fa*) cohort in comparison to the controls (Figure S4.2). The coefficients of correlation were calculated by Pearson's method.

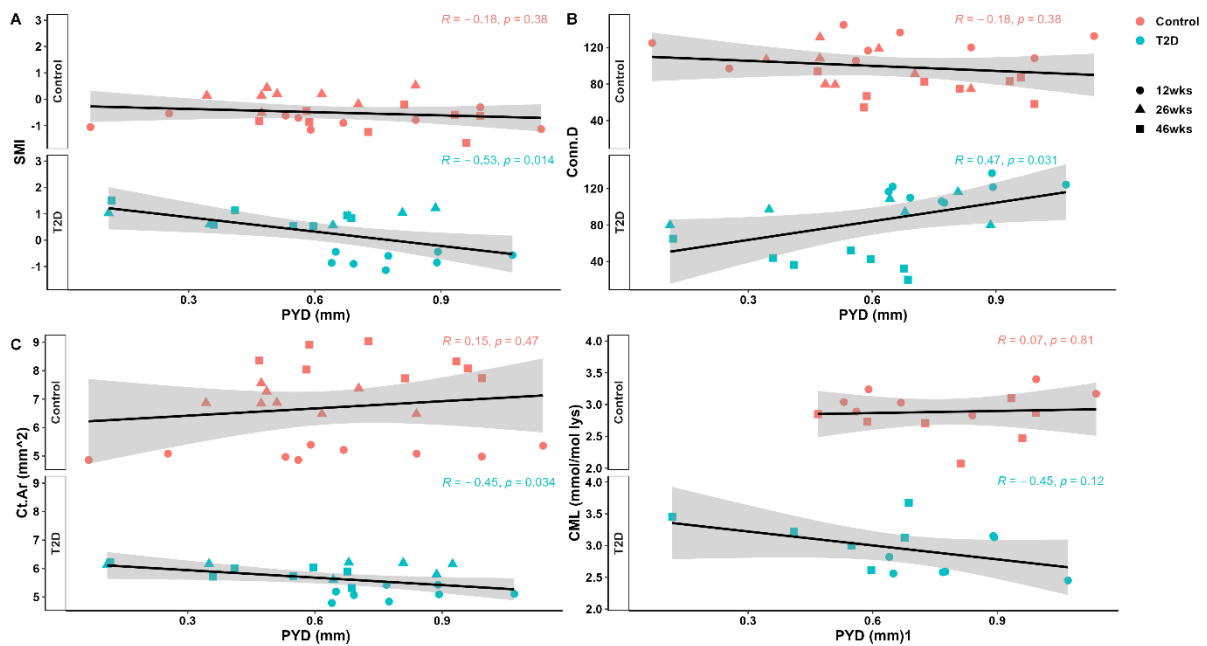


Figure S4.2. Correlations between parameters of (A-C) glycaemic control (serum glucose and furosine) and inflammation (IL-6) and (D-F) glycation control, oxidative stress (CML) and cellular metabolism (Sost, PINP). Data for all strains and ages are pooled.

Data was pooled by strain and faceted by age to compare the examine how the relationship differed between Sost and various parameters from 12-weeks to 46-weeks (Table S4.3). The coefficients of correlation were calculated by Pearson's method.

Table S4.3. Correlations for data compared against serum Sost levels, pooled by strain but faceted by age. Significant correlations written in bold.

	12 weeks	26 weeks	46 weeks
<i>Compared to Sost</i>			
Ct.BV/TV	-0.48 (ns)	-0.82 (<i>p</i> = 0.00063)	-0.74 (<i>p</i> = 0.0026)
Ct.Area	0.33 (ns)	-0.82 (<i>p</i> = 0.00055)	-0.91 (<i>p</i> = 0.0000075)
Tb.BV/TV	0.17 (ns)	-0.78 (<i>p</i> = 0.0015)	-0.87 (<i>p</i> = 0.000046)
Tb.Th	0.072 (ns)	-0.79 (<i>p</i> = 0.0013)	-0.87 (<i>p</i> = 0.000057)
SMI	0.085 (ns)	0.83 (<i>p</i> = 0.00045)	0.88 (<i>p</i> = 0.0000031)
P1NP	0.18 (ns)	-0.81 (<i>p</i> = 0.00076)	-0.88 (<i>p</i> = 0.00017)
Body Mass	0.84 (0.0007)	0.52 (0.07)	-0.77 (0.0014)
HbA1c ratio	-0.53 (0.07)	0.18 (ns)	0.42 (ns)

Values are R-value (*p*-value), ns = *p*-value > 0.1, Ct.BV/TV, Cortical bone volume fraction; Tb.BV/TV, Trabecular bone volume fraction; Tb.Th, Trabecular thickness; SMI, Structural model index; P1NP, procollagen type 1 amino terminal propeptide.

Data was pooled by strain and age to examine the relationship between glycation markers and organic composition with various markers (Table S4.4). The coefficients of correlation were calculated by Pearson's method.

Table S4.4. Correlations for data compared against serum HbA1c ratio, Furosine and CML pooled by strain but faceted by age. Significant correlations written in bold.

	<i>Furosine</i>	<i>CML</i>	<i>PINP</i>	<i>Sost</i>	<i>Blood glucose</i>	<i>K_{Ic}</i>	<i>T_{cr}</i>	<i>PYD</i>
<i>HbA1c Ratio</i>	0.16 (ns)	0.29 (ns)	-0.33 (0.04)	0.29 (0.08)	-0.25 (0.09)	-0.09 (ns)	-0.2 (ns)	0.09 (ns)
<i>Furosine</i>	-	0.33 (0.08)	-0.63 (0.000037)	0.69 (0.0000024)	0.38 (0.01)	-0.41 (0.005)	-0.38 (0.01)	- 0.07 1 (ns)
<i>CML</i>	-	-	-0.14 (ns)	-0.14 (ns)	0.19 (ns)	-0.05 (ns)	-0.21 (ns)	-0.23 (ns)

Values are R-value (*p*-value), ns = *p*-value > 0.1, CML, Carboxymethyl-lysine; PINP, procollagen type 1 amino terminal propeptide; Sost, Sclerostin; *K_{Ic}*, Stress intensity at crack initiation; *T_{cr}*, Cracking toughness; PYD, Post-yield displacement.

4.7 References

- Akbari, M., Hassan-Zadeh, V., 2018. IL-6 signalling pathways and the development of type 2 diabetes. *Inflammopharmacology* 26, 685–698. <https://doi.org/10.1007/s10787-018-0458-0>
- Arakawa, S., Suzuki, R., Kurosaka, D., Ikeda, R., Hayashi, H., Kayama, T., Ohno, R. ichi, Nagai, R., Marumo, K., Saito, M., 2020. Mass spectrometric quantitation of AGEs and enzymatic crosslinks in human cancellous bone. *Sci. Rep.* 10, 1–12. <https://doi.org/10.1038/s41598-020-75923-8>
- Backman, S., 1957. The proximal end of the femur: investigations with special reference to the etiology of femoral neck fractures; anatomical studies; roentgen projections; theoretical stress calculations; experimental production of fractures. *Acta Radiol. Suppl.* 1–166.
- Bouxsein, M.L., Boyd, S.K., Christiansen, B.A., Guldberg, R.E., Jepsen, K.J., Müller, R., 2010. Guidelines for assessment of bone microstructure in rodents using micro-computed tomography. *J. Bone Miner. Res.* 25, 1468–1486. <https://doi.org/10.1002/jbmr.141>
- Caliaperoumal, G., Souyet, M., Bensidhoum, M., Petite, H., Anagnostou, F., 2018. Type 2 diabetes impairs angiogenesis and osteogenesis in calvarial defects: MicroCT study in ZDF rats. *Bone* 112, 161–172. <https://doi.org/10.1016/j.bone.2018.04.009>
- Chen, D., Wang, M., 2005. Development and application of rodent models for type 2 diabetes 307–317. <https://doi.org/10.1111/j.1463-1326.2004.00392.x>
- Cheong, V.S., Roberts, B.C., Kadiramanathan, V., Dall’Ara, E., 2020. Bone remodelling in the mouse tibia is spatio-temporally modulated by oestrogen deficiency and external mechanical loading: A combined in vivo/in silico study. *Acta Biomater.* 116, 302–317. <https://doi.org/10.1016/j.actbio.2020.09.011>
- Creecy, A., Uppuganti, S., Merkel, A.R., O’Neal, D., Makowski, A.J., Granke, M., Voziyan, P., Nyman, J.S., 2016. Changes in the Fracture Resistance of Bone with the Progression of Type 2 Diabetes in the ZDSD Rat. *Calcif. Tissue Int.* 99, 289–301. <https://doi.org/10.1007/s00223-016-0149-z>
- Delgado-Calle, J., Sato, A.Y., Bellido, T., 2017. Role and mechanism of action of sclerostin in bone. *Bone* 96, 29–37. <https://doi.org/10.1016/j.bone.2016.10.007>
- Delmas, P.D., Tracy, R.P., Riggs, B.L., Mann, K.G., 1984. Identification of the noncollagenous

- proteins of bovine bone by two-dimensional gel electrophoresis. *Calcif. Tissue Int.* 36, 308–316. <https://doi.org/10.1007/BF02405335>
- Devlin, Van Vliet, M., Motyl, K., Karim, L., Brooks, D.J., Louis, L., Conlon, C., Rosen, C.J., Bouxsein, M.L., 2014. Early-onset type 2 diabetes impairs skeletal acquisition in the male TALLYHO/JngJ mouse. *Endocrinol. (United States)* 155, 3806–3816. <https://doi.org/10.1210/en.2014-1041>
- Deymier, A.C., Nair, A.K., Depalle, B., Qin, Z., Arcot, K., Drouet, C., Yoder, C.H., Buehler, M.J., Thomopoulos, S., Genin, G.M., Pasteris, J.D., 2017. Protein-free formation of bone-like apatite: New insights into the key role of carbonation. *Biomaterials* 127, 75–88. <https://doi.org/10.1016/j.biomaterials.2017.02.029>
- Gallant, M.A., Brown, D.M., Organ, J.M., Allen, M.R., Burr, D.B., 2013. Reference-point indentation correlates with bone toughness assessed using whole-bone traditional mechanical testing. *Bone* 53, 301–305. <https://doi.org/10.1016/j.bone.2012.12.015>
- García-Martín, A., Rozas-Moreno, P., Reyes-García, R., Morales-Santana, S., García-Fontana, B., García-Salcedo, J.A., Muñoz-Torres, M., 2012. Circulating levels of sclerostin are increased in patients with type 2 diabetes mellitus. *J. Clin. Endocrinol. Metab.* 97, 234–241. <https://doi.org/10.1210/jc.2011-2186>
- Granke, M., Makowski, A.J., Uppuganti, S., Does, M.D., Nyman, J.S., 2015. Identifying Novel Clinical Surrogates to Assess Human Bone Fracture Toughness. *JBMR.* <https://doi.org/10.1002/jbmr.2452>
- Granke, M., Makowski, A.J., Uppuganti, S., Nyman, J.S., 2016. Prevalent role of porosity and osteonal area over mineralization heterogeneity in the fracture toughness of human cortical bone. *J. Biomech.* 49, 2748–2755. <https://doi.org/10.1016/j.jbiomech.2016.06.009>
- Hamann, C., Goettsch, C., Mettelsiefen, J., Henkenjohann, V., Rauner, M., Hempel, U., Bernhardt, R., Fratzl-Zelman, N., Roschger, P., Rammelt, S., Günther, K.-P., Hofbauer, L.C., 2011. Delayed bone regeneration and low bone mass in a rat model of insulin-resistant type 2 diabetes mellitus is due to impaired osteoblast function. *Am. J. Physiol. Metab.* 301, 1220–1228. <https://doi.org/10.1152/ajpendo.00378.2011>
- Hamann, C., Rauner, M., Hohna, Y., Bernhardt, R., Mettelsiefen, J., Goettsch, C., Gunther, K.-

- P., Stolina, M., Han, C.-Y., Asuncion, F.J., Ominsky, M.S., Hofbauer, L.C., 2013. Sclerostin Antibody Treatment Improves Bone Mass, Bone Strength, and Bone Defect Regeneration in Rats With Type 2 Diabetes Mellitus 28, 627–638. <https://doi.org/10.1002/jbmr.1803>
- Hunt, H.B., Pearl, J.C., Diaz, D.R., King, K.B., Donnelly, E., 2018. Bone Tissue Collagen Maturity and Mineral Content Increase With Sustained Hyperglycemia in the KK-Ay Murine Model of Type 2 Diabetes. *J. Bone Miner. Res.* 33, 921–929. <https://doi.org/10.1002/jbmr.3365>
- Hunt, H.B., Torres, A.M., Palomino, P.M., Marty, E., Saiyed, R., Cohn, M., Jo, J., Warner, S., Sroga, G.E., King, K.B., Lane, J.M., Vashishth, D., Hernandez, C.J., Donnelly, E., 2019. Altered Tissue Composition, Microarchitecture, and Mechanical Performance in Cancellous Bone From Men With Type 2 Diabetes Mellitus. *J. Bone Miner. Res.* 34, 1191–1206. <https://doi.org/10.1002/jbmr.3711>
- Hygum, K., Starup-Linde, J., Harsløf, T., Vestergaard, P., Langdahl, B.L., 2017. Diabetes mellitus, a state of low bone turnover—a systematic review and meta-analysis. *Eur. J. Endocrinol.* 176, R137–R157. <https://doi.org/10.1530/EJE-16-0652>
- Ignat'eva, N.Y., Danilov, N.A., Averkiev, S. V., Obrezkova, M. V., Lunin, V. V., Sobol', E.N., 2007. Determination of hydroxyproline in tissues and the evaluation of the collagen content of the tissues. *J. Anal. Chem.* 62, 51–57. <https://doi.org/10.1134/S106193480701011X>
- Jämsä, T., Tuukkanen, J., Jalovaara, P., 1998. Femoral neck strength of mouse in two loading configurations: Method evaluation and fracture characteristics. *J. Biomech.* 31, 723–729. [https://doi.org/10.1016/S0021-9290\(98\)00087-6](https://doi.org/10.1016/S0021-9290(98)00087-6)
- Janghorbani, M., Feskanich, D., Willett, W.C., Hu, F., 2006. Prospective Study of Diabetes and Risk of Hip Fracture. *Diabetes Care* 29, 1573–1578. <https://doi.org/10.2337/dc06-0440>
- Janghorbani, M., Van Dam, R.M., Willett, W.C., Hu, F.B., 2007. Systematic review of type 1 and type 2 diabetes mellitus and risk of fracture. *Am. J. Epidemiol.* 166, 495–505. <https://doi.org/10.1093/aje/kwm106>
- Jepsen, Silva, M.J., Vashishth, D., Guo, X.E., van der Meulen, M.C., 2015. Establishing

- Biomechanical Mechanisms in Mouse Models: Practical Guidelines for Systematically Evaluating Phenotypic Changes in the Diaphyses of Long Bones. *J. Bone Miner. Res.* 30, 951–966. <https://doi.org/10.1002/jbmr.2539>
- Karim, L., Bouxsein, M.L., 2016. Effect of type 2 diabetes-related non-enzymatic glycation on bone biomechanical properties. *Bone* 82, 21–27. <https://doi.org/10.1016/j.bone.2015.07.028>
- Karim, L., Moulton, J., Van Vliet, M., Velie, K., Robbins, A., Malekipour, F., Abdeen, A., Ayres, D., Bouxsein, M.L., 2018. Bone microarchitecture, biomechanical properties, and advanced glycation end-products in the proximal femur of adults with type 2 diabetes. *Bone* 114, 32–39. <https://doi.org/10.1016/j.bone.2018.05.030>
- Keller, T.S., 1994. Predicting the compressive mechanical behavior of bone. *J. Biomech.* 27, 1159–1168.
- Lagathu, C., Bastard, J.P., Auclair, M., Maachi, M., Capeau, J., Caron, M., 2003. Chronic interleukin-6 (IL-6) treatment increased IL-6 secretion and induced insulin resistance in adipocyte: Prevention by rosiglitazone. *Biochem. Biophys. Res. Commun.* 311, 372–379. <https://doi.org/10.1016/j.bbrc.2003.10.013>
- Lekkala, S., Sacher, S.E., Taylor, E.A., Williams, R.M., Moseley, K.F., Donnelly, E., 2023. Increased Advanced Glycation Endproducts, Stiffness, and Hardness in Iliac Crest Bone From Postmenopausal Women With Type 2 Diabetes Mellitus on Insulin. *J. Bone Miner. Res.* 38, 261–277. <https://doi.org/10.1002/jbmr.4757>
- LLabre, J.E., Sroga, G.E., Tice, M.J.L., Vashishth, D., 2022. Induction and rescue of skeletal fragility in a high-fat diet mouse model of type 2 diabetes: An in vivo and in vitro approach. *Bone* 156. <https://doi.org/10.1016/j.bone.2021.116302>
- Lloyd, A.A., Gludovatz, B., Riedel, C., Luengo, E.A., Saiyed, R., Marty, E., Lorich, D.G., Lane, J.M., Ritchie, R.O., Busse, B., Donnelly, E., 2017. Atypical fracture with long-term bisphosphonate therapy is associated with altered cortical composition and reduced fracture resistance. *Proc. Natl. Acad. Sci. U. S. A.* 114, 8722–8727. <https://doi.org/10.1073/pnas.1704460114>
- Lorenzo, C., Hanley, A.J., Rewers, M.J., Haffner, S.M., 2014. Calcium and phosphate concentrations and future development of type 2 diabetes: The Insulin Resistance

- Atherosclerosis Study. *Diabetologia* 57, 1366–1374. <https://doi.org/10.1007/s00125-014-3241-9>
- Lu, Y., Zuo, D., Li, J., He, Y., 2019. Stochastic analysis of a heterogeneous micro-finite element model of a mouse tibia. *Med. Eng. Phys.* 63, 50–56. <https://doi.org/10.1016/j.medengphy.2018.10.007>
- McCarthy, Uemura, T., Etcheverry, S.B., Cortizo, A.M., 2004. Advanced glycation endproducts interfere with integrin-mediated osteoblastic attachment to a type-I collagen matrix. *Int. J. Biochem. Cell Biol.* 36, 840–848. <https://doi.org/10.1016/j.biocel.2003.09.006>
- Merlo, K., Aaronson, J., Vaidya, R., Rezaee, T., Chalivendra, V., Karim, L., 2020. In Vitro-Induced High Sugar Environments Deteriorate Human Cortical Bone Elastic Modulus and Fracture Toughness. *J. Orthop. Res.* 38, 972–983. <https://doi.org/10.1002/jor.24543>
- Miranda, E.R., Somal, V.S., Mey, J.T., Blackburn, B.K., Wang, E., Farabi, S., Karstoft, K., Fealy, C.E., Kashyap, S., Kirwan, J.P., Quinn, L., Solomon, T.P.J., Haus, J.M., 2017. Circulating soluble RAGE isoforms are attenuated in obese, impaired-glucose-tolerant individuals and are associated with the development of type 2 diabetes. *Am. J. Physiol. - Endocrinol. Metab.* 313, E631–E640. <https://doi.org/10.1152/ajpendo.00146.2017>
- Nagai, R., Shirakawa, J., Fujiwara, Y., Ohno, R., Moroishi, N., Sakata, N., 2014. Detection of AGEs as markers for carbohydrate metabolism and protein denaturation 55, 1–6. <https://doi.org/10.3164/jcbn.13>
- O’Sullivan, L.M., Allison, H., Parle, E.E., Schiavi, J., McNamara, L.M., 2020. Secondary alterations in bone mineralisation and trabecular thickening occur after long-term estrogen deficiency in ovariectomised rat tibiae, which do not coincide with initial rapid bone loss. *Osteoporos. Int.* 31, 587–599. <https://doi.org/10.1007/s00198-019-05239-5>
- Ogawa, N., Yamaguchi, T., Yano, S., Yamauchi, M., Yamamoto, M., Sugimoto, T., 2007. The Combination of High Glucose and Advanced Glycation End-products (AGEs) Inhibits the Mineralization of Osteoblastic MC3T3-E1 Cells through Glucose-induced Increase in the Receptor for AGEs. *Horm. Metab. Res.* 39, 871–875. <https://doi.org/10.1055/s-2007-991157>
- Parfitt, A.M., Mathews, C.H.E., Villanueva, A.R., Kleerekoper, M., Frame, B., Rao, D.S.,

1983. Relationships between surface, volume, and thickness of iliac trabecular bone in aging and in osteoporosis. Implications for the microanatomic and cellular mechanisms of bone loss. *J. Clin. Invest.* 72, 1396–1409. <https://doi.org/10.1172/JCI111096>
- Pereira, M., Gohin, S., Lund, N., Hvid, A., Smitham, P.J., Oddy, M.J., Reichert, I., Farlay, D., Roux, J.P., Cleasby, M.E., Chenu, C., 2017. Sclerostin does not play a major role in the pathogenesis of skeletal complications in type 2 diabetes mellitus. *Osteoporos. Int.* 28, 309–320. <https://doi.org/10.1007/s00198-016-3718-0>
- Peterson, R.G., Shaw, W.N., Neel, M., Little, L.A., Eichberg, J., 1990. Zucker Diabetic Fatty Rat as a Model for Non-insulin-dependent Diabetes Mellitus. *ILAR J.* 32, 16–19. <https://doi.org/10.1093/ilar.32.3.16>
- Piccoli, A., Cannata, F., Stollo, R., Pedone, C., Leanza, G., Russo, F., Greto, V., Isgrò, C., Quattrocchi, C.C., Massaroni, C., Silvestri, S., Vadalà, G., Bisogno, T., Denaro, V., Pozzilli, P., Tang, S.Y., Silva, M.J., Conte, C., Papalia, R., Maccarrone, M., Napoli, N., 2020. Sclerostin Regulation, Microarchitecture, and Advanced Glycation End-Products in the Bone of Elderly Women With Type 2 Diabetes. *J. Bone Miner. Res.* 35, 2415–2422. <https://doi.org/10.1002/jbmr.4153>
- Picke, A., Campbell, G., Napoli, N., Hofbauer, L.C., Rauner, M., 2019. Update on the impact of type 2 diabetes mellitus on bone metabolism and material properties. *Endocr. Connect.* 8, R55–R70. <https://doi.org/10.1530/EC-18-0456>
- Picke, Alaguero, I.G., Campbell, G.M., Glüer, C., Salbach-hirsch, J., Rauner, M., Hofbauer, L.C., Hofbauer, C., 2016. Bone defect regeneration and cortical bone parameters of type 2 diabetic rats are improved by insulin therapy ☆. *Bone* 82, 108–115. <https://doi.org/10.1016/j.bone.2015.06.001>
- Poundarik, A.A., Wu, P.-C., Evis, Z., Sroga, G.E., Ural, A., Rubin, M., Vashishth, D., 2015. A direct role of collagen glycation in bone fracture. *J. Mech. Behav. Biomed. Mater.* 52, 120–130. <https://doi.org/10.1016/j.jmbbm.2015.08.012>
- Prisby, R.D., Swift, J.M., Bloomfield, S.A., Hogan, H.A., Delp, M.D., 2008. Altered bone mass, geometry and mechanical properties during the development and progression of type 2 diabetes in the Zucker diabetic fatty rat. *J. Endocrinol.* 199, 379–388. <https://doi.org/10.1677/JOE-08-0046>

- Purnamasari, D., Puspitasari, M.D., Setiyohadi, B., Nugroho, P., Isbagio, H., 2017. Low bone turnover in premenopausal women with type 2 diabetes mellitus as an early process of diabetes-associated bone alterations: A cross-sectional study. *BMC Endocr. Disord.* 17, 1–8. <https://doi.org/10.1186/s12902-017-0224-0>
- Reinwald, S., Peterson, R.G., Allen, M.R., Burr, D.B., 2009. Skeletal changes associated with the onset of type 2 diabetes in the ZDF and ZDSD rodent models. *Am. J. Physiol. Metab.* 296, E765–E774. <https://doi.org/10.1152/ajpendo.90937.2008>
- Ritchie, R.O., Koester, K.J., Ionova, S., Yao, W., Lane, N.E., Iii, J.W.A., 2008. Measurement of the toughness of bone : A tutorial with special reference to small animal studies ☆. *Bone* 43, 798–812. <https://doi.org/10.1016/j.bone.2008.04.027>
- Rubin, M.R., Patsch, J.M., 2016. Assessment of bone turnover and bone quality in type 2 diabetic bone disease: current concepts and future directions. *Bone Res.* 4, 16001. <https://doi.org/10.1038/boneres.2016.1>
- Saito, M., Fujii, K., Mori, Y., Marumo, K., 2006. Role of collagen enzymatic and glycation induced cross-links as a determinant of bone quality in spontaneously diabetic WBN/Kob rats. *Osteoporos. Int.* 17, 1514–1523. <https://doi.org/10.1007/s00198-006-0155-5>
- Sassi, F., Buondonno, I., Luppi, C., Spertino, E., Stratta, E., Di Stefano, M., Ravazzoli, M., Isaia, G., Trento, M., Passera, P., Porta, M., Isaia, G.C., D’Amelio, P., 2018. Type 2 diabetes affects bone cells precursors and bone turnover. *BMC Endocr. Disord.* 18, 1–8. <https://doi.org/10.1186/s12902-018-0283-x>
- Schileo, E., Dall’Ara, E., Taddei, F., Malandrino, A., Schotkamp, T., Baleani, M., Viceconti, M., 2008. An accurate estimation of bone density improves the accuracy of subject-specific finite element models. *J. Biomech.* 41, 2483–2491. <https://doi.org/10.1016/j.jbiomech.2008.05.017>
- Seref-ferlengez, Z., Kennedy, O.D., Schaffler, M.B., 2015. Bone microdamage , remodeling and bone fragility : how much damage is too much damage ? *Bonekey Rep.* 4, 1–7. <https://doi.org/10.1038/bonekey.2015.11>
- Siegmund, T., Allen, M.R., Burr, D.B., 2008. Failure of mineralized collagen fibrils : Modeling the role of collagen cross-linking 41, 1427–1435. <https://doi.org/10.1016/j.jbiomech.2008.02.017>

- Stabley, J.N., Prisby, R.D., Behnke, B.J., Delp, M.D., Physiology, A., Science, E., 2015. Type 2 diabetes alters bone and marrow blood flow and vascular control mechanisms in the ZDF rat 225, 47–58. <https://doi.org/10.1530/JOE-14-0514>.Type
- Tice, M.J.L., Bailey, S., Sroga, G.E., Gallagher, E.J., Vashishth, D., 2022. Non-Obese MKR Mouse Model of Type 2 Diabetes Reveals Skeletal Alterations in Mineralization and Material Properties. *JBMR Plus* 6, 1–14. <https://doi.org/10.1002/jbm4.10583>
- Valcourt, U., Merle, B., Gineyts, E., Viguet-Carrin, S., Delmas, P.D., Garnero, P., 2007. Non-enzymatic Glycation of Bone Collagen Modifies Osteoclastic Activity and Differentiation. *J. Biol. Chem.* 282, 5691–5703. <https://doi.org/10.1074/jbc.M610536200>
- van Greevenbroek, M.M.J., Schalkwijk, C.G., Stehouwer, C.D.A., 2013. Obesity-associated low-grade inflammation in type 2 diabetes mellitus: Causes and consequences. *Neth. J. Med.* 71, 174–187.
- Vashishth, D., 2007. The Role of the Collagen Matrix in Skeletal Fragility. *Curr. Osteoporos. Rep.* 5, 62–66.
- Vashishth, D., Gibson, G., Khoury, J., Schaffler, M., Kimura, J., Fyhrie, D., 2001. Influence of nonenzymatic glycation on biomechanical properties of cortical bone. *Bone* 28, 195–201. [https://doi.org/10.1016/S8756-3282\(00\)00434-8](https://doi.org/10.1016/S8756-3282(00)00434-8)
- Verbruggen, A.S.K., McCarthy, E.C., Dwyer, R.M., McNamara, L.M., 2022. Temporal and spatial changes in bone mineral content and mechanical properties during breast-cancer bone metastases. *Bone Reports* 17, 101597. <https://doi.org/10.1016/j.bonr.2022.101597>
- Verbruggen, A.S.K., McNamara, L.M., 2023. Mechanoregulation may drive osteolysis during bone metastasis: A finite element analysis of the mechanical environment within bone tissue during bone metastasis and osteolytic resorption. *J. Mech. Behav. Biomed. Mater.* 138, 105662. <https://doi.org/10.1016/j.jmbbm.2023.105662>
- Wallenius, V., Wallenius, K., Dickson, S.L., Jansson, J.-O., Ahrén, B., Rudling, M., Ohlsson, C., Carlsten, H., 2002. Interleukin-6-deficient mice develop mature-onset obesity. *Nat. Med.* 8, 75–79.
- Wang, X., Shen, X., Li, X., Mauli Agrawal, C., 2002. Age-related changes in the collagen network and toughness of bone. *Bone* 31, 1–7. [https://doi.org/10.1016/S8756-3282\(01\)00697-4](https://doi.org/10.1016/S8756-3282(01)00697-4)

- Wang, Z., Li, L., Du, R., Yan, J., Liu, N., Yuan, W., Jiang, Y., Xu, S., Ye, F., Yuan, G., Zhang, B., Liu, P., 2016. CML/RAGE signal induces calcification cascade in diabetes. *Diabetol. Metab. Syndr.* 8, 1–12. <https://doi.org/10.1186/s13098-016-0196-7>
- Wehner, T., Wolfram, U., Henzler, T., Niemeyer, F., Claes, L., Simon, U., 2010. Internal forces and moments in the femur of the rat during gait. *J. Biomech.* 43, 2473–2479. <https://doi.org/10.1016/j.jbiomech.2010.05.028>
- Willett, T.L., Suttly, S., Gaspar, A., Avery, N., Grynepas, M., 2013. In vitro non-enzymatic ribation reduces post-yield strain accommodation in cortical bone. *Bone* 52, 611–622. <https://doi.org/10.1016/j.bone.2012.11.014>
- Willett, T.L., Voziyan, P., Nyman, J.S., 2022. Causative or associative: A critical review of the role of advanced glycation end-products in bone fragility. *Bone* 163, 116485. <https://doi.org/10.1016/j.bone.2022.116485>
- Wölfel, E.M., Fiedler, I.A.K., Dragoun Kolibova, S., Krug, J., Lin, M.-C., Yazigi, B., Siebels, A.K., Mushumba, H., Wulff, B., Ondruschka, B., Püschel, K., Glüer, C.C., Jähn-Rickert, K., Busse, B., 2022a. Human tibial cortical bone with high porosity in type 2 diabetes mellitus is accompanied by distinctive bone material properties. *Bone* 165, 116546. <https://doi.org/10.1016/j.bone.2022.116546>
- Wölfel, E.M., Jähn-Rickert, K., Schmidt, F.N., Wulff, B., Mushumba, H., Sroga, G.E., Püschel, K., Milovanovic, P., Amling, M., Campbell, G.M., Vashishth, D., Busse, B., 2020. Individuals with type 2 diabetes mellitus show dimorphic and heterogeneous patterns of loss in femoral bone quality. *Bone* 140, 115556. <https://doi.org/10.1016/j.bone.2020.115556>
- Wölfel, E.M., Schmidt, F.N., vom Scheidt, A., Siebels, A.K., Wulff, B., Mushumba, H., Ondruschka, B., Püschel, K., Scheijen, J., Schalkwijk, C.G., Vettorazzi, E., Jähn-Rickert, K., Gludovatz, B., Schaible, E., Amling, M., Rauner, M., Hofbauer, L.C., Zimmermann, E.A., Busse, B., 2022b. Dimorphic Mechanisms of Fragility in Diabetes Mellitus: the Role of Reduced Collagen Fibril Deformation. *J. Bone Miner. Res.* 37, 2259–2276. <https://doi.org/10.1002/jbmr.4706>
- Yadav, R.N., Sihota, P., Neradi, D., Bose, J.C., Dhiman, V., Karn, S., Sharma, S., Aggarwal, S., Goni, V.G., Bhadada, S.K., Kumar, N., 2022. Effects of type 2 diabetes on the viscoelastic behavior of human trabecular bone. *Med. Eng. Phys.* 104, 103810.

<https://doi.org/10.1016/j.medengphy.2022.103810>

Yamaguchi, T., 2010. Bone fragility in type 2 diabetes mellitus. *World J. Orthop.* 1, 3–9.

<https://doi.org/10.5312/wjo.v1.i1.3>

Yamamoto, M., Sugimoto, T., 2016. Advanced Glycation End Products, Diabetes, and Bone Strength. *Curr. Osteoporos. Rep.* 14, 320–326. <https://doi.org/10.1007/s11914-016-0332-1>

Zákány, J., Duboule, D., 1993. Correlation of expression of Wnt-1 in developing limbs with abnormalities in growth and skeletal patterning. *Nature* 362, 546–549. <https://doi.org/10.1038/362546a0>

Zeitoun, D., Caliaperoumal, G., Bensidhoum, M., Constans, J.M., Anagnostou, F., Bousson, V., 2019. Microcomputed tomography of the femur of diabetic rats: alterations of trabecular and cortical bone microarchitecture and vasculature—a feasibility study. *Eur. Radiol. Exp.* 3, 17. <https://doi.org/10.1186/s41747-019-0094-5>

Zhang, G., Qin, L., 2005. A comparative study between axial compression and lateral fall configuration tested in a rat proximal femur model 20, 729–735. <https://doi.org/10.1016/j.clinbiomech.2005.03.016>

Zhao, C., Liu, G., Zhang, Y., Xu, G., Yi, X., Liang, Jing, Yang, Y., Liang, Jun, Ma, C., Ye, Y., Yu, M., Qu, X., 2020. Association between serum levels of bone turnover markers and bone mineral density in men and women with type 2 diabetes mellitus. *J. Clin. Lab. Anal.* 34, 1–11. <https://doi.org/10.1002/jcla.23112>

Zimmermann, E.A., Schaible, E., Bale, H., Barth, H.D., Tang, S.Y., Reichert, P., Busse, B., Alliston, T., Ager III, J.W., Ritchie, R.O., 2011. Age-related changes in the plasticity and toughness of human cortical bone at multiple length scales. *Proc Natl Acad Sci* 35, 14416–14421. <https://doi.org/10.1073/pnas.1107966108>

CHAPTER 5

An Investigation of Regional Alterations in the Compositional and Mechanical Properties of Cortical Bone from Zucker Diabetic Fatty (ZDF) Rats

This Chapter has been adapted directly from a manuscript that is under preparation, 'Monahan et al., An Investigation of Regional Alteration in the Compositional and Mechanical Properties of Cortical Bone from Zucker Diabetic Fatty (ZDF) Rats, which will be submitted for peer-review.

5.1 Introduction

In Chapter 3 and Chapter 4, the macro-level tissue mechanics of cortical bone have been investigated through combinations of three-point bend testing and simulated sideways fall testing. While certain differences in bone biomechanics have been observed between the strains, these tests were based at the whole-bone level and these approaches present certain challenges in determining true tissue-level responses and how these might be altered during disease. Since bone has a complex hierarchical arrangement, tissue quality can be examined at multiple length scales from the macroscale down to the nanoscale. Already, Chapter 3 and Chapter 4 have highlighted that there are distinct sub-tissue changes taking place in the mineral and, to a lesser extent, the collagen phase of T2 diabetic tissue in ZDF rats. Therefore, determining the mechanics of the tissue in isolation of structural features becomes increasingly important. Furthermore, Chapter 4 has emphasised that the cellular events that lead to biophysical changes in the bone matrix may be driven by an altered bone turnover process in

T2D. For example, it was shown that P1NP, a serum marker of bone formation, was reduced in the ZDF (*fa/fa*) rats at 46-weeks and sclerostin was increased with the addition of the bone mineral density distribution analysis displaying a more homogeneously distributed mineral and a reduction in the tissue volume at low and high mineral density with age, indicating a reduction in bone forming cell activity as well as reduced matrix mineralisation. A recent study by Wölfel *et al.* (2020a) examined regional differences (endocortical and periosteal) in femoral cortical bone quality from two different type-2 diabetic patient cohorts, that had T2D and T2D with high porosity and found that the latter group had lower osteon density and lower mineralization with higher mineral heterogeneity. They also reported some regional differences between cohorts, where osteon density and crystallinity was lower in the endocortical region of the high porosity group, indicating that femoral bone quality was reduced in heterogeneous patterns within the cortical tissue (Wölfel *et al.*, 2020). However, due to the inability to control for disease duration and severity, this study had a high level of variability within the data of the diseased groups and, like other human studies, could not provide further information on the role of disease progression on the tissue quality. While animal models provide a platform to investigate such features in a more controlled manner, providing a direct link between bone turnover and tissue mechanics still presents distinct challenges in rodent bones.

In contrast to humans, rodent bones lack Haversian systems and do not undergo Haversian remodelling observed in human bones (Wittig and Birkedal, 2022). In rodents, bone maturation initiates in the outer and inner circumference of the cortex, forming a layer of lamellar bone around it. Meanwhile, within the cortex, a region of disorganized woven bone persists due to endochondral ossification, where traces of calcified cartilage remain (Vanleene *et al.*, 2008). Interestingly, Birkhold *et al.* (2016) have shown that bone formation and resorption in periosteal and endocortical regions of mice bone is highly dependent on age and mechanical stimulation. In particular, adults and elderly mice showed increased endocortical resorption and formation, resulting in cortical thinning and bone loss. Additionally, the study found that the periosteal surface was less responsive to mechanical stimuli compared to the endocortical regions, highlighting differences between the periosteal and endosteal circumferential lamellar regions in rodent bone during bone turnover. This study suggests that an altered bone cellular metabolism and growth process in rodents would lead to distinct regional changes in the endocortical and periosteal regions of rodent bone over time. Already, Id *et al.* (2023) have used TallyHo mice, which is a polygenic, spontaneous, obese mouse model of T2D, to assess regional differences in nanoindentation properties between the endocortical and periosteal

regions and found that the elastic modulus in the periosteal and intracortical region was higher than the endocortical region for both strains. However, this particular study did not assess regional differences in tissue composition nor did they investigate the animal during disease progression (Arora et al., 2023). With this in mind, there is a distinct lack of understanding in how the onset and progression of T2D affects the regional properties of cortical bone, particularly with disease progression.

The objective of this Chapter was to explore regional differences in tissue composition and mechanics as the disease progressed in a Zucker Diabetic Fatty (ZDF) rat model of T2D. The aim was to investigate how these differences affected the regional tissue-level mechanics. Building upon previous Chapters that focused on whole-bone biomechanical properties, this Chapter aims to characterize the true tissue-level properties utilizing Raman spectroscopy, nanoindentation, and micropillar compression testing.

5.2 Materials and Methods

This Chapter investigates regional differences of cortical bone from ZDF (*fa/fa*) rats along different stages of the disease, with 7 - 9 rats per age group per condition. The animal model and details used in this Chapter are the same as was described in previous Chapters. Rats were euthanized at 12- (Early-stage diabetes), 26- (Established diabetes) and 46-weeks (Long-term diabetes) of age. Figure 5.1 shows an outline of the techniques used in this Chapter, whereby site-matched compositional and biomechanical testing was carried out to analyse regional differences of cortical bone during different severities of T2D modelled in ZDF (*fa/fa*) rats. Here, the left femora were dissected, wrapped in PBS then frozen at -20°C . Before experimentation, bones were defrosted for approximately 12 h. The proximal half of the left femur was kept and sectioned in the mid-diaphyseal region to obtain a section of cortical bone and embedded in epoxy resin. Tissue composition was measured from the endocortical and periosteal regions of the anterior quadrant of these samples and site-matched nanoindentation was also carried out to examine tissue-level mechanics. The anterior quadrant was chosen for multiple reasons; (1) previous research has shown that formation occurs in the anterior-medial region, (2) multiple studies have assessed regional differences using the anterior-quadrant and (3) examining the anterior cortex ensures that the microstructure remains unaffected by muscle and tendon attachments (Arora et al., 2023; Birkhold et al., 2016; Razi et al., 2015; Wölfel et al., 2020). Additionally, micropillar compression testing was conducted on endocortical and periosteal regions of adjacent cortical bone sections from one sample per condition at 12- and 46-weeks of age.

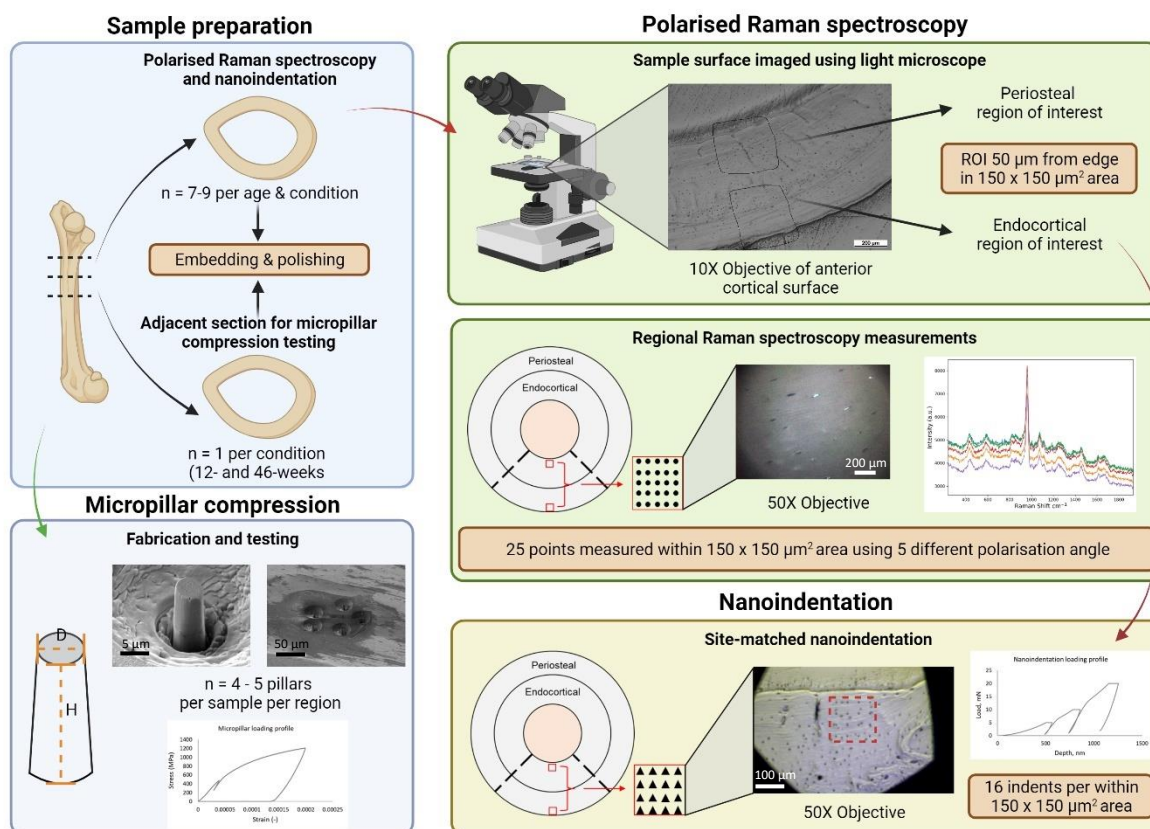


Figure 5.1: Workflow diagram of the different steps in this study. Firstly, samples were prepared by sectioning cortical bone closest to the midshaft region ($n = 7 - 9$, per age and condition) to be used for regional site-matched Raman spectroscopy and nanoindentation. Adjacent sections ($n = 1$, per condition at 12- and 46-weeks) from the region proximal to the midshaft section was made and these samples were used for compressing micropillars from the endocortical and periosteal regions.

5.2.1 Sample preparation

The proximal half of the left femurs from control ($fa/+$) and ZDF (fa/fa) rats were sectioned at the mid-diaphyseal region using a low speed saw (Buehler, Germany) and centrifuged to flush out bone marrow (O'Sullivan, 2020). Two sections of cortical bone were obtained. The cortical section closest to the midshaft was kept for site-matched Raman spectroscopy and nanoindentation. An adjacent section of cortical bone for one sample per condition from the 12- and 46-week cohort was kept for micropillar compression testing. Sections were dehydrated in ascending concentrations of ethanol diluted with dH_2O (50%, 70%, 80%, 90%, 100%, 100%) at $4^\circ C$ for 5 min intervals (O'Sullivan, 2020). The samples were embedded in a mixture of Epothin 2 epoxy resin and hardener (Buehler, Germany) using a 2:1 ratio, vacuumed to remove air bubbles, and left to solidify at room temperature for 72 h. Initially, silicon carbide

paper was used to remove epoxy to expose the test surface. Subsequently, the embedded samples underwent polishing using diamond suspension pastes (9 μm , 3 μm , 1 μm , 0.05 μm) with polishing cloths using a polishing machine (MetaServ® 250 Grinder-Polisher with Vector® LC Power Head, Beuhler, IL, USA). An ultrasonic bath and deionised water were used intermittently to clean the samples between each polishing phase. Mechanical testing of the samples took place within three months of the embedding process to prevent any potential long-term effects of epoxy resin on the nano mechanical properties of bone tissue, according to recommendations by Mittra *et al.* (2006).

5.2.2 Tissue composition

Quantitative polarised Raman spectroscopy (qPRS)

These measurements were carried out as part of a collaboration with Dr. Jakob Schwiedrzik at EMPA Swiss Federal Laboratory (Thun, Switzerland), who helped with the study design. Measurements and analysis were carried out by myself. Local compositional measurements were performed using quantitative polarized Raman spectroscopy (qPRS, WITec Alpha 300 R; Leica, Ulm, Germany; 785 nm laser wavelength and 30 mW power, 50X objective with 0.75 NA). Using qPRS various mineral and collagen properties could be assessed which are described in Table 5.1.

Initially, images of the sample surface were taken using a light microscope after polishing to record a region of interest (ROI) in the endocortical and periosteal regions of the anterior quadrant of cortical bone. This was done so that the qPRS and nanoindentation could be carried out in the same ROI. Images were taken at 5X to capture the detail of the whole anterior quadrant, 10X to record the endocortical and periosteal ROI and finally at 50X to record the details within the ROI where the qPRS will be carried out, which would be used to identify the area to take the qPRS measurements which was done using the 50X objective lens with the Raman spectroscopy camera (Indermaur *et al.*, 2023). ROIs were located 50 μm away from the endocortical or periosteal edges of the cortical bone and spanned a 150 X 150 μm^2 area. Per each endocortical and periosteal ROI, 25 qPRS measurements (total of 50 qPRS measurements per sample) were collected within the 150 X 150 μm^2 area, ensuring to avoid pores such as lacunae or vascular canals. At each position of the qPRS measurement, 5 Raman spectra, each integrated over 10 seconds, were collected at increasing polarisation angles of incoming laser excitation from 0 degrees to 180 degrees with a 45-degree step (0°, 45°, 90°, 135° and 180°).

The linear polarisation of the exciting laser was adjusted with a motorised $\lambda/2$ plate. There was no analyser plate in the light path after the sample. An edge filter was used to block Rayleigh scattered light. The backscattered light was directed to a spectrometer with a 400 mm lens and a grating of 300 g/mm, equipped with a cooled deep-depletion (CCD). The estimated full width at half maximum (FWHM) of the focal spot was approximately 0.4 μm laterally and 1.7 μm axially, calculated based on the confocal Rayleigh criteria (Kochetkova et al., 2021).

Table 5.1: A description of the properties measured in this study using qPRS and the specified ranges they were measured from.

Parameters	Integration range or peak	Description (Ref)
Mineral: Matrix ratio	Integrated area of $\nu_2\text{PO}_4$ (410–460 cm^{-1}) over amide III (1215–1300 cm^{-1})	Explains tissue mineralisation, reflects BMD (Donnelly et al., 2010b)
Crystallinity	1/FWHM $\nu_1\text{PO}_4$	Measure of crystal size and perfection
Carbonate: Phosphate ratio	Integrated area of the carbonate ν_2 peak (1050-1100 cm^{-1}) over of the ν_1 phosphate (920 – 990 cm^{-1})	Measure of carbonate substitution in to the mineral structure (Awonusi et al., 2007; Donnelly et al., 2010b)
Carbonate: Amide I ratio	Integrated area of the carbonate ν_2 peak over Amide I (1600–1700 cm^{-1})	Proposed to be a reflection of bone turnover (McCreadie et al., 2006; Morris and Mandair, 2011)
Amide I status	Intensity ratio of sub-band: I_{-1670}/I_{-1640}	Reflects transition from collagen helical structure to disordered structure (Unal et al., 2016)
Amide III status	Intensity ratio of sub-band: I_{-1245}/I_{-1270}	Reflects transition from collagen helical structure to disordered structure; Proposed to indicate collagen fibre orientation where $\sim 1245 \text{ cm}^{-1}$ reflects the perpendicular direction and $\sim 1270 \text{ cm}^{-1}$ reflects the parallel direction (Dehring et al., 2006; Unal et al., 2021)
Matrix maturity ratio	Intensity ratio of sub-band: I_{-1660}/I_{-1683}	Nonquantitative measure of collagen maturity (Kochetkova et al., 2023; Unal et al., 2021)

Spectral analysis was carried out in batch mode using a Python v3.6 code developed by Kochetkova *et al.* (2021), where each spectra was baseline corrected using a second-order polynomial fit for local minima. The bands of interest were further fit with the Lorentzian function superposition using a least square scheme (`scipy.optimize.leastsq`). Additional information regarding the background subtraction and peak-fitting processes can be found elsewhere (Kochetkova et al., 2022, 2021). Figure 5.1 shows the raw Raman spectra, and the corresponding background corrected Raman spectra is shown in Figure 5.2.

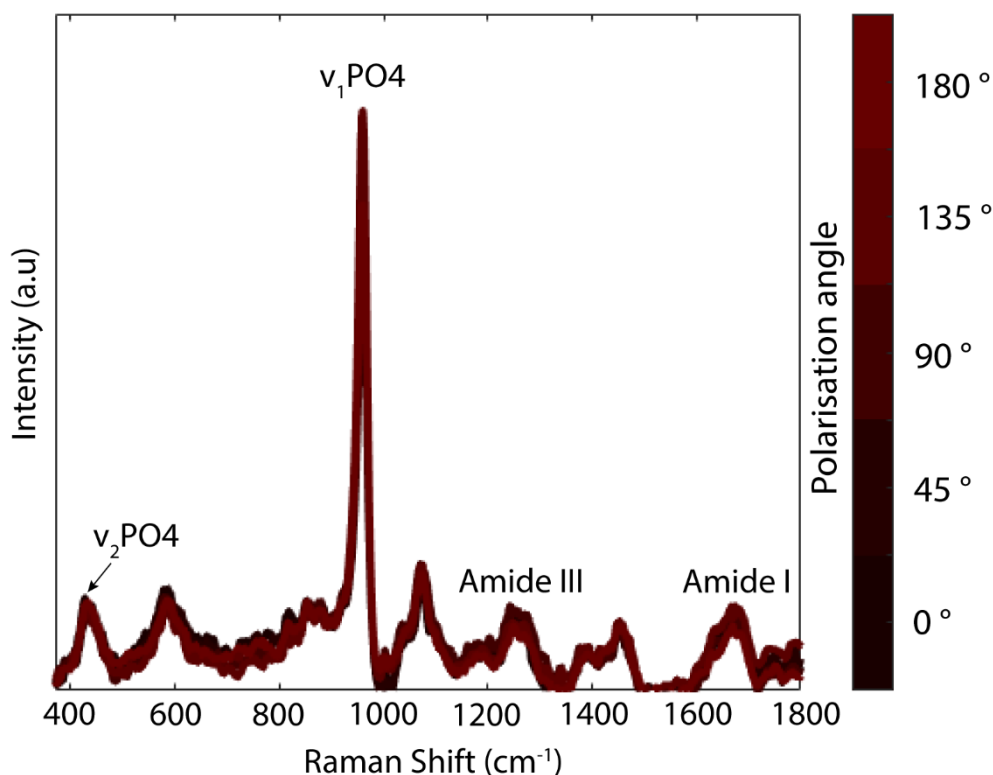


Figure 5.2: Quantitative polarised Raman spectra that has been baseline corrected and smoothed showing the different peaks used to calculate the mineral and collagen properties. The legend shows different colours representing the 5 different polarisation angles of the spectra.

5.2.3 Tissue-level mechanical properties

Site-matched nanoindentation

Site-matched nanoindentation was conducted in the same regions that were analysed using qPRS. For this, 16 site-matched indents in a 4 X 4 matrix were performed in the endocortical and periosteal regions (32 indents in total) using the NanoIndenter G200 (Keysight Technologies, Ca, USA) with a Berkovich diamond indenter tip. The machine was calibrated using fused silica. The indents were positioned at least 100 μm away from the sample's edge and 40 μm apart from neighbouring indents within the array. The loading profile, as depicted in Figure 5.1, involved two conditioning steps reaching loads of 25% and 50% of the maximum load, followed by a third step reaching the maximum load of 20 mN. After each loading peak, there was a 120-second hold period, reducing the effects of time-dependent plasticity based on previous studies (Britton and Vaughan, 2023; Mittra et al., 2006; Sullivan et al., 2020). Upon unloading, the thermal expansion rate was measured. The indenter was held at 10% of the maximum load for 120 s to calibrate the thermal drift correction factor before further data

analysis. Hardness and Elastic modulus were calculated using the Oliver and Pharr method (Oliver and Pharr, 1992) using Equations 5.1 – 5.3.

$$H = \frac{P_{max}}{A_c} \quad (5.1)$$

$$E_r = \frac{\sqrt{\pi}S}{2\beta\sqrt{A_c}} \quad (5.2)$$

$$\frac{1}{E_r} = \frac{(1 - \nu^2)}{E} + \frac{(1 - \nu_i^2)}{E_i} \quad (5.3)$$

Where H is hardness, P_{max} is the maximum load, A_c is the area of contact of the indenter, E_r is the reduced modulus, S is the contact stiffness, β is a constant ($\beta = 1.034$ for a Berkovich tip), E_i is the indenter elastic modulus ($E_i = 1141$ GPa), ν is Poisson's ratio ($\nu = 0.3$) and ν_i is the indenter Poisson's ratio ($\nu_i = 0.07$).

Micropillar compression testing

These measurements were carried out as part of a collaboration with Dr. Jakob Schwiedrzik at EMPA Swiss Federal Laboratory (Thun, Switzerland), with all samples prepared at University of Galway by myself, while compression testing carried out by Dr. Christian Minnert, EMPA. Micropillar fabrication, testing and analysis was carried out using methods from Kochetkova *et al.* (2021). The embedded bone samples were glued to custom made SEM stubs. Samples were then sputtered with and 11 nm thick Au film (Leica EM ACE600, Germany). A thin layer of silver paste (Plano GmbH, Germany) was carefully spread along the sample's sides, reaching down to the aluminium holder to reduce any potential drift resulting from electrostatic charging when exposed to electron or ion beams (Kochetkova *et al.*, 2021). Micropillars were formed using a focused ion beam workstation (Tescan Lyra, Czech Republic) using a protocol detailed in previous work by Schwiedrzik *et al.* (2017, 2014). An adjacent section of cortical bone for one sample per condition from the 12- and 46-week cohort was kept for micropillar compression testing. Micropillars were created on the anterior quadrant of adjacent cortical bone sections as where qPRS and nanoindentation was carried out, where 4 – 5 micropillars were created in the endocortical and periosteal regions. The diameter and height of each pillar was recorded using high-resolution scanning electron microscopy (HRSEM) imaging (Hitachi

S-4800, Japan) (Figure 5.1). Pillars were compressed using a flat punch indenter tip with a 20 μm diameter. The compression was performed in displacement control, reaching a maximum displacement of 2 μm (20%) (loading rate: 10 nm/s), corresponding to a strain rate of 10^{-3} s^{-1} . An intermittent unloading segment in the elastic region was included, allowing for the calculation of elastic moduli (Kochetkova et al., 2021). The loading profile can be seen in Figure 5.1. Elastic modulus values were determined for each pillar based on partial unloading from the beginning of the experiment, yield stress was computed as the stress required for a plastic deformation of 1% using Equations outlined previously by Kochetkova *et al.* (2021). Post-compression images of the micropillars were recorded.

5.2.4 Statistical Analysis

All statistical analyses were carried out using R statistical software (version R-4.1.0). In this study comparisons were made across three distinct components, comparing (a) region vs. region within strains, (b) longitudinally within strains in both regions and (c) between strains within regions at all ages. To compare region vs region (i.e., comparing same cohort but different regions) a Wilcoxon Signed-Rank test was used. To compare longitudinally within strains in both regions a Kruskal-Wallis Rank-Sum test was used, and the p -value was adjusted using the Bonferroni method. To compare between strains within a region a Wilcoxon Rank-Sum was used, and the p -value was adjusted using the Bonferroni method. When comparing combined average difference similar statistics as described previously in Chapters 3 and 4 were used. Alpha levels of $p \leq 0.05$ were considered significant for a 95% confidence interval. Data are represented as mean \pm standard deviation.

5.3 Results

5.3.1 Tissue composition

Quantitative polarised Raman spectroscopy (qPRS)

Figure 5.3 and Table 5.2 shows the combined mean results for tissue composition measured via Raman spectroscopy. The ν_2 phosphate mineral: matrix ratio ($\nu_2 \text{ PO}_4^{3-}/ \text{Amide III}$) decreased by 22.04% ($p < 0.05$) from 26- to 46-weeks in the T2D (*fa/fa*) cohort but no difference was observed in the controls (Figure 5.3 (A)). As for the ν_2 carbonate mineral: matrix ratio ($\nu_2 \text{ CO}_3^{2-}/ \text{Amide I}$), both strains had an increase with age from 12- to 26- and 26- to 46-weeks, however, at 46-weeks T2D (*fa/fa*) rats had a 6.84% ($p < 0.05$) lower ratio than age-matched controls (Figure 5.3 (B)). In the diabetic (*fa/fa*) cohort, the carbonate: phosphate ratio increased from 26- to 46-weeks ($p < 0.05$) and showed a trending increase from 12- to 46-

weeks of age ($p = 0.06$), yet no difference with age was observed in the controls (Figure 5.3 (C)). Crystallinity also increased with age for both strains (Figure 5.3 (D)). However, controls had a greater increase with age than the diabetic (fa/fa) rats, where controls exhibited a 9.83% ($p < 0.0001$) and the T2D (fa/fa) rats showed a 1.97% ($p < 0.05$) increase with age from 12- to 46-weeks. Interestingly, at 26-weeks the crystallinity of the T2D (fa/fa) rats was 2.51% lower than their age-matched controls. Enzymatic crosslink ratio, Amide I status and Amide III status were not significantly different with age or between strains (Table 5.2).

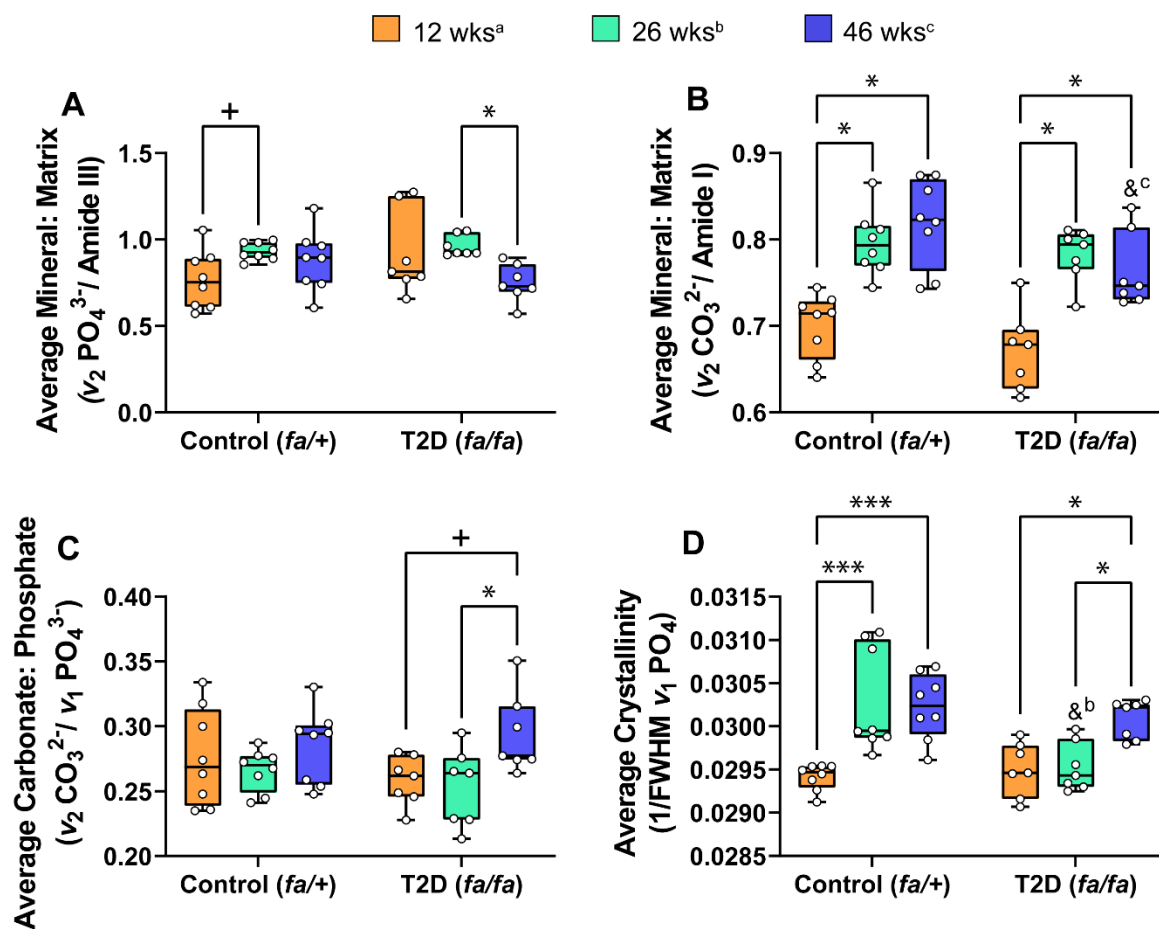


Figure 5.3: Combined average tissue composition from properties measured using polarised Raman spectroscopy such as (A) $v_2 PO_4^{3-} / \text{Amide III}$ ratio, (B) $v_2 CO_3^{2-} / \text{Amide I}$ ratio, (C) $v_2 CO_3^{2-} / v_1 PO_4^{3-}$ ratio and (D) crystallinity. + (trending significance), * ($p < 0.05$), ** ($p < 0.01$) and *** ($p < 0.001$) significance with age within strain, & significance between strain at 12^a, 26^b, and 46^c weeks.

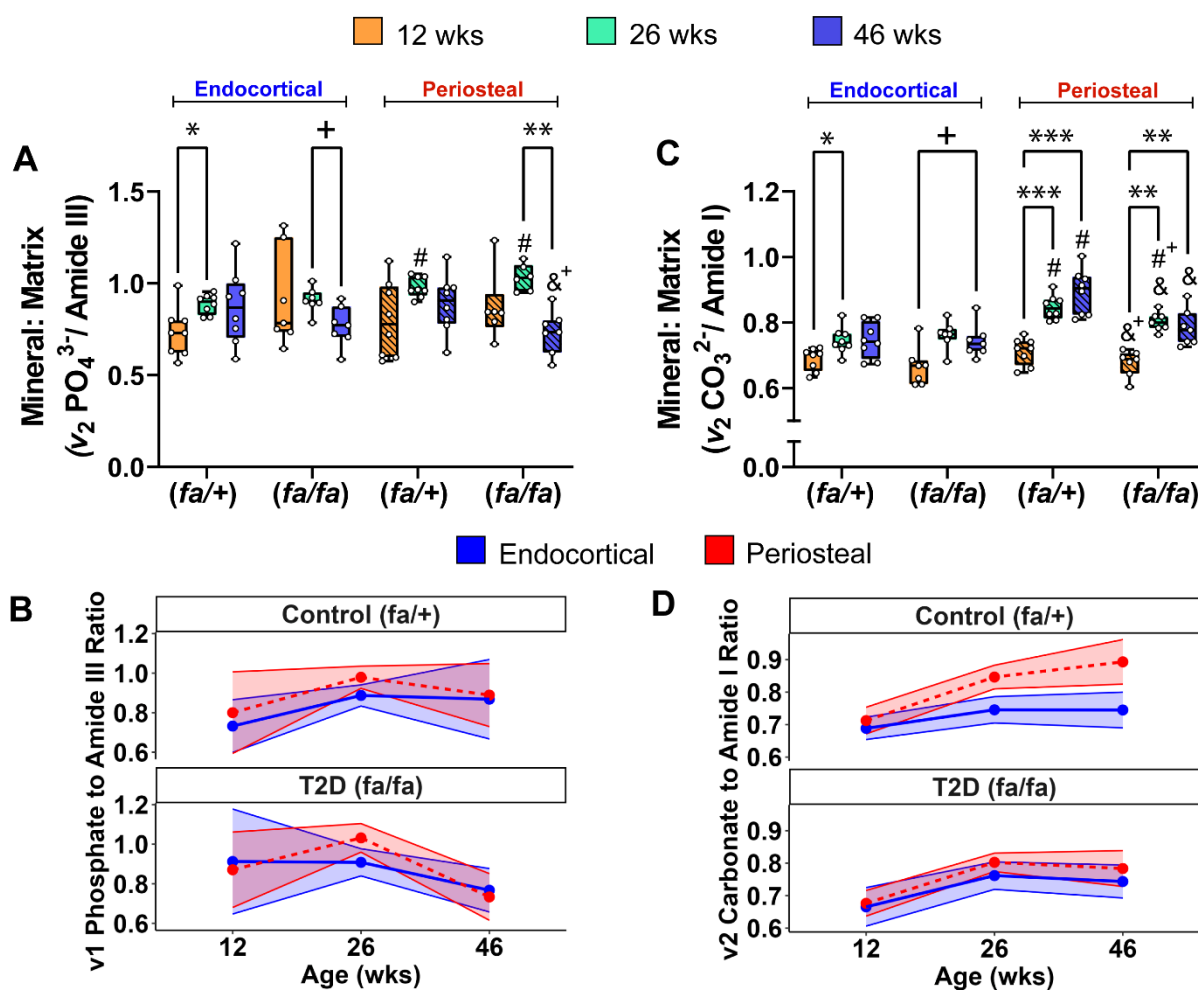


Figure 5.4: Comparing regional differences at 12-, 26- and 46-weeks for T2D (*fa/fa*) and controls (*fa/+*) rats, where each data point represents the mean of all 25 spectra per sample per region expressed as median and interquartile range for different mineral: matrix ratios from the (A and B) v_2 PO_4^{3-} / Amide III ratio (polarisation independent) and (C and D) v_2 CO_3^{2-} / Amide I ratio (polarisation dependant). (B and D) depicts regional difference comparing endocortical (blue) and periosteal (red) faceted by strain. + (trending significance), * ($p = 0.05$), ** ($p < 0.01$) and *** ($p < 0.001$) significance with age within strain, # represents a regional difference within the strain and the & represents a difference between strains within a region at 12-, 26-, and 46-weeks.

Figure 5.4 shows results from the mineral: matrix ratios comparing regional differences measured from the endocortical and periosteal regions via Raman spectroscopy. At 26-weeks, both strains had a higher v_2 phosphate mineral: matrix ratio (v_2 PO_4^{3-} / Amide III) in their periosteal region than their endocortical region (Controls: $p < 0.01$; T2D (*fa/fa*): $p < 0.05$). The diabetic (*fa/fa*) rats exhibited a significant reduction in their v_2 phosphate mineral: matrix ratio from 26- to 46-weeks in the periosteal region (-28.88%, $p < 0.01$) and a trending reduction (-

15.52%, $p = 0.052$) in the endocortical region (Figure 5.4 (A)). This difference was not shown in the control cohort. Interestingly, the diabetic (*fa/fa*) rats at 46-weeks displayed a trend ($p = 0.054$) towards a lower ν_2 phosphate mineral: matrix ratio in the periosteal region than age-matched controls. No differences between strains were observed in the endocortical region. Similarly, the ν_2 carbonate mineral: matrix ratio ($\nu_2 \text{CO}_3^{2-}/\text{Amide I}$) was higher in the periosteal region of the controls when compared to the endocortical region (+13.45% , $p < 0.001$). This regional difference was not exhibited by the T2D (*fa/fa*) cohort (+5.38% , $p = 0.07$). In the periosteal region, the ν_2 carbonate mineral: matrix ratio increased with age for control and T2D (*fa/fa*) rats with age, when only a non-significant trending increase was shown in the endocortical region of the T2D rats ($p = 0.052$) (Figure 5.4 (C)). An increase was observed from 12- to 26-weeks in the endocortical region of controls ($p < 0.05$) but similar to the diabetic (*fa/fa*) rats no significant increase was observed from 12- to 46-weeks. These regional difference with age for both strains are clearly shown in Figure 5.4 (D). Notably, diabetic (*fa/fa*) rats had a 5.06% ($p = 0.07$), 5.56% ($p < 0.05$) and 12.32% ($p < 0.01$) lower ν_2 carbonate mineral: matrix ratio in comparison to age-matched controls within the periosteal region.

Figure 5.5 shows results of further mineral properties comparing regional differences measured from the endocortical and periosteal regions via Raman spectroscopy. The periosteal region of T2D (*fa/fa*) rats at 46-weeks exhibited a significantly lower crystallinity than their endocortical region (-1.45%, $p < 0.05$). This clear regional difference can be seen in Figure 5.5 (B). Interestingly, crystallinity of the control rats increased from 12- to 26- and 26- to 46-weeks in both the endocortical and periosteal regions (Figure 5.5 (A)). While an increase from 12- to 46- (+2.89%, $p < 0.001$) and 26- to 46-weeks (+3.06%, $p < 0.01$) was demonstrated in the endocortical region of the T2D (*fa/fa*) cohort, there was no difference with age shown in their periosteal region. In both the endocortical and periosteal regions, T2D (*fa/fa*) rats at 26-weeks had 2.94% and 2.11% ($p < 0.01$) lower crystallinity than their age-matched healthy counterparts, respectively. At 46-weeks T2D (*fa/fa*) rats displayed a trend towards a 1.16% ($p = 0.07$) lower crystallinity than the controls in the periosteal region. The ν_2 carbonate: ν_1 phosphate ratio increased with age from 12- to 26- and 26- to 46-weeks was significantly increased with age in the periosteal region of T2D (*fa/fa*) rats but not in the endocortical regions (Figure 5.5 (C)). Controls exhibited no difference with age in both regions. There was no difference in the ν_2 carbonate: ν_1 phosphate ratio between strains in both regions.

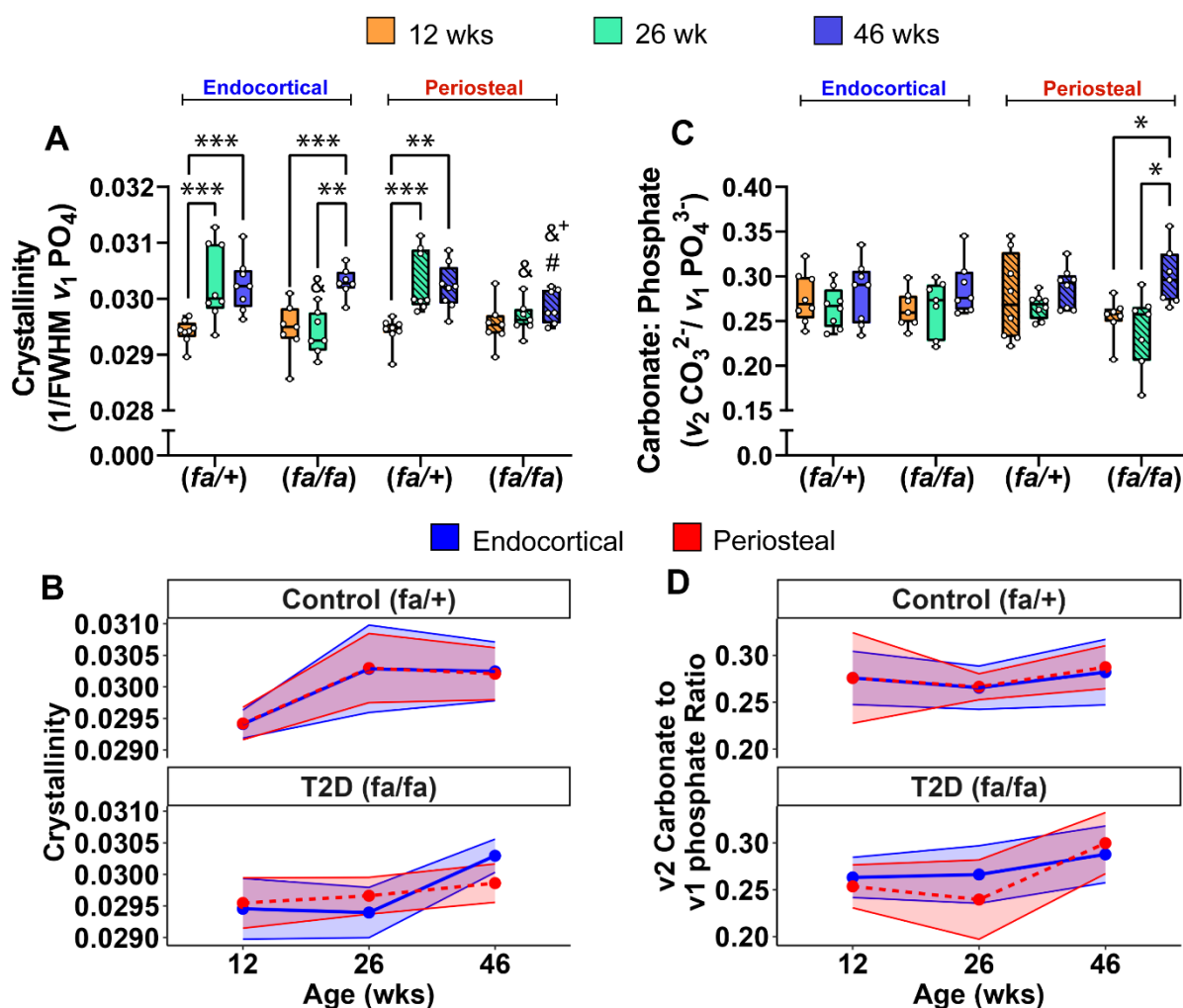


Figure 5.5: Mineral properties comparing regional differences at 12-, 26- and 46-weeks for T2D (*fa/fa*) and controls (*fa/+*) rats, where each data point represents the mean of all 25 spectra per sample per region expressed as median and interquartile range for (A and B) crystallinity and (C and D) carbonate: phosphate ratio. (B and D) depicts regional difference comparing endocortical (blue) and periosteal (red) faceted by strain. + (trending significance), * ($p < 0.05$), ** ($p < 0.01$) and *** ($p < 0.001$) significance with age within strain, # represents a regional difference within the strain and the & represents a difference between strains within a region at 12-, 26-, and 46- weeks.

Figure 5.6 shows results for collagen properties comparing regional differences measured from the endocortical and periosteal regions via Raman spectroscopy. Figure 5.6 (C) shows the regional changes in Amide III status for both strains. The periosteal region of controls at 26-weeks had a lower Amide III status than the endocortical region (-6.70%, $p < 0.05$). With age, T2D (*fa/fa*) rats exhibited a 13.17% ($p < 0.05$) reduction from 26- to 46-weeks, but no other change with age was demonstrated by any other group. Furthermore, in the periosteal region

of 26-week old T2D (*fa/fa*) rats the Amide III status was 5.05% higher than their age-matched controls ($p < 0.05$). There were also no differences observed in the enzymatic crosslink ratio or Amide I found regionally or between strains (Table 5.3).

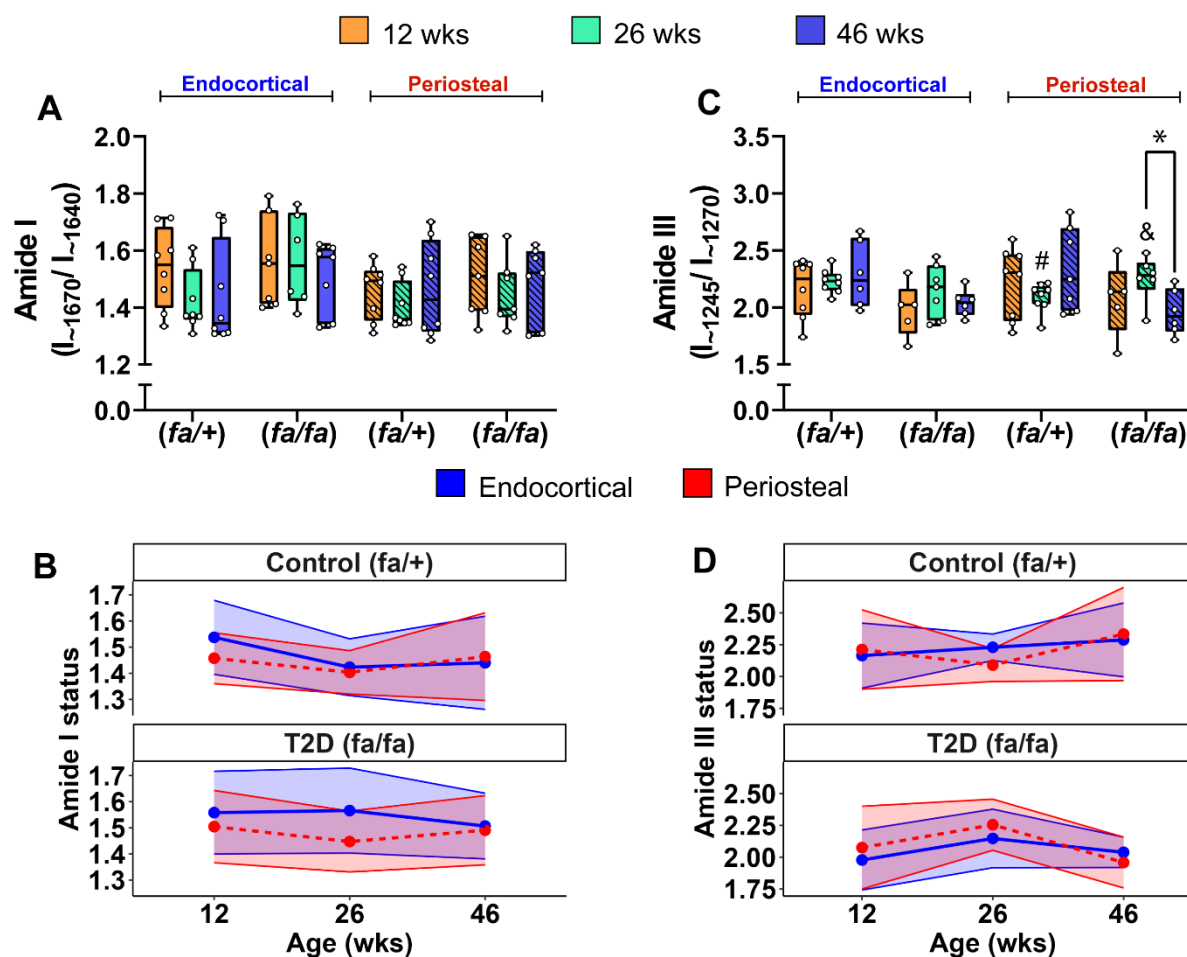


Figure 5.6: Collagen properties comparing regional differences at 12-, 26- and 46-weeks for T2D (*fa/fa*) and controls (*fa/+*) rats, where each data point represents the mean of all 25 spectra per sample, per region expressed as median and interquartile range for (A and B) Amide I status and (C and D) Amide III status. (B – D) depicts regional difference comparing endocortical (blue) and periosteal (red) faceted by strain. + (trending significance), * ($p < 0.05$), ** ($p < 0.01$) and *** ($p < 0.001$) significance with age within strain, # represents a regional difference within the strain and the & represents a difference between strains within a region at 12-, 26-, and 46-weeks.

Table 5.2: Combined average tissue-level mechanical and compositional properties for T2D (*fa/fa*) and control rats.

	Control (<i>fa/+</i>)			T2D (<i>fa/fa</i>)		
	12 weeks ^a (n = 8-9)	26 weeks ^b (n = 8)	46 weeks (n = 7-9)	12 weeks ^a (n = 8-9)	26 weeks ^b (n = 8)	46 weeks (n = 7-9)
Nanoindentation						
Elastic Modulus, GPa	21.12 ± 1.98	23.47 ± 1.01 ^a	23.52 ± 0.94 ^a	20.37 ± 1.68	22.45 ± 1.69 ^{+, a}	23.57 ± 2.07 ^a
Hardness, GPa	0.56 ± 0.06	0.61 ± 0.04 ^a	0.59 ± 0.06	0.52 ± 0.06 ⁺	0.57 ± 0.07 ⁺	0.62 ± 0.08 ^a
Micropillar compression (n = 4-5 pillars, n = 1 per condition)						
Elastic Modulus, GPa	12.51 ± 2.37	-	21.15 ± 3.11 ^a	18.64 ± 2.38 [*]	-	18.79 ± 2.55
Yield Stress, MPa	319.20 ± 59.13	-	541.44 ± 68.60 ^a	586.79 ± 166.89 [*]	-	446.26 ± 107.03 ⁺
Raman Spectroscopy						
Mineral: matrix ratio	0.77 ± 0.17	0.93 ± 0.05 ^{a+}	0.88 ± 0.18	0.92 ± 0.24	0.96 ± 0.06	0.75 ± 0.11 [*]
Crystallinity	0.0294 ± 0.0002	0.0303 ± 0.0006 ^a	0.0302 ± 0.0004 ^a	0.0295 ± 0.0003	0.0295 ± 0.0003 ^{**}	0.0300 ± 0.0002 ^{a, b}
Carbonate: phosphate ratio	0.28 ± 0.04	0.27 ± 0.02	0.29 ± 0.03	0.26 ± 0.02	0.25 ± 0.03	0.29 ± 0.03 ^{a+, b}
Carbonate: Amide I ratio	0.70 ± 0.04	0.80 ± 0.04 ^a	0.82 ± 0.05 ^a	0.67 ± 0.05	0.78 ± 0.03 ^a	0.76 ± 0.04 ^{*, a}
Enzymatic crosslink ratio	1.18 ± 0.10	1.20 ± 0.13	1.20 ± 0.10	1.18 ± 0.08	1.26 ± 0.18	1.17 ± 0.10
Amide I	1.50 ± 0.12	1.41 ± 0.09	1.45 ± 0.17	1.53 ± 0.14	1.49 ± 0.14	1.50 ± 0.13
Amide III	2.19 ± 0.28	2.15 ± 0.10	2.34 ± 0.33	2.03 ± 0.23	2.17 ± 0.21	1.99 ± 0.15

Values are mean ± SD. T2D, Type-2 diabetic.

Difference from aged matched lean control (*fa/+*) rats with * ($p < 0.05$), ** ($p < 0.01$), *** ($p < 0.001$) and ⁺ (*trending influence*).

^a significantly different from 12-weeks determined by a multiple comparisons Tukey test

^b significantly different from 26-weeks determined by a multiple comparisons Tukey test

- samples not tested

5.3.2 Tissue-level mechanical properties

Nanoindentation

Table 5.2 shows the combined mean tissue indentation modulus and hardness, measured at 12-, 26- and 46-weeks in both T2D (*fa/fa*) and healthy, control rats. Elastic modulus increased with age for both strain from 12- to 26- and 12- to 46-weeks (Table 5.2). T2D (*fa/fa*) rats at 26-weeks exhibited a non-significant trend towards a 4.35% ($p = 0.056$) lower elastic modulus than age-matched controls. Mean tissue hardness of the T2D (*fa/fa*) rats increased from 12- to 46-weeks (+19.23, $p < 0.01$), but no significant differences were found in the control cohort. At 12- and 26-weeks, T2D (*fa/fa*) rats showed a trend towards a -7.14% ($p = 0.07$) and -6.56% ($p = 0.055$) lower hardness than their age-matched healthy controls. No difference in hardness between strains was found at 46-weeks.

Figure 5.7 and Table 5.3 shows results for tissue indentation modulus and hardness comparing regional differences measured from the endocortical and periosteal regions. At 26-weeks, controls exhibited a 3.19% ($p < 0.05$) greater elastic modulus in their periosteal region than their endocortical. However, T2D (*fa/fa*) rats only displayed a non-significant trend towards a higher periosteal elastic modulus than endocortical ($p = 0.07$). From 12- to 26-weeks elastic modulus increased with age for controls in both regions (Endocortical: $p < 0.01$; Periosteal: $p < 0.05$) but only in the periosteal ($p < 0.01$) region for the T2D (*fa/fa*) rats (Table 5.3). From 12- to 46-weeks, elastic modulus increased for all ages and strains except the periosteal region of controls. Although non-significant, T2D (*fa/fa*) rats at 26-weeks displayed a trend towards a lower elastic modulus than age-matched controls in the endocortical region (-6.13%, $p = 0.07$).

Hardness was increased from 12- to 46-weeks in the endocortical (+17.24%, $p < 0.05$) and periosteal (+14.40%, $p < 0.05$) regions of the T2D (*fa/fa*) rats, but no increase with age was observed in both regions of the control groups. Despite this, at 26-weeks the hardness in the endocortical region of T2D (*fa/fa*) rats only showed a trend towards a lower hardness (-7.29%, $p < 0.10$) in comparison to age-matched controls, with no other differences observed.

Table 5.3: Regional differences in tissue-level mechanics and composition between the endocortical (E) and periosteal (P) regions.

	Control (<i>fa/+</i>)						T2D (<i>fa/fa</i>)					
	12 weeks ^a (n = 8-9)		26 weeks ^b (n = 8)		46 weeks (n = 7-9)		12 weeks ^a (n = 8-9)		26 weeks ^b (n = 8)		46 weeks (n = 7-9)	
	E	P	E	P	E	P	E	P	E	P	E	P
<i>Nano-indentation</i>												
Elastic Modulus, GPa%	20.51 ± 1.63	21.62 ± 2.27	23.10 ± 1.17 ^a	23.83 ± 0.69 ^{##, a}	23.72 ± 1.09 ^a	23.35 ± 0.82	20.43 ± 1.80	20.32 ± 1.67	21.68 ± 1.63 [*]	23.34 ± 1.37 ^{E+, a}	23.34 ± 2.52 ^a	23.80 ± 1.66 ^a
Hardness, GPa	0.54 ± 0.03	0.57 ± 0.07	0.59 ± 0.04	0.63 ± 0.03	0.62 ± 0.06	0.60 ± 0.06	0.52 ± 0.05	0.51 ± 0.06	0.55 ± 0.05 ⁺	0.61 ± 0.08 ^a	0.61 ± 0.10 ^a	0.60 ± 0.07 ^a
<i>Micropillar compression</i> (<i>n</i> = 4-5 pillars, (<i>n</i> = 1 per condition))												
Elastic Modulus, GPa	11.21 ± 2.50	13.82 ± 2.45	-	-	21.56 ± 0.79 ^a	20.71 ± 5.43 ^a	17.14 ± 2.52 [*]	20.15 ± 4.40 [*]	-	-	17.91 ± 0.81 [*]	19.68 ± 4.28
Yield Stress, MPa	318.15 ± 61.92	320.25 ± 56.34	-	-	500.35 ± 46.90 ^a	582.53 ± 90.30 ^a	552.07 ± 173.86 [*]	621.51 ± 159.91 ^{**}	-	-	468.76 ± 79.95	423.77 ± 134.11
<i>Raman Spectroscopy</i>												
Mineral: matrix ratio	0.73 ± 0.13	0.80 ± 0.21	0.89 ± 0.05 ^a	0.98 ± 0.06 ^{##}	0.87 ± 0.20	0.89 ± 0.16	0.91 ± 0.27	0.87 ± 0.19	0.91 ± 0.07	1.03 ± 0.07 ^{##}	0.77 ± 0.11	0.73 ± 0.12 ^{+, b}
Crystallinity	0.0294 ± 0.0002	0.0294 ± 0.0003	0.0303 ± 0.0007 ^a	0.0303 ± 0.0005 ^a	0.0303 ± 0.0005 ^a	0.0302 ± 0.0004 ^a	0.0295 ± 0.0005	0.0296 ± 0.0004	0.0294 ± 0.0004 ^{**} , ^a	0.0297 ± 0.0003 ^{**}	0.0303 ± 0.0003 ^a	0.0299 ± 0.0003 ^{+, ###}
Carbonate: phosphate ratio	0.276 ± 0.029	0.276 ± 0.05	0.265 ± 0.02	0.267 ± 0.01	0.282 ± 0.04	0.287 ± 0.02	0.263 ± 0.02	0.254 ± 0.02	0.266 ± 0.03	0.240 ± 0.04	0.288 ± 0.03	0.300 ± 0.03 ^{a, b}

Carbonate: Amide I ratio	0.69 ± 0.03	0.71 ± 0.05	0.75 ± 0.04 ^a	0.85 ± 0.04 ^{a+,##}	0.75 ± 0.06 ^{a+}	0.89 ± 0.07 ^{a+,###}	0.67 ± 0.06	0.68 ± 0.04 ^{+,E+}	0.76 ± 0.04 ^a	0.80 ± 0.03 ^{a,*}	0.74 ± 0.05 ^a	0.78 ± 0.06 ^{a,**}
Enzymatic crosslink ratio	1.17 ± 0.09	1.18 ± 0.11	1.21 ± 0.16	1.20 ± 0.14	1.14 ± 0.11	1.10 ± 0.08	1.16 ± 0.08	1.18 ± 0.11	1.26 ± 0.18	1.28 ± 0.20	1.19 ± 0.10	1.15 ± 0.09
Amide I	1.54 ± 0.14	1.46 ± 0.10	1.43 ± 0.12	1.40 ± 0.09	1.44 ± 0.18	1.46 ± 0.17	1.56 ± 0.16	1.51 ± 0.14	1.57 ± 0.16	1.45 ± 0.12	1.51 ± 0.13	1.49 ± 0.13
Amide III	2.16 ± 0.26	2.21 ± 0.31	2.22 ± 0.10	2.09 ± 0.13 ^{##}	2.48 ± 0.57	2.33 ± 0.37	1.98 ± 0.24	2.08 ± 0.33	2.15 ± 0.23	2.26 ± 0.20 [*]	2.04 ± 0.12	1.96 ± 0.20 ^b

Values are mean ± SD. T2D, Type-2 diabetic; E, Endocortical; P, Periosteal.

Difference from aged matched lean control (*fa/+*) rats with * ($p < 0.05$), ** ($p < 0.01$), *** ($p < 0.001$) and + (*trending influence*).

Difference within strain between regions with # ($p < 0.05$), ## ($p < 0.01$) and ### ($p < 0.001$), ^{E+} (*trending influence to endocortical region*).

^a significantly different from 12-weeks

^b significantly different from 26-weeks

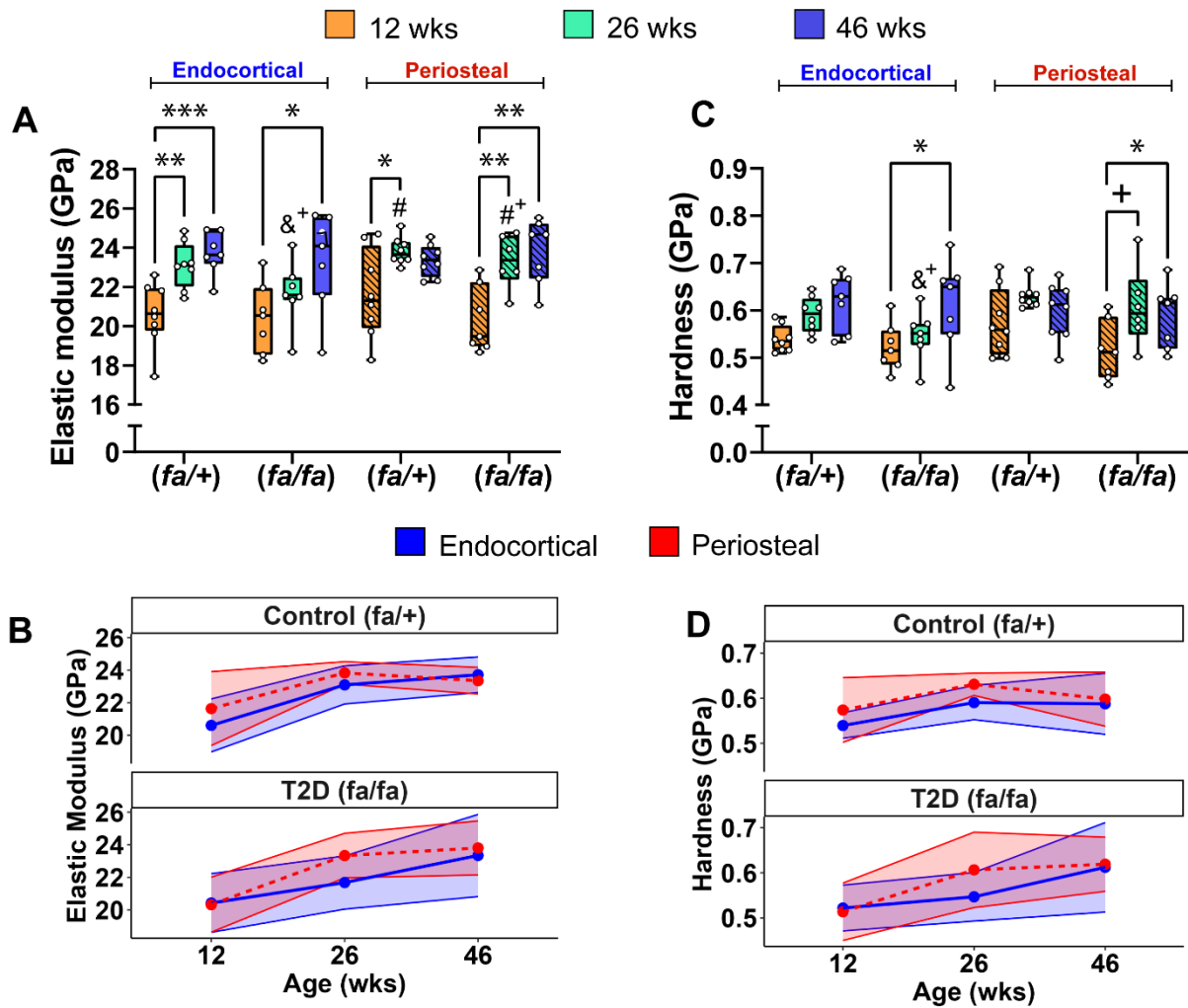


Figure 5.7: Tissue-level mechanical properties comparing regional differences at 12-, 26- and 46-weeks for T2D (*fa/fa*) and controls (*fa/+*) rats, where each data point represents the mean of all 16 indents per region expressed as median and interquartile range for (A) elastic modulus and (B) hardness. (C and D) depicts regional difference comparing endocortical (blue) and periosteal (red) for controls and T2D (*fa/fa*). + (trending significance), * ($p < 0.05$), ** ($p < 0.01$) and *** ($p < 0.001$) significance with age within strain, # represents a regional difference within the strain and the & represents a difference between strains within a region at 12-, 26-, and 46-weeks.

Micropillar compression

Figure 5.8 shows results for micropillar compression testing comparing regional differences measured from the endocortical and periosteal regions. Figure 5.8 (C-F) show the characteristic uniaxial compressive strain curves across each test group. Notably, the measured compressive yield stress and the ultimate compressive strength of the tissue are on the order of 500 MPa and 1,000 MPa, respectively, which is substantially higher than values obtained through traditional

tissue-level testing. Several different loading profiles were observed across groups, with 12-week control micropillars from the endocortical and periosteal regions showing similar loading profiles (Figure 5.8 (C)), while other test cases are more varied and show certain evidence of drop in stress post-yielding. Each boxplot represents the mean of 4 - 6 pillars that were compressed in either the periosteal or endocortical region of one sample per disease state ($n = 1$ per condition at 12- and 46-weeks with $n = 4 - 6$ pillars per region, per sample). There were no regional differences within disease states for the elastic modulus. However, elastic modulus from the endocortical and periosteal region increased by 92.37% ($p < 0.05$) and 49.56% ($p < 0.001$) from 12- to 46-weeks in the control ($fa/+$) rat sample, respectively, but not in the T2D (fa/fa) rat sample (Figure 5.8 (A)). Interestingly, at 12-weeks, micropillars from the diabetic (fa/fa) rat had a higher elastic modulus than the controls in the endocortical (+ 53%, $p < 0.05$) and periosteal (+ 49.87%, $p = 0.05$) region. However, at 46-weeks the micropillars in the endocortical region from the diabetic (fa/fa) sample had a 16.92% lower modulus than the age-matched control pillars ($p < 0.05$). There were no regional differences in yield stress within disease states. The yield stress of the control pillars from both the endocortical and periosteal regions increased with age (Figure 5.8 (B)). However, yield stress was also higher in the pillars of the 12-week T2D (fa/fa) sample in comparison to the age-matched control in both the endocortical (+ 73.52%, $p < 0.01$) and periosteal (+ 94.07%, $p < 0.001$) regions. SEM images of the pillars captured before and after compression testing are shown in Figure 5.9.

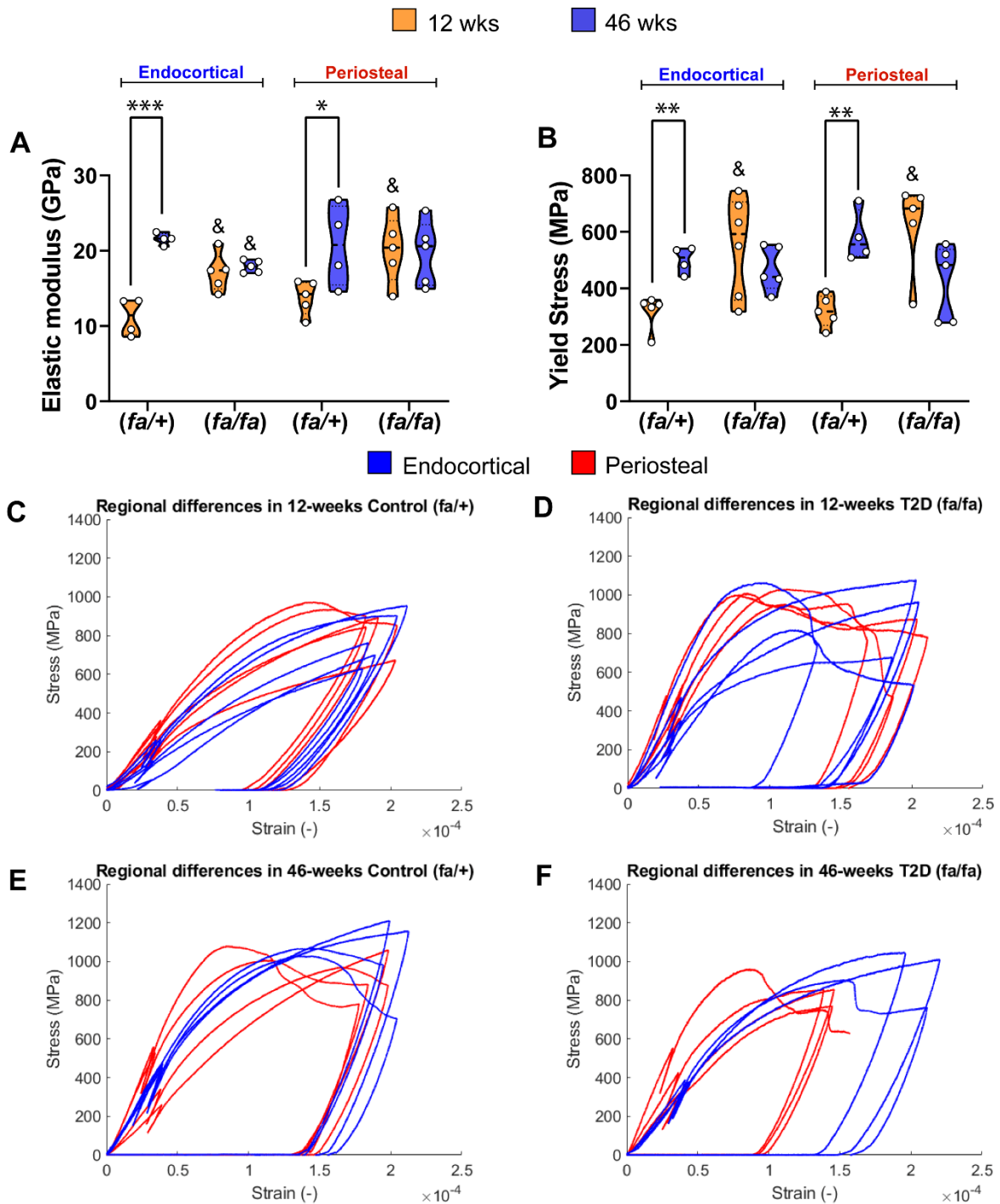


Figure 5.8: Regional differences at 12- and 46-weeks ($n = 1$ per and condition) in (A) elastic modulus and (B) yield stress. Each data point represents results for one pillar. (C-F) exhibits the loading profiles for each profile from the endocortical (blue) and periosteal (red) region for control and T2D (fa/fa) samples. ** ($p < 0.01$) and *** ($p < 0.001$) significance within strain; & indicates a difference between strains 12- and 46-weeks.

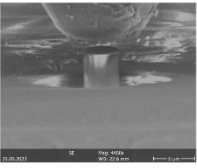
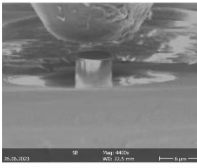
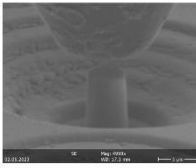
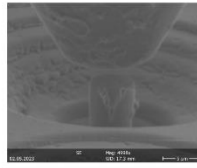
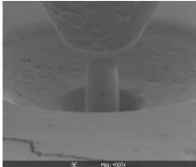
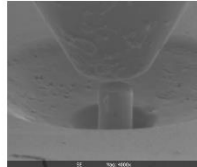
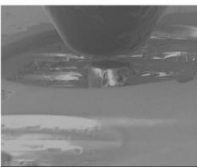

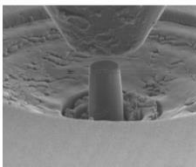
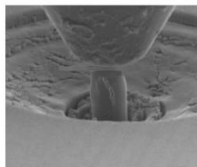
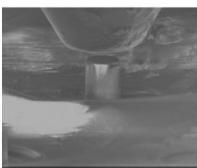
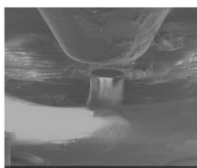
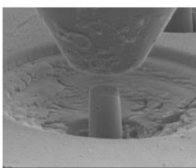
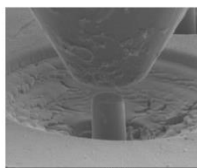
		12 Weeks		46 Weeks	
		Pre	Post	Pre	Post
Control (<i>fa/+</i>)	Peri	 n = 5	 n = 5	 n = 4	 n = 4
	Endo	Not captured n = 5	Not captured n = 5	 n = 4	 n = 4
T2D (<i>fa/fa</i>)	Peri	 n = 5	 n = 5	 n = 5	 n = 5
	Endo	 n = 6	 n = 6	 n = 5	 n = 5

Figure 5.9: Representative post-compression profile of a pillar from the endocortical and periosteal region from a control and diabetic (*fa/fa*) sample.

5.4 Discussion

For the first time, this study has investigated regional differences in tissue composition and mechanics as the disease progresses in a ZDF (*fa/fa*) rat model of T2D. In this study comparisons were made across three distinct components, comparing (a) region vs. region within strains, (b) longitudinally within strains in both regions and (c) between strains within regions at all ages. This study showed that regional differences were mainly evident in the mineral more so than the collagen component of the tissue, particularly in the periosteal region of the cortical bone in T2D (*fa/fa*) and control rats. Regional differences demonstrated by the control cohort were evident through a higher mineral to matrix ratio (v_2 phosphate/ Amide III) and (v_2 carbonate/ Amide I) in the periosteal region when compared to the endocortical region

of control rats at 26-weeks and 26- and 46-weeks, respectively. Furthermore, the diabetic (*fa/fa*) cohort exhibited compositional alterations in the periosteal region when compared to the endocortical region of femoral cortical bone, indicated by a higher mineral to matrix ratio (v2 phosphate/ Amide III) at 26-weeks and a lower crystallinity at 46-weeks in their periosteal rather than their endocortical region. Additionally, whilst controls demonstrated an increase in crystallinity with age in both regions, diabetic (*fa/fa*) rats only showed an increase with age in their endocortical region and no longitudinal change periosteally. The inverse was found in the carbonate: phosphate ratio, where T2D (*fa/fa*) rats showed an increase with age periosteally, when no other longitudinal observations were found in the endocortical region of the diabetic (*fa/fa*) rats and both regions of the controls. Again, the majority of changes found between strains was observed in the periosteal region, where diabetic (*fa/fa*) rats had a lower v2 phosphate mineral to matrix ratio (v2 phosphate/ Amide III) at 46-weeks and lower v2 carbonate mineral: matrix ratio (v2 carbonate/ Amide I) at 26- and 46-weeks in comparison to age- and region-matched controls. Similarly, the diabetic (*fa/fa*) rats had a lower crystallinity at 26 and 46-weeks and a higher periosteal Amide III status at 26-weeks than their age- and region-matched controls. These regional compositional changes may indicate an altered mineralisation or cellular metabolism process in the bone maintenance of ZDF (*fa/fa*) rats as they age and the disease progresses. However, in measuring the tissue-level mechanical properties, there was no difference in indentation modulus or hardness found between strains in both regions, despite the regional differences in composition. Controls had a higher periosteal indentation elastic modulus, in line with a higher mineral: matrix ratio within this region, whereas the T2D (*fa/fa*) rats only displayed a trending higher indentation modulus. Interestingly, hardness increased from 12- to 46-weeks in both regions of the T2D (*fa/fa*) rats but this was not shown in the control cohort. Although previous Chapters have shown compositional changes to tissue quality led to impaired mechanical performance, this study has revealed that on a local level these compositional changes did not lead to altered tissue-level mechanics. Overall, this study provides insight into the regional changes that occur during the growth and maintenance of cortical bone from ZDF (*fa/fa*) rats from diabetes that develops at a young age and progresses into old age.

In previous Chapters, tissue composition and mechanics were explored at the whole bone level and showed that modifications in the cellular activity of ZDF rats may play a significant role in initiating the cellular events that result in mineralisation changes within the bone matrix, ultimately impairing the tissue quality. Moreover, longitudinal bone growth and maintenance

was impaired in these rats, which was evident by a smaller cortical bone area and thickness than controls and reduced trabecular BV/TV with age. Chapter 3 showed that bone growth measured by anterior-posterior and medial-lateral diameter, moment of inertia and cortical bone area did not significantly occur from 26- to 46-weeks in the diabetic (*fa/fa*) cohort, whereas it had increased for controls. In fact, in Chapter 4, femoral thickness decreased from 26- to 46-weeks in the T2D (*fa/fa*) rats but remained unchanged for the controls. In this Chapter, regional differences were explored to assess how diabetes may interrupt bone maintenance and appositional growth particularly with age and disease progression in these ZDF (*fa/fa*) rats. Notably, whilst there was no change with age in the endocortical region, the v_2 carbonate/ Amide I ratio increased with age from 12- to 26 and 26- to 46 weeks for both strains in the periosteal region. The v_2 carbonate/ Amide I ratio has been proposed to be related to turnover rate and remodelling activity in the bone (Isaksson et al., 2010; McCreadie et al., 2006). Carbonate is an impurity that is substituted into the hydroxyapatite mineral structure and carbonate content has been shown to accumulate with age as turnover decreases (Akkus et al., 2004; Kourkoumelis et al., 2019). In rodents, it is understood that age-related bone loss occurs due to increased endocortical resorption and reduced periosteal formation (Razi et al., 2015). This is likely what is being shown in this Chapter whereby the endocortical region did not show an increase in carbonate with age since this mineral is being resorbed and is not given a chance to accumulate carbonate. During bone thickening, the periosteal side forms new bone and the mineral matures since bone formation is high and resorption activity is low (Busa et al., 2005; Donnelly et al., 2010a; Razi et al., 2015). However, as bone ages this process begins to slow down resulting in a slow in cortical thickening and, hence, formation and resorption slow such that it reduces the presence of newly formed bone, resulting in an increase in carbonate content reflecting the older, mature mineral. Controls exhibited no regional difference in v_2 carbonate/ Amide I ratio at 12-week but at 26- and 46-weeks controls displayed greater v_2 carbonate/ Amide I ratio in periosteal regions when compared to the endocortical regions, implying that at 12-weeks young bone was growing and being formed but at 26- and 46-weeks, the formation of new bone slowed and more mature mineral was present in the periosteal region in comparison to the endocortical region. This is again highlighted in the v_2 phosphate/ Amide III ratio which was higher in the periosteal region of control and T2D (*fa/fa*) rats at 26-weeks when compared to endocortical regions. However, the T2D (*fa/fa*) rats showed a trend towards a higher v_2 carbonate/ Amide I ratio in their periosteal regions when compared to their endocortical regions, with no regional change at 12- and 46-weeks. At 26- and 46-weeks, they exhibited a significantly lower v_2 carbonate/ Amide I ratio than controls, suggesting that whilst

the bone growth and maintenance in these T2D (*fa/fa*) rats is occurring with age, this process is happening at a much slower rate when compared to the controls. In fact, mineral maturation may be impaired in these ZDF (*fa/fa*) rats indicated by the fact that only a trending regional difference was observed at 26-weeks and no difference seen between regions at 46-weeks. This was further supported by the trending reduction in ν_2 phosphate/ Amide III ratio of T2D (*fa/fa*) rats at 46-weeks compared to age-matched controls within the periosteal region. Of course, the increased ν_2 carbonate/ Amide I ratio with age can either be explained by an increasing carbonate content or a reducing amide I content. Since there was no difference observed in the Amide I status with age or between strains in any region, the former is accepted. In fact, T2D (*fa/fa*) rats displayed an increase in carbonate: phosphate ratio with age in the periosteal region. However, there is a difficulty in acquiring a precise measurement for the carbonate: phosphate ratio using Raman spectroscopy since the carbonate band (1050 – 1100 cm^{-1}) is partially overlapped by another phosphate band (at $\sim 1076 \text{ cm}^{-1}$) (Awonusi et al., 2007), thus variability was too high in controls to observe differences in the carbonate: phosphate ratio with age.

Previous research has indicated that crystallinity as assessed using vibrational spectroscopy increases with age, which can influence tissue stiffness and strength (Akkus et al., 2004; Yerramshetty et al., 2006). Various human and animal studies of T2D have reported either an increased (Arora et al., 2023; Creecy et al., 2016; Hunt et al., 2019) or unchanged (Creecy et al., 2018b; Hunt et al., 2018; Wölfel et al., 2022b, 2022a) crystallinity in the type-2 diabetic cohorts. To the author's knowledge, crystallinity has not been explored in ZDF (*fa/fa*) rats. Surprisingly, the results from this Chapter showed that, while the combined average crystallinity did increase with age for both control and T2D (*fa/fa*) rats, when examined regionally the T2D (*fa/fa*) rats at 26-weeks exhibited a lower crystallinity in both the endocortical and periosteal regions when compared to age-matched controls. A lower crystallinity may be reflective of a smaller, more disorganised crystalline structure. Notably, Amide III status was also higher in the T2D (*fa/fa*) rats than controls within the periosteal region, which previous research has suggested is reflective of the transition from collagen helical structure to disordered structure (Dehring et al., 2006; Unal et al., 2021). Thus, an increase in Amide III status indicates an increase in collagen fibre disorderliness. Interestingly, Wölfel *et al.* (2020b) reported lower crystallinity in the T2D high porosity group when compared to the T2D group in the endocortical region as well as reporting significantly lower mineral maturity in the high porosity group in endocortical and periosteal regions compared to those in the control and the T2D group. Taken together, they proposed that their results

reflected changes in apatite crystallisation. It is possible that the reduced crystallinity experienced in the T2D (*fa/fa*) rats at 26-weeks may reflect an altered mineralisation process where mineral crystals are not forming or growing as efficiently as controls. This is further highlighted by regionally lower crystallinity in the periosteal region of T2D (*fa/fa*) rats at 46-weeks than their endocortical region. However, it is difficult to fully infer how these changes reflect the cellular metabolism within the tissue without further histological analysis.

A similar study of T2D using TallyHo mice assessed tissue composition and tissue-level mechanics via Raman spectroscopy and nanoindentation, respectively, and found that the TallyHo mice with T2D exhibited a greater indentation modulus and hardness than controls and they attributed these changes to the increased mineral: matrix ratio and trending increase in crystallinity in the diabetic strain (Arora et al., 2023). They also examined regional tissue mechanical properties and found that elastic modulus and hardness were higher in the periosteal region than the endocortical region, however they did not explore regional compositional differences nor did they compare these regional differences between strains (Arora et al., 2023). In this Chapter, the elastic modulus was higher in the periosteal region than the endocortical region at 26-weeks for both strains which may have been due to the higher mineralisation (v_2 phosphate/ Amide III and v_2 carbonate/ Amide I) at this age. Whilst endocortical elastic modulus and hardness trended towards a reduction in the diabetic (*fa/fa*) rats at 26-weeks compared to age-matched controls, ultimately there was no significant differences between strains. Similarly, studies by Wölfel *et al* assessed bone quality from femoral and tibial cortical bone (Wölfel et al., 2022a, 2020) and both studies reported compositional changes such as the T2D with high porosity patients presenting with a lower crystallinity compared to T2D groups and a higher v_2 carbonate/ Amide I ratio compared to T2D and control groups. However, despite reporting these compositional alterations, no differences in the tissue-level indentation modulus or hardness was found regionally or between cohorts (Wölfel et al., 2022a, 2020). They proposed that the observed difference between nano- and micro-scales indicates that T2D is linked to changes in the scaling-up process of mineralisation in bone, rather than alterations in the actual formation of mineral itself. Whilst no tissue-level mechanical differences were captured between strains in this Chapter, previous Chapters have shown that the T2D (*fa/fa*) cohort, particularly at 46-weeks presented with a reduced yield and ultimate strength as well as a reduced cracking toughness. Moreover, post-yield displacement reduced with age for T2D (*fa/fa*) rats when this was not observed in the controls. Consequently, it is possible that using nanoindentation to evaluate mechanical properties of individual lamellae at the nanoscale, as

was done in this Chapter, may not be able to capture the full extent of what is happening to the tissue properties at larger length scales as it omits the presence of porosity, tissue heterogeneity and microdamage to name a few. This may also suggest that differences in tissue mechanics in T2D may indeed have a contribution from these structural features that exist in the tissue. Interestingly, the results from the micropillar compression tests showed that, where the tissue-level yield stresses experienced by the compressed pillars in this Chapter were much higher than stresses measured from macro-level testing in other Chapters. Such a size effect is commonly observed in mechanical testing of materials, where fewer defects exist in the structure at these smaller length scales. However, still it was difficult to observe any true differences in the micropillar mechanical response between T2D and controls.

Several limitations and suggestions for future research should be mentioned. Firstly, this Chapter examined site-matched differences in composition and tissue-level mechanics, whereby Raman spectroscopy and nanoindentation measurements were taken from the same $150 \times 150 \mu\text{m}^2$ area. However, this work is limited by the fact that compositional properties could not be directly correlated to tissue-level mechanics. It would be beneficial for future work to consider site-specific regional testing, where indents would be created, and Raman measurements could be taken from the exact same place as the indents. This would allow direct comparisons to be made between tissue compositional and the tissue mechanics. In addition, future regional work may benefit from not only examining longitudinal regional differences but also implementing the analysis of tissue age by examining tissue composition and mechanics along the cross-section of the cortical tissue moving away from the periosteal and endosteal edge as done in (Donnelly et al., 2010a). This would add another level of analysis to further understand mineralisation and cellular metabolism in ZDF (*fa/fa*) rats. Finally, micropillar compression testing showed that the elastic modulus and yield stress increased with age for the control sample, when no change with age was evident from the T2D (*fa/fa*) sample. However, at 12-weeks the T2D (*fa/fa*) rat sample had a higher elastic modulus and yield stress than controls. This was interesting since in previous Chapters it was shown that post-yield displacement decreased with age in the T2D (*fa/fa*) cohort but not the controls as a result of the diabetic (*fa/fa*) rats at 12-weeks having a higher post-yield displacement than the controls. Whilst this was seemingly captured in micropillar compression test, these results are limited by the fact that only one sample per age, per condition could be examined ($n = 4 - 6$ pillars for each). To probe this further, future work could examine higher samples numbers to investigate the effect of collagen fibre orientation on the local biomechanical properties.

5.5 Concluding Remarks

In conclusion, this study for the first time investigated regional variations in tissue composition and mechanics as T2D progressed in a ZDF (*fa/fa*) rat model. Notably, regional differences were primarily evident in the mineral component, especially in the periosteal region of cortical bone in T2D (*fa/fa*) and control rats. Diabetic rats exhibited an altered ν_2 carbonate/Amide I ratio, ν_2 phosphate/Amide III ratio, and crystallinity, indicating a regional dynamic interplay between bone formation and resorption processes in maintaining bone growth. Despite compositional changes impacting tissue quality, tissue-level mechanical properties, assessed by indentation modulus and hardness, showed no significant differences between strains in both regions. These findings provide valuable insights into the regional changes during the growth and maintenance of cortical bone in ZDF (*fa/fa*) rats with T2D, providing a wider understanding into the complex interaction between tissue composition, mechanics, and disease progression.

5.6 References

- Akkus, O., Adar, F., Schaffler, M.B., 2004. Age-related changes in physicochemical properties of mineral crystals are related to impaired mechanical function of cortical bone. *Bone* 34, 443–453. <https://doi.org/10.1016/j.bone.2003.11.003>
- Arora, D., Taylor, E.A., King, K.B., Id, E.D., 2023. Increased tissue modulus and hardness in the TallyHO mouse model of early onset type 2 diabetes mellitus. *PLOS* 1–22. <https://doi.org/https://doi.org/10.1371/journal.pone.0287825>
- Awonusi, A., Morris, M.D., Tecklenburg, M.M.J., 2007. Carbonate assignment and calibration in the Raman spectrum of apatite. *Calcif. Tissue Int.* 81, 46–52. <https://doi.org/10.1007/s00223-007-9034-0>
- Birkhold, A.I., Razi, H., Duda, G.N., Weinkamer, R., Checa, S., Willie, B.M., 2016. The Periosteal Bone Surface is Less Mechano-Responsive than the Endocortical. *Sci. Rep.* 6, 1–11. <https://doi.org/10.1038/srep23480>
- Britton, M., Vaughan, T., 2023. An experimental investigation on the biomechanics of bone fragility in type-2 diabetes. University of Galway.
- Busa, B., Miller, L.M., Rubin, C.T., Qin, Y.X., Judex, S., 2005. Rapid establishment of chemical and mechanical properties during lamellar bone formation. *Calcif. Tissue Int.* 77, 386–394. <https://doi.org/10.1007/s00223-005-0148-y>
- Creecy, A., Uppuganti, S., Merkel, A.R., O’Neal, D., Makowski, A.J., Granke, M., Voziyan, P., Nyman, J.S., 2016. Changes in the Fracture Resistance of Bone with the Progression of Type 2 Diabetes in the ZDSD Rat. *Calcif. Tissue Int.* 99, 289–301. <https://doi.org/10.1007/s00223-016-0149-z>
- Creecy, A., Uppuganti, S., Unal, M., Clay Bunn, R., Voziyan, P., Nyman, J.S., 2018. Low bone toughness in the TallyHO model of juvenile type 2 diabetes does not worsen with age. *Bone* 110, 204–214. <https://doi.org/10.1016/j.bone.2018.02.005>
- Dehring, K.A., Smukler, A.R., Roessler, B.J., Morris, M.D., 2006. Correlating changes in collagen secondary structure with aging and defective type II collagen by Raman spectroscopy. *Appl. Spectrosc.* 60, 366–372. <https://doi.org/10.1366/000370206776593582>
- Donnelly, E., Boskey, A.L., Baker, S.P., van der Meulen, M.C.H., 2010a. Effects of tissue age

- on bone tissue material composition and nanomechanical properties in the rat cortex. *J. Biomed. Mater. Res. Part A* 92A, 1048–1056. <https://doi.org/10.1002/jbm.a.32442>
- Donnelly, E., Chen, D.X., Boskey, A.L., Baker, S.P., Van Der Meulen, M.C.H., 2010b. Contribution of mineral to bone structural behavior and tissue mechanical properties. *Calcif. Tissue Int.* 87, 450–460. <https://doi.org/10.1007/s00223-010-9404-x>
- Hunt, H.B., Pearl, J.C., Diaz, D.R., King, K.B., Donnelly, E., 2018. Bone Tissue Collagen Maturity and Mineral Content Increase With Sustained Hyperglycemia in the KK-Ay Murine Model of Type 2 Diabetes. *J. Bone Miner. Res.* 33, 921–929. <https://doi.org/10.1002/jbmr.3365>
- Hunt, H.B., Torres, A.M., Palomino, P.M., Marty, E., Saiyed, R., Cohn, M., Jo, J., Warner, S., Sroga, G.E., King, K.B., Lane, J.M., Vashishth, D., Hernandez, C.J., Donnelly, E., 2019. Altered Tissue Composition, Microarchitecture, and Mechanical Performance in Cancellous Bone From Men With Type 2 Diabetes Mellitus. *J. Bone Miner. Res.* 34, 1191–1206. <https://doi.org/10.1002/jbmr.3711>
- Indermaur, M., Casari, D., Kochetkova, T., Willie, B.M., Michler, J., Schwiedrzik, J., Zysset, P., 2023. Tensile Mechanical Properties of Dry Cortical Bone Extracellular Matrix: A Comparison Among Two Osteogenesis Imperfecta and One Healthy Control Iliac Crest Biopsies. *JBMR Plus* 00, 1–12. <https://doi.org/10.1002/jbm4.10826>
- Isaksson, H., Turunen, M.J., Rieppo, L., Saarakkala, S., Tamminen, I.S., Rieppo, J., Kröger, H., Jurvelin, J.S., 2010. Infrared spectroscopy indicates altered bone turnover and remodeling activity in renal osteodystrophy. *J. Bone Miner. Res.* 25, 1360–1366. <https://doi.org/10.1002/jbmr.10>
- Kochetkova, T., Groetsch, A., Indermaur, M., Peruzzi, C., Remund, S., Neuenschwander, B., Bellon, B., Michler, J., Zysset, P., Schwiedrzik, J., 2022. Assessing minipig compact jawbone quality at the microscale. *J. Mech. Behav. Biomed. Mater.* 134, 105405. <https://doi.org/10.1016/j.jmbbm.2022.105405>
- Kochetkova, T., Hanke, M.S., Indermaur, M., Groetsch, A., Remund, S., Neuenschwander, B., Michler, J., Siebenrock, K.A., Zysset, P., Schwiedrzik, J., 2023. Composition and micromechanical properties of the femoral neck compact bone in relation to patient age, sex and hip fracture occurrence. *Bone* 177, 116920. <https://doi.org/10.1016/j.bone.2023.116920>

- Kochetkova, T., Peruzzi, C., Braun, O., Overbeck, J., Maurya, A.K., Neels, A., Calame, M., Michler, J., Zysset, P., Schwiedrzik, J., 2021. Combining polarized Raman spectroscopy and micropillar compression to study microscale structure-property relationships in mineralized tissues. *Acta Biomater.* 119, 390–404. <https://doi.org/10.1016/j.actbio.2020.10.034>
- Kourkoumelis, N., Zhang, X., Lin, Z., Wang, J., 2019. Fourier Transform Infrared Spectroscopy of Bone Tissue: Bone Quality Assessment in Preclinical and Clinical Applications of Osteoporosis and Fragility Fracture. *Clin. Rev. Bone Miner. Metab.* 17, 24–39. <https://doi.org/10.1007/s12018-018-9255-y>
- McCreadie, B.R., Morris, M.D., Chen, T., Sudhaker Rao, D., Finney, W.F., Widjaja, E., Goldstein, S.A., 2006. Bone tissue compositional differences in women with and without osteoporotic fracture. *Bone* 39, 1190–1195. <https://doi.org/10.1016/j.bone.2006.06.008>
- Mitra, E., Akella, S., Qin, Y., 2006. The effects of embedding material, loading rate and magnitude, and penetration depth in nanoindentation of trabecular bone. *J. Biomed. Mater. Res. Part A* 79A, 86–93. <https://doi.org/10.1002/jbm.a.30742>
- Morris, M.D., Mandair, G.S., 2011. Raman Assessment of Bone Quality. *Clin. Orthop. Relat. Res.* 469, 2160–2169. <https://doi.org/10.1007/s11999-010-1692-y>
- O’Sullivan, L., 2020. Time-sequence of Biomechanical Adaption in Trabecular Tissue during Estrogen Deficiency.
- O’Sullivan, L.M., Allison, H., Parle, E.E., Schiavi, J., McNamara, L.M., 2020. Secondary alterations in bone mineralisation and trabecular thickening occur after long-term estrogen deficiency in ovariectomised rat tibiae, which do not coincide with initial rapid bone loss. *Osteoporos. Int.* 31, 587–599. <https://doi.org/10.1007/s00198-019-05239-5>
- Oliver, W.C., Pharr, G.M., 1992. An improved technique for determining hardness and elastic modulus using load and displacement sensing indentation experiments. *J. Mater. Res.* 7, 1564–1583. <https://doi.org/10.1557/JMR.1992.1564>
- Razi, H., Birkhold, A.I., Weinkamer, R., Duda, G.N., Willie, B.M., Checa, S., 2015. Aging leads to a dysregulation in mechanically driven bone formation and resorption. *J. Bone Miner. Res.* 30, 1864–1873. <https://doi.org/10.1002/jbmr.2528>
- Schwiedrzik, J., Raghavan, R., Bürki, A., Lenader, V., Wolfram, U., Michler, J., Zysset, P.,

2014. In situ micropillar compression reveals superior strength and ductility but an absence of damage in lamellar bone. *Nat. Mater.* 13, 740–747. <https://doi.org/10.1038/nmat3959>
- Schwiedrzik, J., Taylor, A., Casari, D., Wolfram, U., Zysset, P., Michler, J., 2017. Nanoscale deformation mechanisms and yield properties of hydrated bone extracellular matrix. *Acta Biomater.* 60, 302–314. <https://doi.org/10.1016/j.actbio.2017.07.030>
- Unal, M., Ahmed, R., Mahadevan-Jansen, A., Nyman, J.S., 2021. Compositional assessment of bone by Raman spectroscopy. *Analyst* 146, 7444–7470. <https://doi.org/10.1039/d1an01560e>
- Unal, M., Jung, H., Akkus, O., 2016. Novel Raman Spectroscopic Biomarkers Indicate That Postyield Damage Denatures Bone’s Collagen. *J. Bone Miner. Res.* 31, 1015–1025. <https://doi.org/10.1002/jbmr.2768>
- Vanleene, M., Rey, C., Ho Ba Tho, M.C., 2008. Relationships between density and Young’s modulus with microporosity and physico-chemical properties of Wistar rat cortical bone from growth to senescence. *Med. Eng. Phys.* 30, 1049–1056. <https://doi.org/10.1016/j.medengphy.2007.12.010>
- Wittig, N.K., Birkedal, H., 2022. Bone hierarchical structure: spatial variation across length scales. *Acta Crystallogr. Sect. B Struct. Sci. Cryst. Eng. Mater.* 78, 305–311. <https://doi.org/10.1107/S2052520622001524>
- Wölfel, E.M., Fiedler, I.A.K., Dragoun Kolibova, S., Krug, J., Lin, M.-C., Yazigi, B., Siebels, A.K., Mushumba, H., Wulff, B., Ondruschka, B., Püschel, K., Glüer, C.C., Jähn-Rickert, K., Busse, B., 2022a. Human tibial cortical bone with high porosity in type 2 diabetes mellitus is accompanied by distinctive bone material properties. *Bone* 165, 116546. <https://doi.org/10.1016/j.bone.2022.116546>
- Wölfel, E.M., Jähn-Rickert, K., Schmidt, F.N., Wulff, B., Mushumba, H., Sroga, G.E., Püschel, K., Milovanovic, P., Amling, M., Campbell, G.M., Vashishth, D., Busse, B., 2020. Individuals with type 2 diabetes mellitus show dimorphic and heterogeneous patterns of loss in femoral bone quality. *Bone* 140, 115556. <https://doi.org/10.1016/j.bone.2020.115556>
- Wölfel, E.M., Schmidt, F.N., vom Scheidt, A., Siebels, A.K., Wulff, B., Mushumba, H.,

Ondruschka, B., Püschel, K., Scheijen, J., Schalkwijk, C.G., Vettorazzi, E., Jähn-Rickert, K., Gludovatz, B., Schaible, E., Amling, M., Rauner, M., Hofbauer, L.C., Zimmermann, E.A., Busse, B., 2022b. Dimorphic Mechanisms of Fragility in Diabetes Mellitus: the Role of Reduced Collagen Fibril Deformation. *J. Bone Miner. Res.* 37, 2259–2276. <https://doi.org/10.1002/jbmr.4706>

Yerramshetty, J.S., Lind, C., Akkus, O., 2006. The compositional and physicochemical homogeneity of male femoral cortex increases after the sixth decade. *Bone* 39, 1236–1243. <https://doi.org/10.1016/j.bone.2006.06.002>

CHAPTER 6

Concluding Remarks and Future Perspectives

6.1 Summary of Key Contributions

Type-2 Diabetes (T2D) mellitus has emerged as an independent risk factor for skeletal fragility fracture, and the principal comorbidity with osteoporosis. Current screening methods like Dual X-Ray Absorptiometry (DEXA) are unable to fully predict fracture probability and FRAX are unable to provide quantitative measures of fracture probability in T2D, due to patients often presenting with normal or high bone mineral density (BMD) (Vandenput et al., 2022). While previous research had suggested that elevated blood glucose levels in T2D leads to non-enzymatic glycation of the organic matrix, and the associated formation of advanced glycated end-products (AGEs), there has been limited experimental evidence that provides any meaningful mechanistic link between AGE accumulation and impaired tissue mechanics in human T2 diabetes (Karim et al., 2018; Wölfel et al., 2022b, 2022a). This highlights that other mechanisms must be responsible for impaired tissue behaviour. As the prevalence of T2D is reaching epidemic proportions (Robertson, 2023; Saeedi et al., 2019), this thesis employed a multiscale approach to investigate the underlying cellular, compositional, structural and biomechanical mechanisms of bone fragility in Zucker Diabetic Fatty (ZDF) (*fa/fa*) rats.

The overall contribution of this thesis has been to present a detailed longitudinal investigation into the mechanisms that lead to bone fragility in a ZDF (*fa/fa*) rat. This work provides new insights into the biological, biophysical, and biomechanical events that could contribute to bone fragility in a ZDF (*fa/fa*) rat model for T2D. Furthermore, this work implements a 46-week

longitudinal animal study, the longest animal study to date of bone fragility in T2D, which reflects three separate disease stages of early, established and long-term diabetes. This thesis shows a strong implementation of the 3R's in animal research, whereby multiple tests were performed on the same bone sample. Moreover, this work for the first time has evaluated regional differences in early to late-stage T2 diabetic rats. The key scientific contributions have been to show that bone fragility in T2D (*fa/fa*) rats occurs through a multifactorial process whereby the downstream effects of altered cellular metabolism in diabetic rats can impair the tissue quality as the disease progresses. Most notably, it was found that the mineral phase of the bone matrix was most affected by the disease, undergoing both spatial and temporal alterations in T2D due to the altered bone turnover process. Several of these alterations were found to be directly correlated to the mechanical integrity of the tissue, as measured by whole bone biomechanical tests. Importantly, these findings challenge the notion that advanced glycation end-products (AGEs) are the main contributors to increased bone fragility in ZDF (*fa/fa*) rats and clearly highlight that both mineral and organic phases of the bone matrix are likely responsible. This section outlines in more detail the key contributions and main findings from each of these studies.

Chapter 3 investigated whether AGEs from radius cortical bone were the main contributing factor to the increased risk of fracture observed in subjects with T2D by examining the geometrical, compositional and mechanical alterations of ulnar bone in ZDF (*fa/fa*) rats as the disease progressed, through the use of micro-CT, Fourier transform infrared spectroscopy (FTIR), fAGE analysis and three-point bend testing. This work revealed significant scientific contributions, demonstrating that ZDF (*fa/fa*) rats exhibit impaired longitudinal bone growth by 12-weeks, leading to substantially reduced bone size by 46-weeks compared to controls (*fa/+*). Structural deficits, including bending rigidity, ultimate moment, and energy-to-failure, were evident in diabetic rats. Tissue-level material properties showed marked alterations, with ZDF (*fa/fa*) rats at 46-weeks having significant reductions in yield and ultimate strength. FTIR analysis indicated changes in tissue composition, revealing a reduced carbonate: phosphate ratio and increased acid phosphate content in ZDF (*fa/fa*) rats with long-term diabetes, indicative of an altered bone cellular processes. Interestingly, while AGE accumulation was higher in the skin of ZDF (*fa/fa*) rats with long-term T2D, bone AGEs did not differ between strains and showed no correlation with bone strength. Furthermore, this multifaceted study contributed to the understanding of the complex mechanism underlying bone fragility in

diabetic ZDF (*fa/fa*) rats, encompassing impaired growth, altered cellular processes and changes in tissue composition.

Chapter 4 established the sequence of events that occurred from the cellular-level to the tissue-level to impact the whole-bone fracture mechanics during T2D using a longitudinal Zucker Diabetic Fatty (ZDF) (*fa/fa*) rat model. This work examined the biological, biophysical and biomechanical factors through the use of biochemical assays on serum, and micro-CT, HPLC, bulk fAGEs analysis, fracture toughness and sideways fall testing on femoral bone. Serum markers revealed disruptions in bone homeostasis and possible impairment of osteoblast activity. Changes in the organic matrix, characterized by elevated Furosine and Carboxymethyl-lysine (CML), were identified in long-term diabetic rats. Micro-CT analysis demonstrated increased cortical porosity, while biomechanical testing indicated reduced tissue-level cracking toughness and work-to-fracture in diabetic bone, emphasizing compromised energy dissipation capacity. This comprehensive study enhanced the understanding of the sequential pathophysiological mechanisms leading to bone fragility in severe T2D.

Finally, Chapter 5 presented a novel investigation into regional differences in tissue composition and mechanics during the growth and maintenance of cortical bone from femurs of ZDF (*fa/fa*) rats as the disease progressed through the use of Raman spectroscopy, nanoindentation and micropillar compression testing. This work examined three distinct components: (a) region vs. region within strains, (b) longitudinal changes within strains in both regions, and (c) differences between strains within regions at various ages. Notably, regional differences were primarily evident in the mineral component, especially in the periosteal region of cortical bone in T2D (*fa/fa*) and control rats. Diabetic rats exhibited an altered ν_2 carbonate/ Amide I ratio, ν_2 phosphate/ Amide III ratio, and crystallinity, indicating a regional dynamic interplay between bone formation and resorption processes in maintaining bone growth. In fact, results from this Chapter have echoed changes in bone growth that had been seen in previous Chapters. Chapter 3 revealed that bone growth, assessed through parameters such as anterior-posterior and medial-lateral diameter, moment of inertia, and cortical bone area, did not exhibit significant changes from 26- to 46-weeks in the diabetic (*fa/fa*) cohort, in contrast to the observed increase in controls. Furthermore, in Chapter 4, femoral thickness decreased from 26- to 46-weeks in the T2D (*fa/fa*) rats while remaining unchanged in the control group. The investigation in this chapter delved into regional disparities, providing insights into how diabetes might disrupt bone maintenance and appositional growth, especially concerning age and disease progression in ZDF (*fa/fa*) rats. Importantly, this work showed that despite

compositional changes impacting tissue quality, tissue-level mechanical properties, assessed by indentation modulus and hardness, showed no significant differences between strains in both regions. These findings provide valuable insights into the regional changes during the growth and maintenance of cortical bone in ZDF (*fa/fa*) rats with T2D, providing a wider understanding into the complex interaction between tissue composition, mechanics, and disease progression.

6.2 Future Recommendations

The work presented in this thesis represents a significant step towards understanding the biological, biophysical, and biomechanical events that could contribute to bone fragility in a ZDF (*fa/fa*) rat model for T2D. Furthermore, this animal model of T2D may be a suitable model to mimic the progression of T2D when developed during childhood or adolescence, given the exact time-point of the onset of diabetes in this strain is known. Additionally, this model is also representative of the small, but still existent, population of humans that develop T2D as a result of a leptin or leptin receptor deficiency (DePaoli, 2014). However, this rodent model has certain limitations, most notably in its male bias, which is common among most other well-established animal models, whereby the female strains either cannot develop frank diabetes or the severity of the disease is very mild. This means that the majority of research on skeletal fragility in rodent models for T2D has been carried out on males, leaving a large gap in the literature and in our understanding of how skeletal fragility can present in females with T2D, particularly in the presence of oestrogen or oestrogen-deficiency (Díaz et al., 2019). To date, only two animal studies using female rodents have been used to investigate bone fragility in T2D (Mehta et al., 2023; Sihota et al., 2020b). Whilst female subjects have been better represented in human studies of T2D (Burghardt et al., 2010; Cirovic et al., 2022; Hunt et al., 2021; Karim et al., 2018; Lekkala et al., 2019; Parle et al., 2020; Piccoli et al., 2020; Wölfel et al., 2022a, 2020), the understanding of disease progression in human studies is limited since disease duration cannot be controlled, while other important factors such as BMI, HbA1C and medications taken are omitted from patient data and confounding factors can interfere. Whilst the use of female rodent models of T2D such as the HFD STZ Sprague Dawley rats has already been examined, future work could utilise this model to carry out a longitudinal study which implements the examination of male and female rats to assess the progression of T2D and its effects on bone fragility. Perhaps another layer of this investigation could assess oestrogen and oestrogen-deficient diabetes in the female cohort.

Results from Chapter 4 demonstrated the downstream effects of an altered cellular metabolism on the biomechanical properties of bone in diabetic (*fa/fa*) rats by assessing serum biological markers. Understanding the potential impact of disrupted bone cell metabolism on subsequent changes in trabecular and cortical bone microstructure is crucial, especially in cases of increased fracture risk that are unrelated to bone density. There is a current lack of methodologies available for clinicians to measure material properties of bone to non-invasively assess fracture risk of patients. This thesis provided novel insight into the cellular mechanisms that underlie that pathogenesis of bone fragility in ZDF rats, future work using histological analysis on regional areas of the bone tissue would be of huge benefit to confirm if the serum cellular markers reflected what was happening within the tissue itself of the ZDF (*fa/fa*) rats. In doing so, this could introduce the potential in identifying a non-invasive serum marker that could be used as a surrogate marker to assess fracture risk. In addition, future work could look to assessing bone material strength index (BMSi) through reference point indentation where the OsteoProbe device (Active Life Scientific, Santa Barbara, CA) could provide non-invasive assessment for the mechanical properties of bone tissue *in vivo* (Farr et al., 2014; Nilsson et al., 2017), with some studies reporting a negative correlation between BMSi and AGEs measured via skin autofluorescence (Furst et al., 2016; Samakkarnthai et al., 2020) but further assessment is required to understand how these measurements could represent fracture risk in a clinical setting. Perhaps future human and animal work could measure the BMSi and examine the cellular aspect either through quantifying serum markers of cellular activity and/ or histology combined with a compositional analysis to assess the mineral component of the bone matrix with the aim to identify whether alterations in the mineral matrix of diabetic subjects may alter the BMSi and whether this can be non-invasively captured via a serum marker. This would help to unite an already fragmented understanding of the underlying mechanisms involved in bone fragility of T2D and move towards the development of an effective fracture risk assessment technique for patients with T2D.

6.3 References

- Burghardt, A.J., Issever, A.S., Schwartz, A. V., Davis, K.A., Masharani, U., Majumdar, S., Link, T.M., 2010. High-resolution peripheral quantitative computed tomographic imaging of cortical and trabecular bone microarchitecture in patients with type 2 diabetes mellitus. *J. Clin. Endocrinol. Metab.* 95, 5045–5055. <https://doi.org/10.1210/jc.2010-0226>
- Cirovic, A., Djukic, D., Djonic, D., Zivkovic, V., Nikolic, S., Djuric, M., Milovanovic, P., 2022. Three-dimensional mapping of cortical porosity and thickness along the superolateral femoral neck in older women. *Sci. Rep.* 12, 1–8. <https://doi.org/10.1038/s41598-022-19866-2>
- DePaoli, A.M., 2014. Leptin in common obesity and associated disorders of metabolism. *J. Endocrinol.* 223, T71–T81. <https://doi.org/10.1530/JOE-14-0258>
- Díaz, A., López-Gruoso, R., Gambini, J., Monleón, D., Mas-Bargues, C., Abdelaziz, K.M., Viña, J., Borrás, C., 2019. Sex Differences in Age-Associated Type 2 Diabetes in Rats—Role of Estrogens and Oxidative Stress. *Oxid. Med. Cell. Longev.* 2019, 1–13. <https://doi.org/10.1155/2019/6734836>
- Farr, J.N., Drake, M.T., Amin, S., Melton, L.J., McCready, L.K., Khosla, S., 2014. In Vivo Assessment of Bone Quality in Postmenopausal Women With Type 2 Diabetes. *J. Bone Miner. Res.* 29, 787–795. <https://doi.org/10.1002/jbmr.2106>
- Furst, J.R., Bandeira, L.C., Fan, W., Agarwal, S., Nishiyama, K.K., McMahon, D.J., Dworakowski, E., Jiang, H., Silverberg, S.J., Rubin, M.R., 2016. Advanced Glycation Endproducts and Bone Material Strength in Type 2 Diabetes. *J. Clin. Endocrinol. Metab.* 101, 2502–2510. <https://doi.org/10.1210/jc.2016-1437>
- Hunt, H.B., Miller, N.A., Hemmerling, K.J., Koga, M., Lopez, K.A., Taylor, E.A., Sellmeyer, D.E., Moseley, K.F., Donnelly, E., 2021. Bone Tissue Composition in Postmenopausal Women Varies With Glycemic Control From Normal Glucose Tolerance to Type 2 Diabetes Mellitus. *J. Bone Miner. Res.* 36, 334–346. <https://doi.org/10.1002/jbmr.4186>
- Karim, L., Moulton, J., Van Vliet, M., Velie, K., Robbins, A., Malekipour, F., Abdeen, A., Ayres, D., Bouxsein, M.L., 2018. Bone microarchitecture, biomechanical properties, and advanced glycation end-products in the proximal femur of adults with type 2 diabetes. *Bone* 114, 32–39. <https://doi.org/10.1016/j.bone.2018.05.030>

- Lekkala, S., Taylor, E.A., Hunt, H.B., Donnelly, E., 2019. Effects of Diabetes on Bone Material Properties. *Curr. Osteoporos. Rep.* 17, 455–464. <https://doi.org/10.1007/s11914-019-00538-6>
- Mehta, D., Sihota, P., Tikoo, K., Kumar, S., Kumar, N., 2023. Type 2 diabetes alters the viscoelastic behavior and macromolecular composition of vertebra. *Bone Reports* 18, 101680. <https://doi.org/10.1016/j.bonr.2023.101680>
- Nilsson, A.G., Sundh, D., Johansson, L., Nilsson, M., Mellström, D., Rudäng, R., Zoulakis, M., Wallander, M., Darelid, A., Lorentzon, M., 2017. Type 2 Diabetes Mellitus Is Associated With Better Bone Microarchitecture But Lower Bone Material Strength and Poorer Physical Function in Elderly Women: A Population-Based Study. *J. Bone Miner. Res.* 32, 1062–1071. <https://doi.org/10.1002/jbmr.3057>
- Parle, E., Tio, S., Behre, A., Carey, J.J., Murphy, C.G., O'Brien, T.F., Curtin, W.A., Kearns, S.R., McCabe, J.P., Coleman, C.M., Vaughan, T.J., McNamara, L.M., 2020. Bone Mineral Is More Heterogeneously Distributed in the Femoral Heads of Osteoporotic and Diabetic Patients: A Pilot Study. *JBMR Plus* 4, 1–10. <https://doi.org/10.1002/jbm4.10253>
- Piccoli, A., Cannata, F., Strollo, R., Pedone, C., Leanza, G., Russo, F., Greto, V., Isgrò, C., Quattrocchi, C.C., Massaroni, C., Silvestri, S., Vadalà, G., Bisogno, T., Denaro, V., Pozzilli, P., Tang, S.Y., Silva, M.J., Conte, C., Papalia, R., Maccarrone, M., Napoli, N., 2020. Sclerostin Regulation, Microarchitecture, and Advanced Glycation End-Products in the Bone of Elderly Women With Type 2 Diabetes. *J. Bone Miner. Res.* 35, 2415–2422. <https://doi.org/10.1002/jbmr.4153>
- Robertson, R.P., 2023. Type 2 diabetes mellitus: Prevalence and risk factors [WWW Document]. UpToDate.
- Saeedi, P., Petersohn, I., Salpea, P., Malanda, B., Karuranga, S., Unwin, N., Colagiuri, S., Guariguata, L., Motala, A.A., Ogurtsova, K., Shaw, J.E., Bright, D., Williams, R., 2019. Global and regional diabetes prevalence estimates for 2019 and projections for 2030 and 2045: Results from the International Diabetes Federation Diabetes Atlas, 9th edition. *Diabetes Res. Clin. Pract.* 157, 107843. <https://doi.org/10.1016/j.diabres.2019.107843>
- Samakkarnthai, P., Sfeir, J.G., Atkinson, E.J., Achenbach, S.J., Wennberg, P.W., Dyck, P.J., Tweed, A.J., Volkman, T.L., Amin, S., Farr, J.N., Vella, A., Drake, M.T., Khosla, S., 2020. Determinants of bone material strength and cortical porosity in patients with type 2

- diabetes mellitus. *J. Clin. Endocrinol. Metab.* 105, 3718–3729. <https://doi.org/10.1210/clinem/dgaa388>
- Sihota, P., Yadav, R.N., Poleboina, S., Mehandia, V., Bhadada, S.K., Tikoo, K., Kumar, N., 2020. Development of HFD-Fed/Low-Dose STZ-Treated Female Sprague-Dawley Rat Model to Investigate Diabetic Bone Fragility at Different Organization Levels. *JBMR Plus* 4, 1–12. <https://doi.org/10.1002/jbm4.10379>
- Vandenput, L., Johansson, H., McCloskey, E. V., Liu, E., Åkesson, K.E., Anderson, F.A., Azagra, R., Bager, C.L., Beaudart, C., Bischoff-Ferrari, H.A., Biver, E., Bruyère, O., Cauley, J.A., Center, J.R., Chapurlat, R., Christiansen, C., Cooper, C., Crandall, C.J., Cummings, S.R., da Silva, J.A.P., Dawson-Hughes, B., Diez-Perez, A., Dufour, A.B., Eisman, J.A., Elders, P.J.M., Ferrari, S., Fujita, Y., Fujiwara, S., Glüer, C.C., Goldshtein, I., Goltzman, D., Gudnason, V., Hall, J., Hans, D., Hoff, M., Hollick, R.J., Huisman, M., Iki, M., Ish-Shalom, S., Jones, G., Karlsson, M.K., Khosla, S., Kiel, D.P., Koh, W.P., Koromani, F., Kotowicz, M.A., Kröger, H., Kwok, T., Lamy, O., Langhammer, A., Larijani, B., Lippuner, K., Mellström, D., Merlijn, T., Nordström, A., Nordström, P., O'Neill, T.W., Obermayer-Pietsch, B., Ohlsson, C., Orwoll, E.S., Pasco, J.A., Rivadeneira, F., Schei, B., Schott, A.M., Shiroma, E.J., Siggeirsdottir, K., Simonsick, E.M., Sornay-Rendu, E., Sund, R., Swart, K.M.A., Szulc, P., Tamaki, J., Torgerson, D.J., van Schoor, N.M., van Staa, T.P., Vila, J., Wareham, N.J., Wright, N.C., Yoshimura, N., Zillikens, M.C., Zwart, M., Harvey, N.C., Lorentzon, M., Leslie, W.D., Kanis, J.A., 2022. Update of the fracture risk prediction tool FRAX: a systematic review of potential cohorts and analysis plan, *Osteoporosis International*. Springer London. <https://doi.org/10.1007/s00198-022-06435-6>
- Wölfel, E.M., Fiedler, I.A.K., Dragoun Kolibova, S., Krug, J., Lin, M.-C., Yazigi, B., Siebels, A.K., Mushumba, H., Wulff, B., Ondruschka, B., Püschel, K., Glüer, C.C., Jähn-Rickert, K., Busse, B., 2022a. Human tibial cortical bone with high porosity in type 2 diabetes mellitus is accompanied by distinctive bone material properties. *Bone* 165, 116546. <https://doi.org/10.1016/j.bone.2022.116546>
- Wölfel, E.M., Jähn-Rickert, K., Schmidt, F.N., Wulff, B., Mushumba, H., Sroga, G.E., Püschel, K., Milovanovic, P., Amling, M., Campbell, G.M., Vashishth, D., Busse, B., 2020. Individuals with type 2 diabetes mellitus show dimorphic and heterogeneous patterns of loss in femoral bone quality. *Bone* 140, 115556.

<https://doi.org/10.1016/j.bone.2020.115556>

Wölfel, E.M., Schmidt, F.N., vom Scheidt, A., Siebels, A.K., Wulff, B., Mushumba, H., Ondruschka, B., Püschel, K., Scheijen, J., Schalkwijk, C.G., Vettorazzi, E., Jähn-Rickert, K., Gludovatz, B., Schaible, E., Amling, M., Rauner, M., Hofbauer, L.C., Zimmermann, E.A., Busse, B., 2022b. Dimorphic Mechanisms of Fragility in Diabetes Mellitus: the Role of Reduced Collagen Fibril Deformation. *J. Bone Miner. Res.* 37, 2259–2276. <https://doi.org/10.1002/jbmr.4706>